THE UNIVERSITY
of EDINBURGH

Investigating Ass1 and its role in renal fibrosis

Sarah Finnie

Doctor of Philosophy

The University of Edinburgh

2019

Author's Declaration

I declare that this thesis has been written entirely by myself and it is the result of my own work except when explicit reference has been made to the contribution of others. This thesis has not been submitted previously for any other degree at any institution. The research was carried out at the Centre for Cardiovascular Science at the Queen's Medical Research Institute at the University of Edinburgh. This work was supervised by Dr Laura Denby and Professor Nicholas Morton.

Acknowledgements

I would firstly like to thank my supervisor Dr Laura Denby for all her support and guidance over the past three years. She was very encouraging of me to gain independence throughout my project and I have come to the end of my PhD a much more competent researcher. Laura was always available to chat over ideas and helped me drive my project forward.

Laura ran a very supportive research group and we were always willing to help each other out. The Denby group were instrumental to the successes of my project and I am very grateful to James, Vicky, Katie, Andrew and Ollie for all the help, support and laughs they have given me. I would like to extend particular thanks to the Ferenbach and Conway groups who gave me great clinical advice and guidance throughout my project. Carolynn Cairns always went above and beyond to help me out in the lab for which I am very thankful. I would also like to thank the Baker group who were extremely knowledgeable of practical lab techniques and were always willing to collaborate. Additionally I am very grateful for Dr Rod Carter, who taught me how to perform metabolic analysis using the Seahorse Analyser. Finally, I would like to thank my funders, the British Heart Foundation, without whom this research would not be possible.

Table of Contents

List of Tables

List of Figures

Abbreviations

- ACAA2: Acetyl-CoA Acyltransferase 2
- AKI: acute kidney injury
- ANOVA: analysis of variance
- ARB: angiotensin receptor blocker
- ARG1: arginase 1
- ASL: argininosuccinate lyase
- ASS1: argininosuccinate synthetase
- BCA: bicinchoninic acid assay
- BSA: bovine serum albumin
- CKD: chronic kidney disease
- COL1A1: collagen 1 subtype a1
- CLDN2: claudin 2
- CPS1: carbamoyl phosphate synthetase
- CTLN1: citrullinemia type I
- DEC1: deleted in oesophageal cancer 1
- DNA: deoxyribonucleic acid
- ECM: extracellular matrix
- EMT: epithelial to mesenchymal transition
- ERK: extracellular signal related kinase
- ESRF: end-stage renal failure
- FACS: fluorescently activated cell sorting
- FAO: fatty acid oxidation
- FGF: fibroblast growth factor
- Gatm: glycine amidinotransferase
- GBM: glomerular basement membrane
- Gcdh: glutaryl-CoA dehydrogenase
- GFR: glomerular filtration rate
- HIF1α: hypoxia inducible factor 1 alpha
- IRI: ischaemia reperfusion injury
- JNK: c-Jun N-terminal kinases
- Lrp2: megalin gene
- MAPK: mitogen activated protein kinase
- miR: microRNA
- MMP: matrix metalloproteinase

- NFκB: nuclear factor kappa B
- NHS: national health service
- OCLN: occludin
- OTC: ornithine transcarbamylase
- PBS: phosphate buffered saline
- PCT: proximal convoluted tubule
- PDGFRβ: platelet derived growth factor receptor beta
- PKD: polycystic disease
- PPARA: peroxisomal proliferator activated receptor alpha
- PT: proximal tubule
- PTEC: proximal tubular epithelial cell
- RAAS: renin-angiotensin-aldosterone system
- RNA: ribonucleic acid
- RPTEC: renal proximal tubular epithelial cells
- rUUO: reversed unilateral ureteric obstruction
- SASP: senescence associated secretory phenotype
- siRNA: small interfering RNA
- STNx: subtotal nephrectomy
- TEC: tubular epithelial cell
- TGFβ: transforming growth factor beta
- TIF: tubulointerstitial fibrosis
- TNFα: tumour necrosis factor alpha
- UUO: unilateral ureteric obstruction
- ZO-1: tight protein junction 1
- ACTA2: alpha smooth muscle actin
- CDKN1A: cyclin dependent kinase inhibitor 1a (p21)
- CDKN2A: cyclin dependent kinase inhibitor 2a (p16)
- COL3A1: collagen 3 subunit 1a
- COL4A1: collagen 4 subunit 1a
- CUBN: cubulin
- HAVCR1: hepatitis A virus cellular receptor 1
- HDAC1: histone deacetylase 1
- ICAM1: intercellular adhesion molecule 1
- MKI67: marker of proliferation Ki-67
- TGFBR1: transforming growth factor beta receptor 1
- TIMP: tissue inhibitor of matrix metalloproteinase

Abstract

Background: The incidence of chronic kidney disease (CKD) is rising and is the 12th most common cause of death worldwide. Currently, the only available treatments are renal replacement therapy and transplantation, both of which are significantly costly for the NHS. Therefore there is an unmet clinical need for new therapies which can tackle the manifestation of renal disease processes and progression to CKD. The pathophysiological process common to all CKDs, regardless of the initiating aetiology, is tubulointerstitial fibrosis (TIF). TIF leads to scarring of the kidney and results in loss of renal function and eventual end-stage renal disease. TIF is driven by a number of pathophysiological processes taking place in several cell types including the proximal tubule. The proximal tubule (PT) is sensitive to injury and in a damaged state has attracted attention as a driver of fibrotic disease due to de-differentiation and pro-inflammatory/ pro-fibrotic signalling. Argininosuccinate synthetase (ASS1), a rate-limiting urea cycle enzyme, is highly expressed in the PT and has been reported to be downregulated in human CKD. Furthermore, urea cycle metabolites such as citrulline have been reported to be dysregulated in renal disease.

Hypothesis: Loss of tubular ASS1 expression is critical in the induction of renal fibrosis.

Results: Renal *Ass1* expression was assessed and compared to sham operated animals in ischaemia-reperfusion injury (IRI), subtotal nephrectomy (STNx), obstructive (UUO) and reversible obstructive (rUUO) murine models. *Ass1* expression was significantly downregulated in all models of injury. *Ass1* loss occurred at early time points and preceded the manifestation of fibrosis. Single cell RNA-seq of the reversible UUO model was adopted to assess *Ass1* expression during the progression and reversal of fibrosis. After obstruction, *Ass1* was significantly depleted in fibrotic tubular epithelial cells. Upon reversal of fibrosis, *Ass1* expression levels almost returned to normal.

ASS1 is highly expressed in human proximal tubular epithelial cells (RPTEC/TERT1). To determine the consequences of *ASS1* depletion, *ASS1* was knocked-down in RPTECs. This induced upregulation of pro-fibrotic genes and downregulation of cell-cell contact genes. In RPTECs*, ASS1* transcription was unaffected by pro-fibrotic, TGFβ. However, ASS1 transcription was significantly reduced in a dose-dependent manner following TNFα treatment and hypoxia.

In order to further interrogate the function of Ass1 in tubular epithelial cells *in vivo*, Ass1 was conditionally knocked out in renal tubular cells specifically using the Pax8 CreER^{T2} floxed *Ass1* transgenic mouse. The effect of Pax8 Cre x *Ass1* flox/wt heterozygous knock-out was assessed to explore if partial loss of *Ass1* exerted a haploinsufficiency effect. Heterozygous

mice did not demonstrate any renal phenotype distinct from controls. A small cohort of Pax8 Cre x Ass1 flox/flox mice homozygous were assessed to interrogate the effects of full knock out of Ass1 in the kidney. Pax8Cre x Ass1 flox/flox female mice exhibited a decrease in ASS1 protein in the kidney. This under-powered study did not reveal any pathological effects in the kidney in the unchallenged state in a period of 10 weeks.

Conclusions: Downregulation of *Ass1* is evident in 3 different models of fibrosis with different aetiologies. Replicating loss of *ASS1 in vitro* in human RPTECs induced a pro-fibrotic, de-differentiated phenotype which is independent of TGF-β signalling but dependent on pro-inflammatory and hypoxic stimuli. A small under-powered cohort of tubular specific Ass1 knock-out mice did not exhibit fibrosis within the kidney in the basal state in a short time-frame. However, using a larger cohort and challenging the tubular Ass1 knock out mouse with an injury such as ischaemia reperfusion may result in an exacerbation of fibrosis. Overall, loss of ASS1 may provide a novel link between initial inflammatory/ hypoxic insult in tubular cells and pro-fibrotic signalling driving renal disease which needs further interrogation *in vivo*.

Chapter: 1 Introduction

1.1 Kidney Function

The kidney is an essential organ which is responsible for maintaining physiological homeostasis through a number of mechanisms. The kidneys perform diverse roles including maintaining the body's pH, regulating electrolyte balance, regulating fluid balance and regulating blood pressure. Additionally, the kidney is responsible for reabsorbing nutrients such as glucose and amino acids, producing hormones such as renin and erythropoietin and activating vitamin D. The specific structure and morphology of the kidney is essential for maintaining these physiological roles. Several functionally distinct cell types coalesce together to form the structurally unique functional unit of the kidney; the nephron. A single kidney contains around 1 million nephrons which together filter around 180 litres blood every day. The nephron is comprised of the glomerulus, proximal tubule, loop of Henlé, distal tubule and collecting duct (Figure 1.1). Each of these components performs a specific function (1).

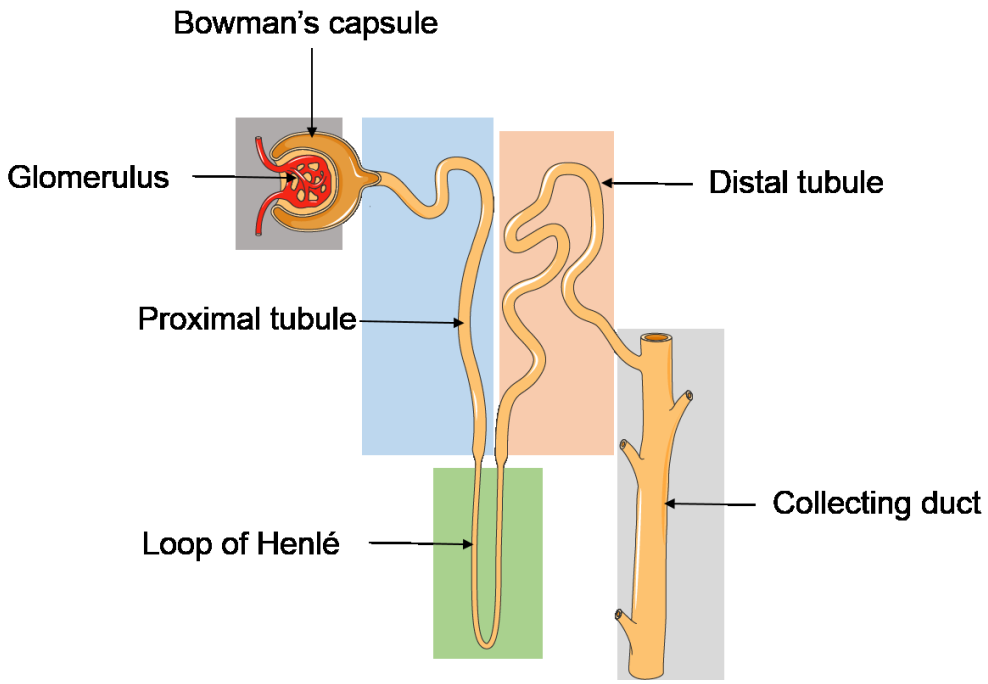

Figure 1.1: Segments of the nephron

1.1.1 The Glomerulus

The glomerulus is the filtering unit of the nephron with multiple filtering layers situated between afferent and efferent resistance vessels. Specialised fenestrated endothelial cells form a bundle of capillaries which provide the first layer of filtration. Filtrate that passes through these fenestrations is further filtered by the glomerular basement membrane (GBM) (2). The GBM is comprised of an array of extra-cellular matrix proteins and serves to support the capillary bundle (3). Finally, specialised peri-vascular epithelial cells, called podocytes, with interdigitating foot processes wrap around the GBM providing the last layer of filtration. The membrane between podocyte foot processes, termed the slit diaphragm, functions to form a size selectivity barrier. It also contains transmembrane proteins that signal back to podocytes to regulate their form and function. Together, these components prevent the passage of red blood cells and large proteins into the urinary space (4). The filtrate, or pre-urine, is then collected in the Bowman's capsule and moves through the tubules for reabsorption of nutrients and fluid balance.

1.1.2 The Tubules

Tubules are luminal structures comprised of polarised tubular epithelial cells which vary in their transporter profile from the proximal tubule to the collecting duct. Each epithelial cell contains an apical and a basolateral membrane which are exposed to the lumen and peritubular capillaries respectively. The proximal tubule (PT) is described in three segments; S1, S2 and S3 (5). S1 comprises the beginning of the proximal convoluted tubule (PCT) and is characterized by a thick brush border with the greatest number of microvilli which provides a very large luminal surface area. S1 also contains more mitochondria and endocytic compartments than S2 or S3. S2 comprises the remainder of the PCT and has a less pronounced brush border with shorter microvilli as well as fewer mitochondria other organelles. Segment 3 comprises the straight PT and terminates at the outer stripe of the medulla. S3 has the least pronounced brush border and the fewest number of mitochondria within the PT (6). The proximal tubule is responsible for the vast majority of tubular reabsorption (6). Glucose, amino acids, electrolytes and water (60-70%) are all reabsorbed by the PT with reabsorption greatest in S1 and to a lesser extent in S2 and S3. This extensive reabsorption requires energy and the PT is the most energy dependent component of the nephron (7).

The remaining segments of nephron, the loop of Henle, distal tubule and the collecting duct are responsible for the concentration of urine. After the majority of nutrients are absorbed by the PT, the loop of Henle descends into the medulla and is responsible for the concentration of pre-urine. The distal tubule and collecting duct are responsible for the fine balance of electrolytes and serve as a pathway to the ureter. Together the distal tubule and collecting duct contribute between 5-10% sodium reabsorption which is entirely dependent on dietary intake (8). These regions of the nephron rely on a fine balance provided by precise passive and active transport of electrolytes and water (9).

Any disturbance to renal homeostasis results in pathological changes to the kidney itself as well as systemic changes such as blood pressure and acid-base balance. One of the most severe pathologies of the kidney is chronic kidney disease which leads to renal failure and end-stage kidney disease for which the treatments are costly and in the exception of transplant, non-curative.

1.1.3 Chronic kidney disease

Chronic kidney disease (CKD) is the progressive loss of renal function and filtrative capacity of the kidney over time. CKD is defined as a decreased glomerular filtration rate (GFR), a measure of renal function, of less than 60mL/min, or markers of renal damage for more than three months. Markers of renal damage include albuminuria, electrolyte imbalance and abnormal histology (10). CKD is diagnosed irrespective of cause and patients with CKD are classified into 5 stages based on their renal GFR. CKD is a progressive disease which ultimately leads to end-stage kidney failure (ESKF). ESKF requires renal replacement therapy with dialysis or ideally a renal transplant. The incidence of CKD is rising and is estimated to affect 11% of adults (11,12). This poses a massive financial burden on the NHS due to cost of kidney failure services comprising an estimated 1.3% of the NHS budget annually (13).

Additionally, CKD is not just a disease of the kidney. Patients often present with complications such as anaemia due to decreased erythropoietin production and iron deficiency. Furthermore dysregulated vitamin D, calcium and phosphate metabolism results in mineral bone disease (10). Of note, CKD is highly interlinked with cardiovascular disease and patients often display co-morbidities including hypertension, atherosclerosis and myocardial infarction (14). Moreover, there is a significant correlation between declined GFR and

increased death from cardiovascular disease (15,16). The fact that CKD not only causes ESKF but also the aforementioned diseases, has prompted the World Health Organisation to name CKD as the 12th most common cause of death worldwide (17).

There are a number of aetiologies and risk factors associated with CKD which include hypertension (18), diabetes, obesity, inherited disorders such as polycystic kidney disease, human immunodeficiency virus (19) and acute kidney injury (20) as well as CKD of unknown cause (12,21). However, regardless of the cause, there is always a common mechanistic pathway leading to CKD; renal fibrosis.

1.1.4 Manifestations of renal fibrosis

Renal fibrosis encompasses a number of pathological events including architectural changes within the nephron such as glomerulosclerosis (GS) and tubulointerstitial fibrosis (TIF). There are also several intracellular events which contribute to fibrogenesis such as myofibroblast activation, tubular de-differentiation and metabolic dysfunction. Finally, infiltration of a variety of immune cells within the kidney is a common characteristic amongst all renal diseases. There is an unmet clinical need for efficacious therapeutics combatting the progression of CKD and the loss of functional filtration due to scarring. Therefore, deeper understanding of the various mechanisms involved in the progression of CKD will lead to improved therapies. The various factors which contribute to the progression of renal fibrosis and subsequent kidney disease is summarised in Figure 1.2.

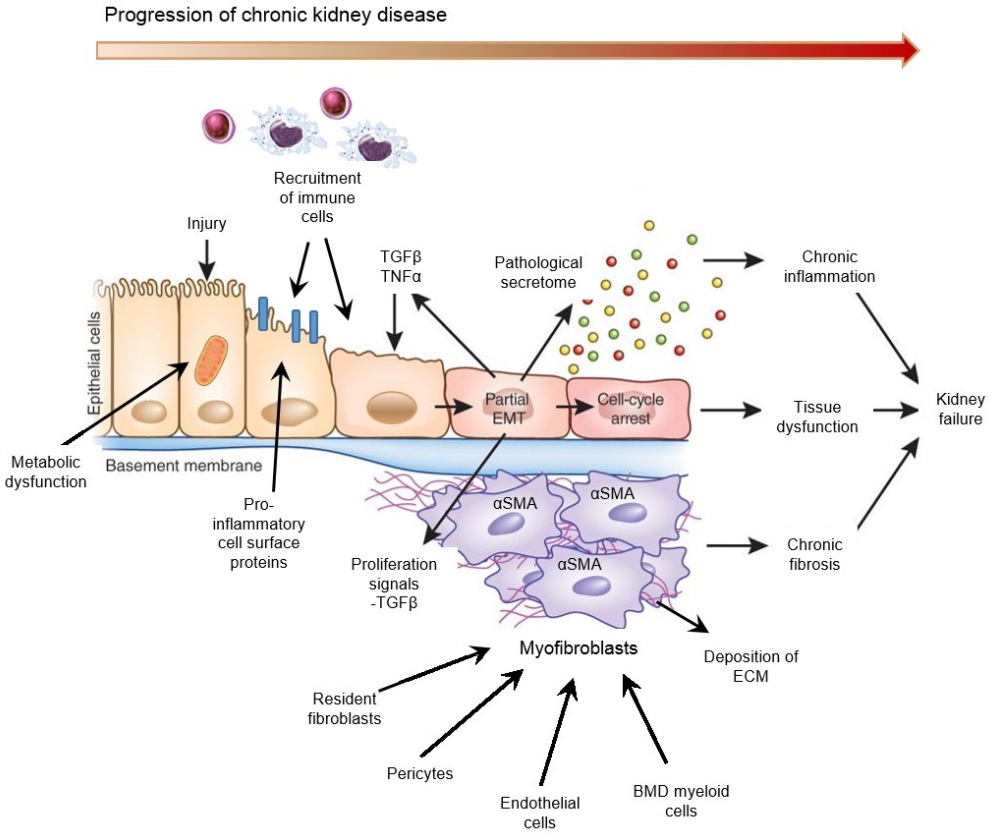

Figure 1.2: Summary of the mechanisms contributing to the progression of renal fibrosis. After injury to the tubular epithelia a number of intracellular processes such as metabolic dysfunction, recruitment of immune cells and partial epithelial-to-mesenchyme-transition occur. Pathological signals induce proliferation of myofibroblasts from several sources and exacerbate chronic inflammation. Together these events lead to fibrosis, tissue dysfunction and inflammation which leads to progression of kidney failure. Diagram adapted from Ovadya et al. (22).

1.1.5 Myofibroblast activation and extra-cellular matrix accumulation

Renal fibrosis is caused by deposition of excess extra-cellular matrix (ECM) in the glomeruli and tubular interstitium. Renal fibrosis is characterised by recruitment of myofibroblasts resulting in excess accumulation of abnormal ECM leading to scar formation and impaired renal function (10). ECM proteins play a structural role in a normal, functioning kidney and the processes of accumulation and degradation of ECM components are tightly balanced. When homeostatic control of ECM production and degradation is lost in the kidney, perhaps due to injury, excess ECM proteins accumulate within the glomerulus and the tubular interstitium, leading to fibrosis and structural changes in the kidney. These structural changes progress to functional changes over time resulting in CKD.

There are several families of ECM proteins, of which many have been described to play a role in the development of fibrosis. Collagens comprise a

large proportion of kidney ECM proteins and during the onset of renal fibrosis excessive deposition of Collagen I and Collagen III in the glomeruli and tubulointerstitium occurs. Furthermore, collagen fragments are found in the urine of patients with CKD which is correlated with serum creatinine and eGFR (23). In addition to collagens, other ECM components such as extracellular proteoglycans, glycoproteins and basement membrane proteins such as laminin are found to be upregulated in renal TIF (24). Matrix metalloproteinases (MMPs) are also thought to play a role in the development of fibrosis. Primarily MMPs are involved in the proteolytic degradation of ECM proteins, however, some MMPs such as MMP-2 and MMP-9 have been reported to be upregulated in animal models of renal fibrosis and human CKD. MMP-2 and MMP-9 have been reported to interact with inflammatory mediators such as tumour necrosis factor alpha (TNF-α) and monocyte chemoattractant protein (MCP-1) as well as activating growth factors such as transforming growth factor beta (TGF-β) and fibroblast growth factor (FGF) (25). Inflammation and activation of these growth factors are hallmarks of renal fibrosis and subsequent CKD. In order to prevent the progression of renal fibrosis we must understand the origins and stimuli of fibrosis. The main cell type responsible for secreting excess accumulation of ECM is the renal myofibroblast.

The myofibroblast is the activated form of the fibroblast and is broadly characterised by its ability to proliferate, contract and secrete vast amounts of ECM. All myofibroblasts express alpha smooth muscle actin (α-SMA) the platelet derived growth factor receptor beta (PDGFRβ) which are used to identify myofibroblasts. However, these markers are not myofibroblast specific and several other cell types express these markers. (26,27). The number of myofibroblasts present within the kidney is an accurate indicator of poor outcome in CKD due to increased fibrosis and they are rarely present in the healthy kidney parenchyma (28). The origin of myofibroblasts has been a hotly debated topic. Fate mapping experiments in rodents have elucidated several origins which contribute to the renal fibroblast population differentially dependent on the disease model. Progenitors include Gli1+ pericytes, resident fibroblasts, bone marrow derived myeloid cells and endothelial cells (29,30). Epithelial cells were until recently thought to be a major contributor to the myofibroblast pool via epithelial to mesenchyme transition (EMT). Recently, this theory has been disproved, however, the role epithelial cells play in the pathogenesis of renal fibrosis will be covered in depth later (29,31).

Activation and proliferation of fibroblasts is a central event in the development of fibrosis. However, all the mechanisms that activate this cell type have yet to be fully understood. Transforming growth factor beta (TGFβ) is known as the master regulator of fibrosis and is a driver of fibrosis in all forms of CKD. TGFβ can bind TGFβ receptors on myofibroblasts resulting in activation of canonical (Smad dependent) and non-canonical (non-Smad dependent) pathways resulting in the transcription of ECM components and subsequently driving fibrosis (32). TGFβ has been reported to be upregulated in human CKD and animal models of renal fibrosis and exogenous administration of TGFβ exacerbates TIF and glomerulosclerosis (33,34). It has deleterious effects on most kidney cells in the setting of fibrosis. Furthermore, deletion of TGFβ receptors in mice has ameliorated excess collagen production and attenuated fibrosis (35-37). However, TGFβ is also involved in a number of central biological processes including proliferation, differentiation, apoptosis and immune signalling. Although targeting TGFβ signalling may provide a potential strategy to treat renal fibrosis, the adverse effects on the immune system pose serious concerns (38). However, myofibroblasts are not the only cell type which has been shown to contribute to the progression of fibrosis.

1.1.6 Tubular epithelial cells and fibrosis

Tubular epithelial cells (TECs) comprise the majority of renal mass and exist as highly differentiated cells which express a number of transporters and have a very high ATP demand. Our knowledge of the role that TECs play in the progression of fibrosis has developed in recent years. Previously, TECs were thought to be purely victims of fibrogenic signalling but now it is appreciated that TECs can act as drivers of fibrosis (27).

Tubules and particularly proximal tubules are sensitive to repeated injury. Fate mapping techniques have revealed that after ischaemia reperfusion injury, surviving epithelial cells are able to proliferate and repair the injury and this repopulation is not mediated by any other progenitor population (39-41). While a single injurious event induces repair, multiple assaults to TECs lead to the initiation of fibrogenesis. This was shown by Takaori and colleagues who developed a targeted injury model specific to the proximal tubule. They found that a single mild injury induced adaptive repair mechanisms while repeated injuries led to maladaptive repair and the development of fibrosis within the interstitium and glomeruli (42). The mechanism whereby PT injury can induce

glomerular damage is not yet fully understood but there is evidence to suggest that epithelial cell cycle arrest in G2/M phase can induce fibrogenesis by increasing JNK activation (43). These mechanisms are important as patients that are exposed to acute kidney injury (AKI) have an increased likelihood of developing CKD later in life. Moreover, the severity of the AKI increases the risk of developing CKD (44). Initial damage to tubules may pave the way for some individuals to develop progressive renal disease. Injuries sustained by TECs in patients can include continued inflammatory insult, hypoxia, ischaemia reperfusion injury as well as physical injury caused by albuminuria (45,46). Although the precise mechanisms whereby injured TECs initiate fibrosis have yet to be fully elucidated, TECs can undergo several pathogenic responses which may contribute to fibrosis.

Injured TECs have been shown to undergo cell cycle arrest after injury. This could occur as a result of DNA damage, mitochondrial dysfunction, inflammation as well as other cell stressors (47). Cell cycle arrest is part of a maladaptive repair process which results in cells losing the ability to divide and is described as senescence. Damaged TECs re-enter the cell cycle in order to proliferate and repair themselves. Some of these cells become arrested in the G2/M phase and become senescent. Senescence has been observed in many CKDs such as diabetic nephropathy, hypertensive CKD and IgA nephropathy as well as mouse models of renal disease. Incidence of senescence also increases with age (27). Additionally, senescent TECs can adopt a secretory phenotype which can result in the secretion of pro-fibrotic and pro-inflammatory cytokines, chemokines and proteases which take part in paracrine signalling with other pro-fibrotic cell types in the interstitium (47).

Another important phenotypic switch that can occur in the setting of fibrosis is tubular de-differentiation. Although there are parallels with cellular senescence, tubular de-differentiation or partial EMT is a distinct process which is emerging as an important cornerstone of fibrogenesis. Complete EMT is a process whereby epithelial cells lose their epithelial characteristics and adopt a mesenchymal, motile phenotype (48). Specifically it is defined as loss of e-cadherin and ZO-1 expression as well as acquisition of collagen 1, vimentin, fibronectin and α-smooth muscle actin. This has long been observed *in vitro* with stimulation by TGFβ and was thought to be the main origin of the myofibroblast in the kidney. The complete EMT theory is now highly disputed as there is little evidence of this process taking place *in vivo* (31). However,

evidence of partial EMT is evident by positive staining of EMT markers in biopsies of patients with renal graft dysfunction as well as the presences of EMT mRNAs in the urine of patients with diabetic nephropathy (49,50). There is also evidence to suggest that partial EMT occurs *in vivo*, whereby epithelial cells lose some epithelial traits but do not transition fully into a myofibroblast. Tubular dedifferentiation and subsequent proliferation occurs in response to injury and is an attempt to resolve the injury. However, while dedifferentiating, TECs have been shown to secrete a number of pro-inflammatory factors and TECs have also been proven to secrete matrix components (51,52). If tubules continue to dedifferentiate due to ongoing injury this can lead to a self-perpetuating cycle of maladaptive repair, inflammation and eventually fibrosis (24). Therefore, there is a fine balance to be struck between repair mechanisms and progressive scar formation and fibrosis which requires more in-depth understanding.

As tubular injury and phenotypic switching is the initiating process in the development of CKD, finding strategies to combat pathological changes in tubular cells could provide a novel therapeutic approach to prevent patients from developing CKD.

1.1.7 Metabolic dysfunction in CKD

Recently, tubular metabolic dysfunction has become a well-recognised feature of renal fibrosis. The kidney is one of the most highly metabolic organs in the body and is mitochondria rich with a high energy demand (13). The kidney relies primarily on oxidative phosphorylation to produce enough ATP to satisfy this high energy demand. The predominant substrates for oxidative phosphorylation are fatty acids, which are metabolized to the greatest extent by proximal TECs (14). It is appreciated that nephron number is correlated with renal function and loss of functional nephrons in CKD leads to increased filtrating and reabsorbing demands in remaining cells to maintain homeostasis. This induces a higher energy requirement of remnant cells, particularly tubular epithelial cells. Eventually increased metabolic load of tubular cells results in hypertrophy and consequently cells exhaust themselves and become apoptotic (53). Defective metabolism affects the kidney at many levels, whether it be sub-cellular mitochondrial dysfunction, lipid accumulation within the kidney parenchyma or metabolic syndrome associated renal disease (54-56).

Changes in cellular metabolism and fuel source preference are hallmarks of disease which have been well characterised in cancer, including the Warburg effect (57). Additionally, mitochondrial dysfunction is a commonly occurring event in several disease states including kidney disease (58,59). Mitochondrial dysfunction is an event which occurs early in TECs after injury. Lan and colleagues investigated metabolic switching in tubules undergoing atrophy and found that tubules which did not successfully regenerate exhibited decreased mitochondrial number and increase rate of glycolysis. They found this process to be governed by TGFβ (60). Mitochondrial dysfunction occurs in many disease states which triggers the increased production of reactive oxygen species which initiate cellular senescence, inflammatory and pro-fibrotic pathways which are highly relevant in the setting of CKD (27,58,61,62).

During the progression of CKD and with increasing age, lipids accumulate within the kidney, further promoting the concept of metabolic dysfunction contributing to disease. Defective mitochondrial fatty acid oxidation (FAO) and decreased expression of Peroxisome Proliferator Activated Receptor Alpha (PPAR-α) have been implicated as mechanisms for excess lipid accumulation (63). Recent efforts have been made to elucidate the role of cellular metabolism within the kidney during fibrogenesis. Kang and colleagues conducted microarray analysis of kidneys and found that cellular metabolism and specifically FAO to be dysregulated in human CKD and mouse models of renal fibrosis. They implicated TGFβ as the main architect of FAO dysfunction and found that inhibiting TGFβ signalling rescued defective fatty acid oxidation. This was found to be beneficial in several models of fibrosis (64). Calorie restriction has also been found to rescue impaired FAO and therefore prevent the accumulation of lipid and slow the development of fibrosis (63).

Another indicator of the link between renal fibrosis and metabolism is the strong relationship between obesity, metabolic syndrome and CKD. Rates of CKD have been rising in line with increased incidence of obesity and metabolic syndrome has been proven to contribute to the pathogenesis of progressive renal disease (54,65). Therefore, metabolic dysfunction is undoubtedly a pathological series of events which requires further investigation in the setting of CKD.

1.1.8 Inflammation in CKD

Inflammation is a driving factor of several chronic diseases and is important in inducing many pathological events that exacerbate renal fibrosis. Inflammation is a protective response which in most instances is resolved. However, when the kidney is injured and cannot be repaired, chronic activation of leukocytes ensues, resulting in pathological inflammation (66,67). The number of inflammatory infiltrates correlates with extent of fibrosis and a myriad of mediators are responsible for this (68). Upon sustained renal insult, recruitment of a number of immune cells occurs including macrophages, T cells, mast cells and dendritic cells. These leukocytes produce a plethora of pro-inflammatory and pro-fibrotic factors such as interleukin 1 beta (IL-1β), inducible nitric oxide synthase, TGF-β and tumour necrosis factor alpha (TNF-α) (69). Some of these factors are involved in promoting the survival and activation of myofibroblasts, tubular dedifferentiation and microvascular rarefaction. Not only are cells recruited from the circulation but resident cells of the kidney can be activated and produce inflammatory cytokines and chemokines themselves (27). Tubular cells particularly can participate in the inflammatory response by recruiting leukocytes and promoting proinflammatory pathways such as NFκB and JNK pathways (67,70,71).

It is evident that there are several cellular players in the setting of renal fibrosis and cross-talk between these cell types is important. Understanding how fibroblast activation, tubular de-differentiation, metabolic dysfunction and inflammation are all linked is essential for furthering our insights into mechanisms driving fibrosis and contributing to CKD.

1.1.9 Current and future therapeutic strategies in CKD

CKD incidence is on the rise, however, there have been very few recent developments in therapeutic strategies despite the increased numbers of patients suffering with this disease. The most advantageous strategies include addressing comorbidities and lifestyle choices that exist in the CKD populations. Cessation of smoking, weight loss and control of diabetes are effective methods to slow down the progression of CKD (72). Additionally, the most widely used pharmacological agents for use in CKD are inhibitors of the renin-angiotensin-aldosterone system (RAAS). Angiotensin converting enzyme

(ACE) inhibitors and angiotensin receptor blockers (ARBs) are both anti-hypertensive agents which have been found to be effective drugs to slow the progression of fibrosis. As well as RAAS inhibition other blood pressure lowering drugs such as calcium channel antagonists have also been found to be effective in the treatment of CKD as a combination therapy (73). However, none of the current strategies are able to resolve renal fibrosis and stop the progression of CKD. Therefore with more preclinical research, the mechanisms driving renal fibrosis and subsequent CKD will be fully elucidated and novel drug targets will be revealed that may provide efficacious treatment for CKD.

The pathogenic mechanisms that drive renal fibrosis are diverse and involve many cell types. Therefore, developing new strategies for the treatment of CKD has proved challenging. Finding new drug targets based on mechanisms elucidated by renal researchers is important to slow the progression of CKD and add to the limited pharmacological arsenal available to nephrologists.

1.1.10 Targeting Transforming growth factor beta

TGFβ has earned its title as the “master regulator of renal fibrosis” and is the predominant initiator of ECM production. TGFβ has been reported to be upregulated in several CKDs and overexpression of TGFβ in animal models induces glomerulosclerosis and tubulointerstitial fibrosis. Therefore, TGFβ has been identified as potential drug target and has been the focus of novel anti-fibrotic therapies (32).

However, promising as these anti-TGFβ treatments sound, the TGFβ pathway interacts with many other ubiquitous pathways such as MAP kinase signalling, Wnt; beta catenin signalling, epidermal growth factor receptor (EGFR) signalling, p53 signalling and others (74). The pleiotropic effects of TGFβ signal transduction mean that targeting TGFβ results in several off-target effects. Indeed, targeting TGFβ directly using monoclonal antibodies have not yielded promising results in clinical trials due to lack of efficacy (32,75). Furthermore, anti-TGFβ treatment has many concerns regarding adverse effects on the inflammatory pathways. Animal models have revealed that TGFβ receptor 2 knockout curtailed fibrotic pathways but conversely promoted inflammatory pathways by induction of nuclear factor kappa b (NFκB) signalling (76). Although several clinical trials have been conducted which focus on anti-TGFβ therapy, none have been shown to improve clinical end-points and the risk of

adverse effects from pleiotropic signalling is a concern. As TGFβ has not yet proven to be a viable drug target despite its central role in the induction of fibrotic pathways, it is important to investigate other potential drug targets involving other pathways ongoing during fibrogenesis.

1.1.11 Targeting Tumour necrosis factor

Another cytokine which plays are major pathological role in the context of renal fibrosis is TNFα. This pro-inflammatory cytokine is known to be upregulated at early stages in animal models of renal fibrosis and is also elevated in patients with CKD (77-79). As inflammatory processes are thought to initiate fibrogenesis, anti-TNFα therapies have been investigated in animal models of CKD. Neutralisation of TNFα was found to attenuate fibrosis in the UUO model effectively (80). Additionally there have been promising results in clinical trials adopting anti-TNFα therapies. Anti-TNFα treatment was found to reduce the renal functional decline in a cohort of patients with rheumatoid arthritis (81). Moreover, as anti-TNF therapies are already approved by the Medicines and Healthcare products Regulatory Agency and the Food and Drug Administration, concerns over drug safety would be avoided if these agents were found to be beneficial in CKD.

1.1.12 Targeting microRNAs

A strategy that has potential as a novel target in the treatment of renal fibrosis and CKD is targeting microRNAs (miRNAs). MicroRNAs are small non-coding RNAs approximately 16-22 nucleotides long which are important mediators of post-transcriptional regulation in nearly all physiological and pathological processes. MiRNAs function to repress target mRNA expression whether by blockage of protein translation or direct degradation of their mRNA target. MiRNAs are attractive drug targets as each miRNA can bind to hundreds of mRNA targets and prevent their expression (82). Several miRNAs have been reported to be upregulated in renal fibrosis including miR-21, -214, -199, -433, -132 and -212 to name a few (83). Some of these miRNAs have been extensively investigated and some of their mRNA targets have been identified. MiR-21, for example, has been found to target and repress genes in a number of pathways including fatty acid oxidation, lipid oxidation, Wnt signalling, ERK/MAPK signalling and TGFβ inhibitory pathways. These processes have been shown to be dysregulated in fibrogenesis. Therefore inhibiting miR-21

would be able to de-repress these pathways and exert subsequent anti-fibrotic actions. Other miRNAs are downregulated in renal fibrosis such as the miR-29 family, -126, -34, -30 family and let-7 family. These miRNAs have been reported to target ECM genes, TGFβ signalling and NFκB signalling. These anti-fibrotic miRNAs could, in theory, be overexpressed to ameliorate fibrosis (84).

MiRNAs can be pharmacologically manipulated by inhibiting their expression with anti-miR oligonucleotides which target and block miRNA activity. Additionally anti-miRs tend to accumulate in the kidney which makes them very attractive for the treatment of renal disease. Levels of anti-fibrotic miRNAs can also be increased using miR-mimics which are chemically synthesised oligonucleotides (85). Although these treatment strategies are in their infancy an anti-miR 122 has been developed against hepatitis C infection which is currently in phase II clinical trials (86,87). This gives hope that pro- and anti-miR therapies may provide benefit to patients with CKD in the future.

Metabolomics and renal disease

A discussed earlier, defective cellular metabolism has been identified as an important pathological change that takes place during the progression of renal disease. Metabolomics can be used to measure levels of metabolites in specific organs as well as in blood and urine to reveal activity of metabolic pathways. Metabolomics has revolutionised how we detect changes in the metabolome during the onset of disease. Several studies have investigated changes in the metabolome to reveal novel biomarkers of renal disease and also to elucidate defective metabolic pathways that may be contributing to CKD (88,89). Metabolomics has been used to great effect to measure differences in the metabolome of real patients versus healthy controls.

1.2 Hypothesis and aims of this thesis

The studies presented in this thesis were conducted to gain further understanding of defective metabolic pathways occurring during renal injury. Studying several murine models of renal disease allows for more robust conclusions to be drawn and provides a more valid reflection of human disease. This thesis investigates the use of these three preclinical models to identify metabolic genes that may play a novel role in the development of fibrosis.

I hypothesised that genes involved in metabolic pathways are downregulated in the progression of renal fibrosis in preclinical models and identification of specific genes that is downregulated in all three models would provide a robust candidate gene for further investigation. The hypothesis was tested using a number of aims:

- To identify genes that are upregulated in a mouse protected from renal fibrosis using microarray data (anti-fibrotic anti-miR-214 treatment)
- To identify genes that are downregulated in kidneys subjected to UUO and upregulated in reversed UUO using RNA-seq
- To produce a curtailed number of candidate genes for further investigation
- To measure expression levels of candidate genes in the STNx and IRI models of renal fibrosis
- To determine a final candidate gene that will be used for further experiments

Chapter: 2 Materials and Methods

2.1 *In Vivo* experiments

Male mice between eight and ten weeks were used throughout animal studies unless otherwise specified. All animals were housed in the animal unit at Little France at 21±1°C, humidity of 50±10% and a controlled light/dark cycle with light from 7am-7pm. The animals had access to water and standard chow *ad libitum* and all procedures were performed in accordance with the UK Home Office Animals (Scientific Procedures) Act of 1986 after ethical review by The University of Edinburgh.

2.1.1 Metabolic Cages and Urine Analysis

In order to perform urine analysis, timed metabolic cages were employed to harvest urine over a 24 hour period. Mice were singly housed within a metabolic cage (courtesy of Professor Matthew Bailey) for 24 hours and urine was collected and frozen at -20^{o}C. Urine analysis was carried out by Dr Forbes Howie in the Specialist Assay Service at The University of Edinburgh.

2.1.2 Assessment of blood pressure by tail cuff plethysmography

Mice were placed in an incubator at 28^{o}C for 15 minutes prior to blood pressure assessment in order to dilate vessels in the tail. Systolic and diastolic blood pressure were measured using the CODA high throughput system with 4 activated channels (Kent Scientific, UK). Mice were subjected to tail cuff measurement twice on consecutive days to allow for habituation to the system. On the third run, measures were used for analysis. The runtime information was as follows: 15 total readings with 5 acclimatisation readings and 10 valid readings. The occlusion pressure within the tail cuff was 250 mmHg with a deflation time of 15 seconds. Mean ±SD systolic and diastolic valid readings were calculated for each mouse. Mean arterial pressure was calculated as follows:

Mean arterial pressure = $\frac{\text{systolic BP + 2 (diastolic BP)}}{3}$

2.1.3 Assessment of urea cycle metabolites

Whole blood was collected either by cardiac puncture at time of termination or by venopuncture in live animals. Whole blood was dropped onto predefined areas of a Guthrie Card and allowed to dry for 24 hours and frozen at -20^{o}C. Levels of urea cycle metabolites in blood samples were kindly assessed by Dr Julien Baruteau at University College London according to the published LC-MS/MS protocol (90).

2.1.4 Surgical Procedures

All surgical procedures were carried out on mice under inhalational anaesthetic (isoflurane) and the subcutaneous analgesics were used to relieve post-operative pain. Mice were weighed and their general health assessed regularly for 1 week and thereafter checked and weighed weekly until culling. After 1 week wound clips were removed. Mice were group housed after surgery to decrease recovery time.

Termination was carried out by overdose of isoflurane. All animals were weighed and their tibia length measured. Cardiac puncture was performed to collect blood followed by perfusion of PBS through the left ventricle to remove as many red cells from the circulation as possible. Serum was extracted from whole blood by centrifugation at 5000g for 15 minutes. Various organs were harvested and stored appropriately for downstream analysis.

2.1.5 Unilateral ureteric obstruction (UUO) and reversible unilateral ureteric obstruction (rUUO)

UUO surgeries were carried out by either Dr Laura Denby, James O'Sullivan or myself on C57BL/6JOlaHsd male mice purchased from Charles River. After induction of anaesthesia, laparotomy was performed and the small and large intestines moved to the side using a damp cotton-bud and prevented from drying out with damp gauze. The right kidney and ureter were located and the ureter was separated from surrounding connective tissue by blunt dissection. Two sloops were tied around the ureter to prevent out-flow of urine from the kidney. The intestines were replaced carefully into the body cavity using a damp cotton-bud and the abdominal wall was closed using dissolvable sutures (Ethicon 6/0). The skin was closed using skin clips and the animal was allowed

to recover in a hot box at 37°C for 24 hours. Renal obstruction was maintained for up to 7 days after which the mouse was terminated and tissues collected.

2.1.6 Reversible unilateral ureteric obstruction model (rUUO)

As with the UUO model, C57BL/6JOlaHsd purchased from Charles River were used throughout rUUO procedures. rUUO surgery was carried out according to the protocol published previously by Gary Borthwick (91).

2.1.7 Subtotal nephrectomy (STNx)

Subtotal nephrectomy surgery was carried out either by Dr Laura Denby or James O'Sullivan and assisted by myself. Surgeries were carried out on SV/129 mice purchased from Envigo. SV/129 mice were used for these experiments as they are sensitive to subtotal nephrectomy and develop fibrosis to larger extent compared to C57BL mice (92). Animal cohorts were culled and assessed at several time points. Our group adopted the refined, one-step flank surgery method of subtotal nephrectomy developed by Dr Laura Denby (93). After induction of anaesthesia the right nephrectomy was carried out. A precise flank incision was made through the skin and fascia to reveal the right kidney. The ureter and renal artery and vein were clamped using a vascular clip before tying off the kidney using sloops. Once obstruction of the blood supply to the kidney was ensured, the kidney was removed and the wound closed using sutures and clips. The remaining contralateral kidney was accessed in the same manner as the first. After clamping of the renal pedicle, the superior and inferior poles of the kidney were removed using surgical scissors and weighed to ensure a similar mass of kidney was removed in each surgery. Bleeding from the resected kidney was prevented using Spongostan™ sponges (Ethicon, UK) which were applied to each cut end of the kidney. The vascular clamp was removed as quickly as possible to avoid excess ischaemia. Once bleeding had stopped the wound was closed using sutures and wound clips. Sham surgery consisted of flank incisions and exposing the kidneys on each side before closing the wound.

2.1.8 Ischemia-reperfusion injury (IRI)

IRI surgery was performed by Dr Victoria Banwell and animal cohorts were assessed at several different time points post-surgery. C57BL/6JOlaHsd mice were purchased from Charles River and were used for all IRI surgeries.

Laparotomy was performed and the right kidney was rendered ischaemic using vascular clips around the renal pedicle for 18 minutes. After ischaemic injury, the vascular clips were removed allowing reperfusion. The wound was closed using sutures and wound clips. After various lengths of time cohorts of mice were culled for tissue.

2.1.9 Transgenic mice

Pax8 CreER^{T2} mouse sperm (EM: 10364) and Ass1 flox/flox mice (EM: 05208) mouse embryos were purchased from the EMMA repository. International strain designations were C57BL/6J-Tg (Pax8-cre/ERT2) CAmat/AmatH and C.129P2 (B6)-Ass1tm1.1Ekoe/Cnbc respectively.

Ai14 tdTomato mice on a C57BL/6J background were used which carry a Cre reporter allele with a loxP-flanked STOP cassette preventing transcription of CAG promoter driven red fluorescent protein (tdTomato). Ai14 tdTomato mice were kindly donated by the Conway group at Edinburgh University.

2.1.10 Breeding of transgenic mice

Ass 1 flox/flox mice were originally bred on a Balb/c background, therefore these mice were back-crossed to C57BL/6J mice for 5 generations. Ideally back-crosses would be carried out for 10 generations but due to time constraints in this project, that was not possible. Pax8 CreERT2 mice were originally bread on a C57BL/6J background.

In order to obtain Pax8CreER^{T2} x *Ass1* flox/flox crossed mice; Pax8-CreER^{T2} homozygous mice were bred with *Ass1* flox/flox homozygous mice. Their offspring were heterozygous for both the *Cre* expression (Cre/wt) and the *Ass1* flox expression (*Ass1* flox/wt). These heterozygous offspring were bred together to obtain a mixture of genotypes including mice homozygous for both Pax8 Cre/Cre and *Ass1* flox/flox which were used in tubular *Ass1* knockout studies.

In order to obtain Pax8CreER^{T2} x Ai14 tdTomato crossed mice; Pax8CreER^{T2} homozygous mice were bred with Ai14 tdTomato homozygous mice. Their offspring were heterozygous for Cre and Ai14. These mice could be used in reported studies as only one copy of the Cre and one copy of the Ai14 tdTomato is necessary for assessment of tdTomato expression.

2.1.11 Pax8CreER^{T2} and Ass1 flox/flox genotyping

Ear clips were taken from mice at 3 weeks of age and processed by Transnetyx which provided genotyping results.

2.1.12 Activation of Cre recombinase with tamoxifen

In mice which carried the Pax8 CreER^{T2} allele, tamoxifen was used to induce recombination of Cre within Pax8 expressing tissue. Tamoxifen (Sigma, UK) was made up at 20mg/mL in sunflower oil. Tamoxifen was dissolved in sunflower oil in a shaking incubator at 52^{o}C until dissolved with occasional vortexing. Tamoxifen was kept in solution for up to 1 week and administered to mice at 200mg/kg by oral gavage. Three doses were given on alternate days and mice were monitored closely and weighed frequently after gavage.

2.2 *Ex Vivo* Experiments

2.2.1 Electrolyte analysis of serum and urine

Serum or urine (Section 2.1.1) was assessed for levels of sodium, potassium and chloride ions using the Spotchem EL^{TM} Electrolyte Analyser (Woodley Laboratory Diagnostics, UK). Urine was diluted 1 in 5 with water before measurement and serum did not require dilution. Electrolyte levels were measured according to manufacturer's instructions.

2.2.2 Kidney digestion for flow cytometry and fluorescence activated cell sorting (FACS)

Mice were anaesthetised under isoflurane and exsanguinated by cardiac puncture. Animals were then perfused with 5mL ice cold PBS through the heart in order to remove as many red blood cells as possible. Kidneys were harvested and stored in ice cold PBS. A quarter or half a kidney was used for flow cytometry and FACS respectively. Kidney tissue was weighed prior to digestion. Digestion buffer was made up according to Table 2.1 in RPMI media (Gibco, Thermo Fisher Scientific, UK) supplemented with 10% fetal calf serum (FCS) and 1% Pen/Strep (penicillin and streptomycin).

Digestion Buffer Component	Manufacturer	Concentration
Collagenase V	Sigma C6885	0.425mg/ml
Collagenase D	Roche 11088882001	0.625mg/ml
Dispase	Gibco 17105-041	1mg/ml
DNase	Roche 10104159001	30µg/ml

Table 2.1: Reagents for Fluorescence Activated Cell Sorting kidney digest

Using a scalpel, kidney tissue was cut up in a petri dish with the addition of 4mL Digestion Buffer before transferring to a gentleMACS C tube (Miltenyi Biotec, UK). Tissue was homogenised in gentleMACS tubes using the gentleMACS dissociator before tubes were transferred to a shaking water bath set to 37^{o}C for 30 minutes. After incubation with collagenases, tissue was further homogenized using the gentleMACS dissociator (Miltenyi Biotech, UK).

The enzymatic activity of the digestion buffer was neutralized by the addition of 4mL FACS buffer (sterile PBS with 2% FCS and 0.2% EDTA). The kidney cell suspension was then filtered through three serially smaller cell strainers (100µm, 70µm and 40µm) to ensure a single cell suspension. The filtered cell suspension was then pelleted at 500xg for 5 minutes at 4^{o}C using a Heraeus^{TM} Megafuge^{TM} (Thermo Fisher Scientific) and the supernatant discarded. Red blood cells were lysed by addition of 1mL red cell lysis buffer (Sigma, UK) for 1 minute before neutralizing with 15mL FACS buffer. This was followed by pelleting at 500xg for 5 minutes at 4^{o}C and ensuring red cells were absent and discarding the supernatant.

Pellets were resuspended in FACS buffer and transferred to a round bottom plate (Corning) according to number of control wells and experimental wells:

- Control wells: unstained controls for each tissue used, FMOs (fluorescence minus one: all antibodies used in the panel excluding one) and single stain controls for which beads are normally used (except LTL which requires cells for single stains).

- Experimental wells: full antibody panel on each experimental kidney.

Cells were pelleted in the in the plate at 1500xg for 3 minutes at 4^{o}C. Subsequently, the supernatant was flicked off and the pellet disturbed by vortexing. Cells were then blocked for 20 minutes at 4^{o}C using 25uL fc block

per well (BD Biosciences – purified rat anti-mouse CD16/CD32) diluted 1:25. Antibodies were made up 2x desired concentration and added directly to cells in block and mixed by vortexing (Table 2.2). Cells were incubated with pre-conjugated antibodies for 30 minutes at 4°C protected from light. After incubation, 120µL FACS buffer was added to the cells which were pelleted at 1500xg for 3 minutes at 4°C. The supernatant was flicked off and cells were vortexed to disturb the pellet. 200µL FACS buffer was added to each well and cells were washed by pipetting. This was repeated. Finally cells were resuspended in 150µL FACS buffer and transferred to FACS tubes before flow cytometry or FACS.

Flow cytometry was carried out using the 5L LSRFortessa cell analyser (BD Biosciences). Cell sorting was carried out using the FACS Aria II (BD Biosciences).

Antibody Name	Fluorophore	Cat Number	Company	Final desired concentration	Marker for:
PDGFRβ	PE	136006	Biolegend	1:100	fibroblasts
CD31	Bright violet 605	102427	Biolegend	1:200	Endothelial cells
CD45	APC	561018	BD Bioscience	1:200	Myeloid lineage
F4/80	PE Cy7	25480182	eBioscience	1:200	macrophages
LTL	FITC	FL1321	Vector	1:400	Tubular cells

Table 2.2: Antibodies used for fluorescence activated cell sorting of kidney cell suspension to fibroblasts, endothelial cells, myeloid cells; macrophages and tubular epithelial cells.

2.2.3 Immunofluorescent staining of tissue

Immunofluorescent staining was carried on tissue fixed in BD Pharmigen™ zinc fixative (BD Biosciences). Fixed tissue was kept in fixative for 24 hours before transferring to 70% ethanol before paraffin embedding. Tissues were sectioned at 3µm using a microtome, transferred to slides and baked at 60°C overnight.

Slides were de-waxed using xylene and rehydrated along an ethanol gradient. Antigen retrieval was achieved by boiling slides for 2 minutes in a microwave on full power followed by 8 minutes on 50% power in a 1:1 ratio of citrate buffer: tri-sodium citrate.

All incubations were carried out in a humidified chamber. Slides were washed 3 times in PBS-T and subsequently blocked in 20% goat serum (Vector Laboratories, UK) in PBS-T for 1 hour at room temperature. After washing three times in PBS-T slides were incubated overnight at 4°C with primary antibody diluted 1:200 in block (see Table 2.4 for antibodies used).

The next day, slides were washed in PBS-T three times and incubated with secondary antibody diluted in block for 1 hour at room temperature. Slides were mounted with coverslips using ProLong Gold Antifade Mountant with DAPI (Thermo Fisher Scientific, Paisley, UK). Images were taken using the Zeiss AxioScope or Andor Spinning Disk microscopes.

2.3 Microarray

This microarray was carried out as described by Denby et al. (94). Data were deposited in the National Center for Biotechnology Information Gene Expression Omnibus database (accession #GSE48194) available online at https://www.ncbi.nlm.nih.gov/geo/.

Total RNA was extracted using miRNeasy kit (Qiagen) from kidneys of animals treated with control anti-miR (n=4) or anti–miR-214 (n=4); in vitro transcription was performed using the Ambion Illumina TotalPrep RNA Amplification Kit (Life Technologies). The microarray was performed using the Illumina MouseWG-6 v2.0 Expression BeadChip Kit (Illumina, Braintree, UK) and data were generated using GenomeStudio (Illumina) (n=4 per group, 1 sample per animal). To assess the statistical significance of pairwise intergroup differences, RP39 was initially used. RP has been specifically developed for the analysis of microarray experiments and has been shown to perform very well with small sample sizes like that used in this study (n=4 per group). The significance cut-off was a FDR adjusted P value of <0.05

2.4 RNA-sequencing

RNA-sequencing (RNA-seq) was carried out on kidney tissue from mice subjected to sham, UUO and rUUO models using three different approaches; mRNA and small RNA sequencing of whole kidney cortex, mRNA sequencing of kidney cell sorted sub-populations and finally single cell RNA sequencing.

2.4.1 RNA-seq of kidney cortex

RNA was extracted from the renal cortex of mice subjected to sham, 7 day UUO or rUUO surgery (1 week, 2 week or 4 week post reversal). Samples (n=4 in each group) were selected for RNA-seq based on high KIM-1 expression levels in UUO kidneys and low KIM-1 expression in rUUO kidneys. RNA samples were sent to Genewiz for sequencing. Small RNA libraries and mRNA libraries were prepared by Genewiz and underwent RNA-sequencing using the Illumina HISeq 2500 platform. Raw reads were then trimmed to remove adaptor contamination and low quality reads using trimGalore (version 0.4.1). Small RNA and mRNA reads were then aligned to the mouse genome (GRCm38) before differential expression analysis. A platform was developed for analysis of log2fold change values and false discovery rates between groups. Kegg pathway data were linked to this dataset in order to visualise patterns in signaling pathways in each experimental group.

2.4.2 RNA-seq of renal cell sub-populations

Kidney cell sub-populations were sorted using FACS with the methodology described in Section 2.2.2. Tubular cells, endothelial cells, macrophages and fibroblasts were sorted and maintained in RLT buffer. RNA was then extracted from each population from each experimental group: sham, 7 day UUO and 4 week rUUO (Table 2.3). The RNA concentration and RNA integrity number were calculated using the Bioanalyzer (Agilent). RNA samples were sent to Genewiz for sequencing. mRNA libraries were prepared and underwent RNA sequencing using the Illumina 2500 platform. Polyadenylated mRNA reads were then aligned to the mouse genome (GRCm38) and the fragments per Kilobase of million mapped reads (FPKM) was calculated for each cell sub-population in each experimental group. R analysis was carried out by James O'Sulliven.

Experiment	Cell sub-population			
	Tubular cells	Endothelial cells	Macrophages	Fibroblasts
Sham	N=4	N=4	N=4	N=4
UUO (7 days)	N=4	N=4	N=4	N=4
rUUO (4 weeks)	N=3	N=4	N=4	N=4

Table 2.3: Renal cell sub-population numbers

2.4.3 Single cell RNA-seq

Single cell suspensions were prepared as in Section 2.2.2 from sham, 2 day UUO, 7 day UUO and 2 week-reversed UUO murine kidneys. Cell suspensions were run through the BD FACS Aria 11 (BD Biosystems). Single cell libraries from whole kidney digests of each group were prepared using a high-throughput droplet-based library preparation workflow (10x). Sequencing was performed by Genewiz on a NextSeq 550 High Output Kit v2 (Illumina) for 150 cycles at 400M PE reads comprising of 2x75bp and 8bp index reads. Alignment was performed by splicing aware aligner STAR 2.5.1b within the cellranger 2.1.0 wrapper before downstream analysis in the R environment. R analysis was carried out by Dr Eoin O'Sullivan and Dr Katie Connor.

2.5 *In vitro* experiments

2.5.1 Cell Culture

Human Renal proximal tubular epithelial cells (RPTEC/TERT1) were used throughout *in vitro* experiments (ATCC® CRL-4031™ LGC Limited, UK). Cells were maintained in DMEM: F-12 (1:1) Medium (2.5 mM L-glutamine, 15 mM HEPES, 0.5 mM sodium pyruvate, and 1200 mg/L sodium bicarbonate). To this basal medium the hTERT Immortalized RPTEC Growth Kit was added (25 ng/mL Hydrocortisone, 3.5 µg/mL Ascorbic Acid, 8.65 ng/mL Sodium selenite, 5.0 µg/mL Transferrin, 5.0 µg/mL insulin, 5 pM Triiodo-L-thyronine, 25 ng/mL Prostaglandin E1, 10 ng/mL rhEGF, 1.2 mg/mL Sodium Bicarbonate (ATCC® ACS-4007™LGC Limited, UK).

For splitting cells, media was aspirated and 3mL trypsin added to each T75 flask. Plates were then incubated at 37°C for 5 minutes until cells had visibly detached from the base of the flask. The flask was then washed vigorously with

media and the cell suspension was added to a 50mL falcon before spinning at 1000xg for 5 minutes. The supernatant was aspirated and the cell pellet was resuspended in 3 mL media and cells were counted using a haemocytometer. Cells were plated according to the density desired.

2.5.2 Immunocytochemistry

Cells were seeded onto coverslips within a 12 well plate and grown in complete media until cells were 100% confluent. Cells were fixed using 4% paraformaldehyde for 30 minutes and washed three times in PBS. Cells were permeabilised for 20 minutes using 0.01% PBS-Tween. Cells were blocked in 20% goat serum (Vector Laboratories, UK) for 1 hour at room temperature and then washed three times in PBS. Coverslips were subsequently transferred into individual humidified chambers and incubated overnight with primary antibodies overnight at 4^{o}C.

The next day, cells were washed in PBS three times and 100µL secondary antibody (1:500) was added to cells and incubated for 1 hour. After washing three times in PBS, coverslips were mounted on to slides with ProLong Gold + DAPI (Thermo Fisher Scientific, UK). Cells were imaged using the Andor Spinning Disk at 60x and x40, x60 or x100 magnification. Image analysis was carried out using ImageJ.

2.5.3 Cytokine treatment of RPTECs

RPTECs were treated once 80% confluent in 6 or 12 well plates. Prior to cytokine treatment, cells were maintained in serum deplete media for 48 hours to ensure all cells were in cell cycle arrest but still viable. Recombinant human TGF-β (R&D systems, UK) or recombinant human TNF-α (R&D Systems, UK) made up in 0.01% serum medium was added to 3 wells of each plate every 24 hours in fresh media. Direct comparisons were made to cells kept in serum deplete media. Images were taken daily to observe any morphological changes. After several different time-points, cells were frozen at -80^{o}C for RNA or protein analysis.

2.5.4 Exposure of RPTECs to hypoxia

RPTECs were seeded and grown until fully confluent in 12 well plates. Plates were exposed to hypoxic condition (1% O_2) for 24 hours. Cells incubated in

normoxic conditions (20% O_2) were used as controls. Hypoxia was induced in 14500 Coy cabinet with an incubator at 37^{o}C and water for humidification, with a gas mixture of 1% O_2, 5% CO_2 and 94% N_2 (Coy Laboratory Products).

2.5.5 Oxygen consumption rate and extra-cellular acidification rate

RPTEC/TERT were seeded onto a Seahorse XFe 24 well microplate (Agilent, UK) ensuring they were confluent on the day measurements were taken. If seeded the night before, 100,000 cells were seeded into each well. On the day of analysis, cells were washed 3 times in Seahorse media and incubated in a CO_2 free chamber for 1 hour. Oligomycin (2μM), FCCP (2.5μM) and antimycin/rotenone (1μM) were loaded into Seahorse injection ports.

The Seahorse XFe analyser (Agilent, UK) was used for both oxygen consumption rate and extra-cellular acidification rate simultaneously. After optimisation, measurement cycles for the run for oligomycin and antimycin/rotenone were set to 3 minute mix, 2 minute wait, and 3 minute measure. Measurement cycles for FCCP were 4 minute mix, 2 minute wait and 2 minute mix. Prior to any drug administration 3 'basal' measurements were taken, oligomycin was then added followed by 3 measurement cycles. FCCP was then added followed by another 3 measurement cycles. Finally, a mixture of antimycin and rotenone were added followed by 3 measurement cycles. Measurements taken by the Seahorse analyser were normalized to protein content as measured by SRB assay.

2.5.6 Sulforhodamine B Assay

Media was removed from cells in Seahorse plate immediately after measures were taken and washed in PBS. Cells were fixed using 25μL cold 50% Trichloroacetic acid for 1 hour at 4^{o}C. The plate was washed gently in running tap water 10 times, ensuring the cell layer was not disturbed. After washing the plate was allowed to air dry overnight in a covered container protected from dust. Subsequently 50μL 0.04% (wt/vol) SRB (Sulforhodamine B sodium salt) (Sigma-Aldrich, UK) solution was added to each well. The plate was left at RT for 1 hour and then washed with 200μL 1% (vol/vol) acetic acid to removed unbound dye. Once the washes appeared clear, the plate was allowed to air dry. Next, 100μL 10mM Tris(base) solution was added to each well and mixed by pipetting. 50μL solution was transferred to a flat bottom 96-well plate

appropriate for absorbance measurement. Absorbance was measured at 510 nm using a microplate reader.

2.5.7 Knock-down of ASS1 in RPTECs

ASS1 was knocked down in RPTECs using Stealth siRNA against ASS1 (Stealth HSS181354, (5'-AGC AGC UGA GCU CAA ACC GGA CCU-3')) and compared to Stealth siRNA Negative Control lo GC (Scramble) (#12935) (both from Thermo Fisher Scientific, UK). (95) Cells were seeded into 6 or 12 well plates and were transfected when 80% confluent. siRNA against *ASS1* and Scramble siRNA were transfected for various time points using RNAiMAX transfection reagent (Thermo Fisher Scientific, Paisley, UK) at 20nM according to manufacturer's instructions.

2.5.8 Western Blot

Prior to immunoblotting, protein was extracted from cells or tissues as follows:

Cells: RIPA buffer with cOmplete protease inhibitor cocktail tablets (Roche, UK) and phosphatase inhibitors cocktail 3 (Sigma-Aldrich, UK) was added to RPTECs (200 µL per well of a 6 well plate) and incubated for 1 hour, shaking, on ice. Once thoroughly lysed, cells were centrifuged at 10000g for 10 minutes to remove cell debris and the supernatant retained for protein quantification.

Tissues: Snap frozen kidney tissue was homogenised in 500 µL RIPA and protease and phosphatase inhibitors with stainless steel balls using the TissueLyser II (Qiagen, UK). Samples were then incubated on ice, shaking for 1 hour prior to spinning at 10 000g for 15 minutes. The supernatant was retained for protein quantification.

Protein was quantified using the Pierce BCA Assay kit according to manufacturer's instructions (Thermo Fisher Scientific, UK). The protein concentration was normalized across samples by diluting with RIPA buffer.

Protein was prepared under reducing and denaturing conditions by boiling in laemelli buffer (Sigma) for 20 minutes in a 1:1 ratio, protein: buffer. 10 µg protein was added to each well of a 10% Bis-Tris pre-cast gel. One well was used for protein ladder (Amersham rainbow ladder, Thermo Fisher Scientific, UK). Electrophoresis was run at 150V for 40 minutes using the Bolt system (Thermo Fisher Scientific, UK). Transfer of protein to nitrocellulose membranes

was carried out in transfer buffer made up in distilled water (Table 2.4) for 1 hour. Immediately after transfer, membranes could be stained for total protein using the Licor total protein stain kit according to manufacturer's instructions. Total protein levels were assessed using the Licor Odyssey clx system using the 700 channel (Licor biosciences, UK). Subsequently membranes were blocked in 10% BSA for 1 hour at room temperature then incubated overnight with primary antibody (Table 2.5) at 4^{o}C.

Transfer buffer component	Dilution
Glycine	14.4g/L
Tris(base)	6.06g/L
Methanol	20% (vol/vol)

Table 2.4: Reagents in transfer buffer for western blot.

After washing 3 times for 10 minutes in TBS-triton the membrane was incubated for 1 hour at room temperature with Licor secondary antibody diluted in a 1% BSA solution. After two washes in TBS-T and a final wash in TBS the membrane was visualised using the Licor Odyssey clx. Signal intensity of the target protein was quantified and normalized to the total protein or loading control housekeeper using Image Studio software.

2.5.9 RNA Extractions

RNA was extracted from tissues and cells using the microRNeasy Kit according to manufacturer's instructions (Qiagen, UK).

2.5.10 Reverse Transcription of RNA

The concentration of total RNA was assessed using the Nanodrop1000 spectrophotometer and subsequently samples were diluted to the same concentration (200ng/µL if possible). cDNA was generated using the Multiscribe reverse transcription kit (Applied Biosystems, Life Technologies, UK). Where possible 1µg was added to 2 µL 10x RT buffer, 2.2 µL $MgCl_2$, 1 µL random hexamers, 0.4 µL RNase inhibitor and 0.5 µL Multiscribe reverse transcriptase and the total reaction was made up to 20 µL with RNase free H_2O in a 96-well plate. Reactions were incubated on a Veriti thermal cycler (AppliedBiosystems, Life Technologies, UK) at the following thermal cycling conditions: 15 minutes at 42^{o}C, 3 minutes at 95^{o}C and forever at 4^{o}C. Following reverse transcription, cDNA was stored at -20^{o}C.

2.5.11 Quantitative Real Time Polymerase Chain Reaction (qRT-PCR)

cDNA and appropriate Taqman probes were defrosted on ice. A mastermix consisting of 5 µL TaqMan gene expression master mix, 0.5 µL TaqMan® gene expression probe and 3.2 µL RNase free water was made up according to the number of reactions being carried out per gene being analysed. A list of the TaqMan® (AppliedBiosystems, UK) probes used can be seen below (Table 2.6). 8.7 µL master mix was added to each well of a 385 well plate before 1.5 µL template cDNA was added to make a final volume of 10 µL. The plate was then centrifuged at 1500xg for 2 minutes to ensure mixing of reagents. The plate was then placed in QuantStudio Real Time PCR System (AppliedBiosystems, UK) for amplification. Cycle threshold (Ct) values for genes of interest were normalized to housekeeper Ct value. Relative expression of a gene was calculated from the ΔΔCt: change in expression in an experimental group normalized to a housekeeper gene relative to a control.

2.5.12 Housekeeper Selection

For each qRT-PCR experiment, a small panel (>2) of housekeepers were run including Ppia, Hprt, Gapdh and 18S. The standard deviation across all samples was assessed for each housekeeper and the gene with the smallest variation was selected for normalization for each group of samples.

2.6 Antibodies

Antibody	Provider/ code	Protocol	Dilution
Anti-ASS1 rabbit monoclonal primary antibody	Abcam (ab170952)	Immunofluorescence (tissue)	1:200
		immunocytochemistry	1:200
		Immunohistochemistry (DAB)	1:250
		Western blot	1:1000
Anti-GAPDH mouse monoclonal antibody	Cell signalling technology (#97166)	Western blot	1:2000
Phalloidin-iFluor 647 Reagent	Abcam (ab176759)	Immunocytochemistry	1:1000
MitoTracker™ Red CMXRos	Invitrogen (M7512)	Immunocytochemistry	1:250
Goat anti rabbit Alexafluor 488		Immunofluorescence	1:500
Goat anti-rabbit IRdye 800CW secondary antibody	Licor	Western blot	1: 10 000
Donkey anti-mouse IRDye 700CW secondary antibody	Licor	Western blot	1: 10 000

Table 2.5: Antibodies used throughout experiments and their applications and dilutions.

2.7 Taqman Probes

Gene	Mouse	Human
Acaa2	Mm00624282_m1	
Acta2	Mm01546133_m1	
Asl	Mm01197741_m1	Hs00902699_m1
Ass1	Mm00711256_m1	Hs01597989_g1
Ccl2		Hs00234140_m1
Cdkn1a		Hs00355782_m1
Cdkn2a		Hs00923894_m1
Cldn2		Hs00252666_s1
Col1a1	Mm00801666_g1	Hs00164004_m1
Col3a1	Mm00802300_m1	
Col4a1	Mm01210125_m1	Hs00266237_m1
Cubn	Mm01325077_m1	
Gatm	Mm00491879_m1	Hs00933793_m1
Gcdh	Mm00433541_m1	Hs00240811_m1
Havcr1	Mm00506686_m1	Hs00930379_g1
Icam1		Hs00164932_m1
Ido2	Mm00524210_m1	Hs01589373_m1
MKI67		Hs04260396_g1
Mmp14	Mm00485054_m1	
Mmp2	Mm00439498_m1	Hs01548727_m1
Mmp9	Mm00442991_m1	Hs00957562_m1
Ocln		Hs05465837_g1
Tgfbr1		Hs00610320_m1
Timp1	Mm01341361_m1	
Tnf	Mm00443258_m1	Hs00174128_m1

Table 2.6: Taqman probes used with mouse and human probe numbers.

2.8 Statistical Analysis

Parametric testing was carried out on *in vivo* experiments that were adequately powered although normality testing was no carried out. For UUO, STNx and IRI the “n” for each group was ascertained from power calculations. For

comparison between two groups an unpaired Student's t test was adopted. For comparison of three or more groups a 1-way analysis of variance (ANOVA) was carried with multiple comparison post-hoc tests. Post-hoc tests included Tukey's test for comparisons between all groups or Dunnett's test for comparison of all test groups with the control. For underpowered *in vivo* experiments statistical analysis was not carried out. For *in vitro* work, experiments were carried out three times in triplicate to give an n=3. Non-parametric statistical tests were carried out on *in vitro* data as normal distribution could not be determined. *In vitro* experiments with less that n=3 were not statistically analysed and instead trends were described. Statistical analysis was carried out using Graphpad-Prism 8. For statistical analysis of RNA-seq and single cell RNA-seq, statistical analysis was carried out in R by Dr Katie Connor and Dr Eoin O'Sulliven respectively.

Chapter: 3 Ass1 expression in murine models of renal fibrosis

3.1 Introduction

3.1.1 Mouse models of renal disease

Several *in vivo* models are used routinely in renal fibrosis research including the unilateral ureteric obstruction model (UUO) and the reversible UUO (rUUO) model, the subtotal nephrectomy model (STNx) and the ischaemia-reperfusion injury model (IRI). All three models lead to the development of tubulointerstitial fibrosis, the final common pathway of all chronic kidney diseases. Each model allows investigation of the mechanisms involved in renal disease with different aetiologies. Each model offers advantages and disadvantages.

3.1.2 Unilateral ureteric obstruction model (UUO)

The UUO model of renal fibrosis is a commonly used model which induces rapid onset of fibrosis within 1 week. It is performed by ligating a single ureter of a single kidney. This leads to build up of urine within the kidney, increased intratubular hydrostatic pressure and subsequent tubular injury (96). The initial tubular damage is followed by rapid tubulointerstitial fibrosis with accompanying infiltration of immune cells and inflammatory response (97). Renal obstruction ultimately leads to destruction of the architecture of tubules due to mechanical stretch. Histologically, tubules appear severely dilated and atrophic. Molecularly, tubular epithelial cells are known to undergo programmed cell death; be it either apoptosis or necrosis. Initial tubular damage is exacerbated by severe inflammation which is caused by substantial infiltration of immune cells, predominantly macrophages but also T cells and neutrophils (97-99). By seven days post-injury, fibrosis has ensued which is characterised by infiltration of myofibroblasts and accumulation of extra-cellular matrix within the tubular interstitium (100).

However, in this model, glomeruli are unaffected and they retain their filtering capacity, therefore, the UUO cannot be used to assess glomerular disease or renal function. This procedure has several advantages including its short time frame in which severe fibrosis ensues. Additionally it has low fatality and the surgical procedure can be performed quickly which cuts down time under

anaesthesia which is better for animal welfare. A disadvantage of UUO is that the procedure is unilateral therefore, it does not induce any accompanying cardiovascular effects seen in patients with CKD. Furthermore, as one kidney is fully functional, clinical biomarkers of renal disease cannot be assessed in urine or plasma.

3.1.3 Reversible UUO

An extension of this protocol is the reversible UUO whereby the cut ureter is re-implanted into the bladder allowing resolution of fibrosis within the kidney over 4 weeks (101). The kidney regains normal morphology and, histologically, fibrosis is resolved. This model allows elucidation of the mechanisms involved in the reversal and resolution of renal fibrosis.

3.1.4 The Subtotal Nephrectomy model of progressive renal fibrosis (STNx)

The Denby lab have refined the STNx protocol to a one-step model of progressive hypertensive CKD in which one whole kidney and 2/3 of the other is removed by flank incisions (93). This procedure models renal insufficiency progressively and provides a more physiologically accurate model to represent chronic fibrosis compared to UUO. Over time (12 weeks) mice develop extensive tubulointerstitial fibrosis and glomerulosclerosis with concurrent hypertension, albuminuria, uraemia, left ventricular hypertrophy and cardiac fibrosis. These pathological events closely mimic what is observed in patients with CKD. This procedure allows assessment of the multi-organ effects observed in human CKD and provides several outputs for phenotypic assessment of renal disease. Blood and urine analysis is possible and therefore many measures that are commonly used in the clinic can be adopted with this model.

3.1.5 Ischaemia-Reperfusion Injury (IRI)

The unilateral ischaemia-reperfusion injury (IRI) model represents an acute kidney injury (AKI). AKI is highly clinically relevant as patients diagnosed with AKI are more likely to develop CKD later in life (44). The renal pedicle of one kidney is clamped and renal ischaemia can be induced for various durations depending on the extent of fibrosis desired (102). The progression of initial ischaemic insult to fibrosis has been thoroughly investigated. IRI results in hypoxia, decreased renal mass as well as initial influx of inflammatory cells.

This inflammatory phase is followed by the progressive development of renal damage and fibrosis. Histologically, tubules appear atrophic with the appearance of intratubular casts. After the inflammatory phase is the fibrotic phase, characterised by excessive deposition of extracellular matrix in the tubular interstitium. The exact mechanisms whereby acute kidney injury transitions in chronic injury are still to be fully elucidated. The murine unilateral IRI provides a clinically relevant model which can be used to investigate the mechanisms involved in fibrosis

3.1.6 Metabolic dysfunction in preclinical models of renal disease

Pathological metabolic changes occur during the progression of renal fibrosis and this has become a new focus for many in the field of renal research. As outlined in detail earlier (Section 1.1.7), metabolic dysfunction has been identified as a common pro-fibrotic mechanism in human disease as well as preclinical models. From intracellular mitochondrial dysfunction, to increased deposition of lipid in the kidneys, to systemic metabolic syndrome; metabolic dysfunction affects renal physiology and pathology at many levels. Investigating how metabolism is altered in multiple pre-clinical models will provide insight into common dysfunctional metabolic pathways in renal fibrosis models with different aetiologies.

3.1.7 MicroRNAs and renal fibrosis

MicroRNAs are small non-coding RNAs approximately 16-22 nucleotides long, which are important mediators of post-transcriptional regulation in nearly all physiological and pathological processes (103). MicroRNAs function by repressing mRNA target translation by blocking protein translation or direct mRNA degradation. miRNAs have the capacity to target hundreds of mRNAs which has gained attraction from a therapeutic stand point as manipulating one miRNA could exert multiple downstream effects in many pathways. Work by Denby and colleagues elucidated a novel driver of renal fibrosis which works independently of classical fibrotic cytokines such as TGF-β. MicroRNA-214 has been shown *in vitro* and *in vivo* to drive fibrosis. Furthermore, miR-214 knockout mice are resistant to fibrosis and protected in UUO. Moreover, treatment with exogenous antagonist of miR-214, anti-miR-214, prevented renal fibrosis in mice subjected to UUO (94). miR-214 has been shown to contribute to the pathogenesis of fibrosis by targeting hundreds of target

transcripts revealed by microarray. However, the precise mechanism whereby miR-214 elicits its deleterious effects has yet to be revealed. This work will use datasets generated by Denby and colleagues to ascertain new pathways that are targeted by miR-214 which may provide new insight into mechanisms driving fibrosis.

3.2 Hypothesis and Aims

The hypothesis of this chapter was as follows: metabolic dysfunction is a fundamental pathological mechanism ongoing in murine models of renal fibrosis.

The aims of this chapter sought to test this hypothesis using an unbiased approach using a number of large transcriptomics datasets to generated novel genes of interest that have a potential role in renal fibrosis:

1. To determine which metabolic pathways are upregulated in kidneys protected from fibrosis (UUO treated with anti-miR 214) vs kidneys unprotected from fibrosis (UUO treated with control anti-miR).

2. To determine if the same metabolic pathways elucidated in Aim 1 are downregulated in the UUO model of fibrosis vs sham and upregulated in the rUUO model vs UUO.

3. To compile a list of candidate pro-fibrotic genes of interest and cross-compare these genes with a publicly available human CKD transcriptomics dataset.

4. To investigate the expression patterns of these genes of interest in two additional models of renal fibrosis, the subtotal nephrectomy and ischaemia reperfusion injury models.

3.3 Results

3.3.1 Investigation of pathways involved in kidneys protected from fibrosis

Previous studies from Denby *et al*. revealed that antagonism of miR-214 prevented the development of fibrosis in mouse models of renal disease. miR-214 antagonism de-represses miR-214 mRNA targets and therefore genes which are upregulated are likely targets of miR-214 binding. We sought to investigate pathways that were altered in kidneys from mice protected from fibrosis by the antagomiR anti-miR-214. A microarray was carried out on UUO kidneys from mice that had either been treated with anti-miR-214 (protected from fibrosis) or a control anti-miR (not protected from fibrosis) and differential expression was assessed between these groups (94).

Genes which were downregulated included extracellular matrix genes such as *Col3a1, Col4a1 and Mmp2* and *Mmp14*. This confirmed that anti-miR-214 downregulated fibrotic pathways and in doing so protected kidneys from fibrosis. In order to reveal which genes/pathways were direct and indirect targets of miR-214, we investigated genes that were upregulated in the anti-miR-214 group.

In order to investigate the pathways that were upregulated in kidneys protected from fibrosis, gene enrichment analysis was carried out using the functional database KEGG (Kyoto Encyclopedia of Genes and Genomes) accessed from http://webgestalt.org/. A list of genes which demonstrated upregulation after anti-miR-214 treatment with their associated fold change values were uploaded via this platform which revealed pathways linked to these genes. This revealed several metabolic pathways enriched in this gene list which included pathways such as “mannose type O-glycan biosynthesis”, “fructose and mannose metabolism” and “glycine, serine and threonine metabolism” (Figure 3.1A).

Expression of genes involved in these specific pathways were visualized on a volcano plot of significantly up- and downregulated genes from the microarray generated using R studio. Lists of genes involved in the pathways generated from Figure 3.1A were downloaded and compared to up- and down-regulated genes generated from the microarray. Genes that are involved in metabolic pathways such as glycine metabolism were shown to be highly upregulated in anti-miR-214 treated kidneys that were protected from fibrosis (Figure 3.1B).

A

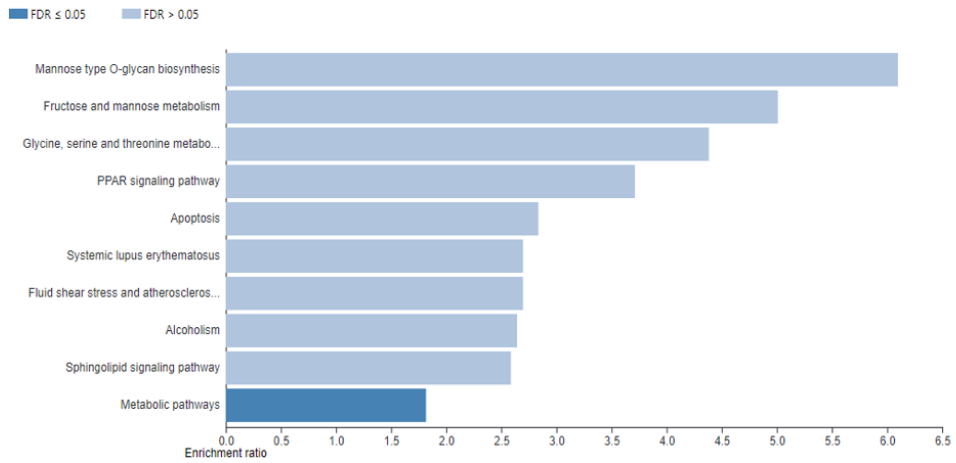

B

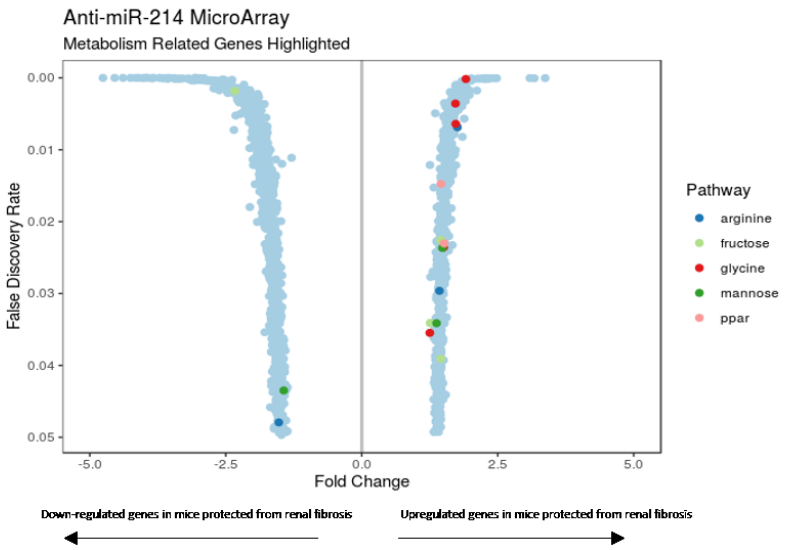

Figure 3.1: Metabolic pathways are upregulated in kidneys protected from fibrosis. A microarray was performed on kidneys from mice treated with either anti-miR-214 (protective against fibrosis) or control anti-miR. (A) Kegg Pathway analysis was performed on genes that were upregulated in the anti-miR-214 group. Several metabolic pathways were upregulated in anti-miR-214 protected kidneys. (B) Volcano plots shows significant genes that are upregulated and downregulated in anti-miR-214 treated kidneys compared to control treated kidneys subjected to UUO. Coloured dots represent genes involved in arginine, fructose, glycine, mannose and ppar pathways.

As many metabolic pathways were upregulated in a model protected from fibrosis, it was important to determine how metabolic pathways are affected during the development of fibrosis and during reversal of fibrosis in a murine model. In this way, I sought to elucidate novel metabolic genes of interest which might provide further insight into the mechanisms driving and repairing fibrosis.

Metabolic pathways which were revealed from genes upregulated in the microarray data were investigated in the UUO and rUUO models.

3.3.2 Selection of genes of interest

In order to dissect metabolic genes that undergo changes in expression during progression and reversal of fibrosis, RNA-seq was performed on cortical kidney tissue from mice subjected to sham surgery, UUO (unilateral ureteric obstruction) or rUUO (reversed UUO). Groups assessed were sham, UUO, 1 week post rUUO, 2 weeks post rUUO and 4 weeks post rUUO. RNA-seq analysis was carried out by Jonathan Manning who developed a platform for interactive analysis of the data including KEGG pathway analysis.

RNA-seq volcano plots demonstrated significantly up- and down- regulated genes in sham vs UUO. We assessed genes that demonstrated an increase or decrease in expression by >2 fold and reached a significant corrected p value or "q" value of <0.01. We could confirm that UUO induced significant upregulation of injury and fibrosis associated genes such as Kim1 (*Havcr1*) and *Col1a1* respectively. We also observed significant downregulation of *Egf,* a marker of tubular remodelling, these genes served as internal positive controls as evidence that UUO kidneys were fibrotic (Figure 3.2A).

Additionally, a number of metabolic pathways, including those revealed using the microarray data were investigated in this dataset. Two particular pathways; fatty acid metabolism and arginine/proline metabolism were found to be markedly disrupted after UUO, indicating their involvement in the development of fibrosis (Figure 3.2B,C).

I adopted a robust triangulation methodology compiling multiple internal and external datasets to reveal metabolic genes which might have a role in the development of fibrosis. I sought to reveal genes that were downregulated in UUO compared to sham and upregulated in rUUO compared to UUO. Within metabolic pathways, genes of interest (GOI) were selected (Table 3.1) according to a number of criteria:

1) Significantly downregulated in UUO with a fold change <-2 and upregulated in rUUO >2

2) Upregulated in a UUO kidney protected from fibrosis (previous microarray data of kidney treated with anti-miR-214 compared to control (94))

3) Presence of a single nucleotide polymorphism associated with renal disease assessed using a publicly available CKD GWAS search tool: https://www.ebi.ac.uk/gwas/efotraits/EFO_0003884.

4) Downregulated in human CKD patient samples as reported by Kang *et al* microarray data (64)

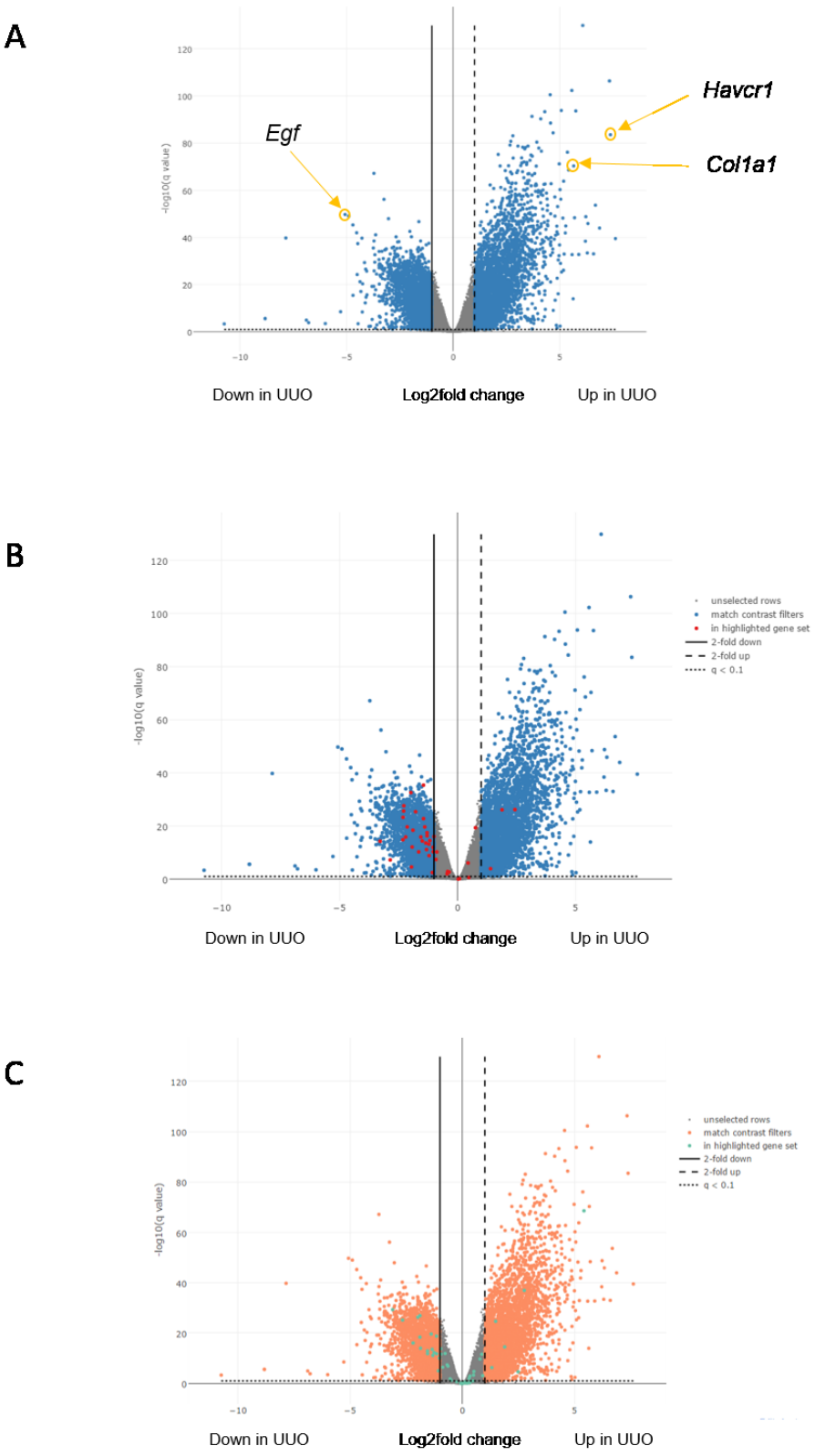

Figure 3.2: Differential expression of genes in the unilateral ureteric obstruction model (UUO). RNA-seq was carried out on RNA extracted from kidneys from mice subjected to either sham or UUO surgery. Volcano plots demonstrates genes > 1 log2fold change increased or decreased in UUO compared to sham (x axis) with q value represented on the y axis. Coloured dots represent individual genes that are significantly differentially expressed. (A) Genes associated with renal fibrosis and tubular injury are depicted by arrows. (B) Volcano plot of sham versus UUO. Red dots represent genes involved in fatty acid metabolism pathways. (C) Volcano plot of sham versus UUO. Turquoise dots represent genes involved in arginine metabolism.

GENE ID	NAME	ROLE	SHAM VS UUO	Corrected p value	UUO VS 4wkR	Corrected p value	Reported SNP?	Fold change: Control vs CKD	Fold change: Control vs Anti-miR-214
Ass1	Arginino succinate synthase	Urea cycle	-8.61	4.827E-30	4.5	4.21E-15		-1.9077	+1.4296
Gatm	Glycine amidino-transferase	Arginine metabolism	-6.34	6.8383E-26	2.88	4.43E-09	SNPs in CKD	-	-
Ehhadh	Enoyl-CoA Hydratase and 3-Hydroxyacyl CoA Dehydrogenase	Peroxi-somal beta oxidation	-9.72	5.6355E-15	3.3	6.83E-05	SNPs in Renal Fanconi syndrome	-1.5311	-
Ido2	Indoleamine 2,3-Dioxygenase 2	Tryptophan metabolism	-9.87	2.75E-25	5.02	5.08E-13		-	-
Gcdh	Glutaryl-CoA dehydrogenase	Fatty acid degradation	-4.88	2.3194E-26	2.29	8.58E-08		-1.7627	+1.4253
Acaa2	Acetyl-CoA acyltransferase 2	Beta oxidation	-2.94	1.38E-16	1.95	1.35E-06		-1.5472	-2.0717

Table 3.1: Genes of Interest dysregulated in renal fibrosis and repair. Gene ID, Name and function with fold change values in sham vs UUO and UUO vs 4wk rUUO (with corrected p value). Reported SNPs associated with renal disease from GWAS. Reported fold change from microarray in control patient biopsy versus CKD biopsy (64) and reported fold change in microarray in control murine kidney vs anti-miR-214 treated murine kidney (94).

In order to validate findings from RNA-seq, cDNA was made from the same samples as the original experiment and qRT-PCR for *Ass1, Gatm, Ehhadh, Ido2, Gcdh* and *Acaa2* was performed (Figure 3.3). Gene expression data revealed that all these candidates apart from *Ehhadh* demonstrated significant downregulation in sham vs UUO and significant upregulation in UUO vs rUUO after 4 weeks (One-way ANOVA with Tukey's multiple comparison). Out of all the genes of interest, Ass1 demonstrated the highest expression level within the kidney and furthermore showed the largest negative fold change in UUO vs sham and the highest positive fold change in rUUO vs UUO.

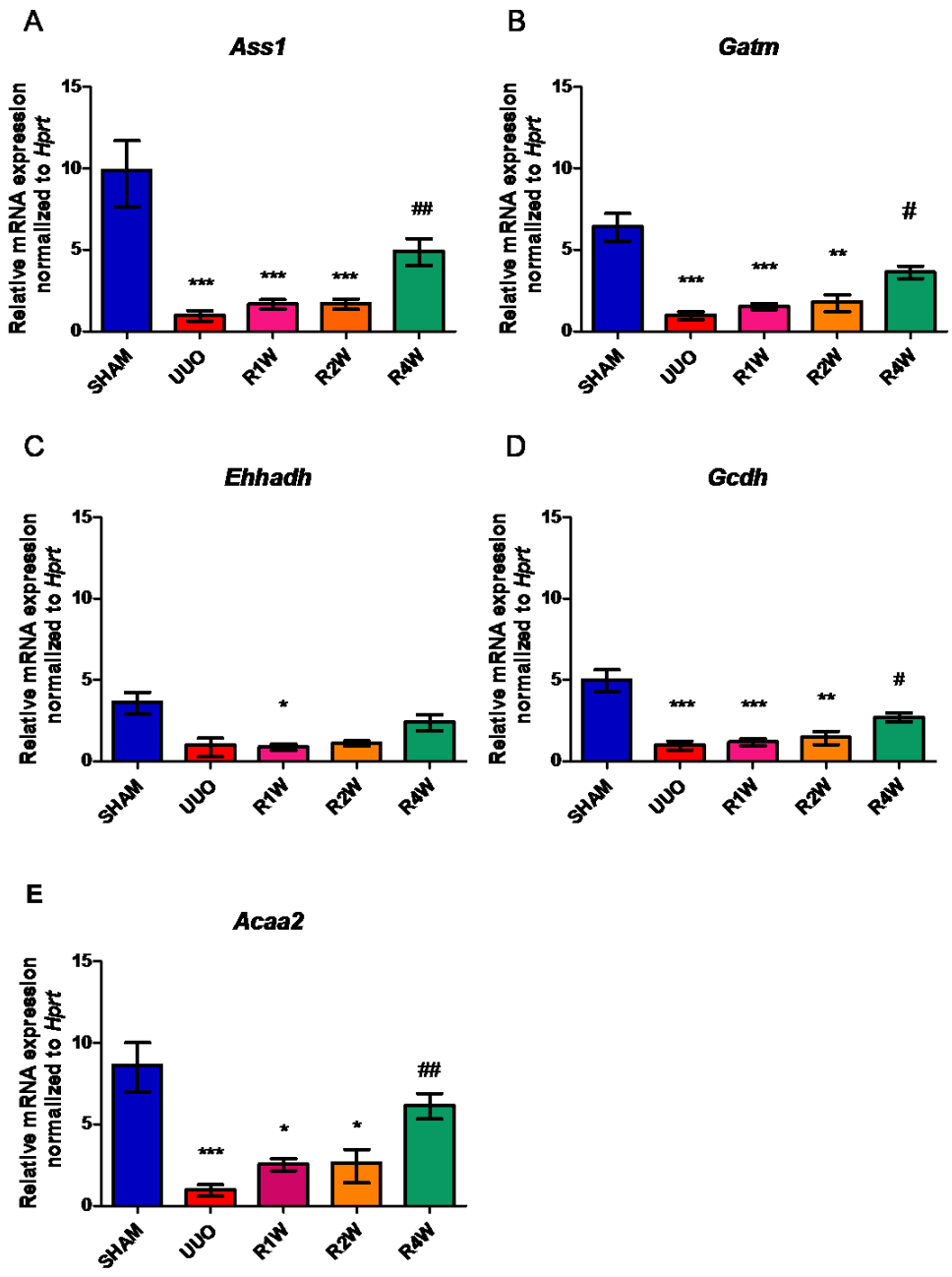

Figure 3.3: qPCR validation of RNAseq genes of interest. Relative mRNA levels of *Ass1, Gatm, Ehhadh, Gcdh* and *Acaa2* in sham (n=6), UUO (n=6), UUO reversed after 1, 2 and 4 weeks; R1W (n=6), R2W (n=6) and R4W (n=6) respectively. Relative expression was calculated from ΔΔcT normalized to *Hprt* housekeeper and compared to sham. *, ** and *** represent $p<0.05$, 0.01 and 0.001 respectively compared to sham by unpaired Student's t test.

3.3.3 Metabolic changes in the kidney are mediated by tubular cells

RNA-seq data from kidneys provides a wealth of knowledge however, as the kidney is comprised of numerous cell types it is important to elucidate if particular cell types are driving these transcriptomic changes or if it is a global effect. To address this caveat, we adopted fluorescence activated cell sorting (FACS) to separate kidney cell sub-populations before RNA extraction and

RNA-sequencing. We sorted 4 subpopulations from whole kidney cell suspension including tubular cells (LTL+ cells), endothelial cells (CD31+ cells), resident macrophages (F480+ cells) and fibroblasts (PDGFRβ+ cells). Subpopulations were sorted from mouse kidneys subjected to either sham surgery, UUO or 4 week rUUO to assess which subpopulations contributed to gene expression changes seen from whole kidney bulk RNA-seq.

Markers of each cell type were assessed by RNA-seq to ensure lack of contamination of one sub-population to another (Figure 3.4). Megalin *(Lrp2)* was used as a tubular marker, *Pecam1* as an endothelial marker, *Cd68* as a macrophage marker and *Pdgfrb* as a marker of fibroblasts. Expression of these markers was confined to their correct sub-population. Moreover these markers exhibited differential expression in sham, UUO and rUUO. Megalin exhibited a 2.39 fold decrease in UUO compared to sham in tubular cells ($P<0.001$). *Pecam1* showed a 1.3 fold increase in UUO compared to sham ($P<0.05$). Cd68 exhibited a 1.45 fold decrease in expression in UUO compared to sham ($P<0.05$) and finally *Pdgfrb* exhibited a 1.81 fold decrease in UUO compared to sham ($p<0.01$).

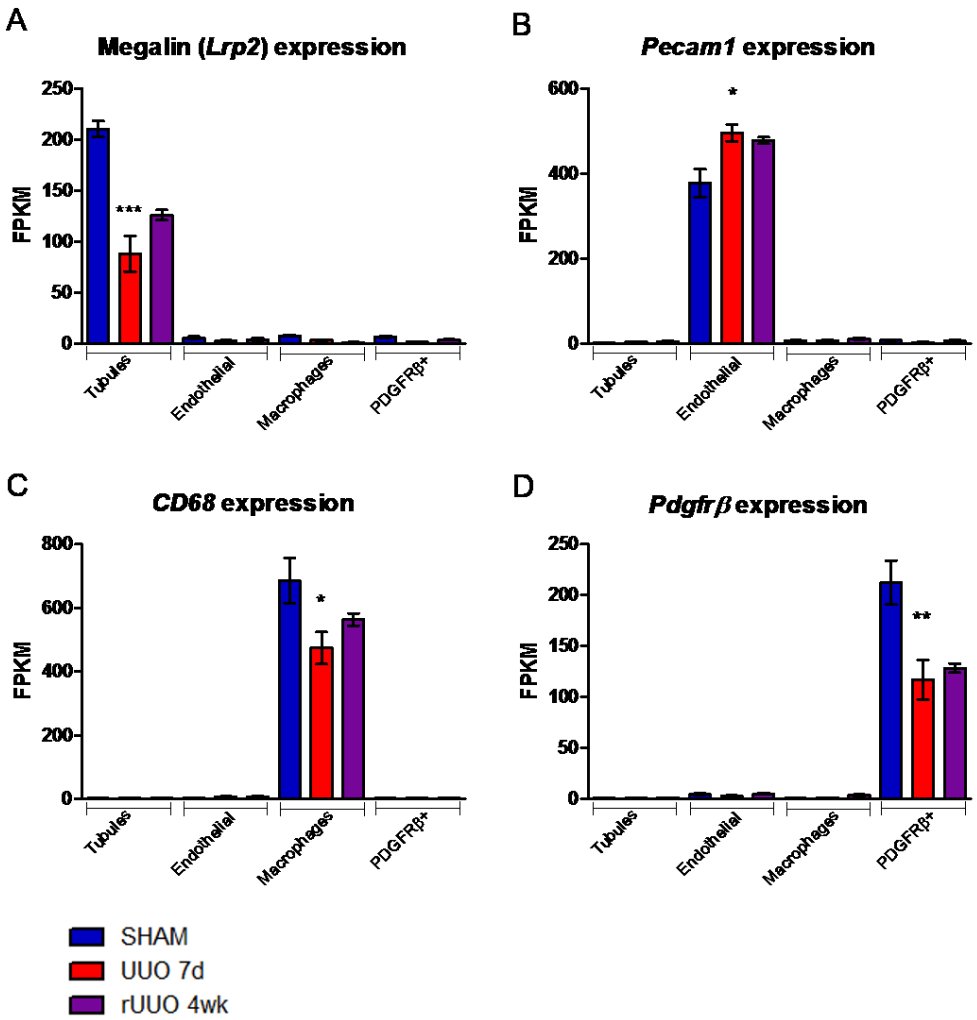

Figure 3.4: Kidney subpopulations express cell specific markers. Differential expression of *Lrp2* (A), *Pecam1* (B), *Cd68* (C) and *Pdgfrβ* (D) in sham, UUO 7 days and rUUO (2 weeks reversed) within kidney subpopulations; tubules, endothelial cells, macrophages and fibroblasts. Gene expression calculated from p-adjusted FPKM (Fragments per Kilobase of transcript per Million mapped reads) and analysed by 1 way ANOVA with Tukey's multiple comparison. ** and *** represent p<0.01 and 0.001 respectively compared to sham.

Next, it was determined which cell sub-population was responsible for the decreases and increases in expression in UUO and rUUO respectively in metabolism genes as seen in bulk cortical RNA-seq. We assessed expression levels of our genes of interest including *Ass1, Gatm, Gcdh* and *Acaa2* (Figure 3.5). *Ass1* expression was detected predominantly in the tubular sub-population and exhibited the same expression pattern as the kidney cortex RNA-seq with a decrease in UUO vs sham (-4.36 fold, p<0.001) and an increase in rUUO vs UUO (+2.54 fold, p<0.01). *Gatm* expression was seen in the macrophage sub-population but to a greater extent in the tubular population. Again, the previous expression pattern was replicated in the tubular

compartment with a decrease in UUO vs sham (-5.89 fold, p<0.001) and an increase in rUUO vs UUO (+2.99 fold, p<0.01). *Gcdh* demonstrated low level expression across endothelial, macrophage and fibroblast sub-populations and high levels of expression in the tubular population. *Gcdh* showed significantly decreased expression in UUO compared to sham (-2.38 fold, p<0.01) however, there was no significant increase in expression in the rUUO group compared to UUO. Finally *Acaa2* was expressed across all sub-populations but only exhibited significantly differential expression in the tubular population with a decreased expression in UUO vs sham (-2.38 fold p<0.01). There was no significant upregulation of *Acaa2* expression in the rUUO group vs UUO. The expression pattern of metabolism genes seen from kidney cortex RNA-seq of decreased expression in UUO compared to sham and increased expression in rUUO compared to UUO is replicated only within the tubular sub-population.

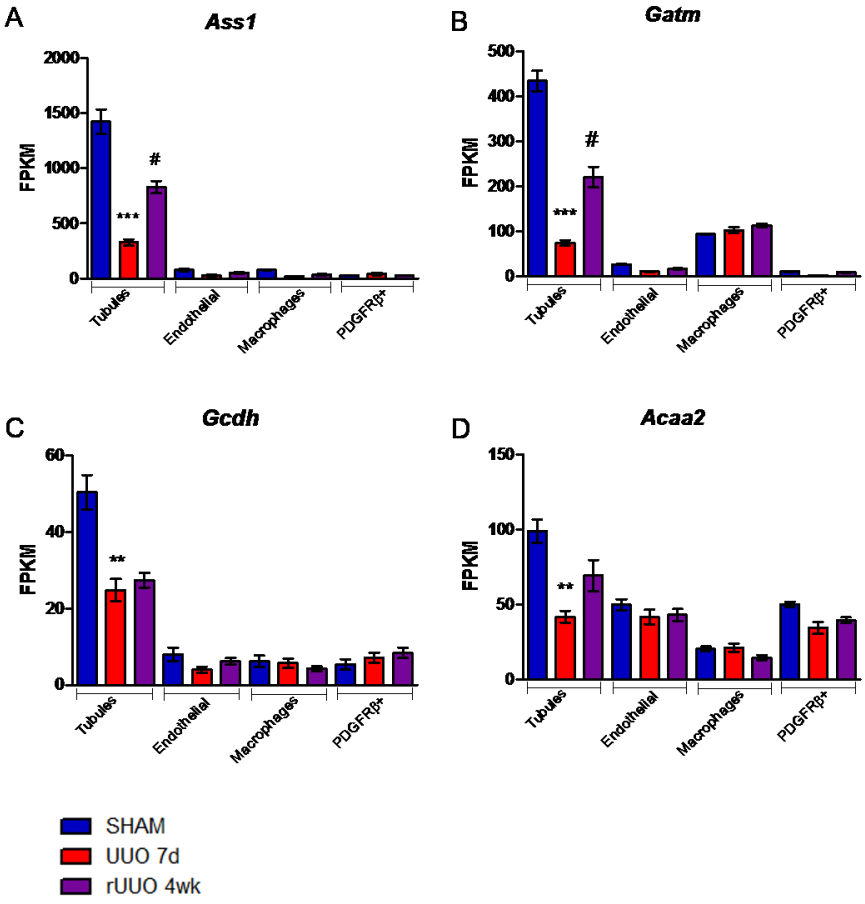

Figure 3.5: Expression of genes of interest in kidney sub-populations in UUO and rUUO. Differential expression of *Ass1* (A), *Gatm* (B), *Gcdh* (C) and *Acaa2* (D) in sham, UUO 7 days and rUUO (4 weeks reversed) within kidney subpopulations; tubules, endothelial cells, macrophages and fibroblasts. Gene expression calculated as p-adjusted FPKM (Fragments per Kilobase of transcript per Million mapped reads) from RNA-seq data and analysed by 1 way ANOVA with Tukey's multiple comparison. ** and *** represent p<0.01 and 0.001 respectively compared to sham and # represents p<0.01 compared to UUO.

3.3.4 Selection of *Ass1* as primary gene of interest

Ass1 was taken forward as our primary gene of interest as it is one of the most downregulated metabolic genes in UUO and one of the most highly upregulated in rUUO. This was demonstrated in both bulk kidney cortex and tubular subpopulation RNA-seq datasets. Furthermore, its expression is significantly decreased in patients with CKD vs healthy controls as seen in previous transcriptomics datasets (64,104). *Ass1* was also significantly upregulated in kidneys protected from fibrosis by anti-miR-214 treatment and finally, it is confined to the tubular compartment of the kidney which enables further investigation in tubular epithelial cell models in subsequent *in vitro* experiments.

3.3.5 *Ass1* expression is depleted to a greater extent than tubular markers

In order to measure proximal tubular number in UUO, the expression of two tubular markers *Lrp2* (megalin) and *Cubn* (cubulin) were assessed from the FACS sorted tubular sub-population RNAseq dataset. Both *Lrp2* and *Cubn* were significantly downregulated -2.39 and -2.10 fold respectively in tubules after UUO compared to sham. *Ass1* expression was depleted to a greater extent with a -4.36 fold reduction in expression in UUO compared to sham. After rUUO neither *Lrp2* nor *Cubn* showed significant elevation in expression while *Ass1* demonstrated a significant 2.54 fold increase in expression after reversal of UUO (Figure 3.6 and Table 3.).

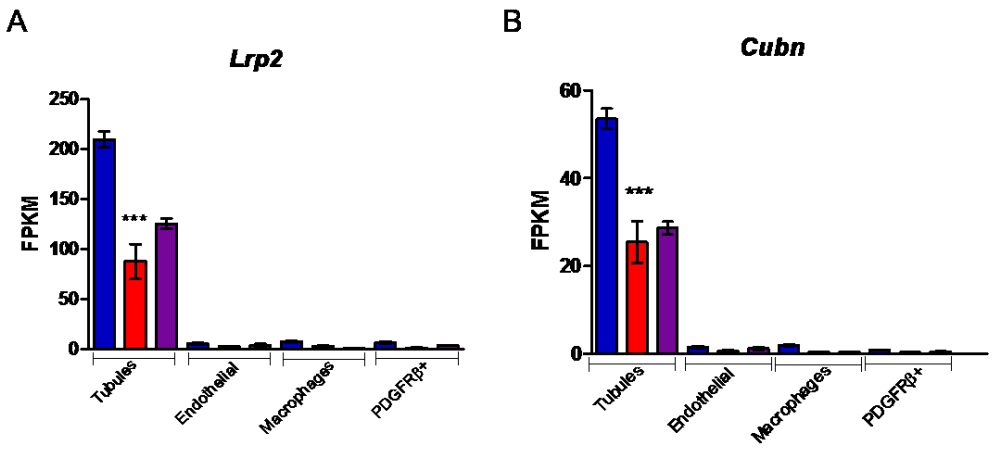

Figure 3.6: Expression of tubular markers kidney sub-populations in UUO and rUUO. Differential expression of *Lrp2* (A) and *Cubn* (B) in sham, UUO 7 days and rUUO (4 weeks reversed) within kidney subpopulations; tubules, endothelial cells, macrophages and fibroblasts. Gene expression calculated as p-adjusted FPKM (Fragments Per Kilobase of transcript per Million mapped reads) from RNAseq data and analysed by 1 way ANOVA with Tukey's multiple comparison. ** and *** represent p<0.01 and 0.001 respectively compared to sham.

Gene	Fold change (SHAM vs UUO)	P value	Fold change (UUO vs rUUO)	P value
Ass1	-4.36	<0.001	+2.54	<0.01
Lrp2	-2.39	<0.001	+1.43	ns
Cubn	-2.1	<0.001	+1.12	ns

Table 3.2: Expression of tubular markers in renal subpopulations in UUO and rUUO. Fold change values of Ass1, Lrp2 and Cubn in Sham vs UUO and UUO vs 4 week rUUO with corresponding *P* values.

3.3.6 Expression of Urea Cycle and Nitric Oxide Synthase Enzymes in subpopulations in the rUUO model

ASS1 is an enzyme which plays its role within the urea cycle in the liver and also the citrulline-nitric oxide cycle in endothelial cells. We used RNA-seq data from kidney subpopulations in the UUO/rUUO models to ascertain expression profiles of these enzymes in the kidney.

Genes encoding the classical urea cycle including N-acetyl glutamate synthase (*Nags*), Carbamoyl phosphate synthase I (*Cps1*), *Ass1*, argininosuccinate lyase (*Asl*), Arginase I (*Arg1*) and finally ornithine transcarbamylase (*Otc*) were assessed in renal cell subpopulations. *Nags, Cps1, Arg1* and *Otc* exhibited no expression within any population within the kidney. *Ass1* and *Asl* were both expressed in the kidney. *Ass1* was highly expressed in tubular cells. *Asl* expression was far less abundant than *Ass1* within the tubular compartment. *Asl* expression was also observed in endothelial, macrophage and fibroblast populations. Furthermore *Asl* demonstrated a similar expression pattern to *Ass1* in UUO and rUUO with a -2.8 fold downregulation in UUO compared to sham and a 2.22 fold upregulation in rUUO compared to UUO (Figure 3.7).

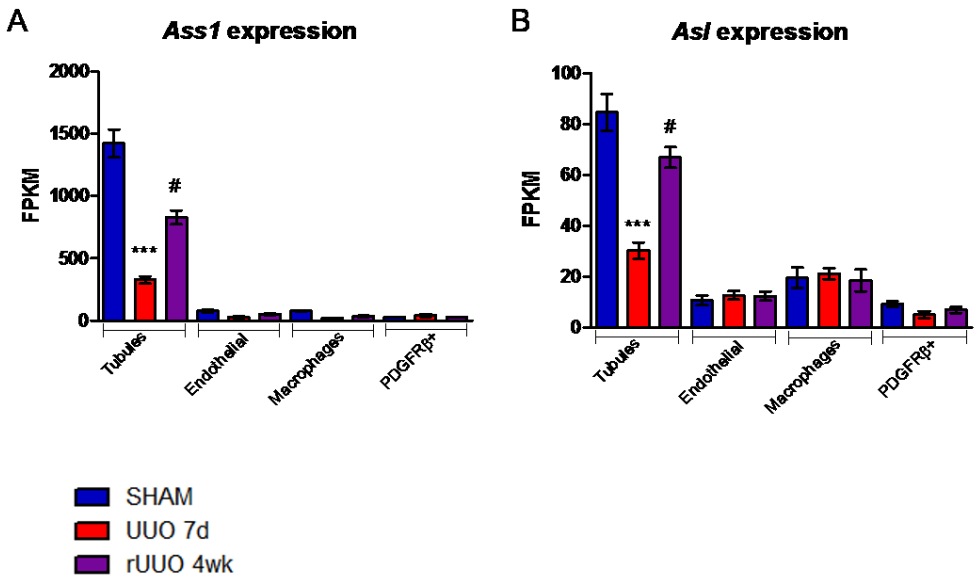

Figure 3.7: Expression of urea cycle genes in kidney sub-populations in UUO and rUUO. Differential expression of *Ass1* (A) and *Asl* (B) in sham, UUO 7 days and rUUO (4 weeks reversed) within kidney subpopulations; tubules, endothelial cells, macrophages and fibroblasts. Gene expression calculated as p-adjusted FPKM (Fragments per Kilobase of transcript per Million mapped reads) from RNA-seq data and analysed by 1 way ANOVA with Tukey's multiple comparison. ** and *** represent $p<0.01$ and 0.001 respectively compared to sham and # represents $p<0.01$ compared to UUO.

Arginine generated from ASS1 and ASL can be used in certain cell types for nitric oxide synthesis termed the citrulline-nitric oxide cycle. Genes encoding the three nitric oxide synthase enzymes *Nos1, Nos2* and *Nos3* were assessed in renal cell subpopulations in UUO/rUUO. All three enzymes demonstrated expression within the kidney however no expression was observed in the tubular subpopulation. *Nos1* demonstrated limited expression in endothelial

cells and fibroblasts. *Nos2* and *Nos3* exhibited expression within the endothelial population only (Figure 3.8). Furthermore, there were no significant changes in expression of any nitric oxide synthase isoform in UUO or rUUO.

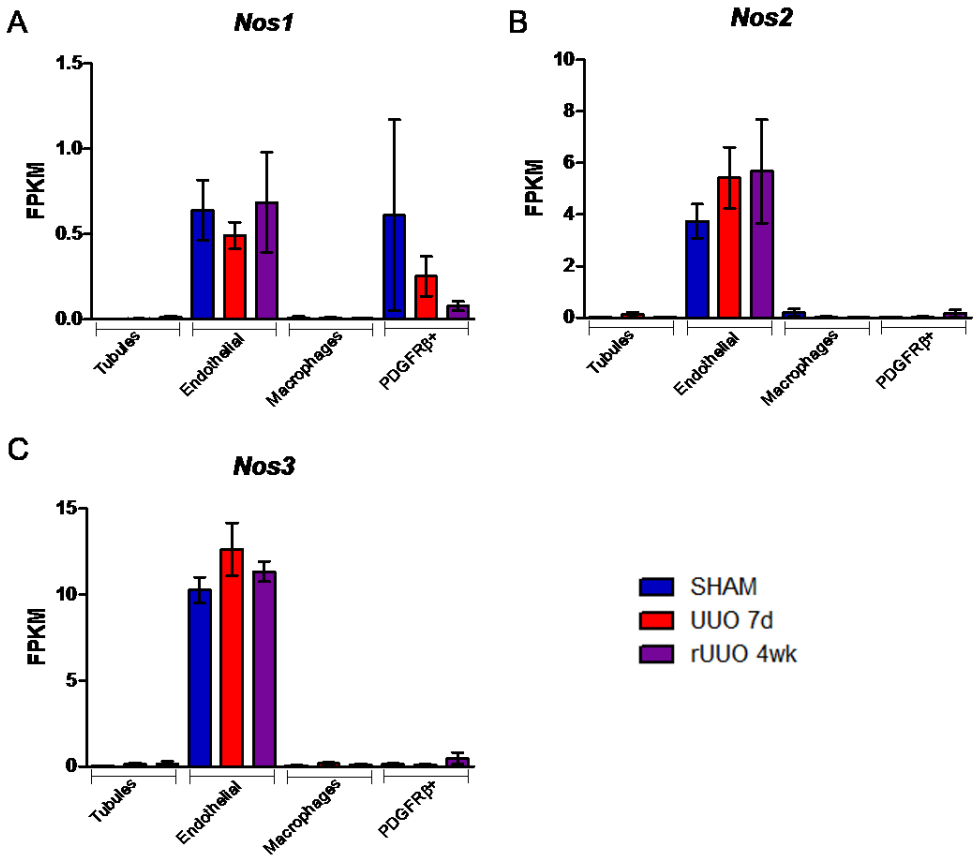

Figure 3.8: Expression of nitric oxide synthase isoforms in kidney sub-populations in UUO and rUUO. Differential expression of *Nos1* (A), *Nos2* (B) and *Nos3* (C) in sham, UUO 7 days and rUUO (4 weeks reversed) within kidney subpopulations; tubules, endothelial cells, macrophages and fibroblasts. Gene expression calculated as FPKM (Fragments Per Kilobase of transcript per Million mapped reads) from RNA-seq data and analysed by 1 way ANOVA with Tukey's multiple comparison. ** and *** represent $p<0.01$ and 0.001 respectively compared to sham and # represents $p<0.01$ compared to UUO.

3.3.7 Correlation between *Ass1* and miR-214 in rUUO Model

As *Ass1* expression was found to be upregulated in anti-miR-214 treated kidneys, we sought to determine whether *Ass1* and miR-214 had a negatively correlated relationship in kidneys from sham, UUO and rUUO interventions. Cortical RNA-Sequencing Data of mRNA and small RNAs was analysed to assess which predicted microRNAs target *Ass1* and whether any of these

microRNAs are negatively correlated with *Ass1* in the rUUO model. RNA-seq and correlation was carried out by Dr Katie Connor.

Integrative miRNA-mRNA analysis was carried out as follows. Small RNA libraries and mRNA libraries were prepared by Genewiz and underwent RNA-sequencing using the Illumina HISeq 2500 platform. Raw reads were then trimmed to remove adaptor contamination and low quality reads using trimGalore (version 0.4.1). Small RNA reads were then aligned to the mouse genome (GRCm38) and annotated to miRBase.

In RStudio (R 3.6.1), lowly expressed reads were removed and normalized. Count tables for both gene and microRNAs were generated using DESeq2 and EdgeR respectively. MicroRNAs underwent differential expression analyses and the predicted gene targets of miRs with at least one significant comparison (Fold Change >1.5, False Discovery Rate <0.05; n=382) were identified using the R package multiMiR (Version 2.2.0). MultimiR acts as an interface for finding miR-mRNA interactions and searches the following databases: TargetScan, PicTar, PITA, MiRanda, miRDB, Diana-microT, EIMMo and MicroCosm.

Eight of the investigated miRs were predicted to target *Ass1*, within this miR-214-3p was predicted by one database (microcosm) with a microcosm score of 17.17.

Database	Mature miRNA accession	Mature miRNA ID	Target	Ensembl ID	Score
elmmo	MIMAT0000237	mmu-miR-204-5p	*Ass1*	ENSMUSG00000076441	0.298
microcosm	MIMAT0000165	mmu-miR-155-5p	*Ass1*	ENSMUSG00000076441	18.33
microcosm	MIMAT0003731	mmu-miR-671-5p	*Ass1*	ENSMUSG00000076441	17.65
microcosm	MIMAT0000661	mmu-miR-214-3p	*Ass1*	ENSMUSG00000076441	17.17

microcosm	MIMAT0005438	mmu-miR-30c-2-3p	*Ass1*	ENSMUSG00000076441	17.17
microcosm	MIMAT0004616	mmu-miR-30c-1-3p	*Ass1*	ENSMUSG00000076441	17.05
miranda	MIMAT0000165	mmu-miR-155-5p	*Ass1*	ENSMUSG00000076441	-0.86
pita	MIMAT0000670	mmu-miR-222-3p	*Ass1*	ENSMUSG00000076441	-11.49

Table 3.3: MicroRNAs predicted to target Ass1 mRNA

To determine if the microRNA was likely to have a mechanistic effect on a predicted gene target, pairwise Pearson correlation coefficients were calculated for each predicted mRNA-miR interaction. Those with a correlation coefficient <-0.6 and FDR adjusted p value <0.05 were considered to be significantly negatively correlated. Using this approach, 28.1% (n=46642 out of n = 166260) of predicted mRNA-miR interaction pairs were considered to be significant within this study. Within this, the only miR significantly negatively correlated with *Ass1* expression was miR-214-3p (R -0.896, FDR.Adj.Pval <0.0001) (Figure 3.9).

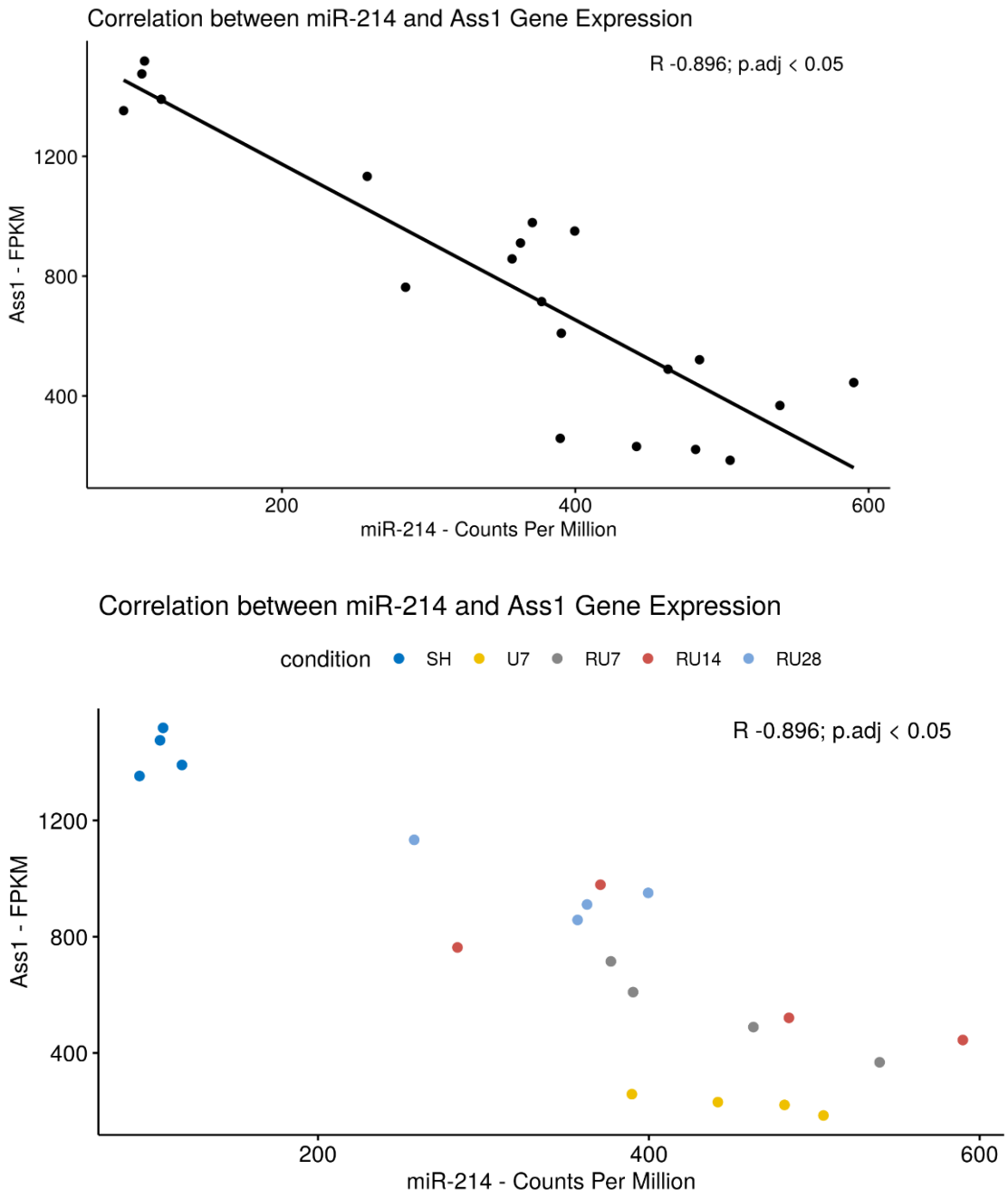

Figure 3.9: Correlation between miR-214 and *Ass1* gene expression. RNA-seq analysis of small RNAs and mRNAs from cortical renal tissue in the UUO/rUUO model elucidated the only microRNA to be significantly correlated to *Ass1* to be miR-214. (B) Coloured dots represent individual samples from sham (dark blue), UUO at 7 days (yellow), rUUO at 7 days (grey), rUUO at 14 days (red) and rUUO at 28 days (light blue).

3.3.8 In-depth investigation of *Ass1* in the rUUO model of renal fibrosis: single-cell RNA-seq

The kidney is comprised of a myriad of cell types with resident cells and transient, infiltrating cells. The cellular milieu changes dramatically with the

onset of disease and the resolution of disease. It was important to assess exactly which cell types *Ass1* is expressed in and how their expression profile changes according to disease state. Single cell RNA-seq allowed for the investigation of the transcriptome of each individual live cell within a sample. This enabled the investigation of *Ass1* in specific cell types in different injury states. The expression profile of *Asl* (enzyme downstream of *Ass1*) was also assessed to ascertain whether these enzymes were always expressed in the same cell type.

The rUUO model was adopted again to assess the expression patterns and abundance of *Ass1* in live renal cells from a sham kidney, a fibrotic kidney and a kidney in which fibrosis has reversed. This experiment compared kidneys from mice subjected to sham, UUO (2 days), UUO (7 days) or 2 week reversed UUO surgeries. Feature plots enabled the investigation of how different renal cells form sub-clusters based on their gene expression signature. Clusters represent kidney cell population including proximal tubular cells (segments 1-3), collecting ducts, endothelial cells and immune cells (Figure 3.10). Ass1 expression was most abundant in the epithelial clusters of cells. Therefore subsequent investigation was carried out only within epithelial cell clusters.

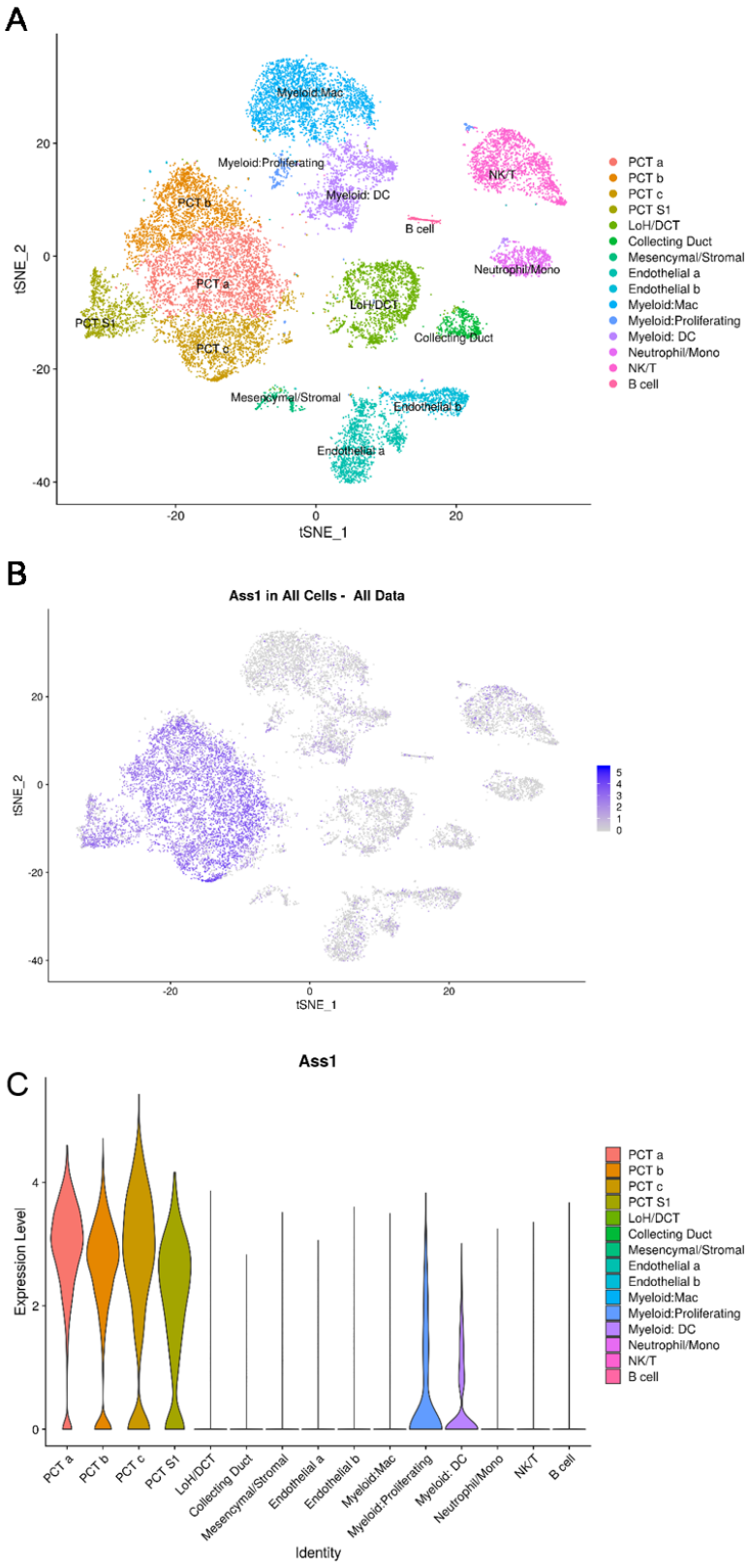

Figure 3.10: Characterisation of Ass1 in the kidney using single cell RNA-seq. Single cell RNA-seq analysis allowed clustering of different populations of renal cells according to their transcriptional profile (A). Ass1 demonstrated abundant expression in the epithelial clusters and low expression in some myeloid cell populations (B, C). Clusters in B are the same in cluster A PCT (proximal convoluted tubule), LoH/DCT (Loop of Henle/ Distal convoluted tubule), NK/T (natural killer/ T cell).

The expression pattern of *Ass1* and *Asl* were investigated in epithelial cells of a sham mouse using tSNE plots (Figure 3.11). Epithelial cells were clustered according to their transcriptome signature. The sub-clusters can be described as 3 proximal tubular cell sub-clusters (blue, red and pink rings: PTa, PTb and PTc), the thick ascending limb (green ring: TAL), and finally distal tubules (orange ring: DT).

Ass1 expression was very abundant within proximal tubular cells, particularly PTa, and expressed to a much lesser extent within PTb, PTc and distal tubules (Figure 3.11A). *Asl*, (Figure 3.11B) the neighbouring enzyme of *Ass1*, was expressed in fewer epithelial cells across the board and was far less abundant in the proximal tubular cells (PTa) compared to *Ass1*.

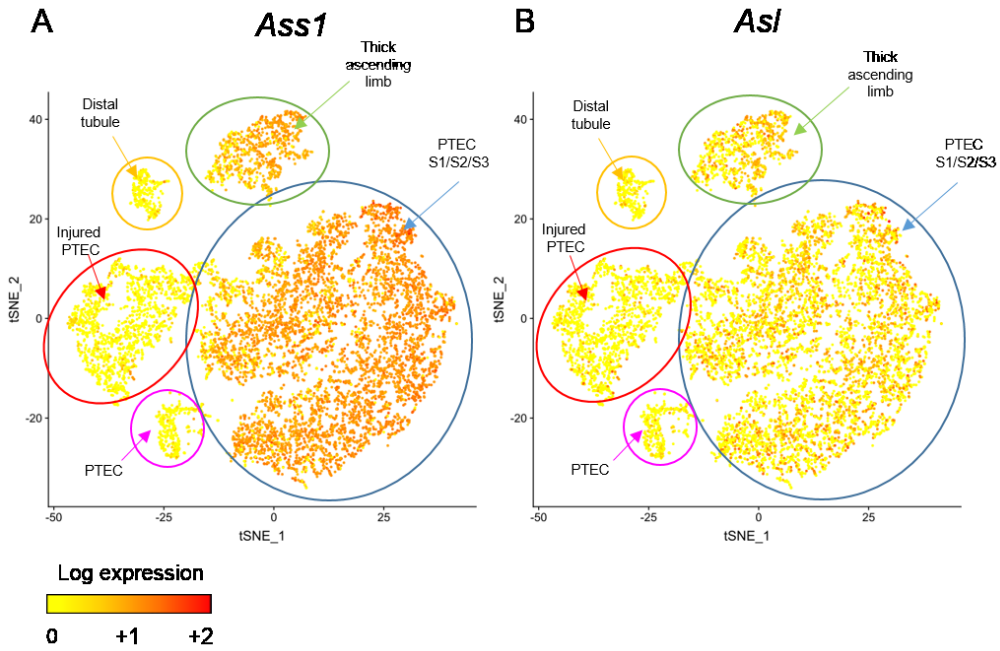

Figure 3.11: Ass1 and Asl expression in epithelial cells. tSNE plots generated from single cell RNA-seq depict the log expression of Ass1 (A) and Asl (B) in epithelial cells from a sham mouse. Epithelial cells are categorised according to their transcript signatures in coloured rings: proximal tubules sub-clusters (blue, red and pink rings), the thick ascending limb (green ring), and distal tubules (orange ring).

Pearson correlation analysis of epithelial cells from scRNA-seq was carried out to determine which cells co-expressed *Ass1* and *Asl* and which cells were *Ass1*-positive but *Asl*-negative a *vice versa*. There was a poor correlation between *Ass1* and *Asl* expression of 0.31. A proportion of epithelial cells co-expressed *Ass1* and *Asl* simultaneously. However, there were 2 other

populations of epithelial cells which expressed either *Ass1* only or *Asl* only (Figure 3.12).

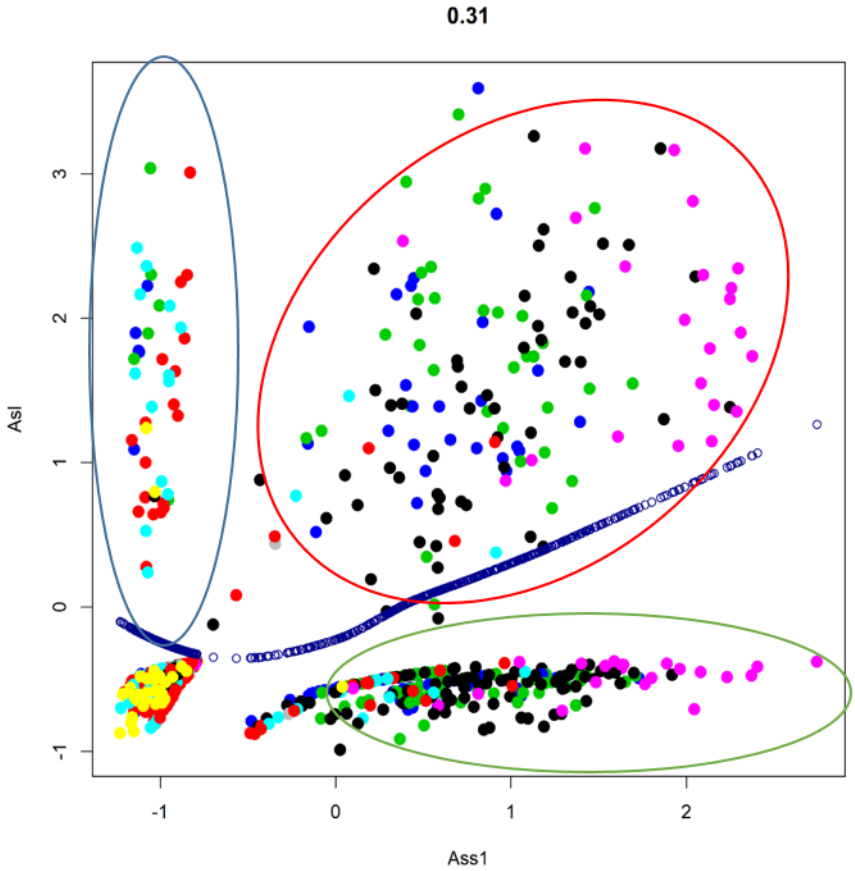

Figure 3.12: Pearson correlation of *Ass1* and *Asl* expression in epithelial cells derived from single cell RNA-seq. Individual epithelial cells (coloured spots) were plotted according to their expression of Asl and Ass1. Blue line represents trend line with R^2 value of 0.31. Coloured rings depict 3 populations: *Asl*-positive (blue), *Asl, Ass1*-double positive (red) and *Ass1*-poisitive (green).

Subsequently, the abundance of *Ass1* and *Asl* expression was assessed in all experimental injury groups within epithelial cells and depicted using Violin Plots (Figure 3.13). In sham, epithelial *Ass1* expression was highly abundant. Following UUO, *Ass1* expression levels were significantly depleted as soon as 2 days after surgery and further depleted 7 days after surgery. After 2 weeks reversal, the log fold expression of *Ass1* were significantly upregulated compared to UUO day 7 (Wilcox Test). Epithelial *Asl* expression was far less abundant in sham than *Ass1* but *Asl* still exhibited a significant decrease in expression in both UUO groups and a significant increase in the rUUO group compared to UUO day 7 (Wilcox Test).

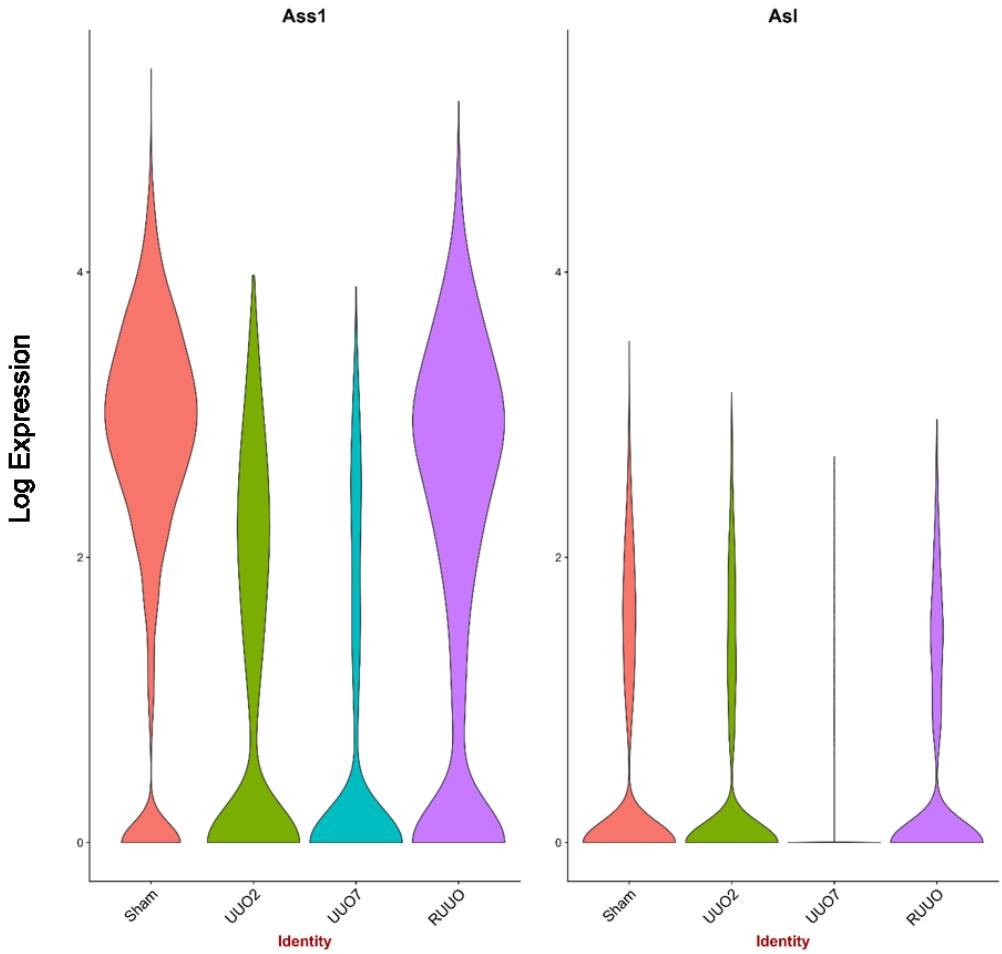

Figure 3.13: *Ass1* and *Asl* expression in epithelial cells from kidneys subjected to UUO/rUUO. Single cell RNA seq was used to determine the expression of *Ass1* and *Asl* in renal epithelial cells from mice subjected to sham, UUO (2 days), UUO (7 days) or 2 week-reversed UUO.

3.3.9 ASS1 protein expression in UUO/rUUO

To determine if ASS1 protein reflects what is seen at the mRNA level, western blot analysis was carried out on kidney tissue lysates from sham, UUO (2 days), UUO (7 days) and rUUO and normalized to housekeeping protein GAPDH. Protein levels were measured using Licor and quantified using Image Studio™ (Figure 3.14). ASS1 protein was highly expressed in renal tissue in sham kidneys. After 2 days of UUO there was no significant difference in ASS1 expression compared to sham ($p=0.3801$, unpaired Student's t test). However 7 days post-UUO there was significant depletion in ASS1 protein levels ($p<0.001$). 2 weeks after reversal of UUO, ASS1 was elevated compared to UUO, however, this did not reach statistical significance ($p=0.233$, One-way ANOVA with Dunnett's multiple comparison).

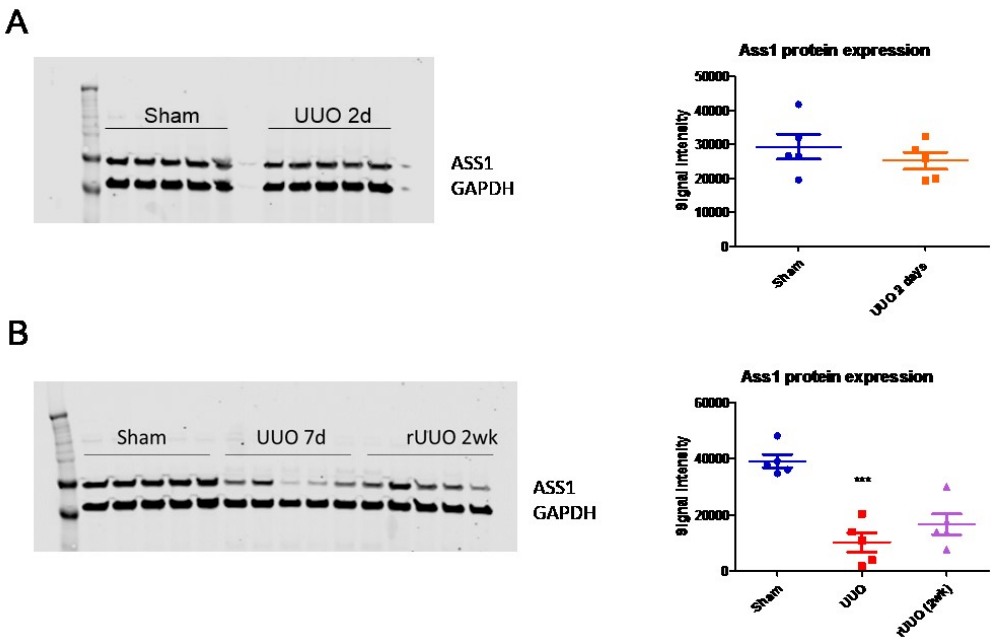

Figure 3.14: Protein analysis of ASS1 in Unilateral ureteric obstruction (UUO) and reversal of obstruction (rUUO). Immunoblot and respective signal intensities of ASS1 protein levels normalized to GAPDH loading control in (A) sham and UUO after 2 days and (B) sham, UUO after 7 days and rUUO after 2 weeks (n=5 per group). Signal intensity of protein bands were determined using ImageStudio Lite software relative to loading control. *** represents $p<0.001$ with one way ANOVA with Dunnett's multiple comparison test.

Finally, ASS1 expression was assessed in kidney slices by immunostaining. Sections of sham and UUO kidney tissue sections were stained for ASS1. ASS1 positive staining was abundant in the tubules of the sham kidney and was absent within the glomeruli. In UUO kidney sections, ASS1 staining was less abundant and some tubules demonstrated no ASS1 positive staining (Figure 3.15).

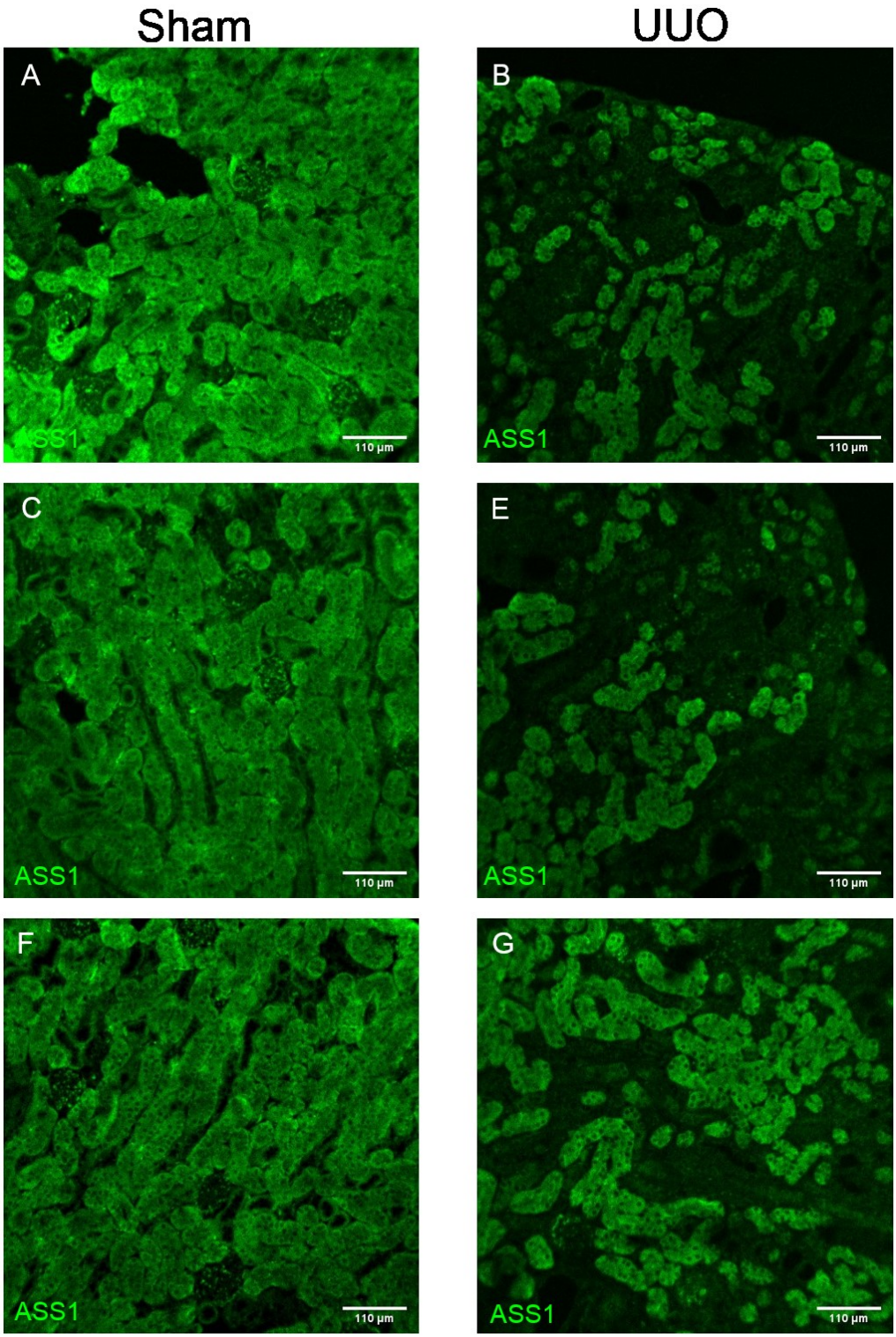

Figure 3.15: ASS1 immunostaining in sham and UUO kidney. Representative images of ASS1 immunostaining in sham (A,C,F) and UUO (B,D,G) kidney sections.

3.3.10 Investigation of *Ass1* expression in translational models

The UUO model of fibrosis allows investigation of renal fibrosis in just 7 days. This rapid onset of fibrosis is confined to the tubules due to ureteric obstruction and the glomeruli are unaffected by UUO. We sought to investigate our findings in two other models of renal fibrosis with distinct aetiologies; the subtotal nephrectomy model and the ischaemia reperfusion injury model. These models reflect human renal disease to a better extent and therefore provide more robust models which are more translational than UUO.

3.3.11 Refined subtotal nephrectomy

To provide evidence that *Ass1* plays a role in the pathogenesis of CKD we conducted further experiments in a more clinically relevant model of CKD; the subtotal nephrectomy model (STNx). The STNx models progressive development of fibrosis over 10 weeks that reflects human CKD more accurately than the rapid onset model of fibrosis; UUO. This refined pre-clinical mouse model undergoes systemic changes as a result of renal fibrosis such as increased blood pressure, cardiac hypertrophy and increased urinary albumin/creatinine ratio (93).

At sacrifice, the body mass and the mass of kidney, liver and heart was measured in each animal. There was no significant difference in body weight between sham and STNx at either time point (One way-ANOVA). Additionally, there was no significant difference in the organ mass of the kidney or liver in either 6 week or 10 week cohort between sham animals and STNx animals. However there was a significant increase in heart mass (normalized to body weight) in STNx animals compared to sham at both time points ($p<0.01$ and $p<0.05$ for 6 and 10 weeks respectively, unpaired Student's t test) (Figure 3.16A,B).

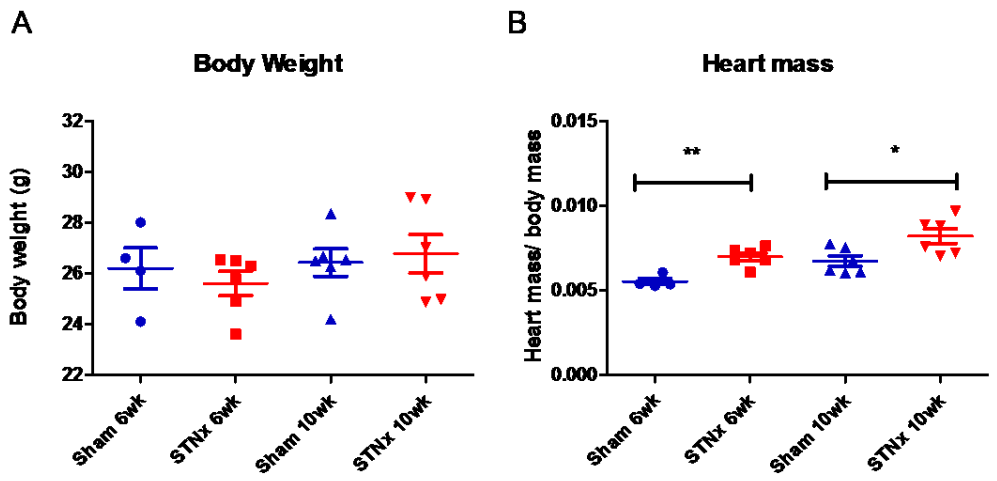

Figure 3.16: Body weight and heart weight in STNx vs sham. Body and heart mass was measured at sacrifice in shams and STNx animals at 6 and 10 weeks post-surgery. Heart weight was normalized to body mass. * and ** represent $p<0.05$ and 0.01 respectively compared to sham by unpaired Student's t test.

The gene expression levels of fibrosis markers were assessed in order to confirm the development of fibrosis in this model in the kidney at 6 weeks and 10 weeks post-surgery (Figure 3.17). Different time points were investigated to reveal the differential expression of genes during the early phase of the fibrotic response (6 weeks post-surgery) and after fibrosis had established within the kidney and cardiovascular impairments had occurred (10 weeks post-surgery). We assessed a panel of fibrosis markers (*Col1a1, Col3a1, Mmp2, Mmp9, Timp1,* and *Acta2*) and found that there was significant elevation in expression of all these markers 10 weeks post STNx and most markers (*Col1a1, Col3a1, Mmp9, Timp1* and *Acta2*) were significantly elevated 6 weeks post STNx (unpaired Student's t test).

Histological analysis of collagen deposition was assessed by picro-sirius red staining of kidney tissue slices Quantification of positive red staining using Image-Pro Plus revealed significantly elevated levels of total collagen after 6 and 10 weeks post-STNx demonstrating the progressive nature of this model. (Figure 3.17B,C) Image analysis was carried out by James O'Sulliven).

The subtotal nephrectomy model allows for the biochemical analysis of urine and serum which is not possible with other pre-clinical models such as UUO which have a remaining functional kidney. Albuminuria is a clinically relevant indicator of renal disease and was measured in STNx compared to sham. Urine was collected at baseline before surgery and 1 week before sacrifice in shams and STNx animals in both 6 week and 10 week cohorts and the extent of

albuminuria was measured. Urine albumin was undetectable in both baseline and sham groups and there were significant increases in urine albumin in both early phase (6 week) and late phase (10 week) STNx animals compared to baseline measurements (One way ANOVA with Dunnett's multiple comparison) (Figure 3.16D). Plasma urea provides another clinical marker of renal disease. Plasma extracted from blood taken at sacrifice at both time points was assessed. Plasma urea was significantly elevated in both early and late phase STNx plasma compared to sham (One way ANOVA with Dunnett's multiple comparison) (Figure 3.17E).

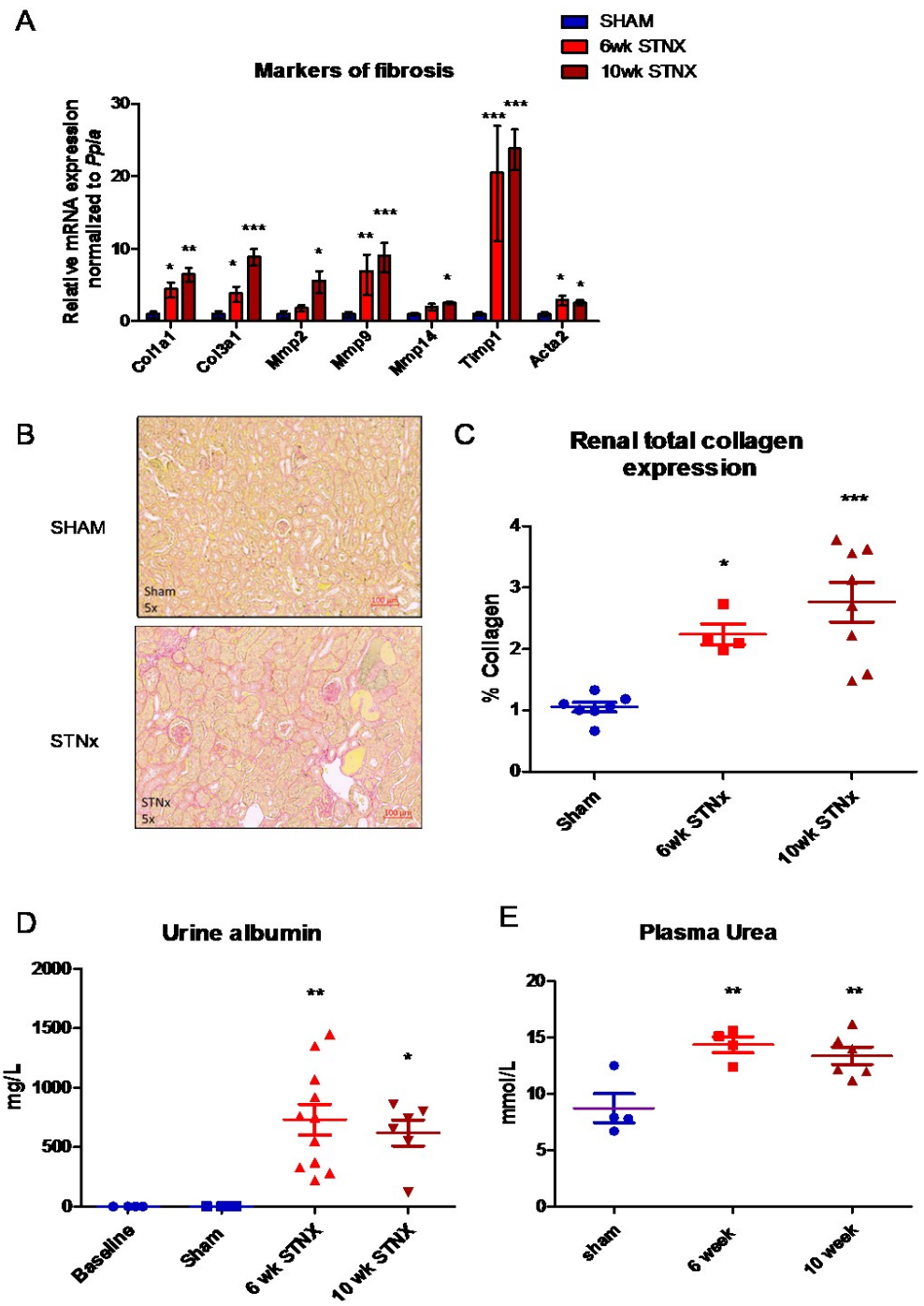

Figure 3.17: The subtotal nephrectomy (STNx) model of progressive renal fibrosis reflects human disease. (A) Relative mRNA levels of genes related to fibrosis in sham (n=4), STNx 6wk (n=6) and STNx 10wk (n=6). Relative expression was calculated from ΔΔcT normalized to Hprt housekeeper and compared to sham. *, ** and *** represent p<0.05, 0.01 and 0.001 respectively compared to sham by unpaired Student's t test. (B) Representative image of picrosirius red stained kidney tissue of sham and STNx at 10 weeks. (C) Corresponding quantification of picrosirius red staining of renal tissue from sham (n=7), 6wk STNx n=4) and 10wk STNx (n=8) mice. Quantification was carried out using Image-Pro Plus.* and *** represent p<0.05 and 0.001 respectively compared to sham by 1-way ANOVA with Dunnett's multiple comparison. (D) Urine (n=20) was collected with metabolic cages at baseline, in shams and STNx animals at 6 and 10 weeks and assessed for presence of albumin. * and ** represent p<0.05 and 0.01 respectively compared to baseline/sham by 1 way ANOVA with Dunnett's multiple comparison. (E) Plasma urea was measured in sham, 6wk and 10wk animals (n=16). ** represents p<0.01 compared to sham by 1 way ANOVA with Dunnett's multiple comparison.

After confirmation of the development of renal fibrosis and systemic pathologies associated with CKD, we assessed whether the expression of our candidate gene, *Ass1*, was altered in both early (6 weeks) and late phases (10 weeks) of STNx compared to sham. Gene expression analysis by qPCR demonstrated that *Ass1* mRNA expression was significantly decreased at both time points in STNx compared to sham (One way ANOVA with Dunnett's multiple comparison) (Figure 3.18A). Another STNx cohort was carried out to measure the expression of Ass1 at early time points (1, 2 and 4 weeks following surgery). Ass1 mRNA expression was consistently depleted at all time points compared to sham (One way ANOVA with Dunnett's multiple comparison) (Figure 3.18B).

Immunofluorescent staining for ASS1 in renal tissue slices from 10 week STNx animals revealed that ASS1 was confined to the proximal tubules within the kidney cortex and was not expressed in the glomerulus. Furthermore, ASS1 expression appeared to be depleted in tubules in 10 week STNx kidneys (Figure 3.18).

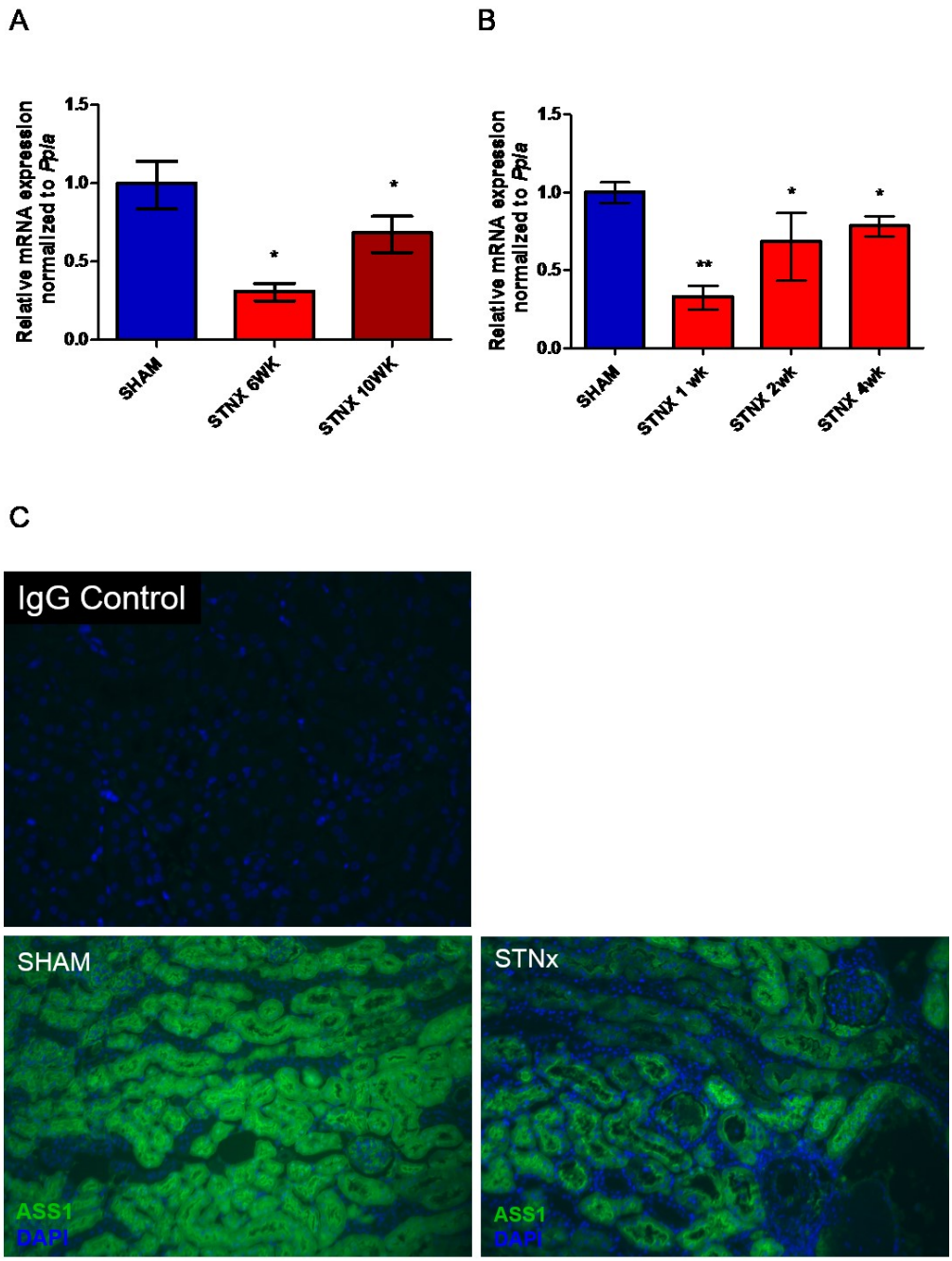

Figure 3.18: ASS1 downregulation in the subtotal nephrectomy (STNx) model of progressive fibrosis. RNA was extracted from kidneys from mice subjected to either sham or STNx surgery and tissue was harvested at mid (6 weeks) and late (10 weeks) time points (A). Tissue was harvested at early time points; 1 week, 2 weeks and 4 weeks (B). qPCR was carried out and *Ass1* expression was assessed in these samples and relative expression was calculated from ΔΔcT normalized to *Ppia* housekeeper compared to sham. (C) Representative image of ASS1 immunostaining in sham and 10 week STNx cortical kidney tissue with IgG control. Images were taken at 20x magnification on the Zeiss Axioscope 2 MOT Plus. * and ** represent $p<0.05$ and $p<0.01$ respectively with One way ANOVA with Dunnett's multiple comparison to sham.

3.3.12 Ischemia Reperfusion Injury Model

Ischaemia reperfusion injury (IRI) models acute kidney injury by unilateral clamping of the renal pedicle for variable durations to induce ischaemia within the kidney. Reperfusion is enabled by removal of the clamp and the animal is allowed to recover. Over time the injured kidney develops fibrosis.

A time course experiment was carried out in order to investigate how the IRI model develops fibrosis over time. IRI kidneys (n=7/8 at each time point) were harvested at 2, 7, 14 and 21 days and gene expression analysis and western blot analysis were carried out compared to sham animals at the corresponding time point (n=4 at each time point).

Markers of fibrosis were assessed by qPCR at all time points. *Col1a1*, a hallmark of fibrosis, was significantly elevated after IRI at all time points compared to sham. As soon as 2 days post-IRI *Col1a1* was 12 fold increased and subsequently it was upregulated by 31, 28 and 44 fold at 7, 14 and 21 days respectively compared to sham values at the same time point (unpaired Student's t test, $p<0.001$). *Col4a1* was not found to be significantly elevated at 2 days post-IRI but after 7 days mRNA was significantly increased by 5 fold compared to sham and this significant elevation was sustained at 15 and 21 days. Finally, *Mmp2* was not significantly elevated 2 days post-IRI but by 7 days post injury mRNA was significantly upregulated by more than 20 fold at 7, 14 and 21 days post-IRI compared to sham (Figure 3.19).

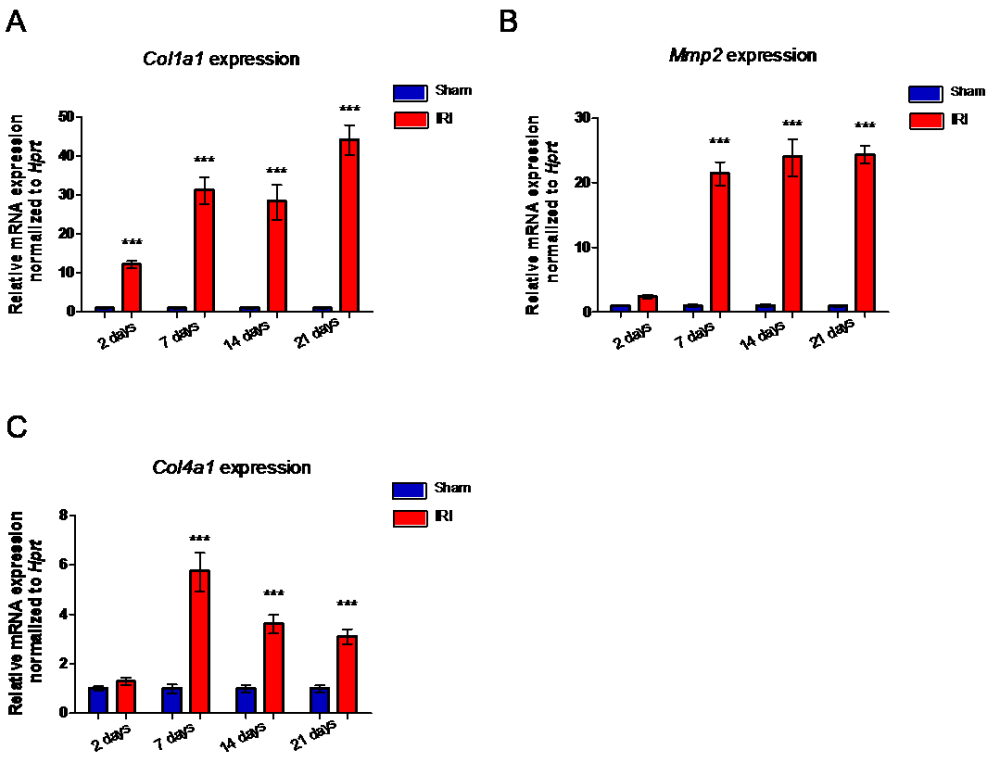

Figure 3.19: Markers of fibrosis are elevated in the ischaemia reperfusion injury model (IRI). (A-C) Relative mRNA levels of genes related to fibrosis in sham (n=4), or IRI (18min) surgery at a number of time points; 2 days (n=8), 7 days (n=8), 14 days (n=8) and 21 days (n=7) post-surgery. Relative expression was calculated from ΔΔcT normalized to *Hprt* housekeeper and compared to sham. *, ** and *** represent p<0.05, 0.01 and 0.001 respectively compared to sham by unpaired Student's t test).

Ass1 mRNA expression was found to be significantly depleted as early as 2 days post-IRI ($p<0.01$) compared to sham and this depletion was sustained at 7 days ($p<0.001$), 14 days ($p<0.01$) and 21 days ($p<0.05$) post-IRI (unpaired Student's t test).

Western blot analysis demonstrated that ASS1 protein was significantly depleted as soon as 2 days after IRI surgery and this loss was sustained at all time points as fibrosis progressed ($P<0.01$, One-way ANOVA with Tukey's multiple comparison (Figure 3.20).

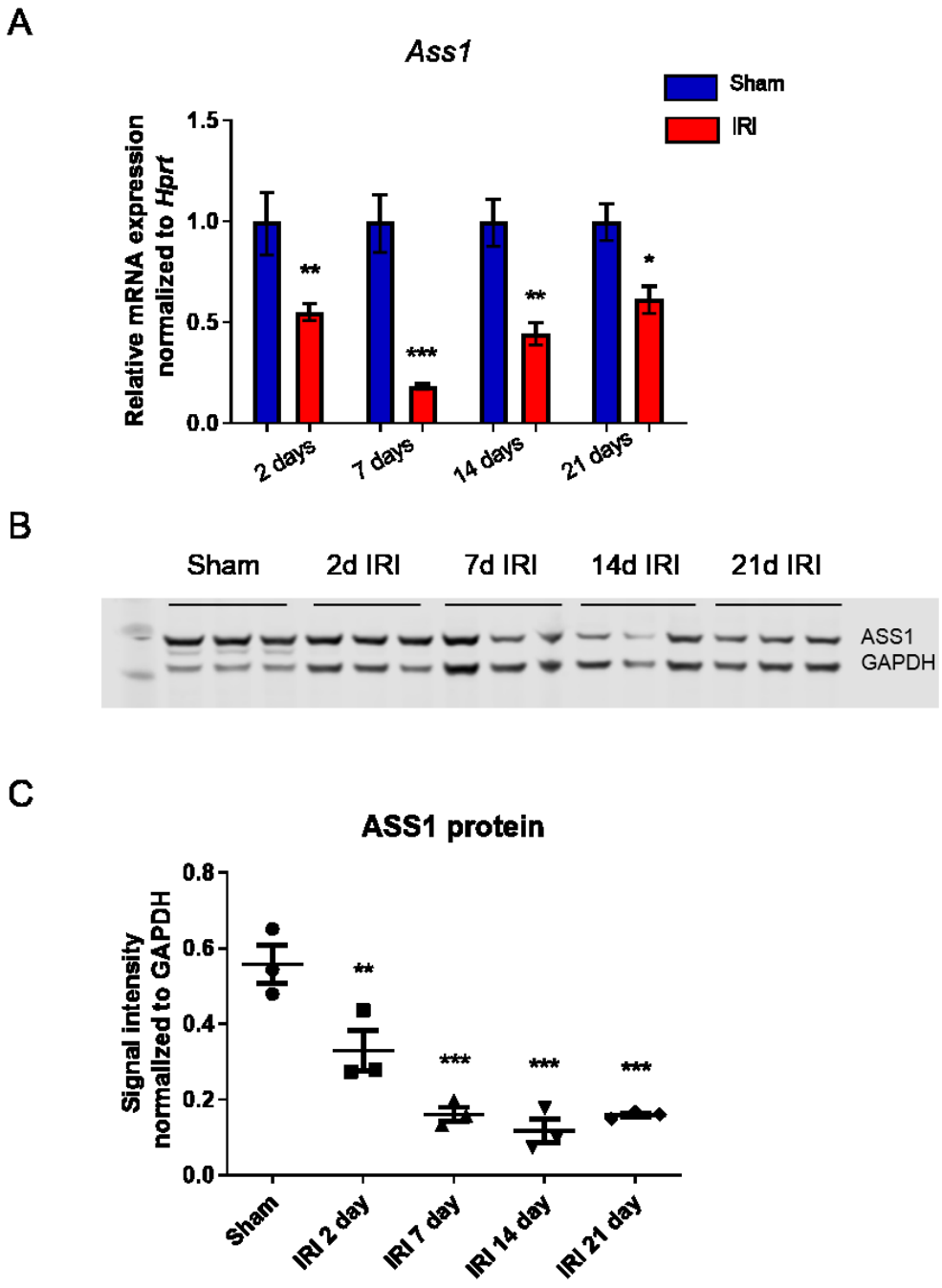

Figure 3.20: ASS1 depletion in the ischaemia reperfusion injury model (IRI). (A) Relative mRNA levels of *Ass1* in sham (n=4) or IRI (18min) surgery at a number of time points; 2 days (n=8), 7 days (n=8), 14 days (n=8) and 21 days (n=7) post-surgery. Relative expression was calculated from ΔΔcT normalized to *Hprt* housekeeper and compared to sham. *, ** and *** represent $p<0.05$, 0.01 and 0.001 respectively compared to sham by unpaired Student's t test. (B) Western blot was carried out on kidney lysates from sham and IRI at all time points (all n=3). Protein expression was measured using the Licor system and normalized to GAPDH housekeeper. ** and *** represent $p<0.01$ and 0.001 respectively compared to sham by 1 way ANOVA with Dunnett's multiple comparison.

The expression of tubular marker, *Cubn*, was assessed by qRT-PCR at all time points. *Cubn* expression did not exhibit significant downregulation until 14 days

after IRI. This reduced expressed was sustained at 21 days (one way ANOVA with Dunnett's multiple comparison) (Figure 3.21).

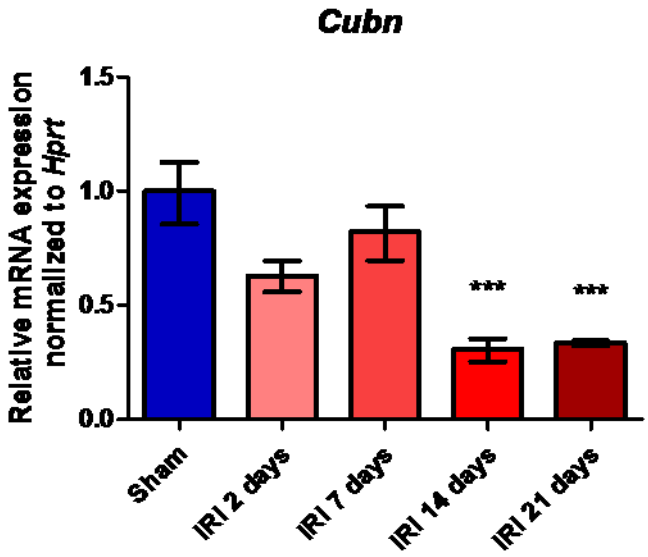

Figure 3.21: Marker of tubular number in ischaemia reperfusion injury. Relative mRNA levels of *Cubn* in sham (n=4) or IRI (18min) surgery at a number of time points; 2 days (n=8), 7 days (n=8), 14 days (n=8) and 21 days (n=7) post-surgery. Relative expression was calculated from ΔΔcT normalized to *Hprt* housekeeper and compared to sham. *, ** and *** represent $p<0.05$, 0.01 and 0.001 respectively compared to sham by One-way ANOVA with Dunnett's multiple comparison.

3.4 Discussion

Pre-clinical murine models provide much insight into the on-going mechanisms driving renal fibrosis and subsequent CKD. Here, three different models have been adopted to explore mechanisms common to fibrosis regardless of aetiology. Using a variety of transcriptomics techniques, it was elucidated that fibrosis is linked to a downregulation in metabolic processes. Moreover, reversal of fibrosis induced an upregulation of genes involved in metabolic pathways. *Ass1* was revealed to be an important gene of interest, highly expressed in tubules, which demonstrated depleted expression in 3 models of renal fibrosis and upregulation of expression when fibrosis was reversed. Furthermore, *Ass1* was shown to be upregulated in kidneys protected from fibrosis by anti-miR-214 and *Ass1* expression and miR-214 demonstrated a strong negatively correlation indicating that Ass1 may be a target of pro-fibrotic miR-214.

Dysregulated metabolism has been reported to be an important driver of renal fibrosis. Here, we found fatty acid oxidation/metabolism to be a metabolic pathway that was shut down in the UUO model of fibrosis. Research conducted by Kang and colleagues supports this finding. Their work demonstrated decreased expression of genes involved in fatty acid oxidation in a genetic murine model of fibrosis (over-expression of Notch 1 in TECs) as well as the folic acid-induced injury model. Furthermore their findings were recapitulated in human studies. Transcriptomics studies and pathway analysis from patients with CKD compared to healthy controls showed an overall decrease in genes pertaining to the fatty acid oxidation pathway (64). Other groups have demonstrated defective fatty acid metabolism in renal fibrosis associated with aging and excess lipid accumulation (63) and AKI followed by exposure to angiotensin 2 (105). As tubular epithelial cells use fatty acid oxidation as their primary mode of generating ATP, losing the ability to metabolise fatty acids is detrimental to TECs which drives injury and subsequent fibrosis.

This work also identified the pathway; arginine biosynthesis and metabolism to be perturbed in UUO. Previous work has identified several amino acids involved in arginine metabolism to be dysregulated in chronic renal failure in rodents and humans. Arginine biosynthesis is achieved in the kidney by conversion of circulating citrulline to arginine which is released from the kidney. Several studies have reported circulating citrulline levels to be upregulated in

renal failure in CKD patients and animal models (106-108). Arginine levels have been reported to be depleted within renal tissue in renal failure, however circulating levels of arginine remain physiologically normal (109-111). Arginine metabolism pathways include the production of nitric oxide (NO) from nitric oxide synthase which is very important in vasodilatation and inflammation. Studies have reported decreased production of NO in patients with renal failure and this depletion could contribute to increased risk of cardiovascular events observed in patients with CKD (108,112).

A large metabolomics study conducted by Rhee and co-workers followed a group of patients with heart disease of which 10% developed CKD. Of the CKD population, metabolomic screening was conducted in plasma and urine. Citrulline was detected as a top ranked metabolite that was significantly upregulated in plasma of patients with CKD compared to healthy controls. Furthermore, higher plasma citrulline levels proved to be a more significant indicator of patients with CKD than creatinine (111). Another study also found high citrulline levels in urine to be a predictor of CKD. Additionally they found citrulline to be negatively correlated with estimated glomerular filtration rate and positively correlated with creatinine levels (107). High citrulline levels have also been seen in pre-clinical models of CKD (113). This supports my finding that arginine metabolism is dysregulated during the progression of renal disease.

Ass1 was selected as a gene with a potential role in the development of CKD. We compiled several transcriptomics datasets from our lab and others which consistently reported *Ass1* to be downregulated in murine models of fibrosis and importantly in human CKD. Moreover, for the first time, *Ass1* was identified as a gene that exhibited marked increases in expression in the rUUO model, where renal fibrosis is largely resolved. Measurement of protein levels of ASS1 revealed that ASS1 was not significantly depleted in UUO kidney after 2 days although *Ass1* mRNA expression was significantly decreased in epithelial cells after 2 days. Seven days after UUO, ASS1 expression was significantly depleted at both mRNA and protein levels. Furthermore, in rUUO ASS1 protein levels were increased after 2 weeks but this did not reach significance. However, Ass1 mRNA was significantly upregulated after 2 weeks rUUO compared to UUO. Unfortunately protein was not available from 4 week rUUO kidneys so we cannot definitively ascertain whether protein levels are significantly increased in rUUO compared to UUO at this time point. However mRNA levels of *Ass1* are significantly elevated after 4 weeks of rUUO. This

suggests that changes in ASS1 protein levels occur later than changes seen at the transcript level. This may be explained by the half-life of ASS1 which has been revealed to be ~40 hours in collecting duct cells *in vitro.* (114). This relative stability of ASS1 means that transcriptional changes are not seen at the protein level immediately.

Additionally, in this project, *Ass1* was found to be significantly depleted in the STNx and IRI models of fibrosis. Therefore, *Ass1* is consistently depleted in three different models of renal fibrosis. This Chapter explored the outcomes from the newly refined subtotal nephrectomy that was developed in the Denby lab. This model results in reliable progressive renal fibrosis over 10 weeks with accompanying renal inflammation, cardiac hypertrophy and elevated blood pressure (93). This model was a great asset to this body of work as it accurately models the progression of CKD in a manner akin to human disease. Another group have also reported ASS1 to be downregulated in the subtotal nephrectomy model as soon as 2 weeks after surgery. They identified early depletion of ASS1 and its partner enzyme ASL as the cause for upregulation of circulating citrulline in chronic renal failure (115). As mentioned previously, elevated citrulline is correlated with both human and rodent CKD. Our data supports this finding as both *Ass1* and *Asl* are depleted in the UUO model of renal fibrosis investigated in this project. Future work investigating these models should include measurement of circulating citrulline and arginine in serum. In this way we could establish whether changes in these amino acids are detectable in unilateral models such as UUO and unilateral IRI or only in models which lack a fully functioning kidney.

Here, it was identified that tubular epithelial cells are the predominant cell type expressing Ass1 in the kidney. Using RNA-seq data from both FACS sorted subpopulations and single cell sequencing has allowed investigation of *Ass1* expression patterns in UUO and rUUO exclusively in tubular epithelial cells. As the kidney is comprised of many cell types, it is important to identify which are responsible for gene expression changes seen in whole kidney homogenate. As *Ass1* expression is predominantly tubular, gene expression analysis from other models such as STNx and IRI could be assessed from whole kidney with the knowledge no other renal cell types were contributing significantly to *Ass1* gene expression patterns.

Single cell RNA-seq has also allowed the investigation of expression profiles from individual cells. Focussing on epithelial cells allowed the observation that *Ass1* and *Asl* are not always expressed in the same cell. tSNE plots as well as Pearson correlation demonstrated that there are 3 populations of cells expressing Ass1 and Asl; Ass1 positive, Ass1-Asl double positive and Asl positive. The classical role of ASS1 is its role in converting citrulline to argininosuccinate which is in turn converted to arginine. It is perhaps an indication that Ass1 and Asl have roles other than citrulline metabolism if they are expressed singly in certain cells. Lee and colleagues also found Ass1 and *Asl* to be distinctly expressed in different regions of the nephron. They carried out deep sequencing on micro-dissected nephrons and found Ass1 to be highly expressed exclusively in the proximal tubule while Asl exhibited lower level expression diffusely through most sections of the nephron (116). Their work supports our findings from tSNE plots which showed Ass1 to be confined mostly to proximal tubular cells while *Asl* exhibited lower level diffuse expression throughout epithelial cells. This evidence could suggest that these genes are playing a role out with their traditional role in the urea cycle.

Another study identified *Ass1* to be downregulated in autosomal dominant polycystic kidney disease (ADPKD). This group found Ass1 to be depleted in genetic knockout mouse models of ADPKD and human ADPKD. The authors attributed loss of *Ass1* to loss of tubular mass which occurs during the onset of ADPKD. They showed that *Ass1* depletion led to changes in arginine levels in the kidney which interfered with glutamine metabolism which they suggested contributes to cyst growth (117). ADPKD is an inherited condition which manifests in cystogenesis but also fibrosis. Trott and colleagues work supports this study as *Ass1* is yet again observed to be downregulated in a fibrotic renal disease. However, in my body of work, tubular loss does not seem to be the only cause of *Ass1* depletion. Another study investigating the characteristics of hepatorenal syndrome, found that *Ass1* mRNA and protein were depleted in a mouse model of bile-duct ligation. This model of hepatorenal syndrome induced renal injury, inflammation and fibrosis. This model provides evidence that *Ass1* is downregulated in models of renal injury in which indirect kidney injury is a downstream effect of hepatic injury (118). This suggests that regardless of aetiology, Ass1 is consistently downregulated with the advent of renal injury.

Tubular loss is a pathological trait of all three models investigated here. Tubular atrophy occurs for a number of reasons and contributes significantly to renal disease. Loss of *Ass1* was demonstrated in all three models and therefore, the fact that *Ass1* loss could be explained purely by tubular loss must be addressed. In the UUO model, *Ass1* loss was confined to the tubular compartment. In order to assess the extent of tubular loss in UUO, expression of tubular markers *Lrp2* and *Cubn* were investigated in live sorted tubular cells for use as a proxy for tubular loss. Both *Lrp2* and *Cubn* showed downregulation after 7 days UUO, however, *Ass1* demonstrated a greater negative fold change in expression in UUO vs sham compared to tubular markers. Therefore, *Ass1* was depleted to a greater extent compared to 2 tubular makers. Both tubular markers demonstrated very similar expression patterns. Furthermore, neither tubular marker exhibited significant elevation in expression after rUUO compared to UUO. This demonstrated no significant increase in tubular number after reversal of obstruction. Conversely, *Ass1* demonstrated significant increases in expression after reversal of obstruction. This suggests that although there are no significant increases in tubular number after rUUO, upregulation of Ass1 is required in the remaining tubular population during resolution of fibrosis.

The extent of tubular loss was also investigated in IRI. Here, *Cubn* expression was measured at various time points following IRI and its expression was not found to be significantly decreased until 14 days post-IRI. This is in contrast to *Ass1* which demonstrated significant depletion as soon as 2 days following IRI. This shows that *Ass1* loss occurs prior to tubular loss, indicating Ass1 depletion is an important event independent of and preceding tubular loss.

This work has revealed a potential interaction between *Ass1* and miR-214. Not only was *Ass1* significantly upregulated in kidneys treated with anti-miR-214 but *Ass1* also demonstrated a very strong negative correlation with miR-214 in UUO/rUUO. As microRNAs function by repressing their target genes, it provides evidence that *Ass1* may be a target of miR-214 due to increased expression of miR-214 correlating strongly with decreased *Ass1* expression in UUO. However, proving direct interaction and repression of an mRNA target by a microRNA is challenging. In mammals microRNAs tend to bind their mRNA targets through imperfect sequence complementarity. Therefore, using computational algorithms to predict miRNA-mRNA binding can be misleading. In order to prove a direct physical interaction between miR-214 and *Ass1* a

reporter based assay could be used. In this way the luminescent signal intensity of a luciferase reporter could be used to detect *Ass1* mRNA target binding by miR-214 (119,120).

This chapter has elucidated metabolic pathways to be dysregulated in renal fibrosis. Ass1, part of arginine biosynthesis and metabolism pathway was found to be consistently downregulated in three different models of renal fibrosis. *Ass1* depletion was an event that occurred early in the progression of renal fibrosis and *Ass1* loss was found to occur prior to tubular loss and was found to be depleted to a greater extent than markers of tubules. Furthermore, Ass1 expression was lost in live transcriptionally active epithelial cells after UUO. Additionally Ass1 expression is rescued in rUUO kidneys in which fibrosis has resolved despite the fact that the number of tubular cells does not significantly increase. This shows that Ass1 expression patterns observed in these models is not entirely a result of tubular loss or gain. This indicates that *Ass1* loss is a molecular mechanism that occurs at the onset of renal fibrosis and the role that this enzyme plays in the progression of fibrosis warrants further investigation.

The role of ASS1 in human renal proximal tubular cells

3.5 Introduction

3.5.1 Argininosuccinate synthetase (ASS1)

ASS1 is the rate limiting step of the urea cycle and is expressed ubiquitously. Its pattern of expression varies according to which cell type it is expressed in. The liver exhibits very high expression of ASS1 and is the main site of urea production. Within the liver, ASS1 localises to the mitochondria. Within endothelial cells, ASS1 associates with calveolae and is expressed at low levels and provides arginine for nitric oxide synthesis (121,122). Within the kidney, ASS1 is highly expressed but confined primarily to the proximal tubule (123). Microdissection of human kidneys has revealed that *ASS1* RNA is highly expressed in all 3 segments of the proximal tubule but very lowly expressed throughout the remainder of the nephron. However, the subsequent enzyme in the urea cycle, argininosuccinate lyase, did not express the same expression pattern within the nephron and exhibited expression in the distal nephron as well as the proximal nephron (116). However the subcellular expression of ASS1 within the kidney is poorly defined and generally referred to as cytosolic (121).

ASS1 functions as part of the urea cycle. However the urea cycle functions differentially depending on the organ. Within the liver, the urea cycle occurs in its entirety but within the kidney only a portion of the urea cycle is carried out.

3.5.2 The Urea Cycle

The urea cycle was the first metabolic cycle to be discovered by Hans Kreb and Kurt Henseleit and functions to detoxify cells by converting ammonia into urea (124). The full urea cycle is carried out by 5 enzymes: carbamoyl phosphate synthetase (CPS), ornithine transcarbamylase (OTC), argininosuccinate synthetase (ASS1), argininosuccinate lyase (ASL) and arginase 1 (ARG1) which are localised within mitochondria and the cytoplasm. Ammonia and bicarbonate are produced in the mitochondria and combined by CPS to give carbamoyl phosphate which is converted by OTC to citrulline. Citrulline is shunted out of the mitochondria and with the addition of aspartate

is converted to argininosuccinate by ASS1. Subsequently this is converted to arginine by argininosuccinate lyase (ASL). Arginine is then converted to urea waste, water and ornithine which is recycled back into the urea cycle (Figure 3.22) (125).

The complete urea cycle takes place primarily in the liver. However, within the kidney, there is very little expression of CPS1, OTC or ARG1 and a truncated version of the urea cycle takes place. Circulating citrulline enters the kidney via the renal artery and is converted to arginine by ASS1 and ASL. Arginine is then excreted via the renal vein and used for a number of processes. The kidney is the main site of arginine production in the body. Production of arginine is essential for protein synthesis in all cell types and plays varying tissue specific roles such as urea production, nitric oxide synthesis, polyamine synthesis, and creatine synthesis (121,122) (Figure 3.23).

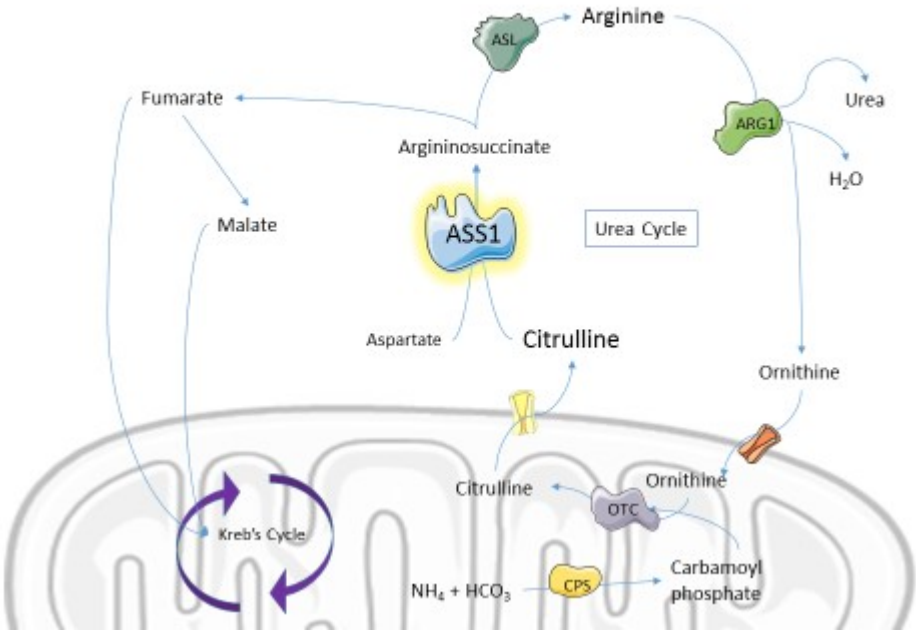

Figure 0.1: Schematic of the urea cycle. CPS (carbamoyl phosphate synthetase), OTC (ornithine transcarbamylase), ASS1 (argininosuccinate synthetase), ASL (argininosuccinate lyase) and ARG1 (arginase 1).

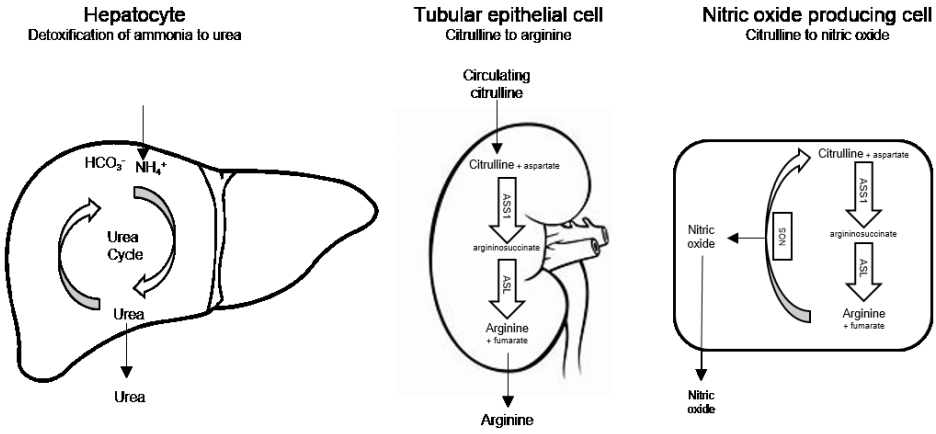

Figure 0.2: The urea cycle in different cell types. Bicarbonate ($HCO3^-$), Ammonia ($NH4^+$) are converted to urea via the urea cycle in hepatocytes of the liver. Circulating citrulline is converted to arginine by argininosuccinate synthetase (ASS1) and argininosuccinate lyase (ASL) in tubular epithelial cells of the kidney. Citrulline is converted to nitric oxide by ASS1, ASL and nitric oxide synthase (NOS) in nitric oxide producing cells.

3.5.3 Urea Cycle Disorders

There are several urea cycle disorders which occur due to deficiencies in the activity of the urea cycle enzymes including ASS1 and ASL. Urea cycle disorders are rare inherited disorders which often result in hyperammonemia which is neurotoxic. This results in a large number of patients with urea cycle disorders dying shortly after birth (126).

Deficiency of ASS1 is characterised as citrullinemia type I and its severity depends on the extent of enzymatic deficiency. CTLN1 is autosomal recessive and symptoms occur shortly after birth and can be fatal. CTLN1 has been associated with liver disease however robust evidence of kidney abnormalities in CTLN1 is lacking. One study reported evidence of renal disease in a small percentage of their cohort with ASS1 deficiency, however, the GFR measuring technique varied within the study cohort and no details of renal function or histology were assessed (127,128).

Another urea cycle disorder, argininosuccinate lyase deficiency, is characterised by dysfunction or absence of the enzyme ASL. The incidence of this inherited disorder is 1:70 000 births which makes it the second most common urea cycle disorder. As well as neurological defects, gastro-intestinal symptoms and liver dysfunction, some patients with ASL deficiency develop some renal pathologies (129-131). Tubulopathies have been reported in a proportion of these patients with one study reporting 46% of their cohort

presenting with hypokalaemia (132). However, in depth diagnoses of potential renal phenotypes is sorely lacking in these patients.

Although insight into renal dysfunction associated with urea cycle disorders is lacking it is interesting to note that some patients with these diseases do develop some renal disease, if poorly described. Together, with the evidence from metabolomics data highlighting elevated citrulline to be a marker of CKD, there is cause to investigate how urea cycle enzymes behave in the context of kidney function and CKD.

3.5.4 The proximal tubule in chronic kidney disease

The proximal tubule comprises the majority of the renal cortex and is made up of proximal tubular epithelial cells (PTEC). The proximal tubule is an essential segment of the nephron and is the main site of electrolyte reabsorption, protein and glucose uptake and pH balance. Therefore, these hard-working cells have a high energy demand and are densely packed with mitochondria. The proximal tubule is highly sensitive to injury and responds to stimulation with a number of pro-fibrotic and pro-inflammatory cytokines and is therefore instrumental in the progression of acute kidney injury to chronic kidney disease (see section 1.1.6).

As demonstrated in Chapter 3, ASS1 is a highly abundant protein in the proximal tubule as seen in mice. The intracellular localisation of ASS1 has not been described fully in PTECs and in addition, the role ASS1 may play in PTECs has not been investigated in the setting of tubular injury and fibrosis. This chapter will characterise the expression of ASS1 in an *in vitro* cell model and will assess how ASS1 transcription and translation are affected in a fibrotic or inflammatory environment.

3.5.5 RPTEC/TERT1 cells provide an improved model for investigating tubular epithelial cell biology

In vitro cell models of tubular epithelial cells have been used extensively to investigate the mechanisms of renal fibrosis, including, HK-2 cells, HKC8 cells, IRPTC and NRK-52E cells. Cell lines can be derived from many species including, human, rat and pig. Cell lines are immortalised by different methods including immortalization by HPV-16 (human papilloma virus-16) transformation, SV40 (adeno-12 simian virus-40) transformation and also by spontaneous immortalization in the case for NRK-52E cells (133). *In vitro*

models are an invaluable tool to assess how renal cells behave in pathological environments. They allow manipulation with drugs as well as biological mediators to elucidate ongoing mechanisms that would be impossible to tease out *in vivo*. However, these *in vitro* cell models have some caveats. *In vitro* models are reductive and do not address the complex interactions that exist between tubular epithelial cells and other cell types such as endothelial cells and cells of the interstitium. Additionally, *in vitro* cell lines often do not demonstrate features of tubular epithelial cells *in vivo* such as ability to polarise, expression of primary cilia and an ability to transport electrolytes (133). Newer *in vitro* models are necessary in order to better model tubular physiology.

RPTEC/TERT1 cells are an *in vitro* model derived from healthy human renal proximal tubular epithelial cells (RPTECs). The RPTEC/TERT1 cell line has been immortalized and made suitable for tissue culture using the human telomerase reverse transcriptase subunit (hTERT) (134). RPTECs are a relatively new cell model and have been used to great success in the field of nephrotoxicity testing (135-137). Additionally, several research groups have been adopting RPTEC/TERT1 cells in place of other *in vitro* tubular epithelial models due to their ability to retain true tubular characteristics. These include the ability to form 3 dimensional tubular structures (138), presence of primary cilia, their ability to transport electrolytes (133) and their ability to endocytose albumin (134). In this chapter, RPTECs will be utilised to investigate the role of ASS1 within proximal tubular epithelial cells.

3.5.6 Metabolic activity of proximal tubular cells

As covered previously in section 1.1.7 metabolic dysfunction is an important pathological event in the progression of tubular injury and subsequent renal fibrosis. Several measures can be used to infer mitochondrial activity *in vitro* such as mitochondrial number and ATP production. However, an improved technique to assess cellular respiration is direct assessment of oxygen consumption rate (OCR) to assess mitochondrial respiration and assessment of extracellular acidification rate (ECAR) to measure glycolytic ATP production. This technique is made possible by the Seahorse XFe Analyser which enables these measures to be made in a 96-well format in real time. Additionally, the Seahorse Analyser allows injection of drugs which manipulate mitochondrial function during OCR and ECAR measurements. In this way, specific questions regarding basal respiration, ATP-linked respiration, maximal respiration and

proton leak can be addressed. The Seahorse Analyser has been successfully adopted as a method for measuring cellular respiration in HK-2 cells as well as isolated podocytes (64,139,140). This chapter will include data generated by the Seahorse Analyser from the more physiologically accurate RPTEC/TERT1 cell model.

3.5.7 Transforming growth factor β signalling in proximal tubular epithelial cells

Transforming growth factor beta (TGFβ) is known as the classical pro-fibrotic cytokine for which the signalling pathway is described in sections 1.1.5 and 1.1.10. TGFβ has long been known to elicit pro-fibrotic effects on fibroblasts, however, its effects in tubular epithelial cells are yet to be fully understood. As the extent of tubulointerstitial fibrosis is the best histologic predictor of CKD severity, the role that tubular cells play in the development of fibrosis warrants investigation. The effects of TGFβ on tubular epithelial cells has been investigated extensively in primary tubular epithelial cells, HK-2 cells and NRK-52E cells. Upon stimulation with TGFβ, epithelial cells undergo morphologic changes and adopt an elongated and spindle shape. Cell-cell contacts are lost and there is a marked rearrangement of the cytoskeleton (141). Additionally TGFβ treatment has been found to decrease albumin uptake in cultured immortalized rat proximal tubular cells which could account for proteinuria seen *in vivo* in models of renal disease and human CKD (142). TGFβ has also been found to promote apoptosis in TECs *in vitro* by p38 MAP kinase signalling, independent of canonical Smad signalling. This may be a mechanism whereby tubular atrophy occurs *in vivo (143).* Furthermore, TGFβ has been found to have an adverse effect on PTECs *in vitro* by impeding fatty acid oxidation and ultimately causing metabolic dysfunction (64). It is clear that TGFβ induces a deleterious effect on TECs with a compounding set of pathological intracellular effects. Characterising the effects of TGFβ signalling in RPTEC/TERT1 cells will be important to elucidate how a more physiologically relevant cell model responds pro-fibrotic signalling.

3.5.8 Tumour necrosis factor alpha in proximal tubular epithelial cells

Inflammation is an essential driver of renal fibrosis and tumour necrosis factor alpha (TNFα) is a central pro-inflammatory cytokine which has been shown to be increased in the circulation and urine of patients with CKD (144). TNFα is

known to stimulate proximal tubular cells *in vitro* and *in vivo* and has been reported to induce antigen presentation in PTECs as well as upregulating a number of chemoattractant proteins such as MCP-1 and ICAM1 which promote recruitment and adhesion of leukocytes (144,145). TNFα activates both TNF receptor I and TNF receptor II which propagate a number of intracellular processes. The canonical signalling pathway functions to activate the transcription factor NFκB which in the basal state is retained in an inactivated state in the cytoplasm by inhibitors of NFκB signalling. Once activated, NFκB exists as a homo- or hetero-dimer of NFκB subunits. There are 15 different possible combinations of 5 different subunits which bind to response elements on DNA and initiate transcription of a number of pro-inflammatory mediators (70). TNFα signalling also activates pro-apoptotic pathways and mitogen activated protein kinases (MAPK) which are responsible for a myriad of cell responses (146). TNFα is secreted by monocytes and macrophages but it also synthesized by resident renal cells including PTECs (147). In response to injury, PTECs are believed to produce TNFα and kick start inflammatory processes which are highly interlinked with fibrotic pathways.

TNFα has also been reported to exert effects on mitochondria and cellular respiration. TNFα has been shown to perturb mitochondrial respiration in hepatocytes as well as cardiomyocytes (148,149). TNFα is thought to increase oxidative stress and therefore cause mitochondrial damage. Dogs treated with etanercept (a TNFα inhibitor) demonstrated increased activity of mitochondrial enzymes and improved heart function in a model of heart failure (150). Furthermore TNFα was found to decrease basal mitochondrial respiration in cultured neuronal cells. Oxygen consumption rate was used to accurately measure aerobic respiration with a Seahorse Analyser (151). The effect of TNFα on mitochondrial respiration of PTECs has not been directly investigated. In this chapter I investigate the direct effects of TNFα treatment on RPTEC mitochondrial respiration to address this.

3.5.9 Ischaemic insult and hypoxia in proximal tubular epithelial cells

During the course of renal fibrosis, the normal tubular interstitium is replaced with fibrous deposits. This results in peritubular microvascular rarefaction and therefore decreased oxygen supply to tubules and resultant ischaemia. The exact mechanism whereby peritubular capillary loss occurs is not fully understood, however, an imbalance of pro- and anti-angiogenic factors may be

to blame. In patients with CKD, there is a negative correlation between capillary density and severity of fibrosis (152). In addition, PTECs have a high oxygen demand due to high ATP demand generated by oxidative phosphorylation (53). Hypoxia not only triggers pro-inflammatory and pro-fibrotic transcription by stabilisation of HIF1α but it also increases production of reactive oxygen species. Therefore investigating the effects of hypoxia on PTECs is an important part of tubular pathophysiology in the setting of renal fibrosis.

3.6 Aims and Hypothesis

As revealed by Chapter 3, ASS1 is lost in three models of renal fibrosis which all have differential aetiologies with fibrosis developing over different time courses. Therefore, I hypothesised that depletion of ASS1 within tubular epithelial cells was critical in the induction of renal fibrosis. However, in order to decipher how loss of ASS1 might lead to the promotion of fibrosis it was required that experiments were carried out *in vitro*. This would allow the elucidation of the potential fibrosis-driving mechanisms that may occur as a result of ASS1 depletion. As ASS1 is highly expressed in the proximal tubule, the cell line, RPTEC/TERT1 was adopted to further investigate the role that ASS1 plays in tubular epithelial cells.

The overarching aim of this chapter was to elucidate the mechanisms whereby loss of Ass1 in tubular epithelial cells may promote the development of renal fibrosis.

The individual aims of this chapter were as follows:

- Characterise the expression of ASS1 in RPTEC/TERT1
- Characterise the metabolic activity of RPTEC/TERT1 and how respiration is influenced by fibrotic and inflammatory stimuli
- Reveal the upstream modulators of ASS1 expression
- Investigate the effect of ASS1 depletion in RPTEC/TERT1 in the context of fibrosis

3.7 Results

3.7.1 Characterisation of human renal proximal tubular epithelial cells (RPTECs)

RPTECs have recently been adopted as an improved *in vitro* model when investigating proximal tubular epithelial cells. We investigated how RPTECs may vary depending on their proliferating vs differentiated state. Once split, RPTECs grow in colonies while proliferating before forming a monolayer. During the proliferation stage, cells adopt an elongated morphology. Once fully differentiated RPTECs begin to form domes which are an indicator of salt transport. Additionally, cells become more rounded and adopt the classical cobblestone morphology. Figure 4.1 A-B shows the morphological difference between proliferating and fully confluent RPTECs. The gene expression profile was assessed in both proliferating (3 days post-split) and fully confluent RPTECs (14 days post-split). Gene expression analysis was conducted in proliferating and confluent RPTECs. Two cell contact genes *CLDN2* and *OCLN* demonstrated increased expression in 14 day confluent cells compared to proliferating cells. *ASS1* mRNA expression was also increased in confluent RPTECs compared to differentiating cells. WNT7A, which is associated with proliferating cells, exhibited decreased expression in confluent cells compared to proliferating cells (Figure 4.1 C).

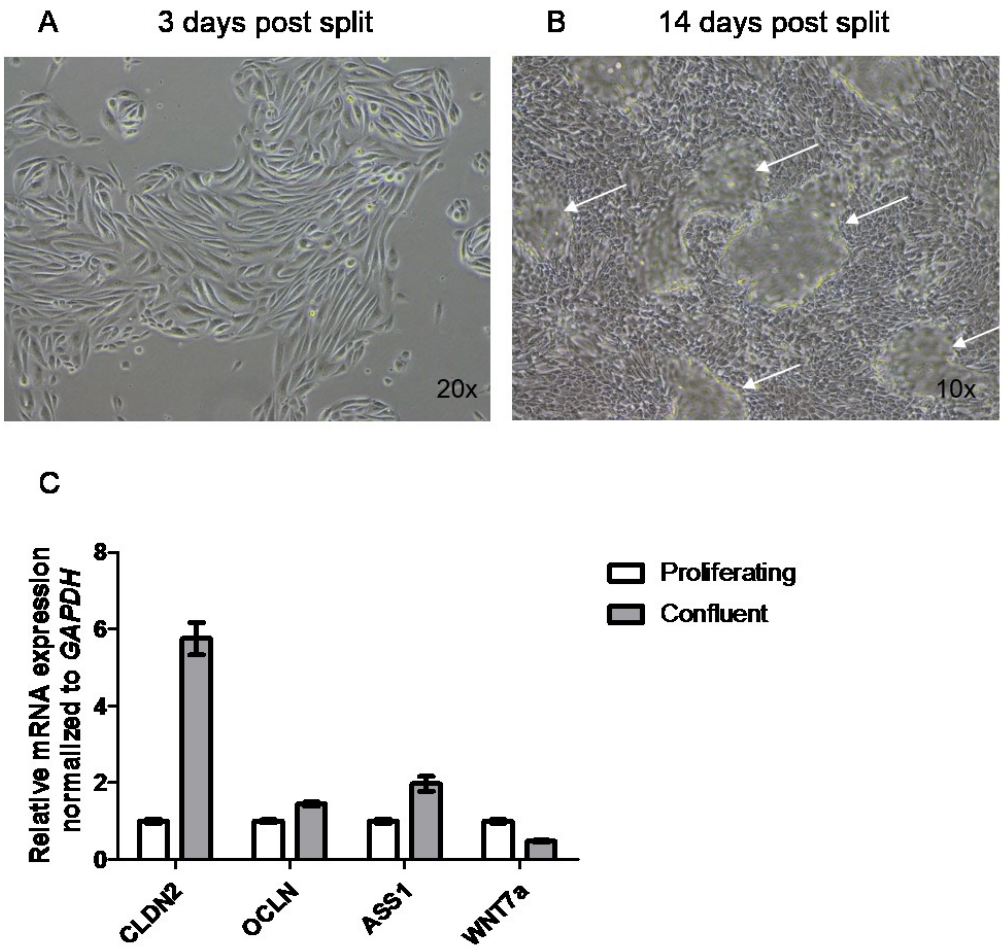

Figure 0.3: RPTEC/TERT cells in a proliferative and fully confluent state. (A, B) Representative bright field images of RPTECs grown for 3 days and 14 days in tissue culture taken at 20x (A) and 10x (B) magnification with evidence of dome formation (arrows). (C) Relative mRNA levels of *CLDN2*, *OCLN*, *ASS1* and *WNT7A* in RPTECs grown for 3 days (proliferating) and 14 days (confluent) in optimal cell culture conditions (n=2). Relative expression of mRNA in differentiating cells was calculated from ΔΔcT normalized to GAPDH housekeeper and compared to mRNA expression in proliferating cells.

3.7.2 Characterisation of intracellular ASS1 expression in RPTEC/TERT1

In order to discern the expression patterns of ASS1 within RPTECs, immunofluorescence was carried out to observe the subcellular localisation of ASS1 in proliferating and confluent cells. Figure 4.2 depicts ASS1 staining in cells fixed 3 days after seeding. ASS1 was stained in conjunction with nuclear stain, DAPI, and F-actin stain, Phalloidin. In proliferating RPTECs, ASS1 positive staining (green) was observed around the nucleus and in the cytoplasm. In actively dividing cells (Figure 4.2 D), ASS1 staining was observed to be surrounding spindle fibres.

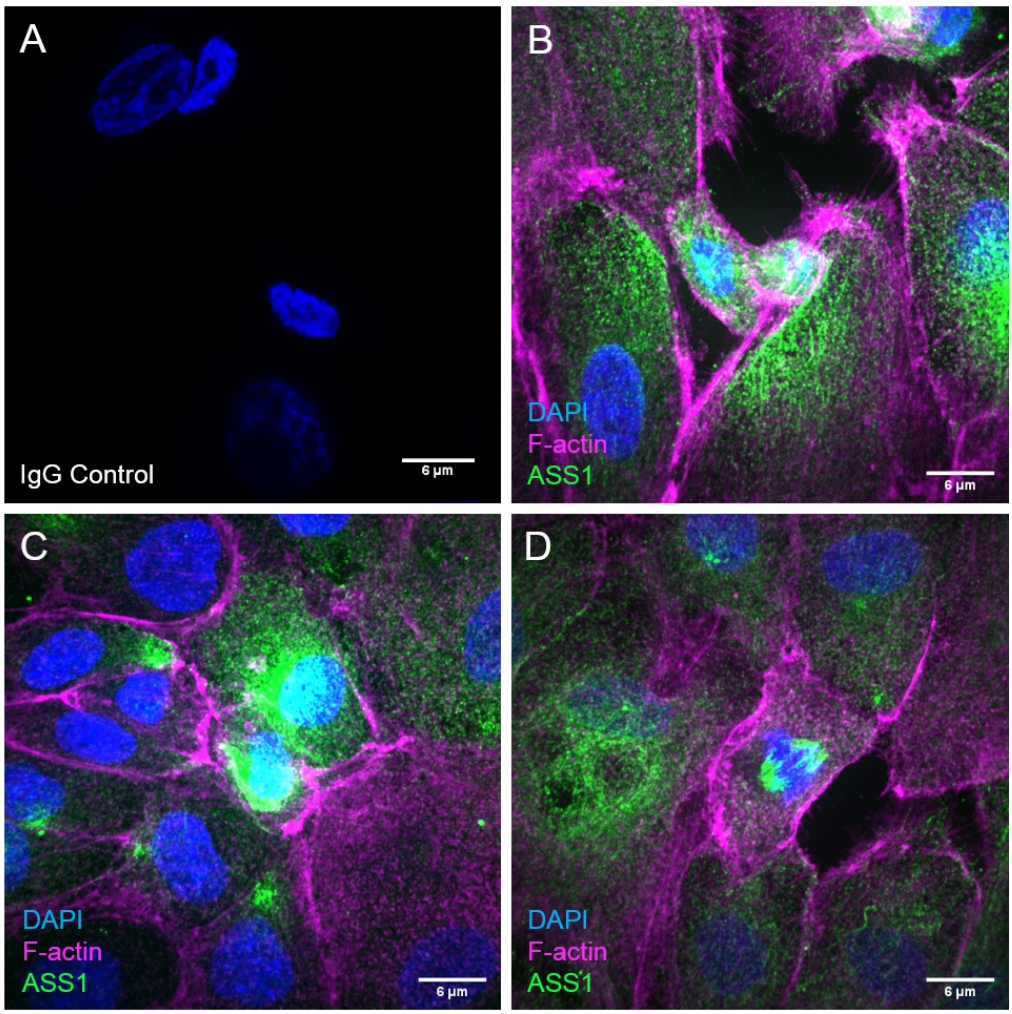

Figure 0.4: ASS1 expression in proliferating RPTECs. A selection of representative z-projected images of RPTECs stained for DAPI (nuclei in blue), F-actin (magenta) and ASS1 (green) taken at 100x magnification with a z-stack using the Andor Spinning disk microscope with IgG control (A). Images were analysed with ImageJ software.

In order to determine the expression pattern for ASS1 in differentiated RPTECs, cells were grown on filters for 14 days to ensure cells were fully differentiated and polarised. When grown on filters, RPTECs have been shown to polarise and microvilli are visible on the apical side of the cells. ASS1 immunostaining was carried out on differentiated RPTECs grown on filters. ASS1 staining was abundant within polarised RPTECs and it was present diffusely throughout the cytoplasm with evidence of punctate staining (Figure 4.3).

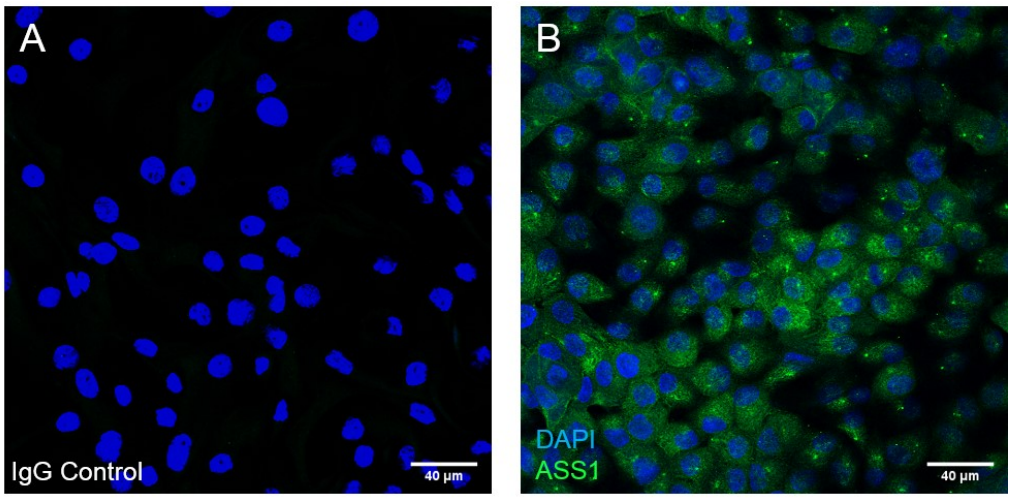

Figure 0.5: ASS1 expression in polarised, differentiated RPTECs. Representative image of RPTECs grown on filters to induce polarisation. Cells were stained for DAPI (nuclei in blue) and ASS1 (green) taken at 40x magnification with the Sp8 Confocal microscope with IgG control (A). Images were analysed with ImageJ software.

3.7.3 ASS1 staining does not co-localise with mitochondria

It has been reported that ASS1 is localised in the vicinity of mitochondria due to part of the urea cycle taking place within the mitochondria. However, this has not been investigated in proximal tubular cells. RPTECs were cultured until confluent and co-stained for ASS1 and live mitochondria. It was observed that ASS1 displayed cytoplasmic staining (green) with some positive staining present around the nucleus. Mitochondria demonstrated abundant positive staining (red) predominantly in the interior of the cell around the nucleus. ASS1 staining was evident in regions of the cell where mitochondrial staining was absent (Figure 4.4).

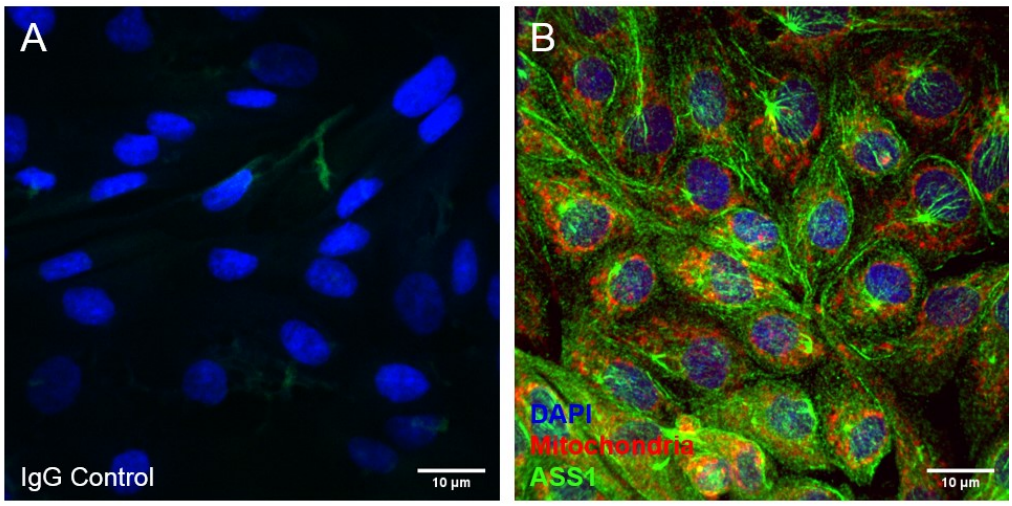

Figure 0.6: ASS1 and mitochondrial expression in RPTECs. A representative z-projected image of RPTECs (B) stained for DAPI (nuclei in blue), mitochondria (red) and ASS1 (green) taken at 60x magnification with a z-stack using the Andor Spinning disk microscope with IgG control (A). Images were analysed with ImageJ software.

3.7.4 RPTECs are highly metabolically active

As the kidneys and the proximal tubule in particular are highly metabolic, we assessed the metabolic activity of RPTECs to ensure they were a reliable cellular model for mirroring the physiology of the PT. The metabolic activity of the RPTECs was assessed using the XFe Seahorse Analyser which measures oxygen consumption and rate (OCR) and extracellular acidification rate (ECR), representing ATP-linked respiration and anaerobic respiration respectively. The Seahorse analyser allows the interrogation of specific components of ATP-linked respiration using a MitoStress test. Three drug treatments (oligomycin, FCCP and antimycin/rotenone) allow investigation of basal respiration, ATP-linked respiration, maximal respiratory capacity and proton leak. Using this technique can reveal how cells respire under different conditions.

Several preliminary experiments were conducted using the Seahorse Analyser to ascertain the optimal seeding density of RPTECs for each experiment as well as optimising the concentration of the drugs used during the MitoStress test.

RPTECs demonstrated an average basal OCR of 583.4523± 119.0912 pmol/min (normalized to protein content) when 100,000 cells were seeded the night before measures were taken under optimum conditions. A MitoStress Test was conducted in order to determine how these cells respire to produce

ATP. After optimisation of drug concentrations, 2 μM oligomycin was added to inhibit ATP synthase and block the production of ATP. Then 2.5μM Carbonyl cyanide-*p*-trifluoromethoxyphenylhydrazone (FCCP) was added to uncouple oxygen consumption from ATP production in order to assess maximal respiratory capacity. Finally, a 1μM mixture of Antimycin A and rotenone (A/R) was added to inhibit complexes I and III to attenuate mitochondrial respiration.

Treatment of RPTECs with oligomycin exerted a decrease in OCR from 583.45± 119.09 to 184.3± 68.5 pmol/min oxygen consumed. FCCP treatment increased the OCR substantially to 1105.7± 337.2 pmol/min and A/R abrogated respiration to 118.01± 48.02 pmol/min. Figure 4.5 And Table 4.1 summarise the biological relevance of these data.

Measure	**OCR (pmols/min)**
Basal respiration	463.5711
ATP-linked respiration	400.9968
Maximal respiration	960.1784
Proton leak	62.5743

Table 0.1: The oxygen consumption rate of RPTECs. Basal, ATP-linked and maximal respiration as well as proton leak were calculated from a MitoStress test carried out on RPTECs which had been seeded overnight.

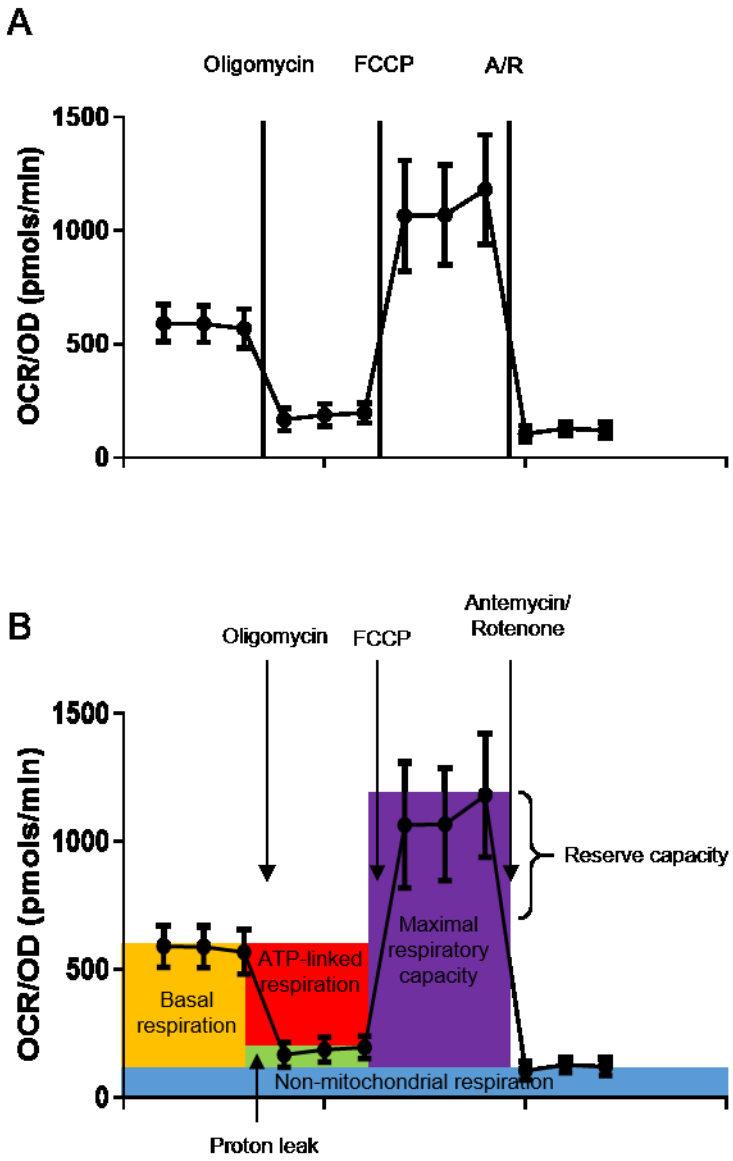

Figure 0.7: Effect of the MitoStress test on the oxygen consumption rate of RPTECs. RPTECs were seeded on to Seahorse XFe 24 well plates and left overnight. The oxygen consumption rate of RPTECs was measured using the Seahorse XFe analyser (4 replicates). Additionally, a MitoStress test was carried out using 2μM oligomycin, 2.5μM FCCP and a 1mM mixture of antimycin A and rotenone. Oxygen consumption rate was normalized to protein content of cells, measured by SRB assay.

During the MitoStress test the extra-cellular acidification rate (ECAR) was also measured to assess anaerobic respiration. Upon treatment of oligomycin the ECAR increased from 113.12± 11.45 to 254.1±27.75 mpH/min. This increased ECAR was unchanged with FCCP and decreased slightly with A/R treatment (Figure 4.6).

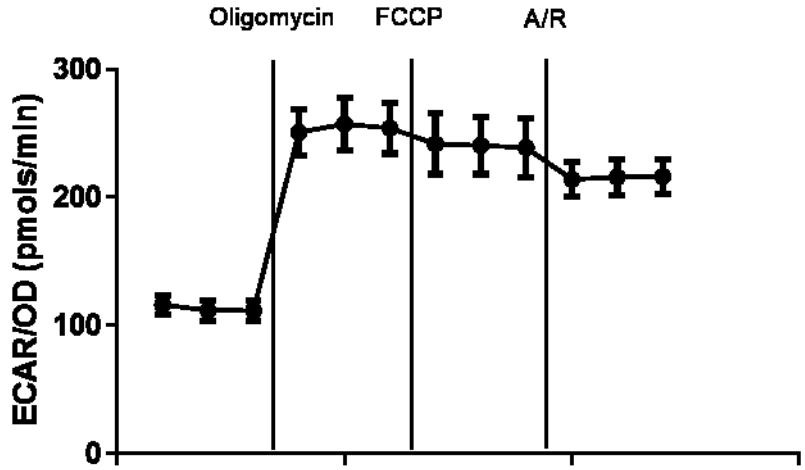

Figure 0.8: Extracellular acidification rate of RPTECs. RPTECs were seeded on to Seahorse XFe 24 well plates and incubated overnight. The extracellular acidification rate of RPTECs was measured using the Seahorse XFe analyser (4 replicates). Additionally, a MitoStress test was carried out using 2μM oligomycin, 2.5μM FCCP and a 1mM mixture of antimycin A and rotenone. Extracellular acidification rate was normalized to protein content of cells, measured by SRB assay.

3.7.5 Upstream mediators of Ass1 expression

As *Ass1* was found to be downregulated in three models of renal fibrosis we sought to elucidate which upstream signalling molecules may be responsible for depletion of *Ass1* expression *in vivo*. A number of factors have been reported to contribute to the progression of fibrosis including molecular signalling cytokines such as TGFβ and TNFα as well a physical drivers such as hypoxia. By reflecting the fibrotic environment seen *in vivo* using cell models, we could ascertain which upstream mediators impact *Ass1* expression.

3.7.6 Transforming growth factor beta induced a fibrotic phenotype in RPTECs without influencing *ASS1* expression

TGFβ is described as the classical fibrotic cytokine that predominates in CKD. RPTECs were treated with increasing doses (5, 10, 20 and 50ng/mL) of recombinant TGFβ for 72 hours in order to assess which dose induced a fibrotic phenotype. *COL1A1* and *TGFBR1* mRNAs were adopted as markers of TGFβ stimulation. Both markers were significantly upregulated compared to control cells with all concentrations of TGFβ apart from the highest concentration (50ng/mL). 10ng/mL was the dose carried forward and used in subsequent TGFβ stimulation experiments (Figure 4.7A). Subsequently, RPTECs were

stimulated with 10ng/mL TGFβ for varying durations of time: 24, 48, 72 and 120 hours. *COL1A1* mRNA was used as a marker of TGFβ signalling and its expression was determined at each time point. *COL1A1* expression was significantly upregulated at all time points compared to control. 72 hours treatment induced a significantly higher expression level of *COL1A1* compared to 120 hours TGFβ stimulation so 72 hours was the time point assessed in subsequent experiments (Figure 4.7B).

The morphology of the cells were assessed using a light microscope. Stimulated cells adopted an elongated phenotype and cells appeared to lose contacts with one another (Figure 4.7C). RPTECs responded to 10ng/mL TGFβ stimulation for 72 hours by upregulating transcription of a number of fibrotic genes such as *COL1A1, COL4A1, MMP2* and *MMP9* compared to control ($p<0.01$, Mann Whitney test, Figure 4.7D).

After confirmation of a fibrotic phenotype in RPTECs, the expression of *ASS1* was assessed. However, there was no significant difference in the expression level of *ASS1* in TGFβ stimulated cells compared to control cells ($p=0.62$, Mann Whitney test, Figure 4.7E).

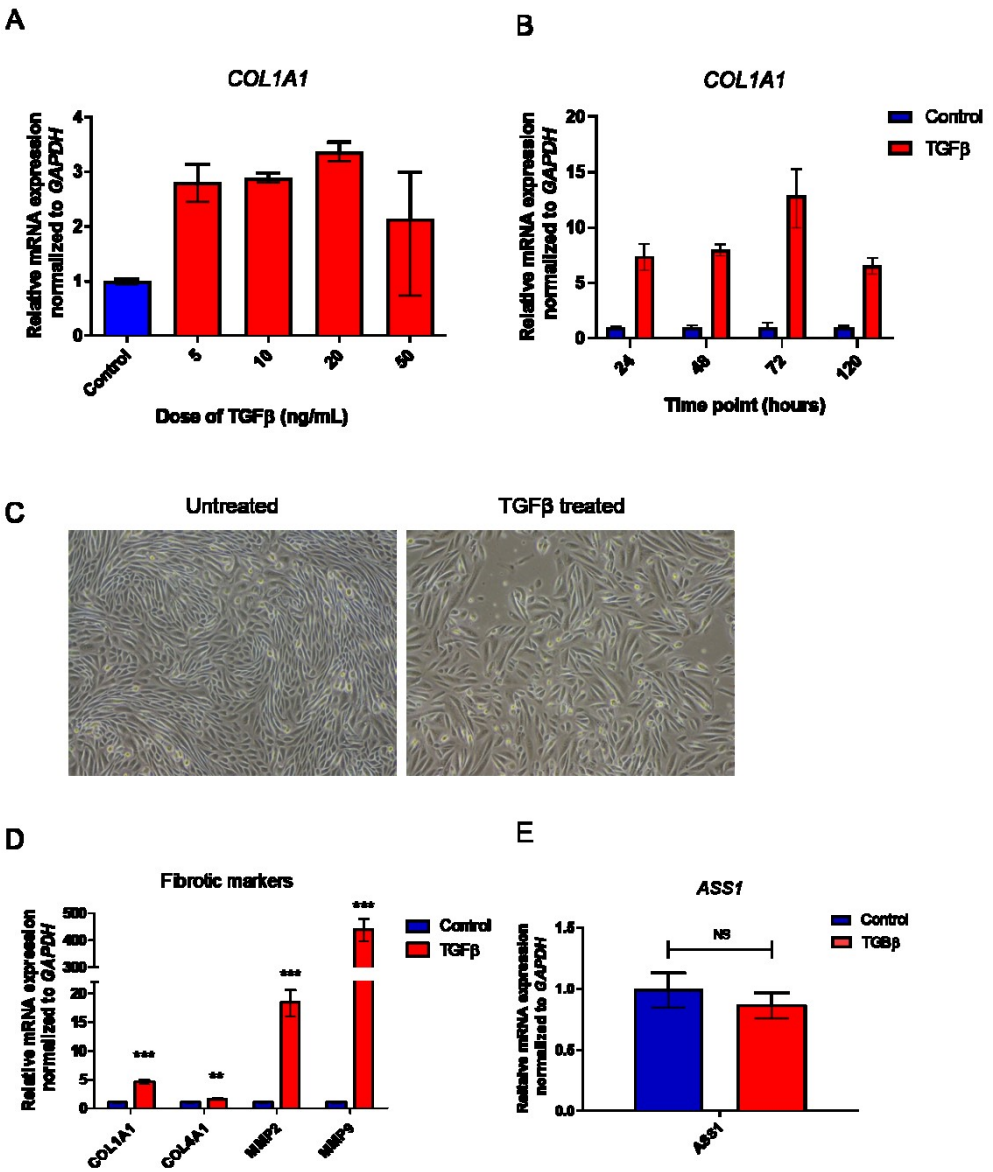

Figure 0.9: Effect of TGFβ stimulation on RPTECs Relative mRNA expression of *COL1A1* mRNA in RPTECs stimulated with TGFβ at increasing doses (A) and increasing length of stimulation (B) compared to control (both n=1). (C) Representative bright field images of untreated RPTECs and TGFβ treated RPTECs taken at 10x magnification. (C) Relative mRNA levels of genes related to fibrosis in RPTECs stimulated with 10ng/mL TGFβ for 72 hours (n=3). (D) Relative expression of *ASS1* expression in RPTECs stimulated with 10ng/mL for 72 hours (n=3). Relative expression was calculated from ΔΔcT normalized to *GAPDH* housekeeper and compared to sham. ** and *** represent p<0.01 and 0.001 respectively compared to control measured by Mann Whitney test.

3.7.7 TGFβ treatment alters the metabolic profile of RPTECs

Subsequently we investigated the effect of TGFβ treatment on the OCR and ECAR in RPTECs to assess its potential actions on metabolic activity. Kang and co-workers found TGFβ treatment to decrease the respiration rate of a

human tubular cell line (64). We sought to assess whether the same effect was seen in human RPTECs.

RPTECs were treated with 10ng/mL TGFβ for 72 hours. Their response to a MitoStress test was assessed and compared to cells kept in control media. Cells treated with TGFβ showed no significant difference in their baseline OCR before stimulation with drugs compared to control media. Furthermore, there were no significant differences in either group upon stimulation with oligomycin (ATP-linked respiration). However, with FCCP treatment, TGFβ stimulated cells exhibited a significant decrease in OCR compared to control media. Antimycin/Rotenone abolished respiration equally in all experimental groups (Figure 4.8). TGFβ stimulation significantly decreased the maximal respiratory capacity of RPTECs compared to control media ($p < 0.01$, Mann-Whitney Test) however, TGFβ did not significantly influence any other parameters of respiration.

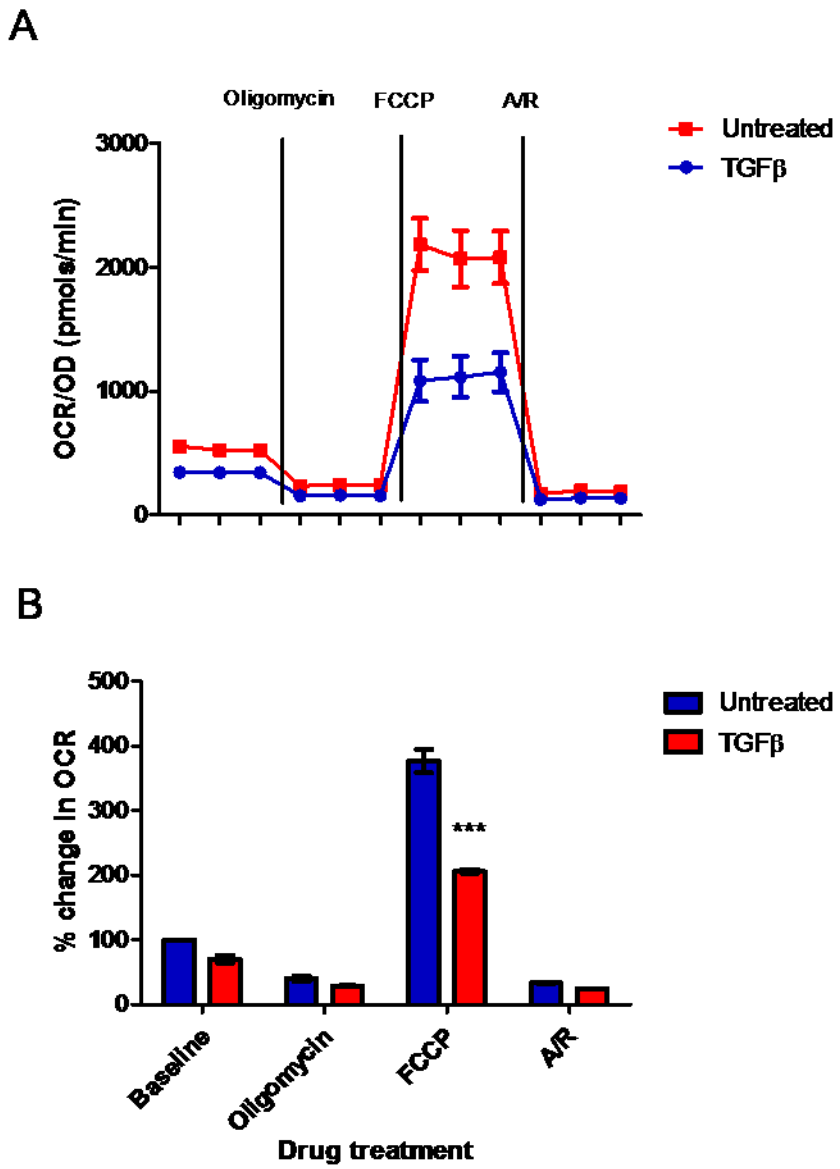

Figure 0.10: Effect of TGFβ on the metabolic activity of RPTECs. (A) Representative trace of oxygen consumption rate of RPTECs stimulated with 10 ng/mL TGFβ or left untreated for 3 days. Where indicated oligomycin (2μM), FCCP (2.5μM) and antimycin/ rotenone (1μM) were added. OCR was measured using the Seahorse XFe analyser and normalized to protein content measured as optical density from SRB assay. (B) Percentage change of OCR in RPTECs in response to drug treatment (n=3). *** represents $p<0.001$ compared to control media, Mann-Whitney test.

3.7.8 TNFα stimulation of RPTECs induced downregulation of ASS1 expression

As TGFβ was found not to effect *Ass1* expression, the promoter region was investigated to elucidate potential transcription factor binding sites in order to reveal upstream mediators that affect transcription of *Ass1*. After running the human *ASS1* promoter sequence through AliBaba 2.0, an online tool for

transcription factor binding predictions, I found two potential NFκB binding sites. Therefore RPTECs were stimulated with TNFα, which initiates the NFκB inflammatory signalling cascade. RPTECs were treated for 72 hours with 10, 20 and 40ng/mL TNFα and gene expression assessed by qPCR. *ASS1* mRNA expression was dampened by TNFα stimulation in a dose-dependent manner. The dose of 20ng/μL was used for subsequent experiments. At this concentration, with n=3, *ASS1* expression was found to be significantly depleted. Additionally, the expression of its neighbouring enzyme *ASL* exhibited no significant change in expression after TNFα treatment. Finally, *ICAM1*, a positive control for TNFα stimulation, was found to be significantly upregulated ($p<0.01$, Mann-Whitney test, Figure 4.9).

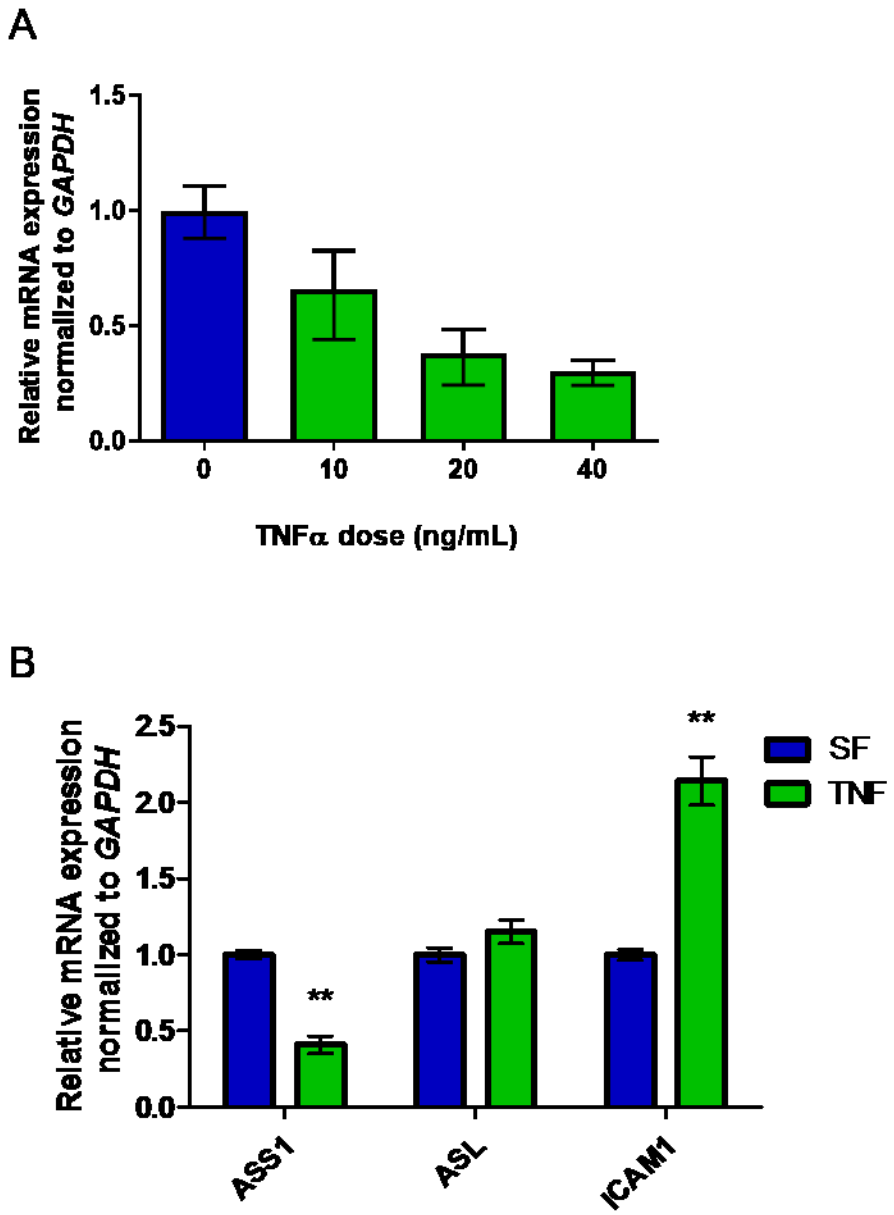

Figure 0.11: Effect of TNFα stimulation on RPTECs. (A) Relative mRNA levels of *ASS1* in RPTECs stimulated with TNF at increasing doses (10, 20 and 40ng/mL) (n=1 with 3 technical replicates) (B) Relative mRNA levels of *ASS1, ASL* and *ICAM1* in RPTECs stimulated by 20ng/mL for 72 hours (n=3). Relative expression was calculated from ΔΔcT normalized to GAPDH housekeeper and compared to sham. ** represents 0.01 respectively compared to control measured by Mann-Whitney test.

3.7.9 TNFα exerts no respiratory changes in RPTECs

We sought to investigate whether TNFα influences the metabolic activity of RPTECs as stimulation with TNFα induced a depletion of Ass1 which is a metabolic enzyme. Furthermore, TNFα has previously been shown to affect the mitochondrial activity of cardiomyocytes (153). RPTECs were treated with

20ng/mL TNFα or cultured in control media for 72 hours and a Mitostress test was carried out as before and the OCR was assessed. TNFα did not significantly alter the OCR of RPTECs compared to control conditions. Basal respiration, ATP-linked respiration, maximal respiratory capacity and proton leak were not significantly changed with TNFα treatment (Figure 4.10) (Mann-Whitney Test).

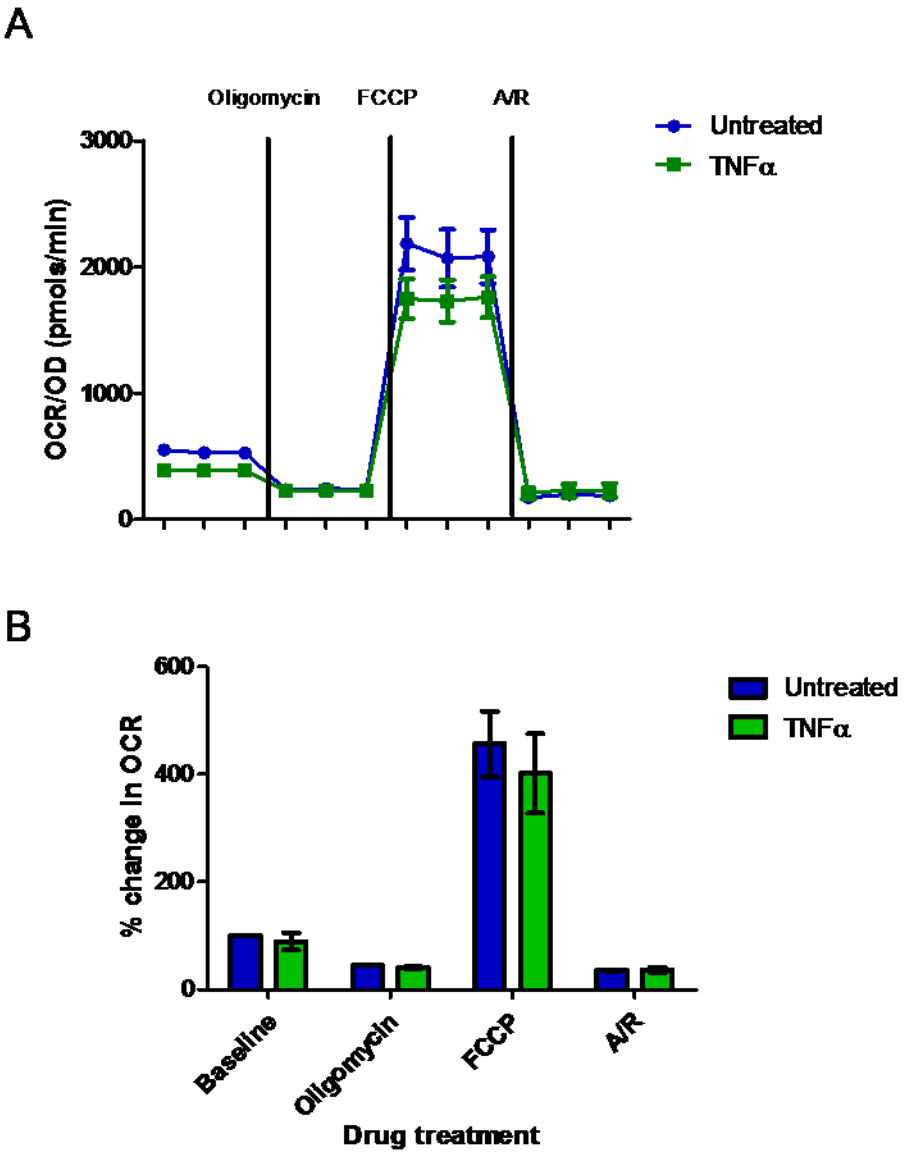

Figure 0.12: Effect of TNFα on the metabolic activity of RPTECs. (A) Representative trace of oxygen consumption rate of RPTECs stimulated with 20 ng/mL TNFα or left untreated for 3 days. Where indicated oligomycin (2μM), FCCP (2.5μM) and antimycin/ rotenone (1μM) were added. OCR was measured using the Seahorse XFe analyser and normalized to protein content measured as optical density from SRB assay. (B) Percentage change of OCR in RPTECs in response to drug treatment (n=3).

3.7.10 Hypoxic conditions induced downregulation of ASS1 expression

In the setting of fibrosis, secreted inflammatory and pro-fibrotic mediators induce changes to tubular epithelial cells. In addition to secreted mediators, tubules are subjected to an ischaemic environment due to microvascular rarefaction and insufficient blood supply to the renal cortex. These ischaemic conditions can be modelled *in vitro* by exposing RPTECs to a hypoxic environment using a hypoxic chamber.

In order to assess the effect of hypoxia on RPTEC phenotype and specifically ASS1 expression, RPTECs were maintained in a hypoxic chamber at 1% oxygen for 24 hours and compared to cells maintained in normoxic conditions. After exposure to these conditions, there was visible evidence of cell death in hypoxic cells compared to normoxic cells. Gene expression analysis was carried out by qPCR in both conditions. ASS1 gene expression was significantly downregulated in RPTECs exposed to hypoxia compared to normoxic cells ($p<0.001$) while its neighbouring enzyme ASL exhibited no significant change in transcription ($p=0.77$). Additionally, endogenous TNF mRNA expression was assessed which demonstrated a significant upregulation in expression compared to normoxic cells ($p<0.001$, Mann-Whitney test).

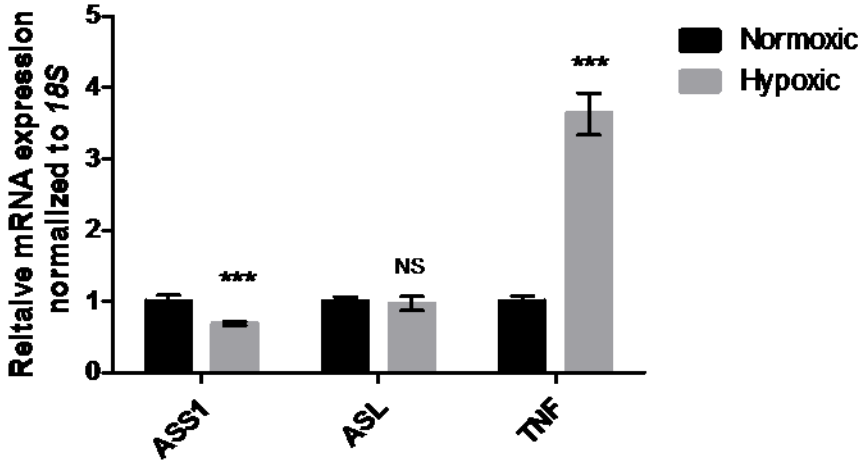

Figure 0.13: Effect of hypoxia on RPTECs. Relative mRNA levels of ASS1, ASL and TNF in RPTECs exposed to hypoxia (1% oxygen) for 24 hours (n=3). Relative expression was calculated from ΔΔcT normalized to 18S housekeeper and compared to sham. *** represents $p<0.001$ compared to normoxic control measured by Mann-Whitney test.

3.7.11 Knock-down of ASS1 in RPTECs

We sought to replicate our *in vivo* finding that ASS1 in lost in models of renal fibrosis *in vitro*. We transfected RPTECs with siRNA against ASS1 for 5 days and achieved 75% knock-down of *ASS1* mRNA vs scramble control which reached significance (Mann Whitney test, $p<0.001$). Western blot analysis demonstrated that ASS1 protein was also depleted (Figure 4.12). There was no observable difference in cell morphology or size in ASS1 knock-down cells compared to scramble control.

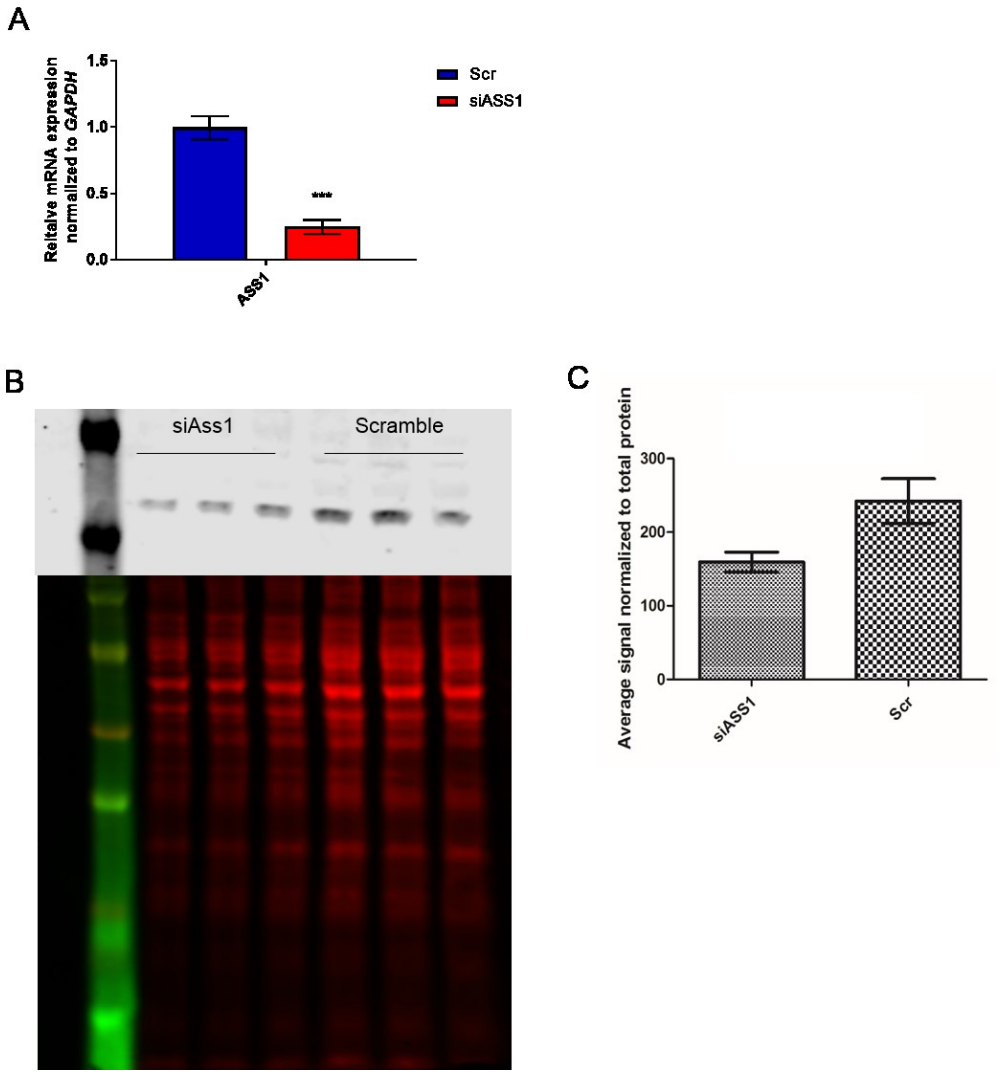

Figure 0.14: Knock-down of ASS1 in RPTECs. ASS1 was knock-down in PRTECs by transfection using stealth siRNA against ASS1 which was demonstrated by qRT-PCR (A) and Western blot (B) with ASS1 expression normalized to total protein and quantified using ImageStudio (C). Relative mRNA expression was calculated from ΔΔcT normalized to GAPDH housekeeper and compared to scramble control. *** represent $p<0.001$, Mann Whitney test.

In order to elucidate a mechanism whereby ASS1 loss may contribute to renal fibrosis, we assessed expression of a number of genes in knock-down vs scramble control which have been reported to be associated with renal fibrosis/ tubular injury/ de-differentiation (Figure 4.13). Firstly we assessed a number of fibrotic markers including *COL1A1, MMP2* and *TGFBR1* which all were significantly elevated in ASS1 knock-down RPTECs vs scramble control. Additionally, we assessed genes associated with cell-cell contacts including *CLDN2* and *OCLN.* Both genes demonstrated significant downregulation in ASS1 knock-down cells compared to scramble control (Mann-Whitney test, $p<0.001$).

As senescence is a hallmark of tubular injury we measured expression of p16 (*CDKN2A*) and p21 (*CDKN1A*). Increased expression of these genes is indicative of tubular senescence. However, siRNA mediated knock-down of ASS1 did not induce upregulation of either of these genes. In fact, p21 (*CDKN1A*) expression demonstrated significant downregulation in ASS1 knock-down cells compared to scramble control (Mann-Whitney test $p<0.05$).

As TNFα was shown to be an upstream mediator of ASS1, the expression of endogenous TNF from RPTECs was assessed in ASS1 knock-down RPTECs. *TNF* mRNA expression was found to be significantly depleted in RPTECs in siASS1 cells compared to scramble control. *ICAM1* and *CCL2* were also assessed as markers of an inflammatory response. *ICAM1* exhibited significant upregulation in ASS1 knock-down cells compared to scramble control while CCL2 exhibited significant downregulation in ASS1 knock-down cells compared to scramble control (Mann-Whitney test, $p<0.001$).

As ASL is the neighbouring enzyme of ASS1 in proximal tubular cells, the expression of ASL was measure in ASS1 depleted cells. There was no significant difference in ASL expression in siASS1 treated cells compared to scramble control (Mann-Whitney test, $p<0.001$). Finally, as HAVCR1 (kidney injury molecule 1) is used commonly as a marker of tubular injury, the mRNA expression of HAVCR1 was assessed in siASS1 RPTECs versus scramble control. However, the depletion of ASS1 had no impact on HAVCR1 transcription.

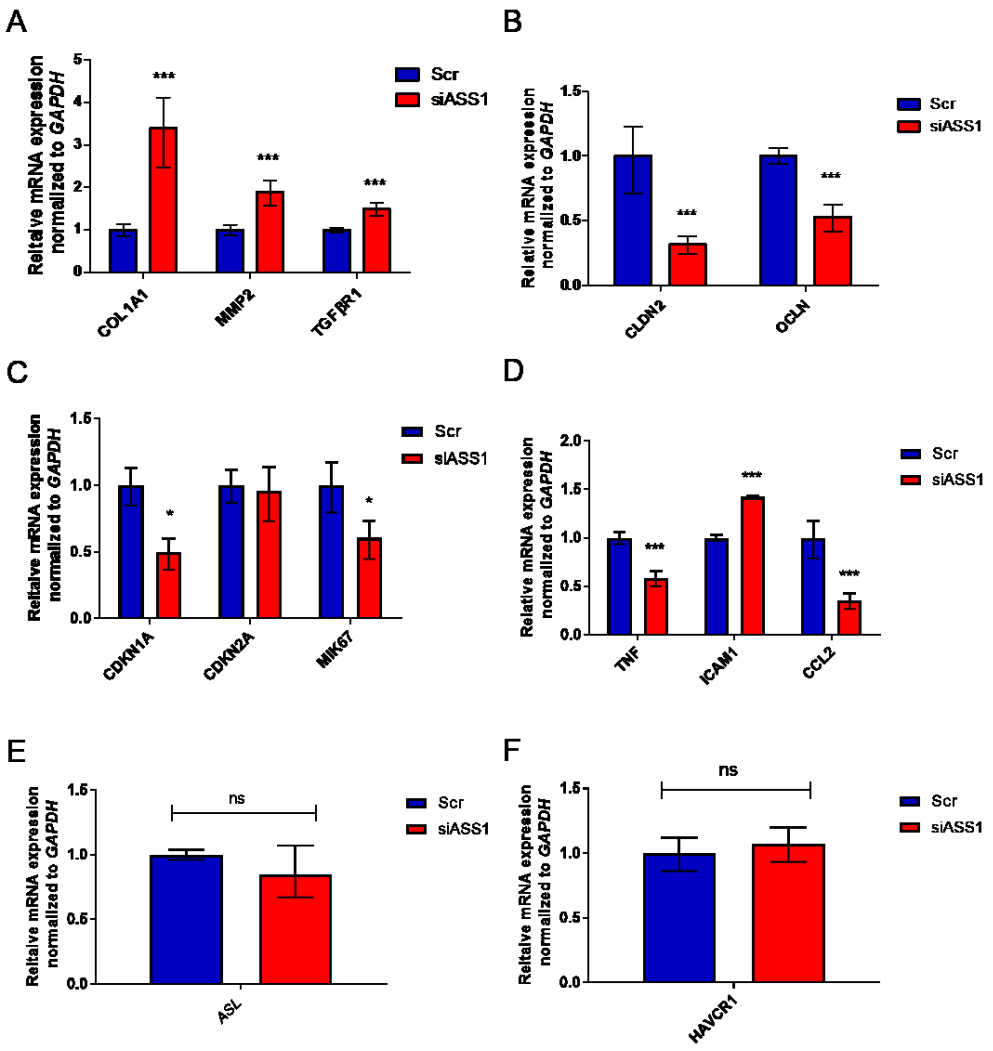

Figure 0.15: Downstream effects of Ass1 knock-down in RPTECs. Relative mRNA levels of fibrosis genes (A), cell-cell contact genes (B), senescence markers (C), inflammatory markers (D) *ASL* (E) and *HAVCR1* (KIM1) in RPTECs treated with siRNA against ASS1 (siASS1) and compared to scramble control (Scr) (n=3). Relative expression was calculated from ΔΔcT normalized to GAPDH housekeeper and compared to scramble control. * and ** represent p<0.05 and 0.01 respectively compared to control by Mann Whitney test.

3.7.12 Pharmacological inhibition of ASS1 with MDLA

Finally, I sought to reveal whether pharmacological inhibition of ASS1 activity exerted the same effects as genetic knock-down of ASS1. α-methyl-DL-aspartic acid (MDLA) is a drug known to inhibit the active site of ASS1 (154-156). RPTECs were treated with MDLA at a range of concentrations for 24 hours before gene expression analysis by qRT-PCR was carried out. *ASS1* and *ASL* expression were assessed to elucidate whether pharmacological inhibition of ASS1 led to a change in the transcription of either of these urea cycle enzymes. Both *ASS1* and *ASL* demonstrated a trend for increased mRNA

expression with increasing doses of MDLA. Subsequently, the expression of *COL1A1* was measured to assess whether inhibition of ASS1 activity led to the same upregulation of *COL1A1* mRNA seen after ASS1 knock-down. However, *COL1A1* demonstrated a trend for decreased transcription with increasing doses of MDLA (Figure 4.13).

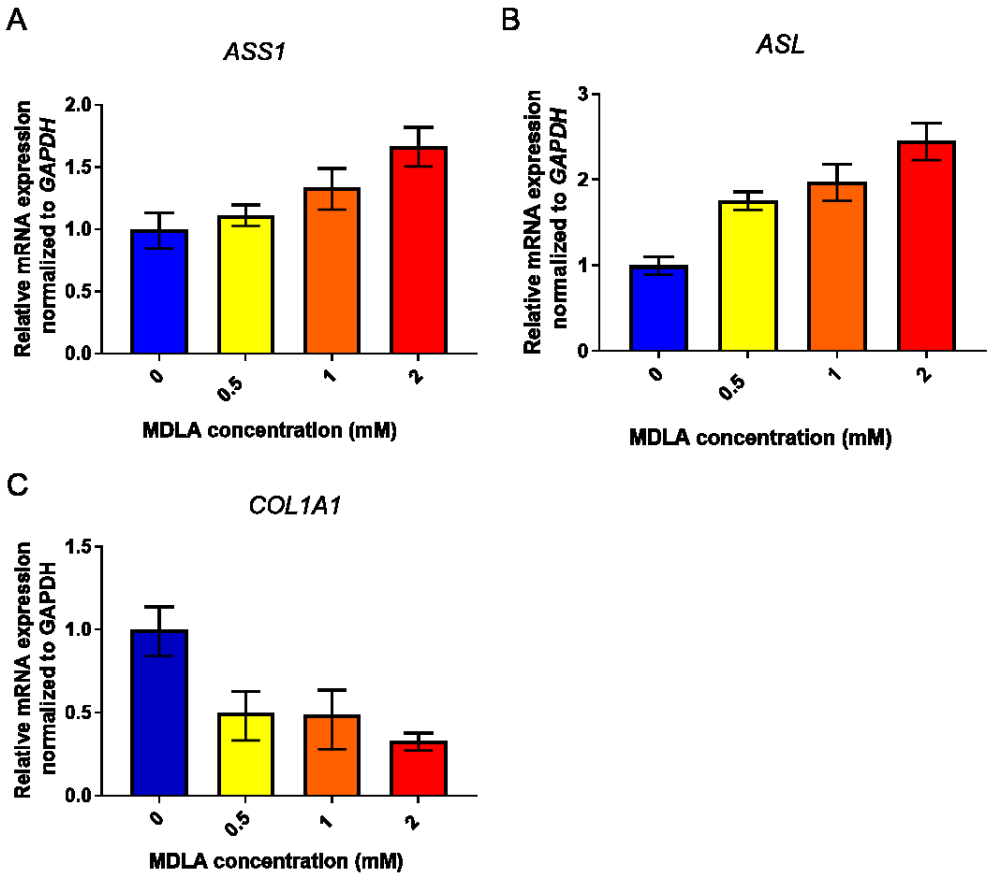

Figure 0.16: Effect of ASS1 pharmacological inhibition in RPTECs. Relative mRNA levels *ASS1* (n=2) (A), *ASL* (n=1) (B) and *COL1A1* (n=2) (C) were assessed in RPTECs treated with an ASS1 inhibitor, MDLA (α-methyl-DL-aspartic acid), at increasing doses (0, 0.5, 1 and 2mM) and compared to untreated RPTECs. Relative expression was calculated from ΔΔcT normalized to *GAPDH* housekeeper and compared to untreated cells.

3.8 Discussion

This chapter successfully utilised RPTEC/TERT cells to characterise the role ASS1 plays in human renal proximal tubular cells. I found that ASS1 is highly expressed in RPTEC/TERT cells and that its site of expression varies according to the proliferative state of the cell. It was revealed that TNFα stimulation and subjection to hypoxia resulted in the downregulation of *ASS1* mRNA expression. This demonstrates that TNFα and hypoxia are capable of mirroring what is seen *in vivo* (Chapter 3) by downregulating *ASS1* expression. However, the classical pro-fibrotic cytokine, TGFβ, did not influence the transcription of *ASS1* although it did induce a fibrotic response and reduce the maximal respiratory capacity of RPTECs. Finally, by recapitulating was is seen during fibrosis *in vivo*, ASS1 was successfully knocked-down in RPTECs. Depletion of ASS1 resulted in differential expression of a number of genes that are involved in the development of fibrosis. Genes known to upregulated in fibrosis included collagen, matrix metalloproteinases and the TGFβ receptor exhibited elevated expression. Conversely, genes involved in cell-cell contacts demonstrated downregulation. Depletion of ASS1 did not induce a senescent phenotype but these transcriptional changes could reflect a de-differentiated phenotype. Tubular de-differentiation is a well described event occurring during the onset of fibrogenic mechanisms. These transcriptional changes seen after ASS1 knock-down were not recapitulated by pharmacological ASS1 activity inhibition by MDLA. A schematic of my current working hypothesis for the mechanism of action of ASS1 in RPTEC is summarised in Figure 4.15.

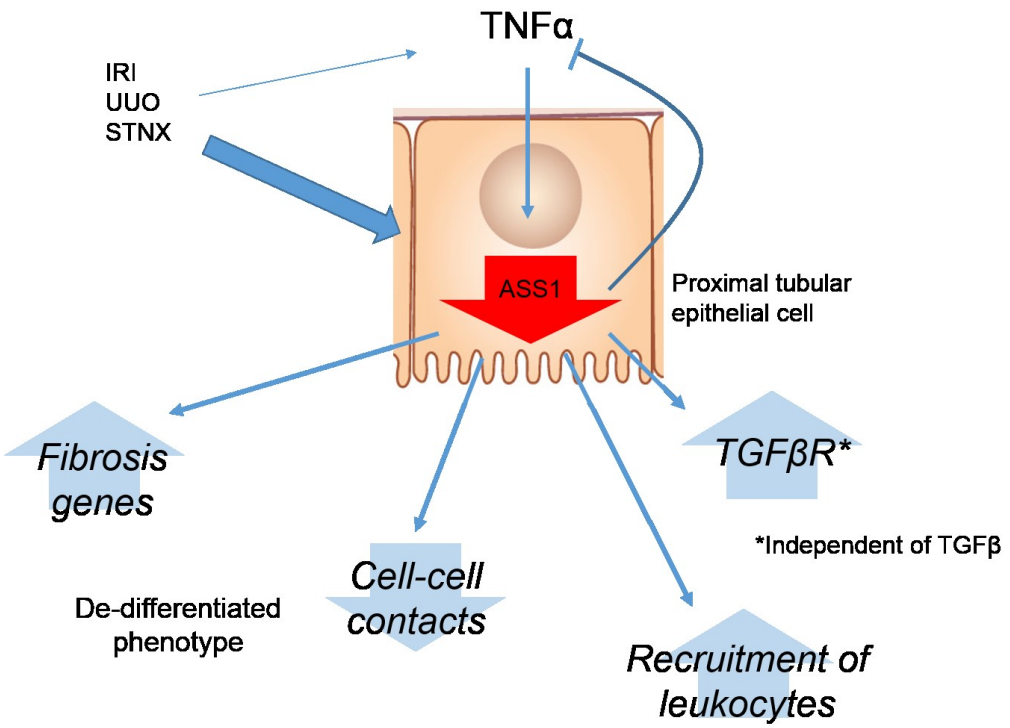

Figure 0.17: Schematic of hypothesised mechanism of action of loss of Ass1 *in vitro*.

RPTEC/TERT provided an ideal cell model for investigating the role that ASS1 plays in the proximal tubule *in vitro*. These cells are derived from human, therefore more relevant to patients than studying cells derived from rat or mouse. Although these are not primary cells, RPTECs retain many of the characteristics of proximal tubular epithelial cells seen *in vivo* (133,138,157). This chapter demonstrated that RPTECs were relatively slow growing and could be investigated in a proliferative state and a fully confluent state. RPTECs could be grown for at least 14 days as a fully confluent monolayer which expressed tight-junction genes and showed evidence of solute transport by the presence of domes. Presence of domes indicates that RPTECs are capable of active transport. HK-2 cells, which are another commonly used immortalized proximal tubule epithelial cell line, do not inherently have the ability undergo active ion transport which is evident by lack of dome formation in these cells (158). Therefore, RPTECs provide a more differentiated model of proximal tubular epithelial cells compared to HK-2 cells. As it is important to replicate as much tubular physiology as possible when using *in vitro* models and RPTECs provide a superior cell model. This chapter also demonstrated that RPTECs provide an excellent cell model for measuring oxygen consumption rate and

extra-cellular acidification rate. Here, RPTECs exhibited very stable measurements with treatment of oligomycin, FCCP and antimycin and rotenone. Many cells, such as HK-2 cells and HKC-8 cells not only exhibit less stable measurements throughout the run but they also demonstrate generally lower OCR values. (64,159). This indicates that RPTEC/TERT are much more metabolically active, which reflects what is seen in PTECs *in vivo (160)*. Furthermore, in this chapter, RPTECs demonstrated an ability to double their oxygen consumption rate after mitochondrial uncoupling by FCCP when seeded the night before which indicates that RPTECs have a large respiratory reserve. A similar pattern of OCR was seen by Secker and colleagues during their assessment of mitochondrial activity in RPTEC/TERT (161).

This chapter, for the first time, has described the subcellular localisation of ASS1 in human renal proximal tubular cells. Previously ASS1 intracellular expression in the kidney has been vaguely described as “cytoplasmic” (121). This study showed that ASS1 expression had differential subcellular expression dependent on the proliferative state of RPTECs. While proliferating cells exhibited strong perinuclear staining and staining adjacent to spindles during mitosis. However, differentiated cells showed diffuse staining throughout the cytoplasm. This provides evidence that ASS1 plays a different role in proliferating cells versus differentiating cells. Polarisation of RPTECs did not alter the expression pattern of ASS1 which remained cytoplasmic and did not favour the apical or basolateral side of RPTECs. Furthermore, unlike hepatocytes, ASS1 staining was not confined around mitochondria (162). This provides evidence that ASS1 could be playing a differential role in proximal tubular epithelial cells and hepatocytes.

Next we investigated the effect of pro-fibrotic and pro-inflammatory signalling on RPTEC respiration and ASS1 expression. TGFβ is known to induce a fibrotic response in tubular epithelial cells and is also known to decrease mitochondrial activity and respiration *in vitro (141)*. Here, RPTECs showed upregulation of a number of genes known to be elevated during fibrosis which is in keeping with other *in vitro* data (163). Additionally, here, it was demonstrated that TGFβ did not influence basal aerobic respiration but did markedly reduce the maximal respiratory capacity of RPTECs. It is known that TGFβ directly and indirectly influences respiration and ATP production in the kidney. TGFβ has been shown to abrogate fatty acid oxidation by targeting metabolic regulators such as *PPARGC* and also has a direct impact on mitochondrial biogenesis and ATP

production (64,164). This is in keeping with the TGFβ mediated decrease in reserve respiratory capacity seen in the chapter. A depleted spare respiratory capacity indicates that cells have a decreased ability to increase their ATP production under times of stress or increased energy demand. This could be as a result of decreased mitochondrial number or decreased mitochondrial complex activity. There is a link between a higher spare respiratory capacity and enhanced survival and resistance to hypoxic injury (165). Therefore, in RPTECs, TGFβ-mediated reduction of spare respiratory capacity may sensitise cells to hypoxic injury. However, despite the fact that TGFβ induces fibrotic and metabolic changes within RPTECs there was no effect on *ASS1* expression after TGFβ stimulation. This indicates that *ASS1* transcription is not TGFβ dependent and *Ass1* depletion observed *in vivo* (chapter 3) must occur as a result of other signalling pathways.

Inflammation is another common pathology that exists in many human renal diseases and all the mouse models of renal fibrosis used in chapter 3 (66,166,167). TNFα levels are elevated during the progression of renal fibrosis in mice and patients (168). Pro-inflammatory signalling by TNFα activates the NF-kB signalling cascade which is a common feature of renal disease and fibrosis. During activation, NF-kB is released from its cytoplasmic anchor, IKK, which allows translocation to the nucleus and NF-kB-mediated transcription of the plethora of genes (169). Promoter analysis carried out here showed a likely NF-kB binding site in the ASS1 promoter which was confirmed by a dose-dependent inhibition of ASS1 transcription after 72 hours of TNFα stimulation in RPTECs. A link between ASS1 and TNFα has been recognised, however, previous studies have found TNFα stimulation to upregulate ASS1 transcription (170). This effect was seen in ovarian cancer cell lines and no investigation until now has investigated how TNFα and ASS1 interrelate in the kidney. It is unusual that TNFα stimulation caused a downregulation in transcription as NF-kB is normally associated with an induction of inflammatory gene transcription such as ICAM1 (171). However, NF-kB subunits have been implicated as transcriptional repressors in different settings. The p65 subunit of NF-kB was found to be a potent inhibitor of gastrin transcription *in vitro*. Chromatin immunoprecipitation (chIP) revealed the presence of histone deacetylase 1 and NF-kB p65 with nuclear corepressor on the gastrin promoter. Together this complex was found to inhibit gastrin transcription (172). Other NF-kB subunit combinations have also been found to act as transcriptional repressors in the

setting of cancer with repression of anti-apoptotic gene transcription (173). Future experiments should be carried out using NF-kB inhibitors to confirm that ASS1 transcriptional repression is mediated by NF-kB subunits and not by non-canonical TNF induced pathways such as MAPK or JNK signalling (174).

The consequences of TNFα stimulation on RPTEC cellular respiration was investigated in this chapter. In previous studies, TNFα stimulation led to decreased basal respiration in neuronal cells in a dose-dependent manner as soon as 1.5 hours after first treatment (151). Additionally TNFα stimulation led to a decrease in basal, ATP-linked and maximal respiration of cardiomyocytes after 24 hours (175). The same was seen in primary proximal tubular epithelial cells which exhibited decreased basal and maximal respiration after TNFα treatment in a dose and time-dependent manner (176). Conversely, in this chapter, TNFα did not exert significant inhibitory effects on basal or maximal respiration as measured by OCR. However, there was a small inhibitory effect that was not statistically significant. In future, subsequent experiments assessing the OCR of RPTECs should be assessed to elucidate if a larger "n" would lead to a significant result. Additionally, a higher dose of TNFα may be required in this cell model to induce a discernible decrease in respiration.

The final upstream stimulus assessed in this chapter was hypoxia. Hypoxia is a key feature of renal fibrosis and progressive renal disease due to microvascular rarefaction and metabolic abnormalities (177). In this chapter, 24 hours of hypoxia induced transcriptional repression of *ASS1* in RPTECs but did not affect the transcription of *ASL*. The main transcription factor responsible for hypoxia-mediated effects is *HIF1α*. The same has been seen in cancer cells. HIF1α was found to downregulate ASS1 expression by binding to an E-box in the proximal region of the promoter (178). Furthermore, HIF1α mediated repression of ASS1 expression is regulated by a clock protein; DEC1 (deleted in oesophageal cancer 1) (179). It is clear that transcription of ASS1 is controlled at many levels and its behaviour varies according to cell type. Future work should be conducted in RPTECs to elucidate exactly how TNFα and HIF1α exert their repressive actions on ASS1. Chromatin immunoprecipitation could be adopted to detect which transcription factors and inhibitors of transcription are bound to the ASS1 promoter during TNFα and HIF1α stimulation.

The final part of this chapter addressed the consequences of ASS1 loss within RPTEC/TERT. ASS1 knock-down was adopted to echo ASS1 depletion within tubular cells *in vivo*. Knock-down induced several transcriptomic changes within RPTECs which altered their phenotype. These effect were independent of depleted enzymatic activity of ASS1 but by knock-down of ASS1 protein. ASS1 depletion markedly induced *COL1A1* expression as well as *MMP2* and *TGFBR1* expression. These transcriptomic changes are similar to those seen after TGFβ stimulation of RPTECs which suggests RPTECs adopt a more de-differentiated, pro-fibrotic phenotype after ASS1 depletion. Additionally, increased expression of the *TGFBR1* indicates that RPTECs may become more sensitive to TGFβ stimulation after ASS1 knock-down. However, *HAVCR1*, the marker of tubular injury, was not upregulated in ASS1 depleted RPTECs (180). This suggests that although ASS1 knock-down cells demonstrate a pro-fibrotic phenotype, this phenotypic change has not led to an injurious response. Further experiments should be conducted to assess the effects of TGFβ stimulation on ASS1 knocked-down RPTECs. In this way, one could investigate whether the pro-fibrotic response of RPTECs to TGFβ is exacerbated after ASS1 depletion.

Further to this, cell-cell contact and tight junction genes were significantly depleted in ASS1 depleted RPTECs which is highly indicative of de-differentiation. ASS1 depleted RPTECs actually responded to trypsinisation by losing their adhesions more quickly than control cells. This indicates that ASS1 knocked-down cells have a less robust monolayer with fewer cell adhesions.

Cellular senescence is a common hallmark of tubular injury progressing to renal fibrosis and is an important mechanism driving CKD (46). Senescence, or permanent cell cycle arrest, is induced by DNA damage of as a result of oxidative and genotoxic stresses. Senescent tubular epithelial cells are resistant to apoptosis and often adopt a senescence associated secretory phenotype (SASP), whereby cells secrete pro-inflammatory and pro-fibrotic factors such as TGFβ, IL-1 and IL-6. Senescence in renal tubular cells is characterised by altered morphology as well as increased expression of cyclin dependent kinase inhibitors, p16 and p21. Additionally, as senescent cells have lost the ability to proliferate, they stop expressing markers of proliferation such as KI67 (181). In this chapter, I wanted to reveal whether ASS1 depletion in RPTECs led to induction of senescence. ASS1 depleted RPTECs demonstrated downregulation of KI67, suggesting that these cells have a lower

proliferative capacity compared to control cells. However ASS1 depleted RPTECs did not exhibit increased expression of either cyclin dependent kinase inhibitor, p16 (*CDNK2A*) or p21 (*CDKN1A*). In fact, p21 exhibited downregulation in ASS1 knocked-down RPTECs. These results are somewhat contradictory as ASS1 depleted cells have a decreased ability to proliferate but do not show signs of cell cycle arrest. Furthermore, ASS1 knocked-down cells did not exhibit a SASP phenotype are there was no evidence of increased *TGFB1* or *IL6* transcription. These results confirm that ASS1 knock-down in RPTECs does not induce a senescent phenotype but could have inhibitory actions on proliferation.

As TNFα was identified as an upstream modulator of ASS1 expression, I next sought to reveal whether knock-down of ASS1 induced a proinflammatory phenotype. As mentioned earlier, PTECs are capable of secreting a number of proinflammatory cytokines and expressing pro-inflammatory chemotactic and adhesion molecules which promote an inflammatory response and contribute to renal injury and fibrosis (182). Firstly, *TNF* mRNA transcription demonstrated downregulation in ASS1-depleted RPTECs. As recombinant TNFα induced a decrease in ASS1 expression it was interesting to see this reciprocal effect. This suggests that loss of ASS1 may exert a negative feedback loop with TNF signalling. Next, I wanted to investigate the effect of ASS1 knock-down on *ICAM1* and *CCL2* (MCP-1) expression. Both these cell surface molecules have been shown to be upregulated on tubular epithelial cells and promote the recruitment of immune cells which exacerbate renal injury and contribute to fibrosis (144). In ASS1 depleted RPTECs, *ICAM1* demonstrated upregulation while *CCL2* demonstrated downregulation compared to control cells. Moreover, as mentioned previously ASS1 knock-down did not induce the expression of IL-6. It appears that RPTECs which lack ASS1 do not exhibit many characteristics of a pro-inflammatory phenotype. However, ICAM1 upregulation is associated with increased tubular epithelial cell adhesion of lymphocytes whereas CCL2 upregulation is associated with recruitment of monocytes (71,171). This suggests that ASS1 depletion may promote tubular interactions with T-cells but not with monocytes. Increased ICAM1 expression has been reported in mouse models and *in vitro* models of renal disease which is associated with increased recruitment of T-cells *in vivo (183)*. Although understudied, T cells have been shown to play an important role in the progression of AKI to CKD (184). Furthermore, increased TEC adhesion of T

cells has been found to be an important underlying mediator of T cell mediated inflammation and renal injury after ischaemia reperfusion injury (185).

Data from chapter 3 indicated that ASL, the neighbouring enzyme of ASS1, demonstrated a similar pattern of expression to ASS1 in murine models of renal fibrosis. Furthermore, Erez and colleagues have reported ASS1 and ASL to exist in a protein complex with NOS3 in lung tissue (186). Here, ASL expression was measured in ASS1 knocked-down RPTECs to reveal whether loss of ASS1 induced the depletion of ASL. ASS1 knock-down did not influence ASL expression. Moreover, upstream ASS1 inhibitory stimuli, TNFα and hypoxia, had no effect on *ASL* transcription. While other studies conclude that ASS1 and ASL are inextricably linked, data from this chapter demonstrates differential upstream signalling between ASS1 and ASL which indicates, in tubular epithelial cells, ASS1 and ASL may play functionally distinct roles.

The final experiment of this chapter endeavoured to reveal whether inhibiting the active site of ASS1 pharmacologically exerted similar effects of depleting ASS1 protein levels. In this way we could reveal whether the disturbance of the amino acid, citrulline, was responsible for the downstream effects of ASS1 knock-down or whether absence of ASS1 protein itself induced these effects. Pharmacological inhibition of ASS1 activity by MDLA led to a dose dependent increase of *ASS1* and *ASL* transcription. This indicates that inhibition of citrulline-aspartate ligation by ASS1 led to an increase in citrulline and aspartate which resulted in upregulation of ASS1 and ASL to rectify the amino acid imbalance. MDLA has been shown previously to increase and decrease levels of citrulline and argininosuccinate respectively (187). In future, the levels of citrulline and aspartate as well as arginine should be assessed in the media of MDLA-treated RPTECs to confirm this effect in this cell type. Subsequently, the expression of *COL1A1* was assessed to determine if MDLA led to the marked upregulation seen after ASS1 knock-down. *COL1A1* was chosen as to test this hypothesis as it was the gene that was most markedly upregulated after ASS1 knock-down and it was very tightly negatively correlated with ASS1 expression. However MDLA treatment did not induce an upregulation of *COL1A1*. In fact *COL1A1* demonstrated evidence of downregulation after MDLA treatment. Although this experiment needs to be repeated once more in order to detect if any of these changes are statistically significant, it provides convincing evidence that inhibition of ASS1 activity does not exert the same effects as ASS1 knock-down.

The data from this chapter has confirmed that ASS1 is highly expressed in RPTECs and downregulation of transcription is achieved by both TNFα and hypoxia but not by TGFβ. TNFα and hypoxia are important hallmarks of renal fibrosis and their inhibitory effects on ASS1 expression mirror what is seen *in vivo.* Replicating ASS1 loss in RPTECs led to phenotypic changes that reflect a de-differentiated, pro-fibrotic cell with some capacity for pro-inflammatory signalling. Furthermore, these effects are independent of urea cycle amino acid disturbance. This project for the first time has elucidated loss of ASS1 in RPTECs may be important in linking proinflammatory and hypoxic signalling with a pro-fibrotic and de-differentiated cellular phenotype.

Chapter: 4 Chapter 5- Phenotype of *Ass1* tubular knockout mice

4.1 Introduction

4.1.1 Cre-lox system

Cre-lox technology is a widely used biological tool capable of deleting, inverting or translocating genetic material by utilising the ability of the Cre recombinase enzyme to recognise specific DNA sites, termed Lox. This genetic engineering technology has harnessed these tools from the bacteriophage P1. Cre recombinase functions to recombine two LoxP sites surrounding a specific portion of DNA (188). Cre recombinase can be adapted to serve different purposes including inducible Cre, promoter specific Cre and fluorescent Cre. Inducible Cre requires stimulation by a drug, often tamoxifen, in order to activate the enzymatic activity of Cre (189). Promoter specific Cre results in Cre only being expressed in cell types which express a specific promoter and thus Cre recombination only occurs in these cells. Finally, fluorescent Cre comprises a fluorescent tag fused to Cre which emits a signal upon successful activation of Cre and is used as a reporter (190). Floxed constructs include two LoxP sites flanking a region of genomic DNA. Design of these constructs can result in activation of Cre mediated gene expression, Cre-mediated gene knockout and also Cre-mediated gene switching. As DNA constructs can be easily introduced into the mouse genome in a heritable manner, the Cre-Lox system can now be used to great effect in transgenic mice by crossing a Cre expressing mouse with a mouse expressing LoxP flanked DNA of the desired target gene (191,192). The Cre-Lox system was employed in this project to allow tubular specific inducible knockout of *Ass1*.

4.1.2 Pax8 CreER^{T2} mouse

Several kidney specific Cre expressing mouse lines are used in renal research. As the kidney is composed of many different cell types, it is important to choose the Cre expressing mouse under the control of the correct promoter which will result in genetic manipulation in the correct cell type. For example, Cre activation under the regulation of the podocin promoter results in recombination occurring specifically in the podocytes of the kidney (193). Additionally, Cre

recombination occurs specifically in the collecting duct of the kidney with the aquaporin-2 Cre mouse line (194).

In this project, a tubular specific Cre expressing mouse was required and the Pax8-CreER^{T2} transgenic mouse was utilised. This transgenic mouse line was generated to use the Pax8 promoter to direct Cre recombination in tubules of the kidney. Pax8 is expressed in the proximal and distal tubules as well as the collecting duct, therefore Cre is expressed in all segments of the tubule. Additionally the Pax8-CreER^{T2} mouse is inducible by tamoxifen administration. To generate this mouse, a fusion protein of the Cre DNA sequence and a mutant form the oestrogen receptor (ER^{T2}) which only contains the ligand binding domain was constructed. This allows temporal control of Cre activation with the administration of a ligand which binds the oestrogen receptor: tamoxifen. Administration of tamoxifen triggers the release of bound ER^{T2} which then is translocated to the nucleus and initiates recombination. Inducible Cre is especially important to avoid targeting the gene of interest during development if the genetic knockout is embryonically lethal (189,195).

4.1.3 *Ass1* floxed mouse

Genetic manipulation of the *Ass1* gene has been adopted in several different mouse lines. Global genetic deletion of *Ass1* was achieved by disruption of exon 4 of the *Ass1* gene which resulted in 0% enzyme activity in the liver. Mice missing the *Ass1* gene survived gestation but did not live more than 2 days after birth due to citrullinemia and hyperammonemia. This mouse was generated to mirror what is seen in severe neonatal citrullinemia type I (CTLN1) (196). Other mouse lines with naturally occurring mutations have been investigated in the setting of CTLN1 including the *fold* mouse and the *bar* mouse. These *Ass1* hypomorphic mice display less severe symptoms compared to the global knockout and have been investigated to elucidate the mechanisms ongoing in patients with CTLN1 (197). The only available floxed *Ass1* transgenic mouse was generated by the Lamers group. They engineered LoxP sites to flank exon 13 of the *Ass1* gene. Non-recombined Ass1 flox/flox mice develop normally and exhibit no phenotype. However, upon recombination by Cre in intestinal enterocytes, Ass1 was entirely knocked out. This group showed that deletion of exon 13 of the Ass1 gene was sufficient to knock Ass1 out in the organ of interest (198).

Therefore, crossing the Pax8-CreER^{T2} mouse with the *Ass1* flox/flox mouse would result in knockout of *Ass1* specifically in the tubules of mice after tamoxifen administration. This would allow interrogation into the spatiotemporal role that *Ass1* plays within the tubular compartment of the kidney, while circumventing *Ass1* knockout in any other cell type or organ (Figure 5.1).

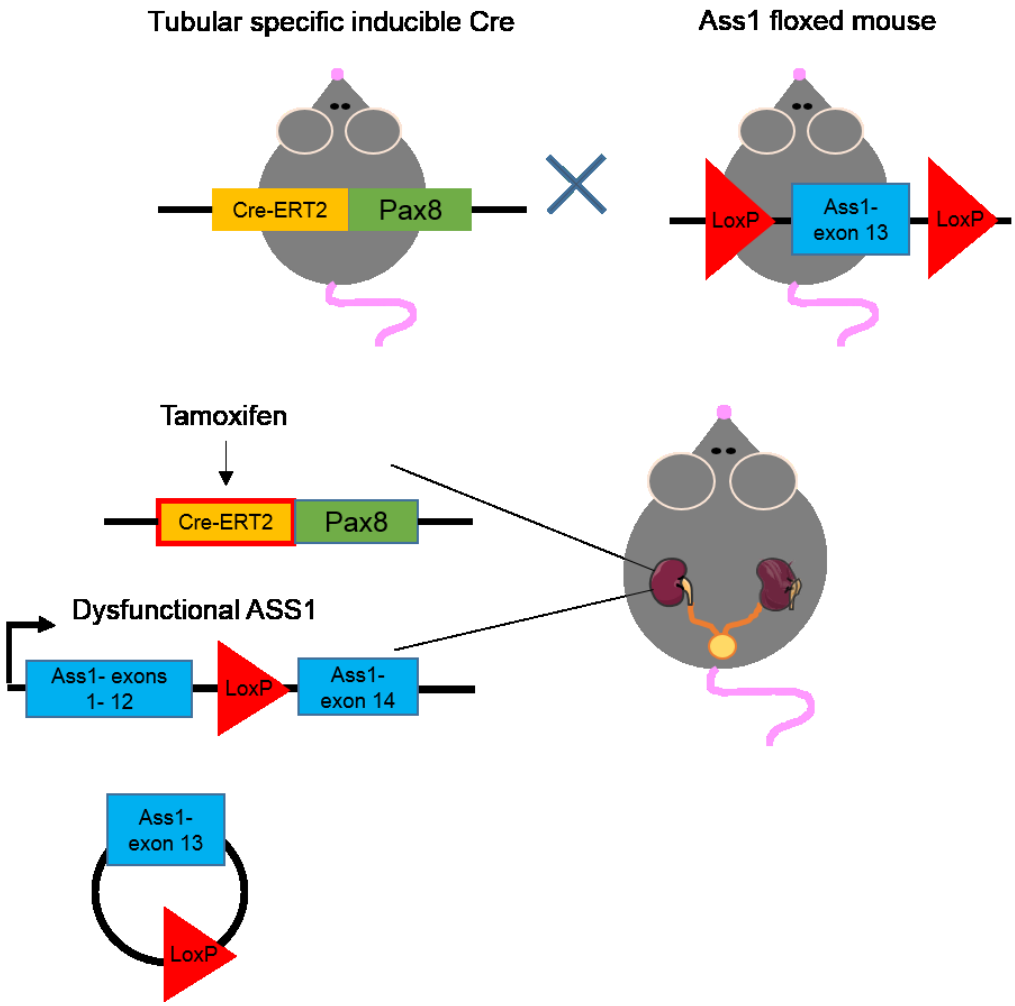

Figure 4.1: Schematic of Pax8CreERT2 and Ass1 flox/flox breeding to yield tubular knockout of Ass1 in the Pax8Cre x Ass1 fl/fl mouse

4.1.4 Ai14 tdTomato reporter mouse

It is important to confirm site-specific Cre recombination when using a specific promoter driven Cre mouse line. The Cre mouse in question should be crossed with a reporter mouse to allow detection of Cre recombination in the desired cell type only, without any off target expression (192). Reporter mice often express fluorescent proteins which are activated upon Cre recombination. The Ai14 tdTomato mouse is created using a construct with a LoxP flanked stop

codon upstream of the tdTomato reporter. Upon introduction into a mouse and recombination by Cre, the loxP sites recombine and the stop codon is excised. This results in constitutive activation of the tdTomato reporter (199). This red reporter can be visualised in tissue of interest using fluorescent activated cell sorting and immunostaining (Figure 5.2).

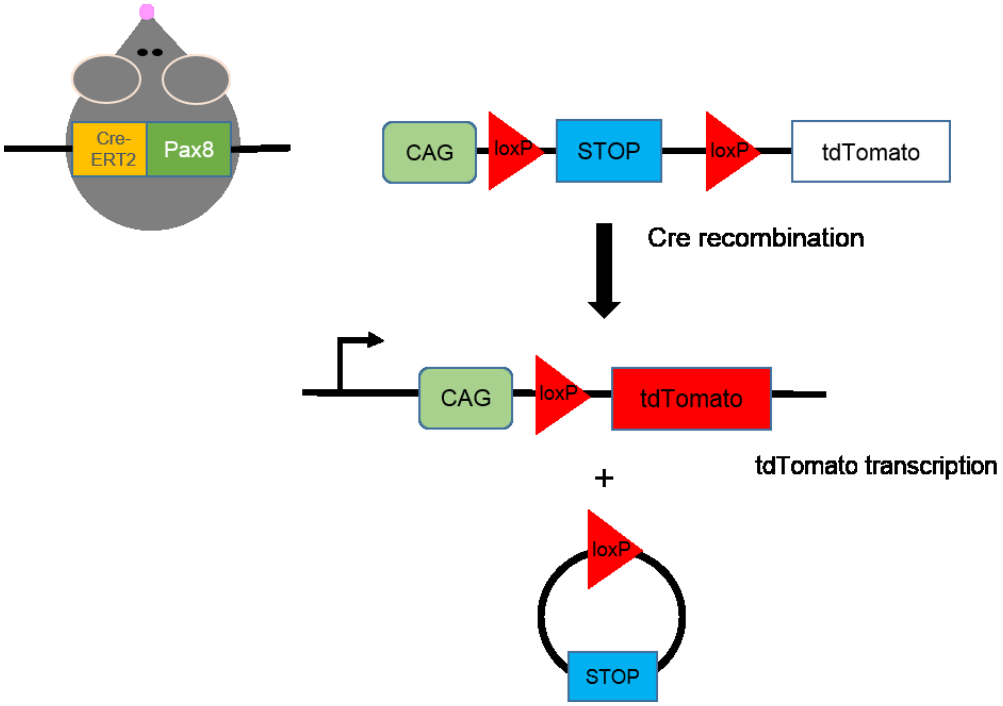

Figure 4.2: Schematic of Pax8CreERT2 cross with Ai14 mouse to yield Pax8 driven tdTomato reporter mouse

4.1.5 Asl$^{neo/neo}$ hypomorphic mouse

ASS1 and argininosuccinate lyase (ASL) are linked in the urea cycle and ASS1 provides arginine as a substrate for ASL. Argininosuccinate lyase deficiency or ASL-D is a heritable disorder which results in the enzyme, ASL, functioning incorrectly (see Section 1.1.15). The Asl$^{neo/neo}$ hypomorph mouse (*Asl* mutant) was developed to explore the phenotype of ASL-D while avoiding the neonatal lethality associated with *Asl* global knockout. These mice were developed by introducing a neomycin cassette into intron 9 of the murine *Asl* gene. This results in 25% residual mRNA, 25% residual protein and 16% enzymatic activity of ASL. These mice survive until 3 weeks of age before multi-organ failure ensues resulting in death. These mice display elevated circulating levels of argininosuccinic acid, citrulline and ammonia. *Asl* mutant mice display a number of pathological phenotypes affecting most organs. The renal

phenotype of these mice has not been extensively investigated however *Asl* mutants exhibit elevated blood pressure, decreased creatinine clearance and smaller glomeruli compared to wildtype counterparts (90,186). However, the tubular phenotype of these mice is relatively unexplored.

4.2 Aims and Hypothesis

The hypothesis of this Chapter was as follows:

Tubular specific deletion of *Ass1* using a transgenic mouse model will induce some degree of tubular dysfunction and fibrosis.

The aims of this Chapter are as follows:

- To ascertain if Ass1 is differentially expressed in the kidney of the $Asl^{neo/neo}$ hypomorphic mouse and if there is a renal phenotype in these mice.
- To validate the site-specific expression of Cre under the control of the Pax8 promoter within the tubular compartment of the kidney only
- To assess any effects of deleting one copy of *Ass1* in the Pax8Cre-Ass1 wt/flox heterozygous mouse
- To achieve tubular knockout of *Ass1* using the Pax8Cre x Ass1 flox/flox homozygous transgenic mouse
- To investigate the renal phenotype of the Pax8Cre x Ass1 flox/flox transgenic mouse

4.3 Results

4.3.1 Renal phenotype of *Asl* mutant mice

Some patients with ASL (argininosuccinate lyase) deficiency have been reported to exhibit decreased renal function and elevated levels of serum creatinine. The *Asl*$^{neo/neo}$ mouse is a transgenic mouse which expresses a mutant copy of the *Asl* gene which results in 25% residual protein expression. Kidney tissue from 3 week old *Asl* mutant mice was kindly donated by Julien Baruteau from University College London.

Gene expression analysis was carried out on renal tissue from *Asl* mutant mice and wildtype littermate controls. Expression of *Asl* was depleted as expected, however, *Ass1* mRNA was also depleted to the same extent. Additionally expression of kidney injury molecule 1 (*Havcr1*) was significantly elevated indicating tubular injury ($p<0.01$, Student's t-test) (Figure 5.1). The relative mRNA expression of *Col1a1*, *Col3a1*, *Tnf* and *Tgfbr1* were also assessed in this cohort and there were no changes in expression between *Asl* mutants and wildtype controls.

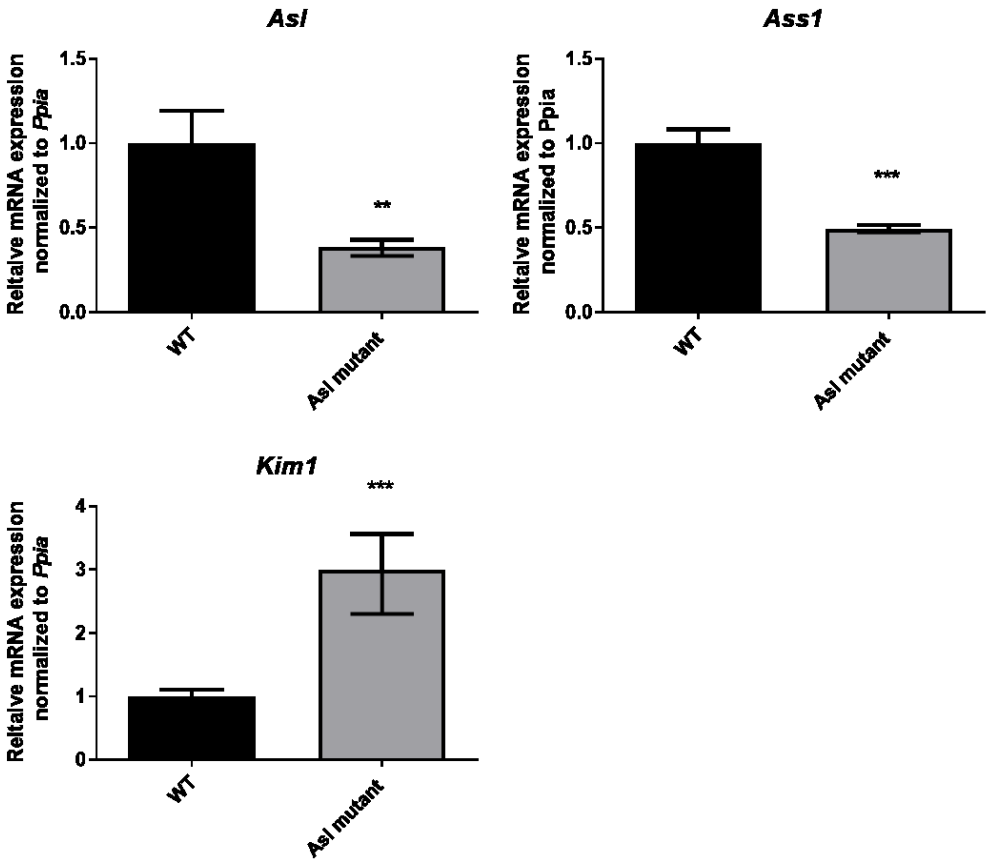

Figure 4.3: Renal phenotype of $Asl^{neo/neo}$ hypomorph mice. Relative mRNA expression of Asl, Ass1 and Kidney injury molecule 1 in kidney tissue from $Asl^{neo/neo}$ hypomorph mice (n=3) compared to Wildtype mice (n=3). Relative expression was calculated from ΔΔcT normalized to Ppia housekeeper and compared to wildtype (WT). * and ** represent $p<0.05$ and 0.01 respectively compared to control by Student's t-test.

4.3.2 Pax8 Cre recombination is specific to renal tubules

Using the $Pax8CreER^{T2}$ mice allowed selective, tamoxifen inducible recombination of Cre only in cells that express *Pax8*. In order to validate the expression profile of *Pax8* specifically in the kidney, Pax8Cre mice were crossed with Ai14 tdTomato reporter mice.

The offspring of these mice expressing Cre were given tamoxifen (n=4) or vehicle (n=4) at 6 weeks of age. Two weeks after tamoxifen administration, mice were culled in order to assess the extent of tdTomato positive cells in kidneys and livers in both groups. Flow cytometry was adopted to assess the number of tdTomato-positive cells which indicated successful Cre recombination. A gating strategy was set up to include only live single cells which were DAPI-negative (UV450). Subsequently the percentage of live cells which were tdTomato-positive were assessed (Figure 5.4). Unstained controls

and Pax8Cre x Ai14 kidneys treated with vehicle exhibited very few tdTomato-positive cells as expected. The Pax8Cre x Ai14 kidneys treated with tamoxifen showed a wide-ranging level of recombination with tdTomato-positive cells varying from 4.47% to 66.9% (Figure 5.5).

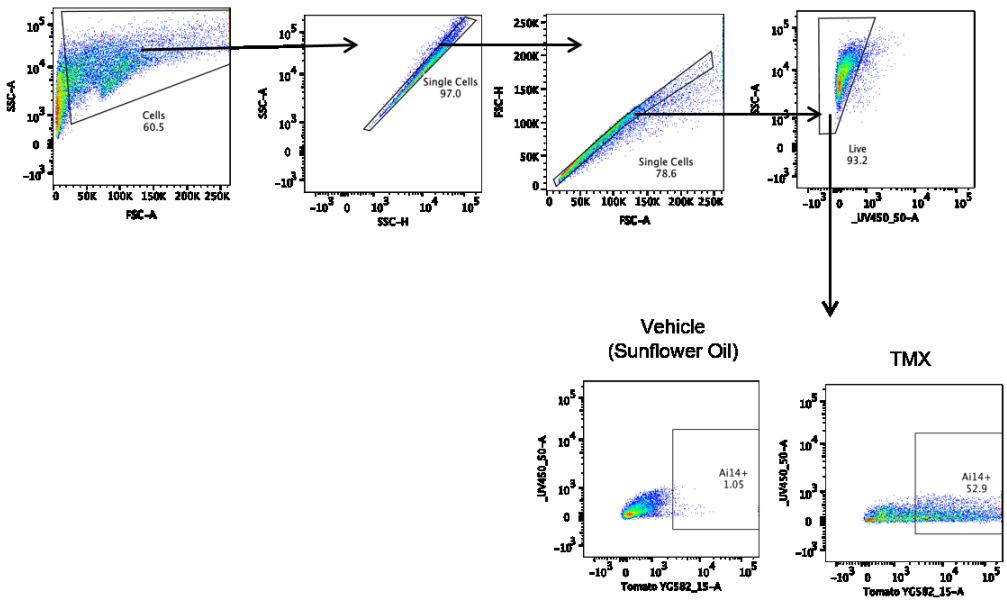

Figure 4.4: Gating strategy for Pax8Cre x Ai14 kidney cells. Kidney cell suspensions were analysed by flow cytometry to determine single, live cells which expressed tdTomato in vehicle control and tamoxifen treated Pax8Cre x Ai14 mice.

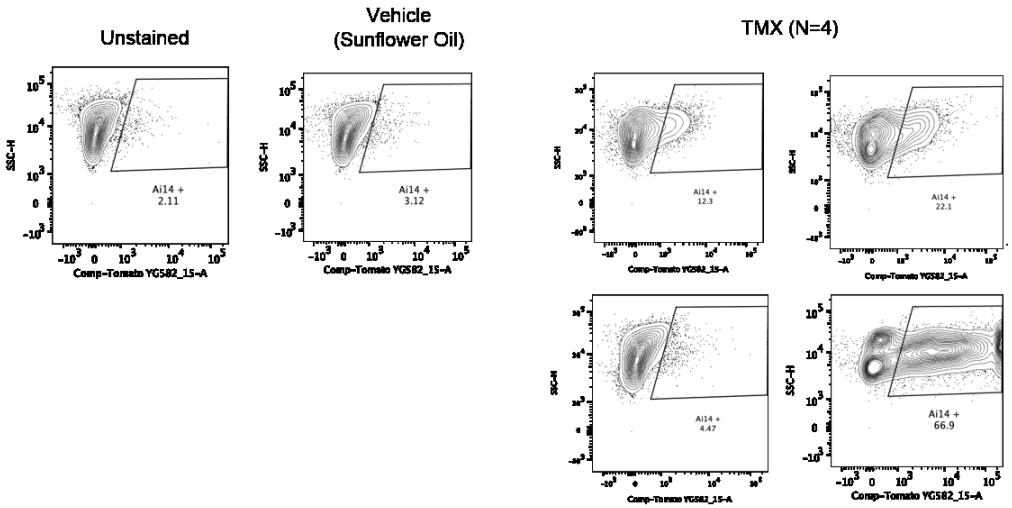

Figure 4.5: Flow cytometry contour plots of tdTomato positivity in Pax8Cre x Ai14 kidney cells. Representative plots showing the percentage of live tdTomato-positive kidney cells (in black box) in Pax8Cre x Ai14 mice administered with vehicle control or tamoxifen. Positive staining was assessed using the PE channel.

In order to characterise which kidney cells exhibited Cre recombination, frozen tissue was sectioned and visualised using a confocal microscope. Cre recombination shown by tdTomato expression was confirmed to have site specificity in the tubular compartment only and was absent in the glomeruli. There was no positive staining found in hepatocytes of the liver (Figure 5.6). Imaging was performed by Dr Duncan Humphries.

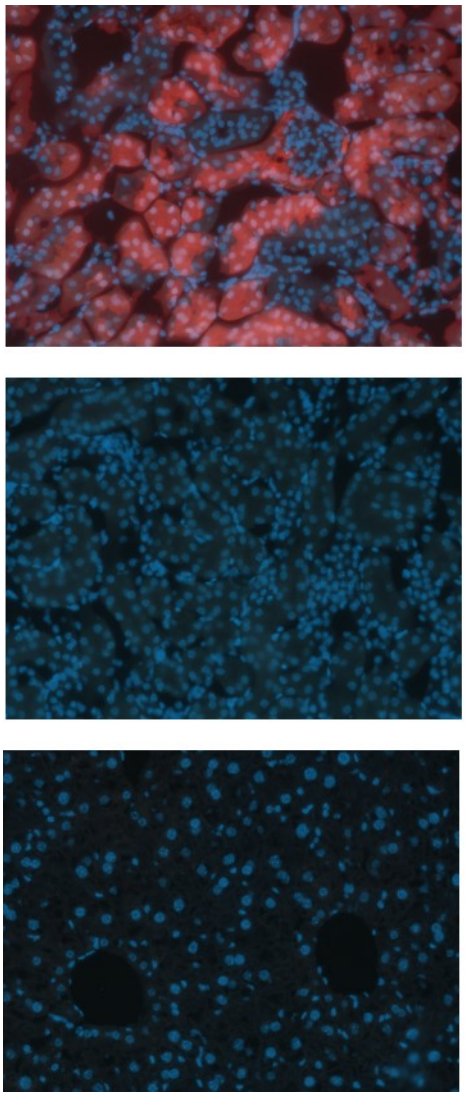

Figure 4.6: Validation of site specific recombination with Pax8Cre-ER^{T2}. Cre recombination was induced by 3 doses of 200mg/kg tamoxifen administration in Pax8Cre x Ai14 tdTomato mice. TdTomato fluorescent reporter was visualised in sectioned tissue using confocal microscopy

4.3.3 Pax8Cre x Ass1 wt/flox heterozygotes express normal levels of ASS1 with no measurable phenotype

Pax8Cre x *Ass1* wt/flox heterozygotes were assessed for any haploinsufficiency effect as they should express only one copy of the *Ass1* gene. A time course study was carried out to investigate whether heterozygotes display a discernible phenotype. Cre recombination was induced by administration of tamoxifen at 6 weeks of age and three cohorts were allowed to age for 2, 4 and 6 weeks. These mice were compared to littermates which received a vehicle control instead of tamoxifen.

Tamoxifen-induced heterozygous Pax8Cre x Ass1 wt/fl mice demonstrated no difference in body weight, heart, liver or kidney weight compared to vehicle control mice (Figure 5.7). Furthermore, there was no significant difference in ASS1 protein expression ($p=0.3$ and $p=0.0971$ at 2 weeks and 4 weeks respectively, Student's t test)) or mRNA expression in heterozygous mice compared to vehicle control mice at any time point. Additionally, there was no significant difference in *Asl* mRNA expression between each group (Student's t-test) (Figure 5.8).

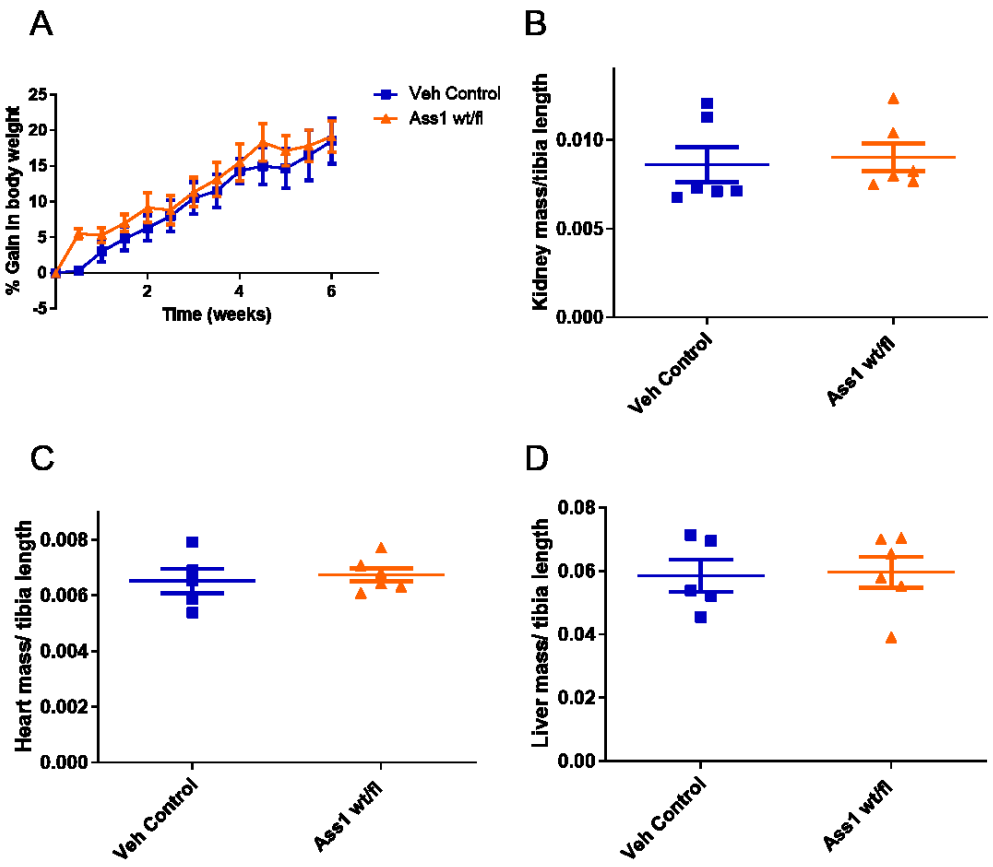

Figure 4.7: Body and organ weights of tubular Ass1wt/fl heterozygous knockout mice. (A) percentage gain in body weight, (B) kidney mass, (C) heart mass and (D) liver mass of Pax8Cre x Ass1 wt/fl mice with (Ass1 wt/fl) and without (Veh control) tamoxifen administration. Organ mass was normalized to tibia length.

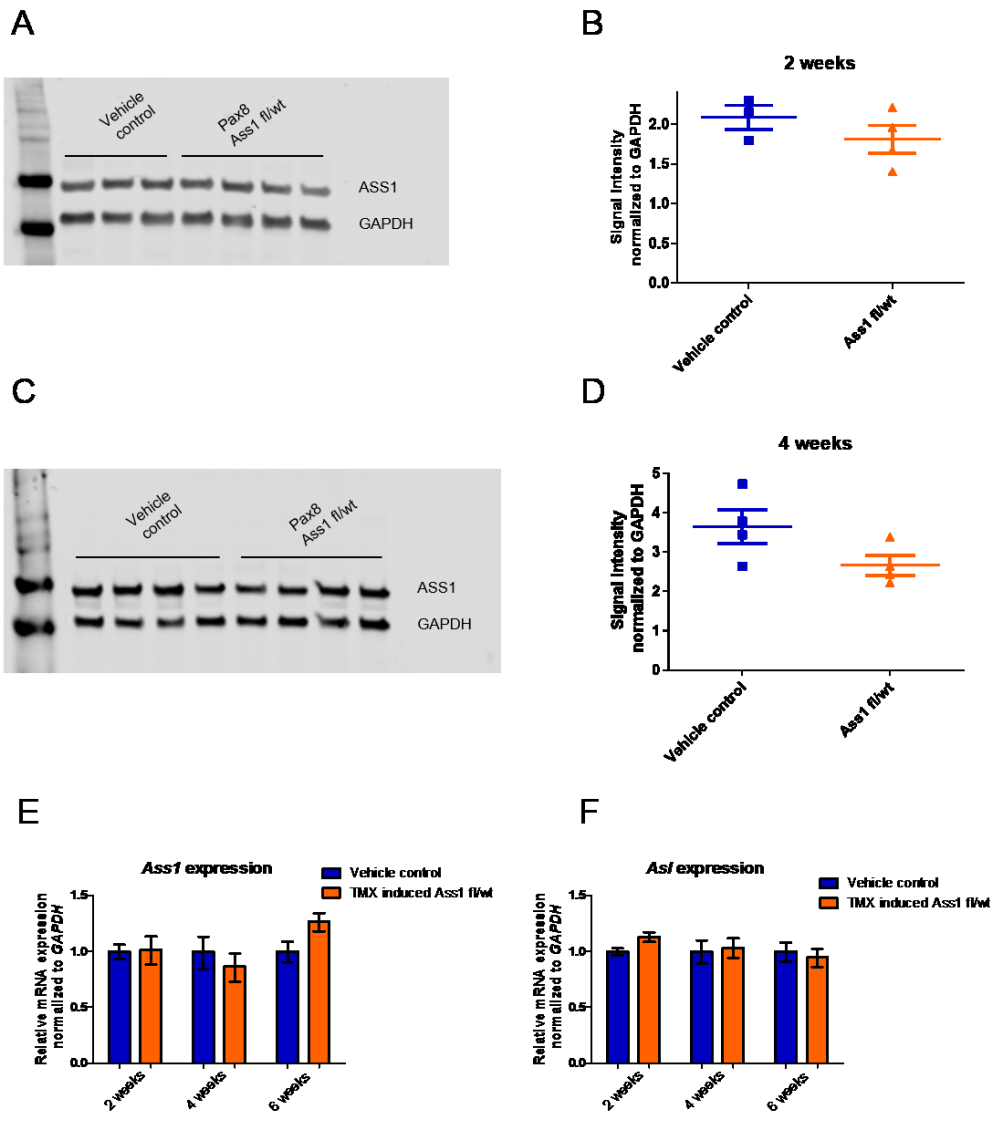

Figure 4.8: Pax8 Cre x Ass1 fl/wt heterozygous mice do not exhibit haploinsufficiency. Western blot was carried out on kidney lysates from tamoxifen induced and vehicle control Pax8 Cre- Ass1 fl/wt mice at 2 weeks (A-B) and 4 weeks (C-D) after treatment with tamoxifen or vehicle. Protein expression was measured using the Licor system and normalized to GAPDH housekeeper. Relative mRNA levels of Ass1 (E) and Asl (F) in kidneys of tamoxifen induced Pax8 Cre- Ass1 fl/wt (n=18) or vehicle control Pax8 Cre- Ass1 fl/wt mice (n=12) at 2 weeks, 4 weeks and 6 weeks after treatment with tamoxifen or vehicle. Relative expression was calculated from ΔΔcT normalized to *Gapdh* housekeeper and compared to vehicle control group.

Expression of KIM1 (*Havcr1*) was assessed to determine whether there was any kidney injury in these transgenic mice. *Havcr1* expression was consistently very lowly expressed in all 3 groups indicating no evidence of tubular injury by heterozygous expression of Ass1 or tamoxifen administration.

Finally, blood pressure was measured in the 6 week cohort of Pax8Cre x Ass1 wt/fl mice with or without tamoxifen administration. There was no significant

difference in mean arterial pressure between each group (p= 0.1665, Student's t-test) (Figure 5.9).

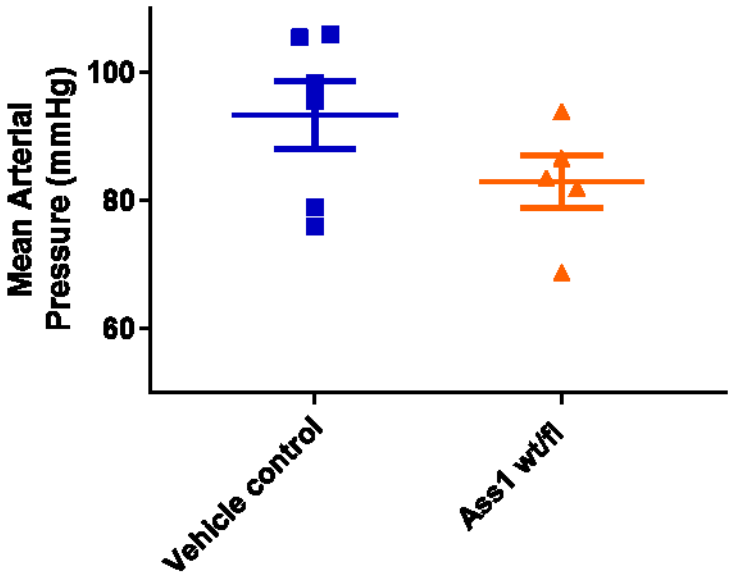

Figure 4.9: Mean arterial pressure of Pax8Cre x Ass1 wt/fl mice. Mean arterial pressure was calculated from systolic and diastolic blood pressure from tamoxifen induced Pax8Cre x Ass1 wt/fl and vehicle control mice.

4.3.4 Tubular specific homozygous knockout of *Ass1*

Pax8Cre x *Ass1* flox/flox homozygous knockouts (KO) were bred and recombination of Cre was induced with 200mg/kg tamoxifen at 6 weeks of age. 10 weeks after tamoxifen administration, Pax8Cre x Ass1 flox/flox mice were culled and their organs harvested and compared to their Pax8Cre x Ass1 wt/wt wildtype (WT) littermates. Due to time constraints and delays with breeding, this cohort was made up of a small number of animals which were a mixture of male and female mice (Table 5.1). Furthermore there were not enough mice of the correct genotype in order to compare against as vehicle control group. Due to the small group size, statistics could not be carried out on data generated from this study.

Genotype	Males	Females	Total
Pax8 Cre- Ass1 wt/wt (WT)	1	2	3
Pax8 Cre- Ass1 fl/fl (KO)	2	2	4

Table 4.1: Number of male and female mice in each experimental group

Kidney cortex lysates were prepared from WT and KO mice and ASS1 protein measured in both groups by western blot. ASS1 was detectable in all mice with only female KOs exhibiting depleted ASS1 protein compared to WT controls (Figure 5.10).

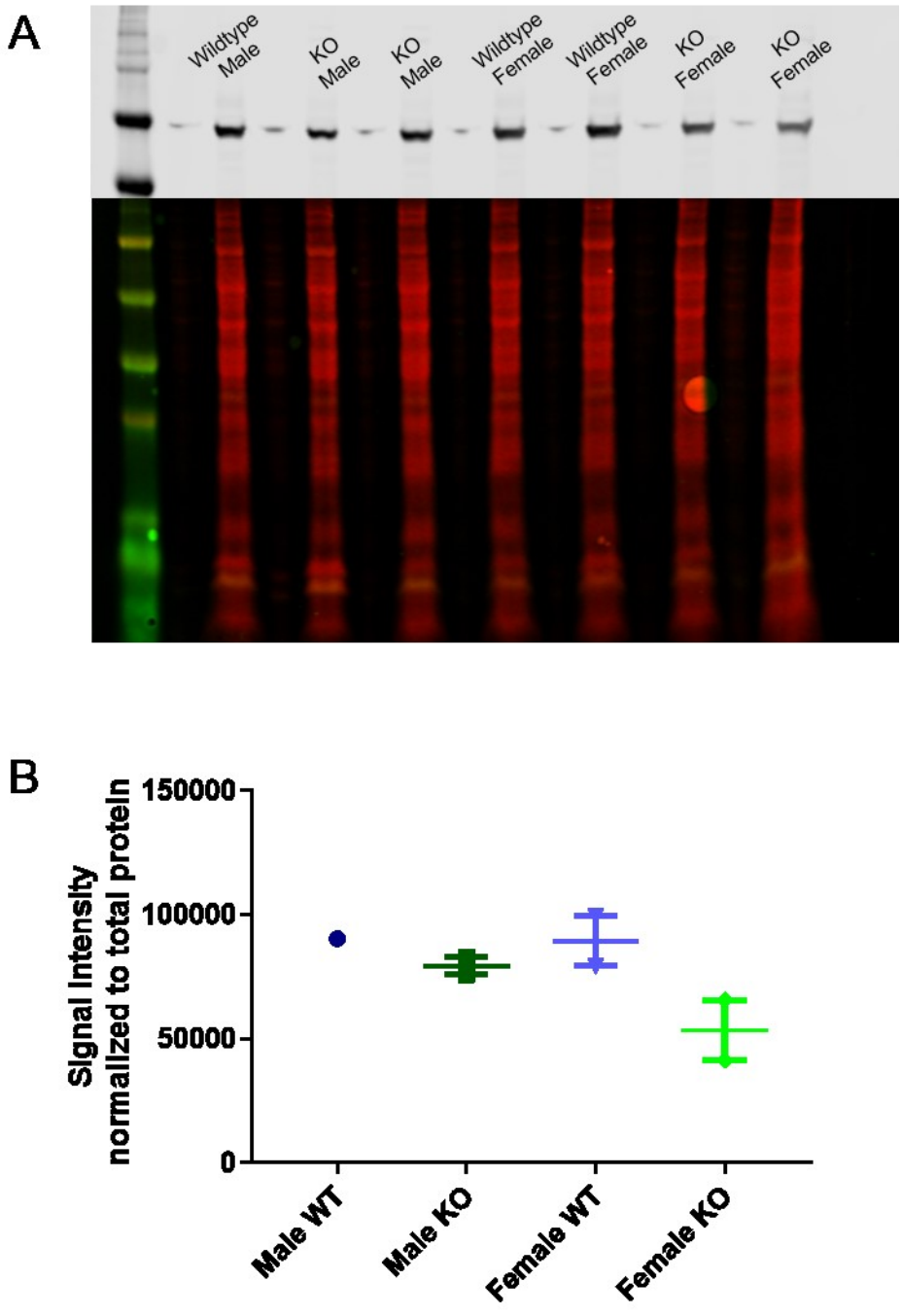

Figure 4.10: ASS1 protein expression in tubular Ass1 KO and controls. (A) Western blot analysis showed ASS1 protein levels in kidney lysates of male and female tamoxifen induced Pax8Cre x Ass1 fl/fl mice (KO) and Pax8Cre Ass1 wt/wt (WT) controls. (B) Protein levels were normalized to total protein content of the membrane and quantified using the Licor system and ImageStudio.

At sacrifice, kidney and heart weights were recorded. Male mice exhibited heavier organs even when normalized to tibia length. KO mice did not demonstrate marked differences in kidney or heart weight compared to WT when sexes were pooled. However, when males and females were analysed separately, there was a trend for increased heart weight in females (Figure 5.11).

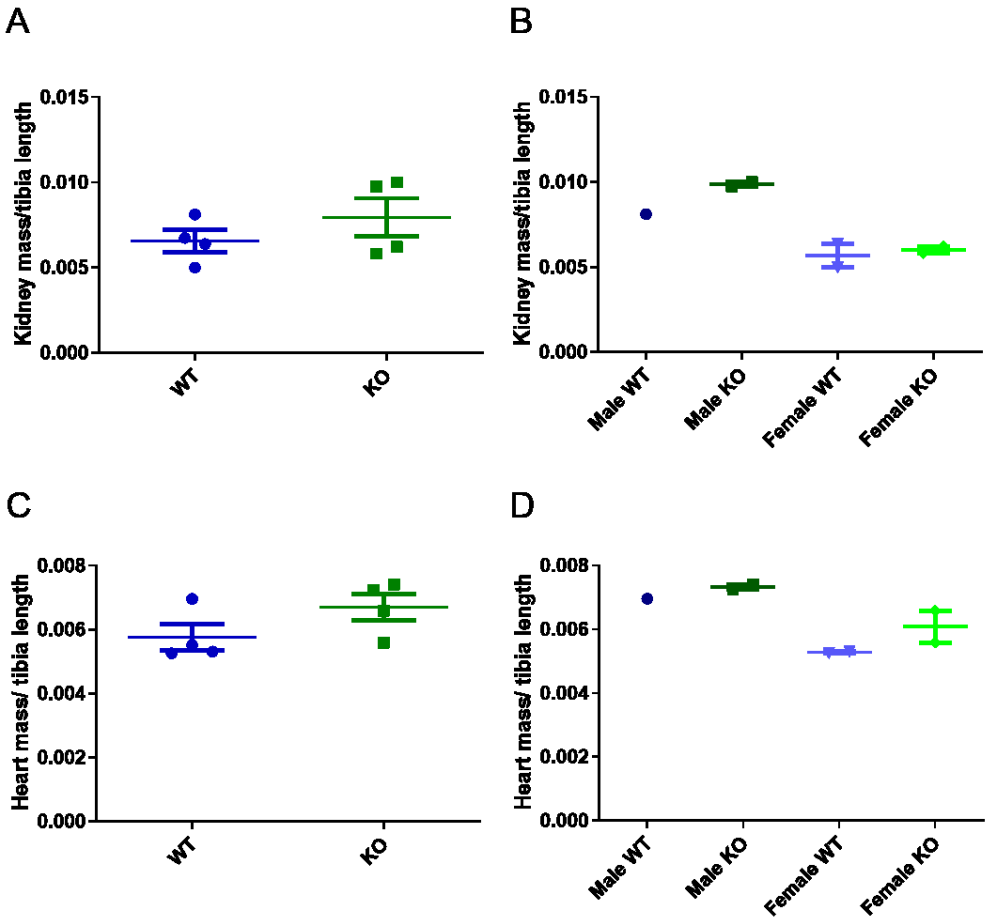

Figure 4.11: Organ weights of tubular Ass1 knockout mice. Organ weights were recorded at sacrifice, 10 weeks after tamoxifen administration of Pax8Cre x Ass1 fl/fl and wildtype controls. Organs were weighed using the same set of sensitive scales throughout and normalized to tibia length.

Gene expression analysis using qPCR was carried out from kidney cortex of WT and KO mice. mRNA expression of *Col1a1, Cubn, Cdh1, Tgfrb1* and *Havcr1* were assessed and there were no differences in expression between WT and KO kidneys of any of these genes (Figure 5.12).

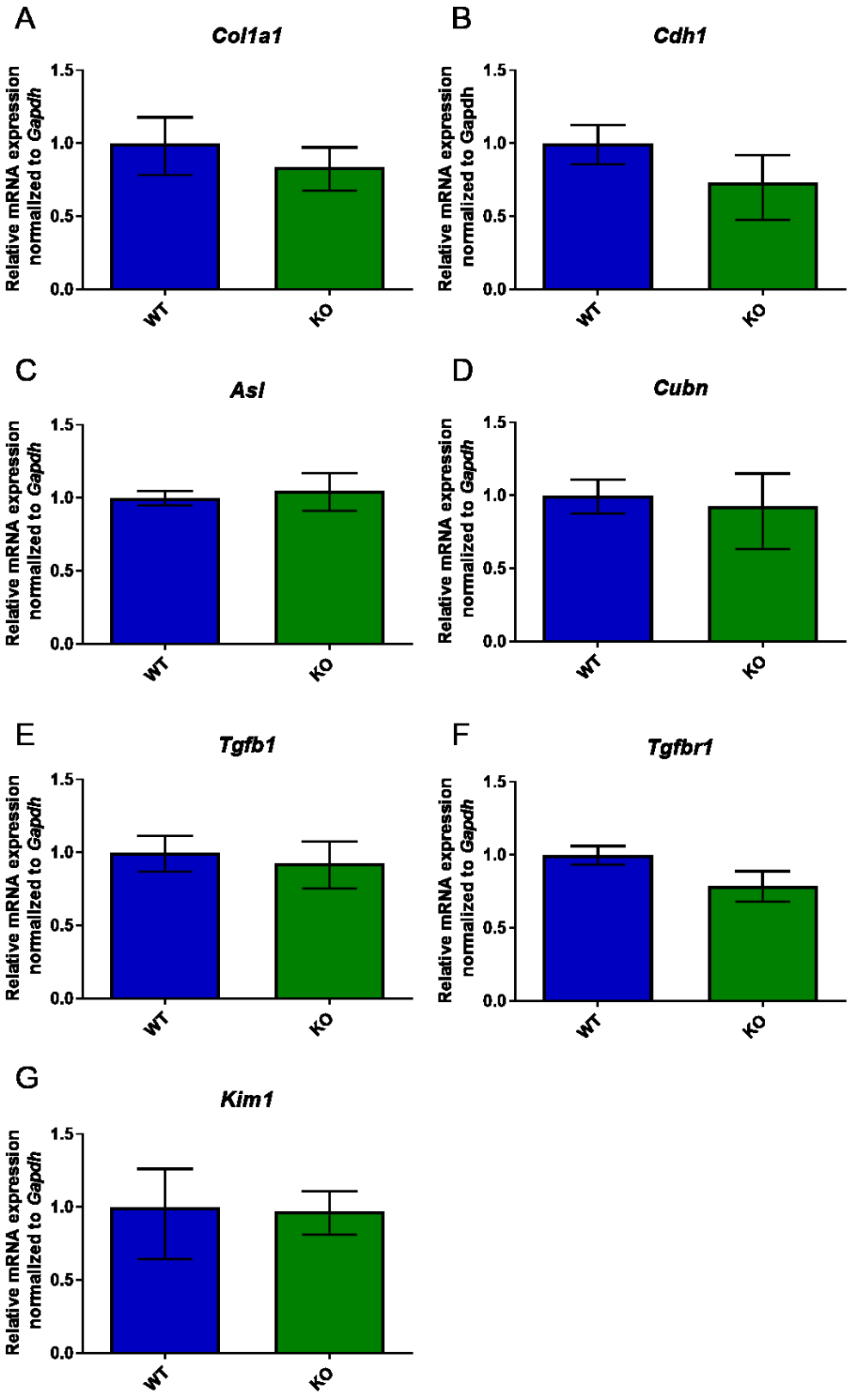

Figure 4.12: Gene expression analysis of tubular Ass1 knockout cortex. Relative mRNA levels of *Col1a1* (A), *Cdh1* (B), *Asl* (C), *Cubn* (D), *Tgfb1* (E), *Tgfbr1* (F) and *Havcr1* (Kim1) (G) were assessed in kidney cortex of tamoxifen induced Pax8Cre x *Ass1* fl/fl mice (n=4) and wildtype littermate controls (n=3). Relative expression was calculated from ΔΔcT normalized to *Gapdh* housekeeper and compared to wildtype control group.

4.3.5 Circulating urea cycle metabolites in tubular Ass1 knockout mice

As ASS1 is part of the urea cycle, levels of circulating amino acids present in the urea cycle were assessed from WT and KO blood. Whole blood was collected from WT and KO mice 10 weeks after induction of Cre recombination by tamoxifen. Drops of whole blood were spotted on Guthrie cards and sent to University College London for processing by Julien Baruteau using mass spectrometry (90).

Circulating citrulline showed no discernible difference between WT and KO when the sexes were pooled together. However upon inspection of males and females analysed separately, circulating citrulline was upregulated in female KOs compared to female WTs and males. Levels of circulating arginine demonstrated no difference between WT and KO but female KO levels were elevated compared to female WT. Circulating argininosuccinic acid levels were consistent in male and female KOs and WTs (Figure 5.13).

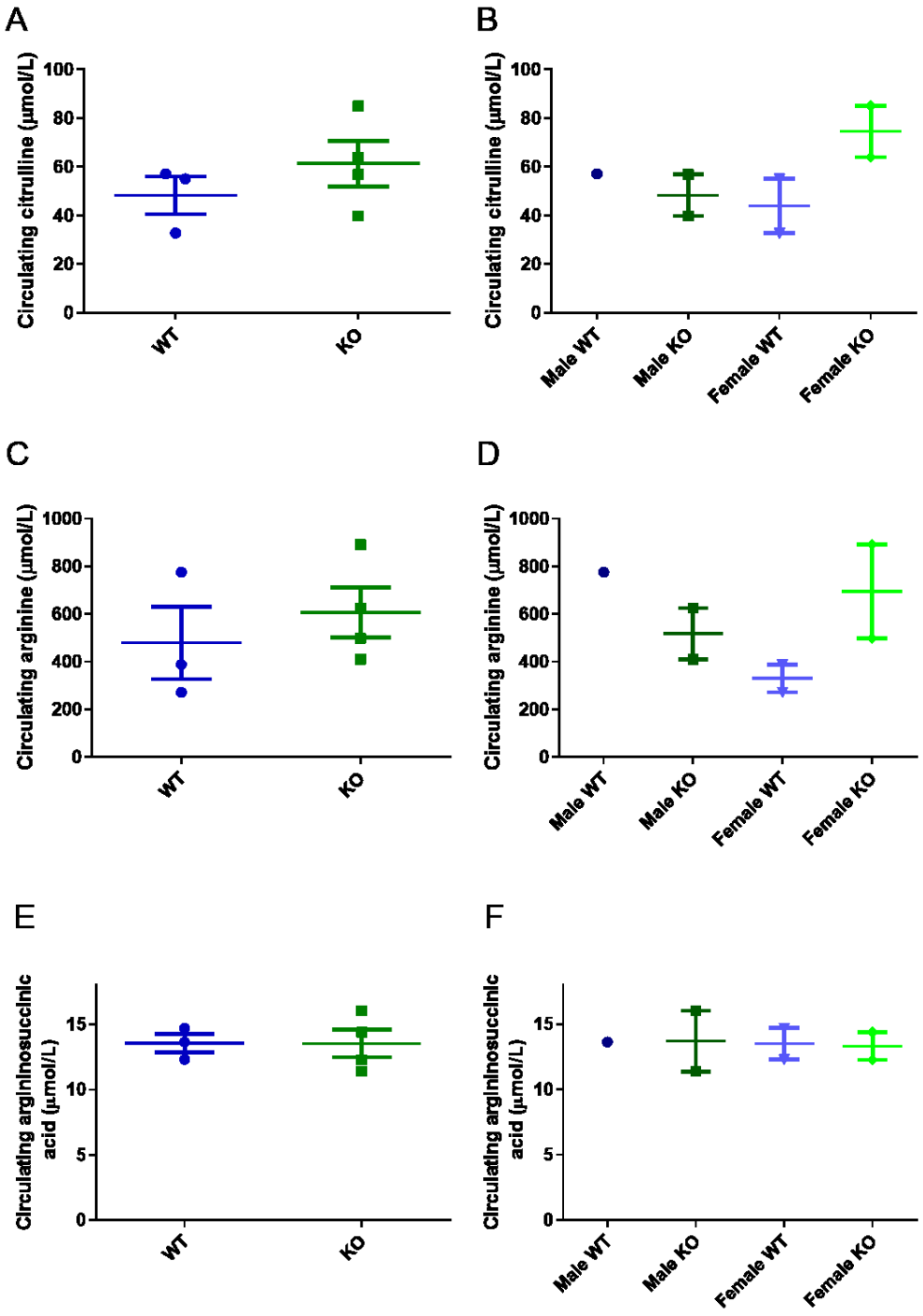

Figure 4.13: Circulating amino acid levels in tubular Ass1 knockout. Mass spectrometry was carried out on dried blood spots from Pax8 Cre x Ass1 fl/fl (n=4) and wildtype littermate controls (n=3) both treated with tamoxifen. Male and female data shown separately. (A-B) Citrulline, (C-D) Arginine and (E-F) Argininosuccinic acid were measured.

4.3.6 Urine and serum markers of chronic kidney disease in tubular *Ass1* knockout mice

Several measures taken in urine and serum are commonly used to assess the progression of CKD in mice and also patients. Serum creatinine is the most commonly used measure of renal function and is used to calculate the estimated GFR. High creatinine values indicate decreased filtering of the kidney which is evidence of CKD (200). The levels of circulating creatinine were low in this cohort and the spread of creatinine values were large. There were no differences in serum creatinine between WT and KO mice. Additionally, serum urea was assessed, which is another common measure used in patients with CKD, referred to a blood urea nitrogen (BUN) (201). There were no differences in serum urea between WT and KO mice (Figure 5.14).

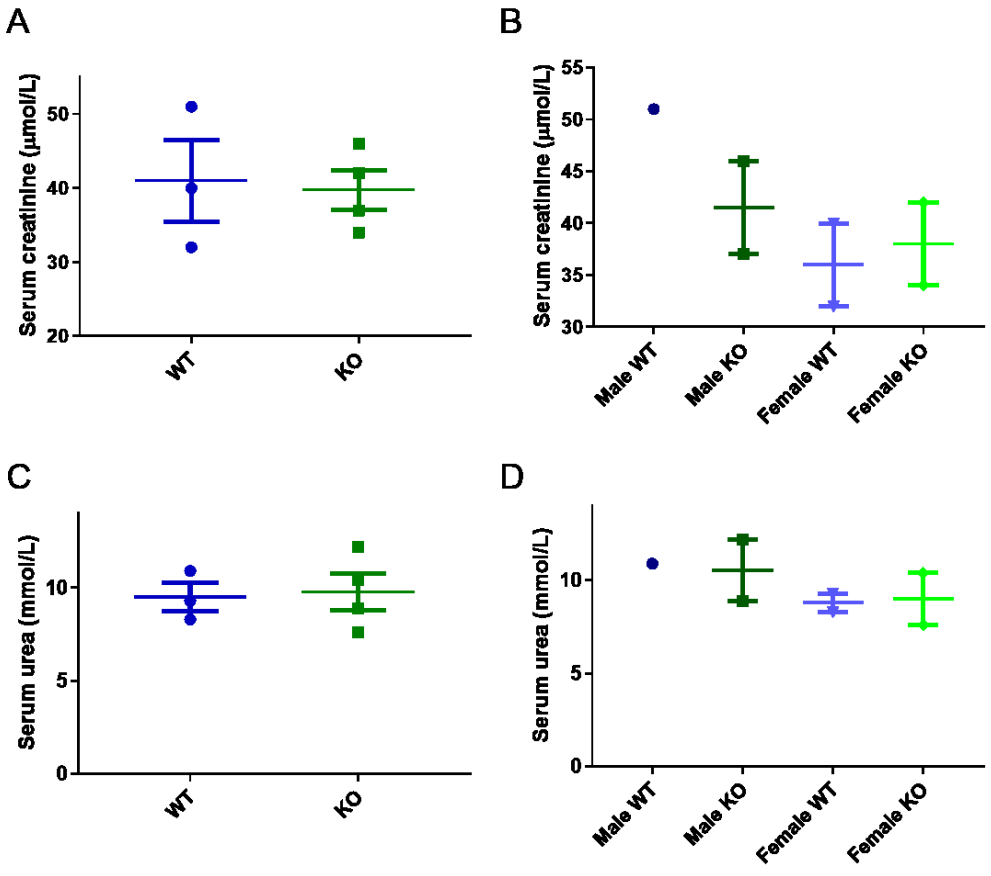

Figure 4.14: Serum creatinine and urea measurements in tubular Ass1 knockout mice. Serum was extracted from whole blood which was taken at termination from Pax8Cre x Ass1 fl/fl (n=4) and wildtype littermate controls (n=3) 10 weeks after tamoxifen administration. Creatinine levels and urea levels were measured using the Specialist Assay Service at The University of Edinburgh.

Urine albumin is also used to detect CKD. Albuminuria is present in patients with CKD and albumin should be absent from the urine in healthy individuals. Albuminuria is also present in mice with renal dysfunction as seen in the subtotal nephrectomy model in Chapter 3 of this thesis. This cohort of mice all demonstrated undetectable levels of albumin in their urine.

4.3.7 Electrolyte levels in tubular Ass1 knockout mice

Ass1 is highly expressed in tubules and tubular dysfunction can impact electrolyte balance including imbalance of sodium, potassium and chloride. Additionally ASL deficiency is associated with hypokalaemia and tubulopathy. The levels of sodium, potassium and chloride were assessed in serum and urine from our cohort of Ass1 tubular KO mice and WT mice.

Serum sodium concentration was found to be consistent in WT and KO mice. Additionally there was no difference between males and females. Serum potassium was unchanged between WT and KO mice but females demonstrated lower serum potassium concentrations that males. Finally, serum chloride concentrations were consistent in male and female WT and KO mice (Figure 5.15).

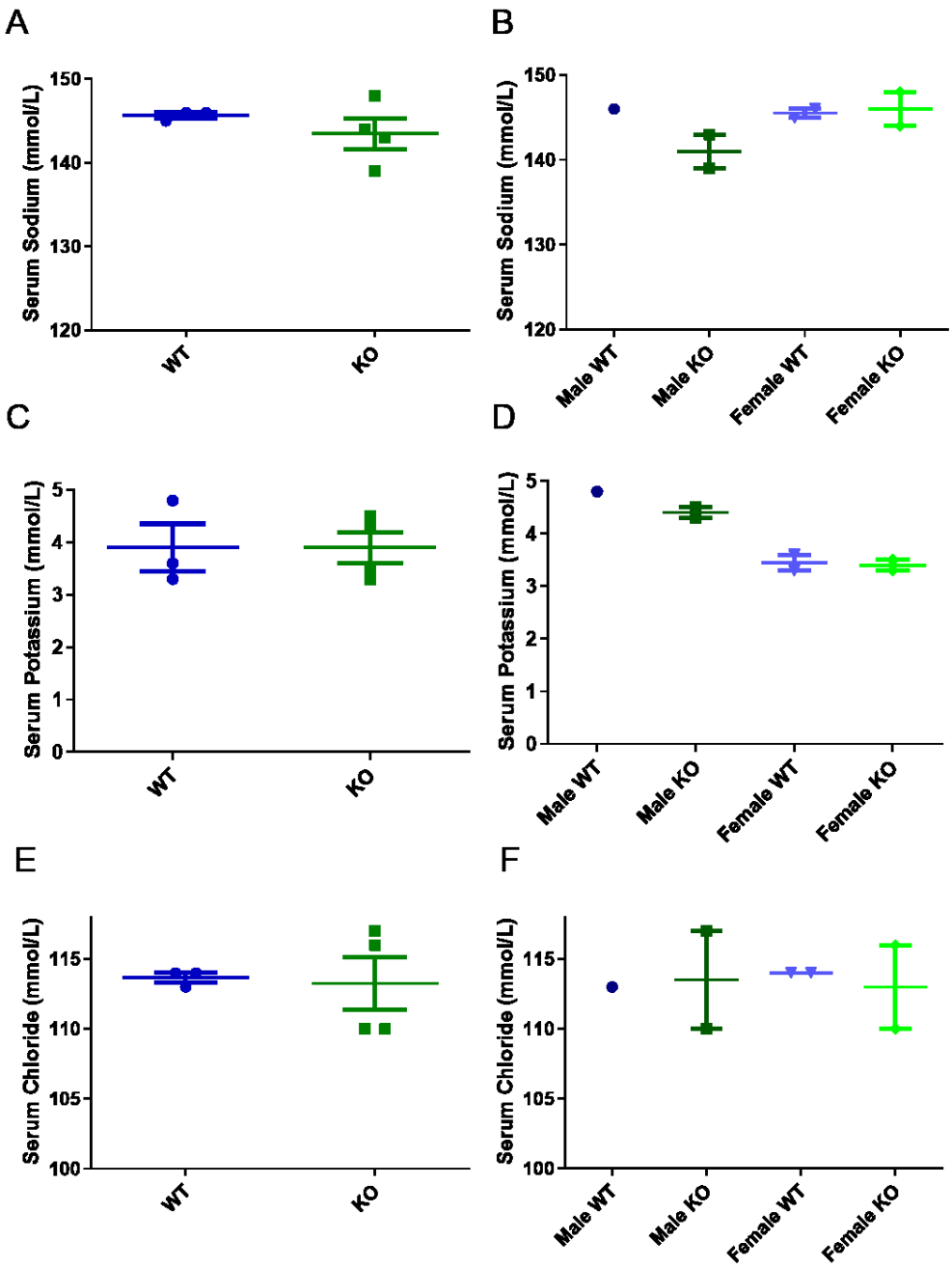

Figure 4.15: Serum electrolyte levels in tubular Ass1 knockout mice. Serum was extracted from whole blood taken at termination 10 weeks after tamoxifen administration of Pax8Cre x Ass1 fl/fl mice (KO) and Pax8Cre x Ass1 wt/wt (WT) controls. Serum electrolytes were assessed using the Spotchem EL™ electrolyte analyser. Data is shown with sexes pooled (A) and separated (B).

Levels of urinary sodium, potassium and chloride can be used to calculate the urine anion gap which indicates the ability of kidney to acidify urine and is an indicator of tubular function. The calculation to establish the urine anion gap is:

$Na^+ + K^+ - Cl^-$

The levels of these electrolytes were measured in the urine of WT and KO mice to ascertain any differences in the urine anion gap. There were no appreciable differences in the urine anion gap in WT or KO mice. However there was a trend for female mice to exhibit is slightly lower urine anion gap (Figure 5.16).

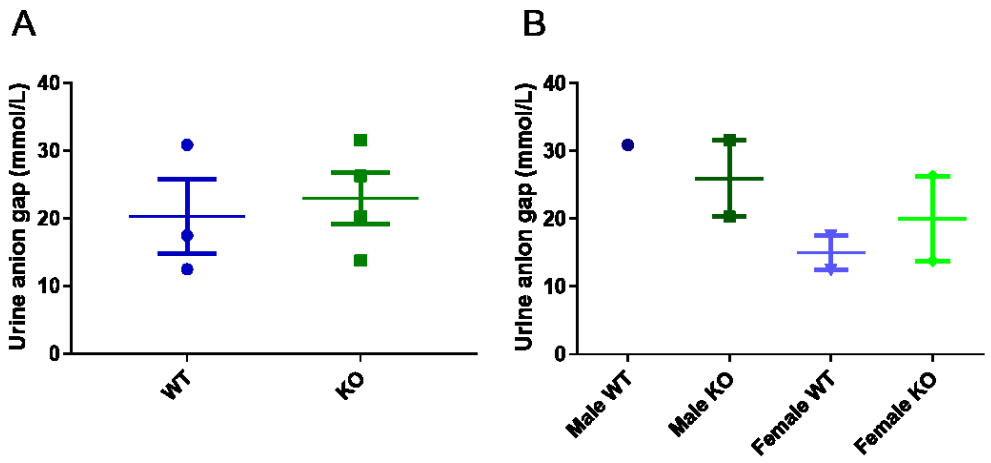

Figure 4.16: Urine anion gap in tubular Ass1 knockout mice. Mice were singly house and urine was collected using metabolic cages 10 weeks after tamoxifen administration in Pax8Cre x Ass1 fl/fl (KO) mice (n=4) and wildtype littermate controls (WT) (n=3). Urine electrolytes were assessed using the Spotchem EL^{TM} electrolyte analyser. Data is shown with sexes pooled (A) and separated (B).

4.3.8 Blood pressure in tubular Ass1 knockout mice

Ass1 is involved in the urea cycle which produces arginine within the kidney. Arginine can be utilised by nitric oxide producing cells for nitric oxide synthase in order to produce nitric oxide which exerts a number of effects including vasodilation. Therefore, we investigated whether blood pressure was influenced by tubular knockout of *Ass1*. Systolic and diastolic blood pressure was assessed using the tail-cuff method in WT and KO mice 8 weeks after tamoxifen administration. Animals were habituated to blood pressure measuring before final measures were taken. Mean arterial pressure (MAP) was calculated from systolic (SBP) and diastolic blood pressure (DBP).

Mean arterial pressure exhibited a trend to increase in KO mice compared to WT mice. Additionally female WT mice demonstrated a trend for decreased blood pressure compared to male mice (Figure 5.17).

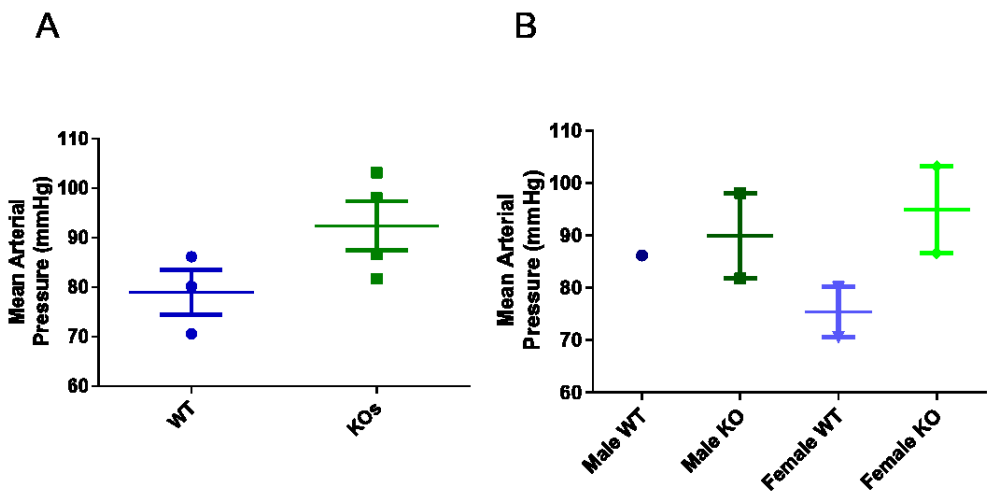

Figure 4.17: Mean arterial blood pressure of Ass1 KO mice. Mean arterial pressure was calculated from systolic and diastolic blood pressure from tamoxifen induced Pax8Cre x Ass1 fl/fl Ass1 knock out mice (KO) and compared to littermate wildtype controls (WT). Data is shown with sexes pooled (A) and separated (B).

4.4 Discussion

The final chapter of this thesis sought to reveal the effects of knocking out *Ass1* specifically within tubular epithelial cells of the kidney. In this way I sought to investigate whether tubular deletion of Ass1 had any impact on tubular function, tubular injury status and finally whether tubular Ass1 knock-out promoted fibrogenesis. In the short time available to me I investigated a small cohort of tubular *Ass1* knock-out males and females. This preliminary study demonstrated that *Ass1* deletion was more effective in tubules of female mice. Successful tubular knock-out of *Ass1* led to a trend for increased circulating citrulline levels and may have increased mean arterial blood pressure. Other functional parameters measured in this study such urine albumin and electrolyte levels showed no discernible difference between *Ass1* tubular knock-out and controls. Furthermore, assessment of tubular injury by *Havcr1* (Kidney injury molecule 1) mRNA expression demonstrated no measurable tubular injury in tubular specific Ass1 knockout mice. Gene expression analysis revealed there was no upregulation of genes commonly associated within fibrosis. For the first time, this study explored the effect of tubular deletion of *Ass1*. Although there was no strong evidence for renal pathological changes in these transgenic mice at baseline in this underpowered study, there is much further work to be carried out to investigate the role Ass1 plays in the development of fibrosis and the progression of CKD.

This chapter also included some preliminary data investigating the effects of global *Asl* hypermorphism on the kidney. As well as the expected depletion of *Asl* mRNA expression, *Asl* mutant mice also demonstrated a pronounced downregulation of *Ass1* mRNA within the kidney. This was unexpected as studies investigating lung tissue of $Asl^{neo/neo}$ mutant mice found ASS1 protein levels to be consistent in mutant and wildtype mice (186). This chapter only investigated mRNA levels of *Ass1* in $Asl^{neo/neo}$ mutant mice kidney tissue. Therefore, a western blot or immunostaining of ASS1 protein levels should be conducted in renal tissue to ensure that ASS1 protein levels are diminished as well as mRNA levels. This chapter also demonstrated that *Havcr1* (Kidney injury molecule 1) was significantly upregulated in $Asl^{neo/neo}$ mutant mice at only 3 weeks of ages. This indicates that global depletion of *Asl* resulted in tubular injury. KIM1 is a commonly utilised marker of tubular injury and therefore other assessments of renal injury should be carried out in these mice. Other groups

have carried out some assessment of kidney function in $Asl^{neo/neo}$ mutant mice including revealing elevated serum creatinine levels and histological identification of smaller glomeruli compared to wildtype controls (186). However, more detailed assessment of renal function should be assessed including assessment of albuminuria, measurement of glomerular filtration rate and identification of fibrosis.

One caveat of using $Asl^{neo/neo}$ global mutant mice to identify pathological changes in kidneys is that these mice exhibit multi-organ failure. They also exhibit elevated levels of circulating ammonia which is in itself toxic to the kidneys and would explain upregulated *Havcr1* expression seen in this chapter. To avoid this caveat, the effect of *Asl* depletion should be investigated in the kidney in isolation. Our collaborators, Baruteau and colleagues, achieved correction of hyperammonemia in $Asl^{neo/neo}$ mutant mice by replacing the faulty *Asl* gene with a fully functional copy of *Asl* in the liver (90). As the liver is the main site of ammonia removal by the urea cycle, this was sufficient to prevent multi-organ failure and extend the lifespan of these treated mutant mice. As the viral vector they used to deliver *Asl* to the liver should not enter the kidneys, it would be interesting to see if evidence of renal failure persisted in mice which had hyperammonemia corrected. Indeed, elevated levels of citrulline seen in $Asl^{neo/neo}$ mutant mice was not corrected in mice with hepatic *Asl* gene transfer. If possible, further work should be carried out to explore the renal phenotype and manifestation of fibrosis in $Asl^{neo/neo}$ mutant mice with hyperammonemia and multi-organ failure corrected. This could elucidate the role that *Asl* and *Ass1* play in tandem in the context of renal fibrosis.

To circumvent the lethal phenotype of global *Ass1* deletion, conditional gene targeting was adopted to ablate *Ass1* expression selectively in tubular epithelial cells. The $Pax8CreER^{T2}$ x *Ass1* flox/flox mouse was adopted to be able to achieve conditional knockout of *Ass1* within *Pax8* expressing tubules (195,198). An advantage of using this mouse was that recombination of Cre was inducible by tamoxifen administration. In this way *Ass1* knockout was controlled spatiotemporally and this avoided manipulating *Ass1* expression during development.

Initially we investigated whether heterozygous deletion of *Ass1* in tubules induced any renal phenotype. This would indicate whether there was a gene dosage effect of partial *Ass1* deletion. Studies investigating the effect of *Mmp2*

deletion found that, in the setting of ureteric obstruction, *Mmp2* knockout significantly prevented renal fibrosis. Moreover, heterozygous mice with only one remaining *Mmp2* allele (*Mmp2*$^{+/-}$) also demonstrated effective protection against fibrosis to a similar extent as homozygous knockout mice (*Mmp2*$^{-/-}$). The authors concluded an important gene dosage effect of *Mmp2* deletion (202). In this chapter, the effect of tubular specific heterozygous *Ass1* knock-out (Pax8Cre x Ass1 wt/fl) was investigated. There was no significant depletion of renal ASS1 protein at any of the time points investigated after tamoxifen administration. Furthermore, there was no difference between groups when assessing *Havcr1* expression or blood pressure. Therefore, the heterozygous Pax8Cre Ass1 wt/fl mice did not exhibit effective renal *Ass1* deletion and there was no evidence of tubular injury or vasoconstriction.

After a gene dosage effect of *Ass1* partial deletion was disproved, full knock-out of Ass1 in tubular epithelial cells was carried out with the Pax8Cre x Ass1 fl/fl mouse. This study found that tubular knock-out of *Ass1* was more efficient in females than in males. There could be several reasons for this including inefficient activity of Cre, incorrect induction of Cre recombinase by tamoxifen or inefficient recombination of loxP sites. It has been reported that in some Cre expressing models, Cre recombination can be more or less efficient depending whether the Cre was transmitted from the male or female parent (192). However, in this study, paternal/ maternal Cre transmission is irrelevant as all mice in this cohort were littermates with the same parents. Until a larger cohort of mice is investigated, it will not be clear whether the more successful knock-out of *Ass1* in females compared to males is a true biological effect or just chance. Furthermore, as evidenced by using the Pax8Cre x Ai14 reporter mouse, Cre recombination was highly variable and inadequate in some mice. This indicates that Cre recombination in the Pax8CreER^{T2} mouse could be inefficient and therefore larger groups of mice should be investigated in future to account for this. Another explanation for inefficient Cre recombination is that the dose of tamoxifen used to induce recombination was not sufficient. Mice in this study were treated with 200mg/kg tamoxifen for three alternate days. Future studies could investigate the effect of elevating the dose of tamoxifen and also could investigate the result of increasing the dosing regimen to every day for 5 days.

This study showed that in female mice, in which tubular *Ass1* knock-out was successful, there was a trend for increased circulating citrulline. As citrulline is

a substrate which the ASS1 enzyme anabolises, it fits that citrulline levels would be elevated due to decreased availability of ASS1 to catalyse the conversion of citrulline to argininosuccinic acid. When *Ass1* was knocked out in enterocytes using the same Ass1 flox/flox mouse by Marion and colleagues, they also found citrulline levels to be elevated. (198). Elevated citrulline seen here, echoes what is seen in patients and animal models of CKD as assessed using metabolomics. Both patients with CKD and animal models of CKD demonstrate increased concentration of citrulline in the blood (107,111). As discussed in Chapter 1, elevated circulating citrulline seen in patients with CKD was a driver to investigate the role of *Ass1* in the kidney. Therefore is it positive to see that a modest decrease in renal ASS1 expression seen in females of this cohort is sufficient to elevate circulating citrulline.

The urine levels of sodium, potassium and chloride were measured to assess any evidence of metabolic acidosis in tubular specific Ass1 knock out mice. Metabolic acidosis is common in patients with CKD and manifests as decreased ammonium (NH_4^+) excretion which correlates with decreased renal filtration and reabsorption and late stage CKD (203). The urine anion gap is calculated from levels of Na^+, K^+ and Cl^- and is used clinically as a surrogate measure of NH_4^+ excretion in the urine (204). A high urine anion gap is correlated with decreased ammonia excretion while a low urine anion gap is correlated with bicarbonate loss. These observations occur in renal tubular acidosis type 1 and type 2 respectively and can also be measured in mice (205). As tubular dysfunction can contribute to ion imbalance and acid imbalance, it was important to ascertain if there were any changes in the urine anion gap in tubular specific Ass1 knock-out mice to reveal if these mice had tubular dysfunction. In this cohort there was no difference in the urine anion gap between knock-outs and wildtype controls. This indicates that in the unchallenged state, tubular specific knock-out of *Ass1* does not impact ammonia excretion or bicarbonate loss. This indicates that tubular mediated acid/base balance has stayed intact.

Serum levels of sodium, potassium and chloride ions were measured to assess if renal transport of electrolytes was affected in tubular specific *Ass1* mice. Furthermore, ASL deficient mice have been reported to exhibit hypokalaemia which has been attributed to a tubulopathy (131). Serum potassium was measured in our cohort to ascertain whether a similar effect could be seen. Levels of sodium, potassium and chloride ions in KO and WT groups were

unchanged. However, it was observed that female mice exhibited lower levels of potassium ions compared to males which is an observation also seen in human studies (206). These results demonstrate that tubular transport of these ions is unaffected by tubular specific knock out of Ass1 in the basal state after 10 weeks.

Blood pressure was assessed in this cohort of tubular specific knock-out mice to determine whether deletion of Ass1 within the tubular compartment influenced mean arterial pressure. There was an observable trend for an increase in blood pressure within the KO group compared to the WT group. This effect was most pronounced in females which had demonstrated depletion of renal ASS1 protein expression. This is in line with what is seen in mice globally deficient in ASL protein. Erez and colleagues showed blood pressure to be significantly increased in $Asl^{neo/neo}$ hypomorph mice compared to wildtype controls. The authors attributed this to depleted availability of arginine for use by nitric oxide synthase. However as ASL was mutated globally, the impact of ASL deficiency specifically within the kidney could not be investigated (186). ASS1 functions upstream of ASL and provides argininosuccinic acid as a substrate for ASL to yield arginine. Furthermore, the kidney is the main site of arginine production in the body. Therefore, lack of tubular ASS1 would theoretically deplete renal arginine levels which could impact nitric oxide synthase mediated production of nitric oxide. As nitric oxide is a potent vasodilator it could be hypothesised that tubular deletion of *Ass1* depletes available nitric oxide resulting in vasoconstriction and elevated blood pressure. This is important in the context of CKD as hypertension and CKD are inextricably linked (207). While hypertension is one of the most important risk factors for developing CKD, hypertension can also occur as a result of CKD (208). Additionally, CKD with hypertension vastly increases the risk of a patient experiencing a cardiovascular effect such as myocardial infarction or stroke (209).

Subsequent experiments with a larger cohort of male and female tubular specific Ass1 knockout mice should be carried out to determine if blood pressure is statistically significantly elevated in KO mice compared to WT and a vehicle control. If this is the case, the circulating levels of nitrate and nitrite should be assessed as an indirect method of assessing nitric oxide levels in the blood (210). This could confirm if tubular specific knockout of Ass1 directly impacts available circulating nitric oxide resulting in elevated blood pressure.

Furthermore, if blood pressure elevation is proven to be a pathological effect of *Ass1* deletion in tubules, then an improved method of blood pressure assessment should be used. The tail cuff plethysmography method used here has several disadvantages. Physical handling and restraint of mice can induce stress and therefore increased blood pressure. The tail cuff method involves extensive handling, restraint and also mild discomfort for the animals which is likely to elevate their heart rate and blood pressure. Telemetry is now termed the “gold standard” for blood pressure assessment over time and is achieved by an implantable device that can measure blood pressure in undisturbed animals with consistent measures taken automatically over time. Telemetry provides superior, more accurate measures of blood pressure but these devices are expensive and implantation of the device requires surgical expertise (211).

It was hypothesised that deletion of Ass1 in tubular epithelial cells would induce aspects of renal disease or fibrosis. Therefore, it was important to investigate multiple measures associated with renal disease and fibrosis to adequately characterise any potential phenotype. Measures assessed in this chapter have addressed many facets of renal function and disease. Measuring urine albumin and serum creatinine levels has addressed the filtering action of kidney in these mice, while measuring electrolyte levels has addressed the tubular phenotype of these mice. Gene expression analysis allowed the investigation of genes known to be markers of renal injury (*Havcr1*) as well as genes known to be involved in the development of fibrosis (*Col1a1*, *Tgfb1* and *Tgfbr1*) and markers of tubular integrity (*Cubn* and *Cdh1*). Finally, measuring blood pressure has addressed that renal disease induces pathological systemic effects such as hypertension and associated cardiovascular disease. Although Pax8Cre x Ass1 fl/fl mice did not exhibit striking changes in many of these parameters, these mice should be utilised in future *in vivo* studies with an additional challenge such as ischaemia reperfusion injury.

Transgenic mouse models can take significant amounts of time to develop pathological phenotypes. Moreover, organ specific transgenic mice may not induce any changes for many months and an additional challenge may be required to accelerate disease progression. Kruger and colleagues developed a transgenic mouse of proximal tubular mitochondrial overload by knocking out carnitine 29 acetyl-transferase (CrAT) specifically within the proximal tubule. These mice did not develop renal disease until 18-20 months of age. However,

an additional high fat diet challenge did accelerate the rate of renal disease development modestly to 12-15 months (212). The Pax8Cre x Ass1 fl/fl mice in this study were only investigated 10 weeks after knockout was induced by tamoxifen. The time scale of this project may not have been long enough to be able to detect any pathological changes that may point towards renal disease. Furthermore, tubular specific *Ass1* KO mice may require an additional physiological challenge in order detect exacerbated renal disease in KO mice compared to controls. Indeed, Miao and colleagues found that proximal tubular specific knockout of the gene *Crry* did not induce any apparent renal disease when left unchallenged. *Crry* is involved in the complement cascade and knockout of *Crry* resulted in spontaneous deposition of C3 complement on the surface of proximal tubular epithelial cells as expected but with no associated renal disease. PT-*Crry* knockout mice were subjected to ischaemia reperfusion injury and this led to exacerbated renal disease in transgenic mice compared to controls. They exhibited higher blood urea, enhanced tubular injury and apoptosis as well as increased inflammatory infiltrates. They concluded that PT-Crry knockout sensitised mice to IRI and therefore Crry provided protection to proximal tubular cells from inflammatory kidney injury (213). Together these studies provide evidence that the tubular specific Ass1 knockout mouse warrants further interrogation over a much longer time scale than conducted in this chapter and also may require challenge with IRI to result in exacerbated injury.

This chapter has investigated the effects of knocking out Ass1 within the tubular compartment of the kidney. While this study demonstrated no striking changes associated with renal disease or fibrosis, there are interesting trends demonstrating a potential blood pressure effect of tubular Ass1 knockout. Additional longitudinal studies over several months could be carried out to assess the long term effects of Ass1 knockout on tubular health and blood pressure. However, the most valuable experiment will be to induce an IRI in tubular specific knockout mice. I hypothesise that tubular deletion of Ass1 will sensitise mice to the pathological effects of IRI and will result in exacerbated fibrosis.

Chapter: 5 General Discussion and Future Perspectives

The studies presented in this thesis focussed on identifying novel pathways and mechanisms that may play a role in the progression of renal fibrosis and subsequent CKD. Arginine metabolism was revealed to be a metabolic pathway that was downregulated in the setting of renal fibrosis. Specifically, Ass1, the rate limiting step of arginine biosynthesis in the kidney, was identified as a gene which demonstrated downregulation in the kidney in three models of renal fibrosis. Ass1 is highly expressed in tubular epithelial cells and is absent in most other renal cell populations. Ass1 expression was depleted in live, transcriptionally active epithelial cells after obstructive injury and expression levels were recovered after reversal of obstruction. After Ass1 loss was identified as a common hallmark of all three *in vivo* models, the role that Ass1 played in RPTECs was investigated. Ass1 was found to be highly expressed in human RPTEC/TERT cells and Ass1 loss was mediated *in vitro* by TNFα and hypoxic signalling. Furthermore, transcriptional inhibition of Ass1 was found to be independent of classical pro-fibrotic TGFβ signalling. Depletion of Ass1 *in vitro* resulted in a phenotypic change that was characterised as pro-fibrotic and de-differentiated but not senescent. These phenotypic changes are synonymous with tubular injury and the promotion of renal fibrosis. Finally, loss of *Ass1* was induced *in vivo* by inducible tubular specific knock-out of *Ass1* using the Pax8CreER^{T2} x Ass1 flox/flox mouse. In a short time frame in an unchallenged state, Ass1 tubular KO did not induce any transcriptional changes seen *in vitro* after Ass1 depletion. Nor did Ass1 tubular KO result in any renal functional changes associated with CKD. However tubular *Ass1* KO did perturb urea cycle amino acids in the kidney and resulted in elevated circulating citrulline. There was also some indication that Ass1 tubular KO did increase mean arterial blood pressure which indicated that Ass1 depletion may have abrogated arginine production in the kidney which is involved with nitic oxide signalling and vasodilation.

CKD is a growing problem worldwide and there has been a lack of new therapeutics which halt the progression of CKD. Additionally, an aging population, the increased prevalence of type II diabetes and obesity will undoubtedly increase the incidence of renal failure. This “silent tsunami” will

greatly impact healthcare systems across the world (214). Therefore, new therapeutics need to focus on targeting the pathophysiological processes driving the early stages of tubular injury and TIF. Reversing fibrosis is possible as was shown in a patient with diabetic nephropathy who received a pancreatic transplant. This transplant and subsequent correction of hyperglycaemia allowed the reversal of renal fibrosis shown by histological analysis of biopsies over 10 years (215). However, although physical manifestations of fibrosis were reversed, there was no evidence of any improvement to renal function. Therefore, we must tackle mechanisms driving renal fibrosis before renal function can no longer be rescued. Superior biomarkers of early-stage renal fibrosis must be developed as well as therapies that abrogate early-stage events such as immune cell recruitment and maladaptive tubular dedifferentiation and senescence. Additionally, due to the elevated risk of developing CKD in patients who have previously experienced an AKI (216), these patients should be monitored closely in order to diagnose early-stage disease as soon as possible. Patient stratification either by genetic predisposition or AKI history will be important in the future to tailor correct treatments based on individual differences (217).

CKD is driven by a number of processes but the common driving pathological mechanism for all forms of CKD is renal fibrosis. Tubular injury has now been identified as an initiating mechanism in the progression of renal fibrosis and tubular phenotypic changes such as de-differentiation and senescence have been shown to be responsible for initiating the fibrotic response (46,160). Ass1 is highly expressed in the kidney and its expression is confined to tubules and predominantly the proximal tubule. Tubular cells are attracting attention as potential new druggable targets for the prevention of the initiation of renal fibrosis after acute kidney injury (AKI). AKI has been found to significantly increase the likelihood of developing progressive CKD and tubular cell dysfunction is central to this phenomenon (218). Studies have demonstrated that inhibition of histone deacetylase 1 resulted in tubular de-differentiation and subsequent increased proliferation of tubular epithelial cells after acute kidney injury. This de-differentiation and proliferation of tubular cells accelerated recovery and reduced fibrosis in zebrafish and mouse models of AKI. Furthermore administration of a drug which inhibited histone deacetylase was found to be affective several days after AKI. This is highly clinically relevant as patients rarely get treated for AKI until the injury has already established. This

provides evidence that correcting dysfunctional mechanisms ongoing in tubular cells is an effective therapeutic strategy against renal fibrosis (219,220). Previously, fibroblasts were seen as the most promising cellular targets for anti-fibrotic therapies in CKD, however anti-TGFβ based therapies have yielded disappointing results (32). Therefore, studies from this thesis may provide insight into how tubular cells undergo de-differentiation via Ass1 loss in a TGFβ-independent manner.

The Denby lab previously identified miR-214 as pro-fibrotic microRNA which exerted its effects in the kidney in a TGFβ-independent manner (94). This thesis identified *Ass1* mRNA as a likely target of miR-214 binding and repression. The precise mechanism whereby miR-214 performs its pro-fibrotic role has not been fully elucidated but repression of Ass1 in tubular cells may be a mechanism which miR-214 adopts to augment fibrogenesis. miR-214, TNFα and hypoxia are all stimuli are present in most renal diseases. All three of these upstream modulators exert an inhibitory action on Ass1 transcription. This provides strong evidence that Ass1 downregulation is an important mechanism in the progression of renal fibrosis as three different signalling pathways present in the fibrotic milieu lead to the same downstream effect. Although the consequences of genetic downregulation of Ass1 *in vivo* were not fully elucidated here, there is much work still to be carried out using the Pax8Cre x Ass1 fl/fl mouse.

The experiment which should be carried out next is ischaemia-reperfusion challenge in Pax8Cre x Ass1 fl/fl mice. This study would definitively show the effect of tubular *Ass1* loss in the setting of renal injury and fibrosis. I hypothesise that tubular knockout of *Ass1* would exacerbate the effects of renal IRI and would increase the extent of renal fibrosis. The same parameters adopted in chapter 5 should be used to assess the renal function of Pax8Cre x *Ass1* fl/fl subjected to IRI. Additionally, the extent of fibrosis should be assessed by gene expression analysis and histological analysis to ascertain the extent of tubular injury and ECM deposition in the kidney. This study should be adequately powered and conducted with the correct control mice in order to make valid comparisons. Pax8Cre x *Ass1* fl/fl mice induced with tamoxifen should be subjected to sham or IRI surgery. Additionally, Pax8Cre x *Ass1* fl/fl mice administered with vehicle control should be subjected to sham or IRI surgery. Furthermore, male and female mice should both be assessed separately. Chapter 5 demonstrated the need to evaluate the physiology and

genetics of males and females individually and CKD itself demonstrates unequal prevalence among males and females. While more females are diagnosed with CKD, it has been observed that the disease is more severe in men with more men progressing to ESKD (221,222). Furthermore, female rats have been reported to have increased protection against an experimental model of CKD than male rats. Male rats developed higher levels of albuminuria and more severe glomerulosclerosis compared to females after L-NAME induced CKD (223). Until recently, *in vivo* studies involving kidney disease have used only male mice. It is growing increasingly more important to evaluate the results of studies in males and females within the field of renal research.

If tubular knockout of *Ass1* led to increased sensitivity of tubular cells to ischemia reperfusion injury mediated fibrosis, further studies should be carried out to abrogate the downregulation of Ass1 *in vivo*. One methodology to reinstate normal Ass1 expression would be to target one of the upstream modulators of Ass1 expression. Anti-miR-214 has already been adopted by the Denby group to prevent the progression of renal fibrosis (94). If Ass1 is found to be a validated target of miR-214 then antagonism of miR-214 would prevent Ass1 downregulation and therefore would prevent Ass1-loss-mediated effects. Another course of action would be to target TNFα. Anti-TNF therapeutics are already licensed to be used in patients and have passed safety requirements. TNFα blockade has shown promise in diseases such as rheumatoid arthritis, spondyloarthritis and other chronic inflammatory diseases. Anti-TNF therapies currently function to neutralise endogenous TNFα and take the form of full length monoclonal antibodies (adalimumab, golimumab and infliximab) as well as a soluble TNF receptors (etanercept) and most recently a PEGylated Fab fragment of a monoclonal antibody (certolizumab) (224). These therapies must be administered intravenously or subcutaneously and incur a high cost to the NHS (225). TNFα blockade has been found to be successful in improving the quality of life for patients who have chronic forms of arthritis, however, it has been reported that there is a high rate of non-responsiveness in certain patients and there is a high risk of developing serious chronic infections as an adverse effect (226,227). These drugs are still in their infancy but they do provide effective treatment for diseases which are driven in part by TNFα. As TNFα is upregulated in patients with CKD and inflammatory pathways are strong initiators of renal fibrosis, TNFα blockade may provide an effective therapy to abate CKD progression. Additionally, antagonising TNF mediated signalling

may prevent Ass1 downregulation, thereby retaining tubular *Ass1* expression and preventing *Ass1*-mediated de-differentiation.

The studies presented in the thesis highlight the complexity of fibrotic signalling within the kidney. This complexity has stunted the finding of new therapeutics to treat patients with CKD. This body of work has identified Ass1 as a potentially important gene in the setting of renal fibrosis. This tubular gene may provide a mechanistic link between pro-inflammatory, hypoxic and miR-214 mediated signalling and tubular de-differentiation and fibrogenesis. The elucidation of Ass1 as an important gene is the development of renal injury and fibrosis may provide insight into novel druggable mechanisms which may benefit patients suffering with progressive CKD in years to come.

Chapter: 6 References

1. Carroll, R. G. (2007) 11 - Renal System and Urinary Tract. in *Elsevier's Integrated Physiology* (Carroll, R. G. ed.), Mosby, Philadelphia. 117-137
2. Satchell, S. C., and Braet, F. (2009) Glomerular endothelial cell fenestrations: an integral component of the glomerular filtration barrier. *American Journal of Physiology-Renal Physiology* **296**, 947-956
3. Farquhar, M. G. (1981) The Glomerular Basement Membrane. in *Cell Biology of Extracellular Matrix* (Hay, E. D. ed.), Springer, Boston, MA. 335-378
4. Ruotsalainen, V., Ljungberg, P., Wartiovaara, J., Lenkkeri, U., Kestilä, M., Jalanko, H., Holmberg, C., and Tryggvason, K. (1999) Nephrin is specifically located at the slit diaphragm of glomerular podocytes. *Proceedings of the National Academy of Sciences* **96**, 7962-7967
5. Jacobson, H. R., and Kokko, J. P. (1976) Intrinsic differences in various segments of the proximal convoluted tubule. *The Journal of Clinical Investigation* **57**, 818-825
6. Zhuo, J. L., and Li, X. C. (2013) Proximal nephron. *The Journal of Comparative Physiology* **3**, 1079-1123
7. Bhargava, P., and Schnellmann, R. G. (2017) Mitochondrial energetics in the kidney. *Nature Reviews Nephrology* **13**, 629-646
8. Palmer, L. G., and Schnermann, J. (2015) Integrated control of Na transport along the nephron. *Clinical Journal of the American Society of Nephrology* **10**, 676-687
9. DiBartola, S. P. (2012) Chapter 2 - Applied Renal Physiology. in *Fluid, Electrolyte, and Acid-Base Disorders in Small Animal Practice (Fourth Edition)* (DiBartola, S. P. ed.), W.B. Saunders, Saint Louis. pp 26-43
10. Webster, A. C., Nagler, E. V., Morton, R. L., and Masson, P. (2017) Chronic Kidney Disease. *The Lancet* **389**, 1238-1252
11. Levey, A. S., Coresh, J., Balk, E., Kausz, A. T., Levin, A., Steffes, M. W., Hogg, R. J., Perrone, R. D., Lau, J., and Eknoyan, G. (2003) National Kidney Foundation Practice Guidelines for Chronic Kidney Disease: Evaluation, Classification, and Stratification. *Annals of Internal Medicine* **139**, 137-147
12. Levey, A. S., Atkins, R., Coresh, J., Cohen, E. P., Collins, A. J., Eckardt, K. U., Nahas, M. E., Jaber, B. L., Jadoul, M., Levin, A., Powe, N. R., Rossert, J., Wheeler, D. C., Lameire, N., and Eknoyan, G. (2007) Chronic kidney disease as a global public health problem: Approaches and initiatives – a position statement from Kidney Disease Improving Global Outcomes. *Kidney International* **72**, 247-259
13. Kerr, M., Bray, B., Medcalf, J., O'Donoghue, D. J., and Matthews, B. (2012) Estimating the financial cost of chronic kidney disease to the NHS in England. *Nephrology, Dialysis, Transplantation* **27 Suppl 3**, iii73-80
14. Weiner, D. E., Tighiouart, H., Amin, M. G., Stark, P. C., MacLeod, B., Griffith, J. L., Salem, D. N., Levey, A. S., and Sarnak, M. J. (2004) Chronic Kidney Disease as a Risk Factor for Cardiovascular Disease and All-Cause Mortality: A Pooled Analysis of Community-Based Studies. *Journal of the American Society of Nephrology* **15**, 1307-1315

15. Thompson, S., James, M., Wiebe, N., Hemmelgarn, B., Manns, B., Klarenbach, S., and Tonelli, M. (2015) Cause of Death in Patients with Reduced Kidney Function. *Journal of the American Society of Nephrology* **26**, 2504-2511
16. Zoccali, C., Abd ElHafeez, S., Dounousi, E., Anastasi, R., Tripepi, G., and Mallamaci, F. (2015) Life-Time Risk, Screening and The Cost of Cardiovascular Comorbidities in CKD Patients. *Prilozi (Makedonska Akademija na Naukite i Umetnostite. Oddelenie za medicinski nauki)* **36**, 85-90
17. Collaborators. (2016) Global, regional, and national life expectancy, all-cause mortality, and cause-specific mortality for 249 causes of death, 1980-2015: a systematic analysis for the Global Burden of Disease Study 2015. *The Lancet* **388**, 1459-1544
18. Sternlicht, H., and Bakris, G. L. (2017) The Kidney in Hypertension. *The Medical Clinics of North America* **101**, 207-217
19. Wyatt, C. M., Winston, J. A., Malvestutto, C. D., Fishbein, D. A., Barash, I., Cohen, A. J., Klotman, M. E., and Klotman, P. E. (2007) Chronic kidney disease in HIV infection: an urban epidemic. *AIDS*, 2101-2103
20. Chawla, L. S., Eggers, P. W., Star, R. A., and Kimmel, P. L. (2014) Acute Kidney Injury and Chronic Kidney Disease as Interconnected Syndromes. *New England Journal of Medicine.* **371**, 58-66
21. Lunyera, J., Mohottige, D., Isenburg, M. V., Jeuland, M., Patel, U. D., and Stanifer, J. W. (2016) CKD of Uncertain Etiology: A Systematic Review. *Clinical Journal of the American Society of Nephrology* **11**, 379-385
22. Ovadya, Y., and Krizhanovsky, V. (2015) A new Twist in kidney fibrosis. *Nature Medicine* **21**, 975
23. Ghoul, B. E., Squalli, T., Servais, A., Elie, C., Meas-Yedid, V., Trivint, C., Vanmassenhove, J., Grunfeld, J. P., Olivo-Marin, J. C., Thervet, E., Noel, L. H., Prie, D., and Fakhouri, F. (2010) Urinary procollagen III aminoterminal propeptide (PIIINP): a fibrotest for the nephrologist. *Clinical Journal of the American Society of Nephrology* **5**, 205-210
24. Eddy, A. A. (1996) Molecular insights into renal interstitial fibrosis. *Journal of the American Society of Nephrology* **7**, 2495-2508
25. Cheng, Z., Limbu, M. H., Wang, Z., Liu, J., Liu, L., Zhang, X., Chen, P., and Liu, B. (2017) MMP-2 and 9 in Chronic Kidney Disease. *International Journal of Molecular Science* **18**, 776
26. Liu, Y. (2011) Cellular and molecular mechanisms of renal fibrosis. *Nature Reviews Nephrology* **7**, 684
27. Qi, R., and Yang, C. (2018) Renal tubular epithelial cells: the neglected mediator of tubulointerstitial fibrosis after injury. *Cell Death & Disease* **9**, 1126
28. Meran, S., and Steadman, R. (2011) Fibroblasts and myofibroblasts in renal fibrosis. *International Journal of Experimental Pathology* **92**, 158-167
29. Humphreys, B. D., Lin, S. L., Kobayashi, A., Hudson, T. E., Nowlin, B. T., Bonventre, J. V., Valerius, M. T., McMahon, A. P., and Duffield, J. S. (2010) Fate tracing reveals the pericyte and not epithelial origin of myofibroblasts in kidney fibrosis. *American Journal of Pathology* **176**, 85-97
30. Humphreys, B. D. (2018) Mechanisms of Renal Fibrosis. *Annual Review of Physiology* **80**, 309-326
31. Koesters, R., Kaissling, B., Lehir, M., Picard, N., Theilig, F., Gebhardt, R., Glick, A. B., Hahnel, B., Hosser, H., Grone, H. J., and Kriz, W. (2010) Tubular overexpression of transforming growth factor-beta1 induces

autophagy and fibrosis but not mesenchymal transition of renal epithelial cells. *American Journal of Pathology* **177**, 632-643
32. Meng, X.-m., Nikolic-Paterson, D. J., and Lan, H. Y. (2016) TGF-[beta]: the master regulator of fibrosis. *Nature Reviews Nephrology* **12**, 325-338
33. Isaka, Y., Fujiwara, Y., Ueda, N., Kaneda, Y., Kamada, T., and Imai, E. (1993) Glomerulosclerosis induced by in vivo transfection of transforming growth factor-beta or platelet-derived growth factor gene into the rat kidney. *Journal of Clinical Investigation* **92**, 2597-2601
34. Bottinger, E. P., and Kopp, J. B. (1998) Lessons from TGF-beta transgenic mice. *Mineral and electrolyte metabolism* **24**, 154-160
35. Xavier, S., Vasko, R., Matsumoto, K., Zullo, J. A., Chen, R., Maizel, J., Chander, P. N., and Goligorsky, M. S. (2015) Curtailing Endothelial TGF-β Signaling Is Sufficient to Reduce Endothelial-Mesenchymal Transition and Fibrosis in CKD. *Journal of the American Society of Nephrology* **26**, 817-829
36. Miyajima, A., Chen, J., Lawrence, C., Ledbetter, S., Soslow, R. A., Stern, J., Jha, S., Pigato, J., Lemer, M. L., Poppas, D. P., Vaughan, E. D., and Felsen, D. (2000) Antibody to transforming growth factor-beta ameliorates tubular apoptosis in unilateral ureteral obstruction. *Kidney International* **58**, 2301-2313
37. Gewin, L., Vadivelu, S., Neelisetty, S., Srichai, M. B., Paueksakon, P., Pozzi, A., Harris, R. C., and Zent, R. (2012) Deleting the TGF-β receptor attenuates acute proximal tubule injury. *Journal of the American Society of Nephrology* **23**, 2001-2011
38. Gewin, L., and Zent, R. (2012) How does TGF-β mediate tubulointerstitial fibrosis? *Seminars in nephrology* **32**, 228-235
39. Humphreys, B. D., Valerius, M. T., Kobayashi, A., Mugford, J. W., Soeung, S., Duffield, J. S., McMahon, A. P., and Bonventre, J. V. (2008) Intrinsic Epithelial Cells Repair the Kidney after Injury. *Cell Stem Cell* **2**, 284-291
40. Humphreys, B. D., Czerniak, S., DiRocco, D. P., Hasnain, W., Cheema, R., and Bonventre, J. V. (2011) Repair of injured proximal tubule does not involve specialized progenitors. *Proceedings of the National Academy of Sciences* **108**, 9226-9231
41. Smeets, B., Boor, P., Dijkman, H., Sharma, S. V., Jirak, P., Mooren, F., Berger, K., Bornemann, J., Gelman, I. H., Floege, J., van der Vlag, J., Wetzels, J. F., and Moeller, M. J. (2013) Proximal tubular cells contain a phenotypically distinct, scattered cell population involved in tubular regeneration. *The Journal of Pathology* **229**, 645-659
42. Takaori, K., Nakamura, J., Yamamoto, S., Nakata, H., Sato, Y., Takase, M., Nameta, M., Yamamoto, T., Economides, A. N., Kohno, K., Haga, H., Sharma, K., and Yanagita, M. (2016) Severity and Frequency of Proximal Tubule Injury Determines Renal Prognosis. *Journal of the American Society of Nephrology* **27**, 2393-2406
43. Yang, L., Besschetnova, T. Y., Brooks, C. R., Shah, J. V., and Bonventre, J. V. (2010) Epithelial cell cycle arrest in G2/M mediates kidney fibrosis after injury. *Nature medicine* **16**, 535
44. Leung, K. C. W., Tonelli, M., and James, M. T. (2012) Chronic kidney disease following acute kidney injury—risk and outcomes. *Nature Reviews Nephrology* **9**, 77
45. Abbate, M., Zoja, C., and Remuzzi, G. (2006) How Does Proteinuria Cause Progressive Renal Damage? *Journal of the American Society of Nephrology* **17**, 2974-2984

46. Chevalier, R. L. (2016) The proximal tubule is the primary target of injury and progression of kidney disease: role of the glomerulotubular junction. *American Journal of Physiology. Renal Physiology* **311**, 145-161
47. Docherty, M. H., O'Sullivan, E. D., Bonventre, J. V., and Ferenbach, D. A. (2019) Cellular Senescence in the Kidney. *Journal of the American Society of Nephrology* **30**, 726-736
48. Kalluri, R., and Weinberg, R. A. (2009) The basics of epithelial-mesenchymal transition. *Journal of Clinical Investigation* **119**, 1420-1428
49. Xu-Dubois, Y.-C., Galichon, P., Brocheriou, I., Baugey, E., Morichon, R., Jouanneau, C., Ouali, N., Rondeau, E., and Hertig, A. (2013) Expression of the transcriptional regulator snail1 in kidney transplants displaying epithelial-to-mesenchymal transition features. *Nephrology Dialysis Transplantation* **29**, 2136-2144
50. Zheng, M., Lv, L.-L., Cao, Y.-H., Zhang, J.-D., Wu, M., Ma, K.-L., Phillips, A. O., and Liu, B.-C. (2012) Urinary mRNA markers of epithelial–mesenchymal transition correlate with progression of diabetic nephropathy. *Clinical Endocrinology* **76**, 657-664
51. Qureshi, O. S., Bon, H., Twomey, B., Holdsworth, G., Ford, K., Bergin, M., Huang, L., Muzylak, M., Healy, L. J., Hurdowar, V., and Johnson, T. S. (2017) An immunofluorescence assay for extracellular matrix components highlights the role of epithelial cells in producing a stable, fibrillar extracellular matrix. *Biology Open* **6**, 1423
52. Lovisa, S., Zeisberg, M., and Kalluri, R. (2016) Partial Epithelial-to-Mesenchymal Transition and Other New Mechanisms of Kidney Fibrosis. *Trends in Endocrinology and Metabolism* **27**, 681-695
53. Schnaper, H. W. (2017) The Tubulointerstitial Pathophysiology of Progressive Kidney Disease. *Advances in Chronic Kidney Disease* **24**, 107-116
54. Prasad, G. V. R. (2014) Metabolic syndrome and chronic kidney disease: Current status and future directions. *World Journal of Nephrology* **3**, 210-219
55. Galvan, D. L., Green, N. H., and Danesh, F. R. (2017) The hallmarks of mitochondrial dysfunction in chronic kidney disease. *Kidney International* **92**, 1051-1057
56. Gai, Z., Wang, T., Visentin, M., Kullak-Ublick, G. A., Fu, X., and Wang, Z. (2019) Lipid Accumulation and Chronic Kidney Disease. *Nutrients* **11**, 722
57. Burns, J. S., and Manda, G. (2017) Metabolic Pathways of the Warburg Effect in Health and Disease: Perspectives of Choice, Chain or Chance. *International Journal of Molecular Science* **18**
58. Che, R., Yuan, Y., Huang, S., and Zhang, A. (2014) Mitochondrial dysfunction in the pathophysiology of renal diseases. *American journal of physiology. Renal physiology* **306**, 367-378
59. Hall, A. M., and Unwin, R. J. (2007) The not so 'mighty chondrion': emergence of renal diseases due to mitochondrial dysfunction. *Nephron Physiology* **105**, 1-10
60. Lan, R., Geng, H., Singha, P. K., Saikumar, P., Bottinger, E. P., Weinberg, J. M., and Venkatachalam, M. A. (2016) Mitochondrial Pathology and Glycolytic Shift during Proximal Tubule Atrophy after Ischemic AKI. *Journal of the American Society of Nephrology* **27**, 3356-3367
61. Wiley, C. D., Velarde, M. C., Lecot, P., Liu, S., Sarnoski, E. A., Freund, A., Shirakawa, K., Lim, H. W., Davis, S. S., Ramanathan, A., Gerencser,

A. A., Verdin, E., and Campisi, J. (2016) Mitochondrial Dysfunction Induces Senescence with a Distinct Secretory Phenotype. *Cell Metabolism* **23**, 303-314
62. Zank, D. C., Bueno, M., Mora, A. L., and Rojas, M. (2018) Idiopathic Pulmonary Fibrosis: Aging, Mitochondrial Dysfunction, and Cellular Bioenergetics. *Frontiers in Medicine* **5**, 10-10
63. Chung, K. W., Lee, E. K., Lee, M. K., Oh, G. T., Yu, B. P., and Chung, H. Y. (2018) Impairment of PPARalpha and the Fatty Acid Oxidation Pathway Aggravates Renal Fibrosis during Aging. *Journal of the American Society of Nephrology* **29**, 1223-1237
64. Kang, H. M., Ahn, S. H., Choi, P., Ko, Y.-A., Han, S. H., Chinga, F., Park, A. S. D., Tao, J., Sharma, K., Pullman, J., Bottinger, E. P., Goldberg, I. J., and Susztak, K. (2015) Defective fatty acid oxidation in renal tubular epithelial cells has a key role in kidney fibrosis development. *Nature Medicine* **21**, 37-46
65. Whaley-Connell, A., and Sowers, J. R. (2017) Obesity and kidney disease: from population to basic science and the search for new therapeutic targets. *Kidney International* **92**, 313-323
66. Silverstein, D. M. (2009) Inflammation in chronic kidney disease: role in the progression of renal and cardiovascular disease. *Pediatric Nephrology* **24**, 1445-1452
67. Meng, X.-M., Nikolic-Paterson, D. J., and Lan, H. Y. (2014) Inflammatory processes in renal fibrosis. *Nature Reviews Nephrology* **10**, 493
68. Vernon, M. A., Mylonas, K. J., and Hughes, J. (2010) Macrophages and renal fibrosis. *Seminars in Nephrology* **30**, 302-317
69. Lv, W., Booz, G. W., Wang, Y., Fan, F., and Roman, R. J. (2018) Inflammation and renal fibrosis: Recent developments on key signaling molecules as potential therapeutic targets. *European Journal of Pharmacology* **820**, 65-76
70. Sanz, A. B., Sanchez-Niño, M. D., Ramos, A. M., Moreno, J. A., Santamaria, B., Ruiz-Ortega, M., Egido, J., and Ortiz, A. (2010) NF-κB in Renal Inflammation. *Journal of the American Society of Nephrology* **21**, 1254-1262
71. Tesch, G. H., Schwarting, A., Kinoshita, K., Lan, H. Y., Rollins, B. J., and Kelley, V. R. (1999) Monocyte chemoattractant protein-1 promotes macrophage-mediated tubular injury, but not glomerular injury, in nephrotoxic serum nephritis. *Journal of Clinical Investigation* **103**, 73-80
72. Tomson, C., and Duffy, S. (2019) Management of chronic kidney disease. *Medicine*.
Available at https://doi.org/10.1016/j.mpmed.2015.05.004
73. López-Novoa, J. M., Martínez-Salgado, C., Rodríguez-Peña, A. B., and Hernández, F. J. L. (2010) Common pathophysiological mechanisms of chronic kidney disease: Therapeutic perspectives. *Pharmacology & Therapeutics* **128**, 61-81
74. Guo, X., and Wang, X.-F. (2009) Signaling cross-talk between TGF-β/BMP and other pathways. *Cell Research* **19**, 71-88
75. Meng, X.-M., Tang, P. M.-K., Li, J., and Lan, H. Y. (2015) TGF-β/Smad signaling in renal fibrosis. *Frontiers in Physiology* **6**, 82-82
76. Meng, X. M., Huang, X. R., Xiao, J., Chen, H. Y., Zhong, X., Chung, A. C., and Lan, H. Y. (2012) Diverse roles of TGF-beta receptor II in renal fibrosis and inflammation in vivo and in vitro. *Journal of Pathology* **227**, 175-188

77. Al-Lamki, R. S., and Mayadas, T. N. (2015) TNF receptors: signaling pathways and contribution to renal dysfunction. *Kidney International* **87**, 281-296
78. Devarapu, S. K., Grill, J. F., Xie, J., Weidenbusch, M., Honarpisheh, M., Vielhauer, V., Anders, H. J., and Mulay, S. R. (2017) Tumor necrosis factor superfamily ligand mRNA expression profiles differ between humans and mice during homeostasis and between various murine kidney injuries. *Journal of Biomedical Science* **24**, 77
79. Tong, F., Luo, L., and Liu, D. (2016) Effect of Intervention in Mast Cell Function Before Reperfusion on Renal Ischemia-Reperfusion Injury in Rats. *Kidney & Blood Pressure Research* **41**, 335-344
80. Meldrum, K. K., Misseri, R., Metcalfe, P., Dinarello, C. A., Hile, K. L., and Meldrum, D. R. (2007) TNF-α neutralization ameliorates obstruction-induced renal fibrosis and dysfunction. *American Journal of Physiology-Regulatory, Integrative and Comparative Physiology* **292**, 1456-1464
81. Sumida, K., Molnar, M. Z., Potukuchi, P. K., Hassan, F., Thomas, F., Yamagata, K., Kalantar-Zadeh, K., and Kovesdy, C. P. (2018) Treatment of rheumatoid arthritis with biologic agents lowers the risk of incident chronic kidney disease. *Kidney International* **93**, 1207-1216
82. Bartel, D. P. (2009) MicroRNAs: target recognition and regulatory functions. *Cell* **136**, 215-233
83. Trionfini, P., Benigni, A., and Remuzzi, G. (2014) MicroRNAs in kidney physiology and disease. *Nature Reviews Nephrology* **11**, 23
84. Lv, W., Fan, F., Wang, Y., Gonzalez-Fernandez, E., Wang, C., Yang, L., Booz, G. W., and Roman, R. J. (2018) Therapeutic potential of microRNAs for the treatment of renal fibrosis and CKD. *Physiological Genomics* **50**, 20-34
85. Lima, J. F., Cerqueira, L., Figueiredo, C., Oliveira, C., and Azevedo, N. F. (2018) Anti-miRNA oligonucleotides: A comprehensive guide for design. *RNA biology* **15**, 338-352
86. Janssen, H. L., Reesink, H. W., Lawitz, E. J., Zeuzem, S., Rodriguez-Torres, M., Patel, K., van der Meer, A. J., Patick, A. K., Chen, A., Zhou, Y., Persson, R., King, B. D., Kauppinen, S., Levin, A. A., and Hodges, M. R. (2013) Treatment of HCV infection by targeting microRNA. *The New England Journal of Medicine* **368**, 1685-1694
87. Lanford, R. E., Hildebrandt-Eriksen, E. S., Petri, A., Persson, R., Lindow, M., Munk, M. E., Kauppinen, S., and Orum, H. (2010) Therapeutic silencing of microRNA-122 in primates with chronic hepatitis C virus infection. *Science* **327**, 198-201
88. Davies, R. (2018) The metabolomic quest for a biomarker in chronic kidney disease. *Clinical Kidney Journal* **11**, 694-703
89. Grams, M. E., Shafi, T., and Rhee, E. P. (2018) Metabolomics Research in Chronic Kidney Disease. *Journal of the American Society of Nephrology* **29**, 1588-1590
90. Baruteau, J., Perocheau, D. P., Hanley, J., Lorvellec, M., Rocha-Ferreira, E., Karda, R., Ng, J., Suff, N., Diaz, J. A., Rahim, A. A., Hughes, M. P., Banushi, B., Prunty, H., Hristova, M., Ridout, D. A., Virasami, A., Heales, S., Howe, S. J., Buckley, S. M. K., Mills, P. B., Gissen, P., and Waddington, S. N. (2018) Argininosuccinic aciduria fosters neuronal nitrosative stress reversed by Asl gene transfer. *Nature Communications* **9**, 3505
91. Hesketh, E. E., Vernon, M. A., Ding, P., Clay, S., Borthwick, G., Conway, B., and Hughes, J. (2014) A murine model of irreversible and

reversible unilateral ureteric obstruction. *Journal of Visualized Experiments* **94**. doi: 10.3791/52559.

92. Hamzaoui, M., Djerada, Z., Brunel, V., Mulder, P., Richard, V., Bellien, J., and Guerrot, D. (2020) 5/6 nephrectomy induces different renal, cardiac and vascular consequences in 129/Sv and C57BL/6JRj mice. *Scientific Reports* **10**, 1524
93. O'Sullivan, J., Finnie, S. L., Teenan, O., Cairns, C., Boyd, A., Bailey, M. A., Thomson, A., Hughes, J., Bénézech, C., Conway, B. R., and Denby, L. (2019) Refining the Mouse Subtotal Nephrectomy in Male 129S2/SV Mice for Consistent Modeling of Progressive Kidney Disease With Renal Inflammation and Cardiac Dysfunction. *Frontiers in Physiology* **10,** 1365
94. Denby, L., Ramdas, V., Lu, R., Conway, B. R., Grant, J. S., Dickinson, B., Aurora, A. B., McClure, J. D., Kipgen, D., Delles, C., van Rooij, E., and Baker, A. H. (2014) MicroRNA-214 Antagonism Protects against Renal Fibrosis. *Journal of the American Society of Nephrology* **25**, 65-80
95. Barbone, D., Van Dam, L., Follo, C., Jithesh, P. V., Zhang, S. D., Richards, W. G., Bueno, R., Fennell, D. A., and Broaddus, V. C. (2016) Analysis of Gene Expression in 3D Spheroids Highlights a Survival Role for ASS1 in Mesothelioma. *PLoS One* **11**, e0150044
96. Chevalier, R. L., Forbes, M. S., and Thornhill, B. A. (2009) Ureteral obstruction as a model of renal interstitial fibrosis and obstructive nephropathy. *Kidney International* **75**, 1145-1152
97. Ucero, A. C., Benito-Martin, A., Izquierdo, M. C., Sanchez-Nino, M. D., Sanz, A. B., Ramos, A. M., Berzal, S., Ruiz-Ortega, M., Egido, J., and Ortiz, A. (2014) Unilateral ureteral obstruction: beyond obstruction. *International Urology and Nephrology* **46**, 765-776
98. Nikolic-Paterson, D. J. (2010) CD4+ T cells: a potential player in renal fibrosis. *Kidney International* **78**, 333-335
99. Tang, P. M.-K., Nikolic-Paterson, D. J., and Lan, H.-Y. (2019) Macrophages: versatile players in renal inflammation and fibrosis. *Nature Reviews Nephrology* **15**, 144-158
100. LeBleu, V. S., Taduri, G., O'Connell, J., Teng, Y., Cooke, V. G., Woda, C., Sugimoto, H., and Kalluri, R. (2013) Origin and function of myofibroblasts in kidney fibrosis. *Nature Medicine* **19**, 1047-1053
101. Hesketh, E. E., Vernon, M. A., Ding, P., Clay, S., Borthwick, G., Conway, B (2014) A Murine Model of Irreversible and Reversible Unilateral Ureteric Obstruction. *Journal of Visualized Experiments.* **94**
102. Le Clef, N., Verhulst, A., D'Haese, P. C., and Vervaet, B. A. (2016) Unilateral Renal Ischemia-Reperfusion as a Robust Model for Acute to Chronic Kidney Injury in Mice. *PLoS ONE* **11**, e0152153
103. Ha, M., and Kim, V. N. (2014) Regulation of microRNA biogenesis. *Nature Review Molecular and Cellular Biology* **15**, 509-524
104. Beckerman, P., Qiu, C., Park, J., Ledo, N., Ko, Y. A., Park, A. D., Han, S. Y., Choi, P., Palmer, M., and Susztak, K. (2017) Human Kidney Tubule-Specific Gene Expression Based Dissection of Chronic Kidney Disease Traits. *EBioMedicine* **24**, 267-276
105. Bataille, A., Galichon, P., Chelghoum, N., Oumoussa, B. M., Ziliotis, M. J., Sadia, I., Vandermeersch, S., Simon-Tillaux, N., Legouis, D., Cohen, R., Xu-Dubois, Y. C., Commereuc, M., Rondeau, E., Le Crom, S., and Hertig, A. (2018) Increased Fatty Acid Oxidation in Differentiated Proximal Tubular Cells Surviving a Reversible Episode of Acute Kidney Injury. *Cellular Physiology and Biochemistry* **47**, 1338-1351

106. Swendseid, M. E., Wang, M., Schutz, I., and Kopple, J. D. (1978) Metabolism of urea cycle intermediates in chronic renal failure. *The American Journal of Clinical Nutrition* **31**, 1581-1586
107. Chen, D. Q., Cao, G., Chen, H., Liu, D., Su, W., Yu, X. Y., Vaziri, N. D., Liu, X. H., Bai, X., Zhang, L., and Zhao, Y. Y. (2017) Gene and protein expressions and metabolomics exhibit activated redox signaling and wnt/beta-catenin pathway are associated with metabolite dysfunction in patients with chronic kidney disease. *Redox Biology* **12**, 505-521
108. Baylis, C. (2006) Arginine, arginine analogs and nitric oxide production in chronic kidney disease. *Nature Clinical Practice Nephrology* **2**, 209-220
109. Tizianello, A., De Ferrari, G., Garibotto, G., Gurreri, G., and Robaudo, C. (1980) Renal metabolism of amino acids and ammonia in subjects with normal renal function and in patients with chronic renal insufficiency. *Journal of Clinical Investigation* **65**, 1162-1173
110. Simon, N., and Hertig, A. (2015) Alteration of Fatty Acid Oxidation in Tubular Epithelial Cells: From Acute Kidney Injury to Renal Fibrogenesis. *Frontiers in Medicine* **2**, 52
111. Rhee, E. P., Clish, C. B., Ghorbani, A., Larson, M. G., Elmariah, S., McCabe, E., Yang, Q., Cheng, S., Pierce, K., Deik, A., Souza, A. L., Farrell, L., Domos, C., Yeh, R. W., Palacios, I., Rosenfield, K., Vasan, R. S., Florez, J. C., Wang, T. J., Fox, C. S., and Gerszten, R. E. (2013) A combined epidemiologic and metabolomic approach improves CKD prediction. *Journal of the American Society of Nephrology* **24**, 1330-1338
112. Schmidt, R. J., and Baylis, C. (2000) Total nitric oxide production is low in patients with chronic renal disease. *Kidney International* **58**, 1261-1266
113. Mathew, A. V., Zeng, L., Byun, J., and Pennathur, S. (2015) Metabolomic Profiling of Arginine Metabolome Links Altered Methylation to Chronic Kidney Disease Accelerated Atherosclerosis. *Journal of Proteomics & Bioinformatics* **Suppl 14**, 001
114. Sandoval, P. C., Slentz, D. H., Pisitkun, T., Saeed, F., Hoffert, J. D., and Knepper, M. A. (2013) Proteome-wide measurement of protein half-lives and translation rates in vasopressin-sensitive collecting duct cells. *Journal of the American Society of Nephrology* **24**, 1793-1805
115. Chen, G.-F., and Baylis, C. (2010) In vivo renal arginine release is impaired throughout development of chronic kidney disease. *American Journal of Physiology - Renal Physiology* **298**, 95-102
116. Lee, J. W., Chou, C.-L., and Knepper, M. A. (2015) Deep Sequencing in Microdissected Renal Tubules Identifies Nephron Segment–Specific Transcriptomes. *Journal of the American Society of Nephrology* **26**, 2669-2677
117. Trott, J. F., Hwang, V. J., Ishimaru, T., Chmiel, K., Zhou, X., Shim, K., Stewart, B., Mahjoub, M. R., Jen, K. Y., Barupal, D., Li, X., and Weiss, R. H. (2018) Arginine reprogramming in ADPKD results in arginine-dependent cystogenesis. *American Journal of Physiology. Renal Physiology* **315**, 1855-1868
118. Varga, Z. V., Erdelyi, K., Paloczi, J., Cinar, R., Zsengeller, Z. K., Jourdan, T., Matyas, C., Nemeth, B. T., Guillot, A., Xiang, X., Mehal, A., Haskó, G., Stillman, I. E., Rosen, S., Gao, B., Kunos, G., and Pacher, P. (2018) Disruption of Renal Arginine Metabolism Promotes Kidney Injury in Hepatorenal Syndrome in Mice. *Hepatology* **68**, 1519-1533

119. Nicolas, F. E. (2011) Experimental validation of microRNA targets using a luciferase reporter system. *Methods in Molecular Biology* **732**, 139-152
120. Ritchie, W., Rasko, J. E., and Flamant, S. (2013) MicroRNA target prediction and validation. *Advances in Experimental Medicine and Biology* **774**, 39-53
121. Haines, R. J., Pendleton, L. C., and Eichler, D. C. (2011) Argininosuccinate synthase: at the center of arginine metabolism. *International Journal of Biochemistry and Molecular Biology* **2**, 8-23
122. Husson, A., Brasse-Lagnel, C., Fairand, A., Renouf, S., and Lavoinne, A. (2003) Argininosuccinate synthetase from the urea cycle to the citrulline-NO cycle. *European journal of biochemistry* **270**, 1887-1899
123. Park, J., Shrestha, R., Qiu, C., Kondo, A., Huang, S., Werth, M., Li, M., Barasch, J., and Suszták, K. (2018) Single-cell transcriptomics of the mouse kidney reveals potential cellular targets of kidney disease. *Science* **360**, 758-763
124. Nickelsen K., Graßhoff G. (2009) Concepts from the Bench: Hans Krebs, Kurt Henseleit and the Urea Cycle. In: Hon G., Schickore J., Steinle F. (eds) Going Amiss In Experimental Research. Boston Studies In The Philosophy Of Science, vol 267. Springer, Dordrecht. 91-117
125. Engelking, L. R. (2015) Chapter 10 - Urea Cycle (Krebs-Henseleit Ornithine Cycle). in *Textbook of Veterinary Physiological Chemistry (Third Edition)* (Engelking, L. R. ed.), Academic Press, Boston. 58-64
126. Helman, G., Pacheco-Colon, I., and Gropman, A. L. (2014) The urea cycle disorders. *Seminars in Neurology* **34**, 341-349
127. Mori, T., Nagai, K., Mori, M., Nagao, M., Imamura, M., Iijima, M., and Kobayashi, K. (2002) Progressive Liver Fibrosis in Late-onset Argininosuccinate Lyase Deficiency. *Pediatric and Developmental Pathology* **5**, 597-601
128. LaBrecque, D. R., Latham, P. S., Riely, C. A., Hsia, Y. E., and Klatskin, G. (1979) Heritable urea cycle enzyme deficiency-liver disease in 16 patients. *The Journal of Pediatrics* **94**, 580-587
129. Nagamani, S. C., Erez, A., and Lee, B. (2012) Argininosuccinate lyase deficiency. *Genetics in Medicine : Official Journal of the American College of Medical Genetics* **14**, 501-507
130. Kölker, S., Cazorla, A. G., Valayannopoulos, V., Lund, A. M., Burlina, A. B., Sykut-Cegielska, J., Wijburg, F. A., Teles, E. L., Zeman, J., Dionisi-Vici, C., Barić, I., Karall, D., Augoustides-Savvopoulou, P., Aksglaede, L., Arnoux, J.-B., Avram, P. (2015) The phenotypic spectrum of organic acidurias and urea cycle disorders. Part 1: the initial presentation. *Journal of Inherited Metabolic Disease* **38**, 1041-1057
131. Kolker, S., Valayannopoulos, V., Burlina, A. B., Sykut-Cegielska, J., Wijburg, F. A., Teles, E. L., Zeman, J., Dionisi-Vici, C., Baric, I., Karall, D., Arnoux, J. B., Avram, P., Baumgartner, M. R., Blasco-Alonso, J., Boy, S. P., Rasmussen, M. B., Burgard, P. (2015) The phenotypic spectrum of organic acidurias and urea cycle disorders. Part 2: the evolving clinical phenotype. *Journal of Inherited Metabolic Disease* **38**, 1059-1074
132. Baruteau, J., Jameson, E., Morris, A. A., Chakrapani, A., Santra, S., Vijay, S., Kocadag, H., Beesley, C. E., Grunewald, S., Murphy, E., Cleary, M., Mundy, H., Abulhoul, L., Broomfield, A., Lachmann, R., Rahman, Y., Robinson, P. H., MacPherson, L., Foster, K., Chong, W. K., Ridout, D. A., Bounford, K. M., Waddington, S. N., Mills, P. B., Gissen, P., and Davison, J. E. (2017) Expanding the phenotype in

argininosuccinic aciduria: need for new therapies. *Journal of Inherited Metabolic Disease* **40**, 357-368
133. Slyne, J., Slattery, C., McMorrow, T., and Ryan, M. P. (2015) New developments concerning the proximal tubule in diabetic nephropathy: in vitro models and mechanisms. *Nephrology, Dialysis, Transplantation* **30 Suppl 4**, 60-67
134. Wieser, M., Stadler, G., Jennings, P., Streubel, B., Pfaller, W., Ambros, P., Riedl, C., Katinger, H., Grillari, J., and Grillari-Voglauer, R. (2008) hTERT alone immortalizes epithelial cells of renal proximal tubules without changing their functional characteristics. *American Journal of Physiology. Renal Physiology* **295**, 1365-1375
135. Simon, B. R., Wilson, M. J., and Wickliffe, J. K. (2014) The RPTEC/TERT1 cell line models key renal cell responses to the environmental toxicants, benzo[a]pyrene and cadmium. *Toxicology Reports* **1**, 231-242
136. Wilmes, A., Bielow, C., Ranninger, C., Bellwon, P., Aschauer, L., Limonciel, A., Chassaigne, H., Kristl, T., Aiche, S., Huber, C. G., Guillou, C., Hewitt, P., Leonard, M. O., Dekant, W., Bois, F., and Jennings, P. (2015) Mechanism of cisplatin proximal tubule toxicity revealed by integrating transcriptomics, proteomics, metabolomics and biokinetics. *Toxicology in Vitro* **30**, 117-127
137. Ellis, J. K., Athersuch, T. J., Cavill, R., Radford, R., Slattery, C., Jennings, P., McMorrow, T., Ryan, M. P., Ebbels, T. M. D., and Keun, H. C. (2011) Metabolic response to low-level toxicant exposure in a novel renal tubule epithelial cell system. *Molecular BioSystems* **7**, 247-257
138. Secker, P. F., Luks, L., Schlichenmaier, N., and Dietrich, D. R. (2018) RPTEC/TERT1 cells form highly differentiated tubules when cultured in a 3D matrix. *Altex* **35**, 223-234
139. Han, S. H., Malaga-Dieguez, L., Chinga, F., Kang, H. M., Tao, J., Reidy, K., and Susztak, K. (2016) Deletion of Lkb1 in Renal Tubular Epithelial Cells Leads to CKD by Altering Metabolism. *Journal of the American Society of Nephrology* **27**, 439-453
140. Okamoto, K., Rausch, J. W., Wakashin, H., Fu, Y., Chung, J.-Y., Dummer, P. D., Shin, M. K., Chandra, P., Suzuki, K., Shrivastav, S., Rosenberg, A. Z., Hewitt, S. M., Ray, P. E., Noiri, E., Le Grice, S. F. J., Hoek, M., Han, Z., Winkler, C. A., and Kopp, J. B. (2018) APOL1 risk allele RNA contributes to renal toxicity by activating protein kinase R. *Communications Biology* **1**, 188-188
141. Tian, Y.-C., Fraser, D., Attisano, L., and Phillips, A. O. (2003) TGF-β1-mediated alterations of renal proximal tubular epithelial cell phenotype. *American Journal of Physiology-Renal Physiology* **285**, 130-142
142. Russo, L. M., del Re, E., Brown, D., and Lin, H. Y. (2007) Evidence for a Role of Transforming Growth Factor (TGF)-β1 in the Induction of Postglomerular Albuminuria in Diabetic Nephropathy. *Amelioration by Soluble TGF-β Type II Receptor* **56**, 380-388
143. Dai, C., Yang, J., and Liu, Y. (2003) Transforming Growth Factor-β1 Potentiates Renal Tubular Epithelial Cell Death by a Mechanism Independent of Smad Signaling. *Journal of Biological Chemistry* **278**, 12537-12545
144. Ho, A. W. Y., Wong, C. K., and Lam, C. W. K. (2008) Tumor necrosis factor-α up-regulates the expression of CCL2 and adhesion molecules of human proximal tubular epithelial cells through MAPK signaling pathways. *Immunobiology* **213**, 533-544

145. Wuthrich, R. P., Glimcher, L. H., Yui, M. A., Jevnikar, A. M., Dumas, S. E., and Kelley, V. E. (1990) MHC class II, antigen presentation and tumor necrosis factor in renal tubular epithelial cells. *Kidney International* **37**, 783-792
146. Benedetti, G., Fredriksson, L., Herpers, B., Meerman, J., van de Water, B., and de Graauw, M. (2013) TNF-α-mediated NF-κB survival signaling impairment by cisplatin enhances JNK activation allowing synergistic apoptosis of renal proximal tubular cells. *Biochemical Pharmacology* **85**, 274-286
147. Jevnikar, A. M., Brennan, D. C., Singer, G. G., Heng, J. E., Maslinski, W., Wuthrich, R. P., Glimcher, L. H., and Kelley, V. E. R. (1991) Stimulated kidney tubular epithelial cells express membrane associated and secreted TNFα. *Kidney International* **40**, 203-211
148. Stadler, J., Bentz, B. G., Harbrecht, B. G., Di Silvio, M., Curran, R. D., Billiar, T. R., Hoffman, R. A., and Simmons, R. L. (1992) Tumor necrosis factor alpha inhibits hepatocyte mitochondrial respiration. *Annals of Surgery* **216**, 539-546
149. Mariappan, N., Elks, C. M., Fink, B., and Francis, J. (2009) TNF-induced mitochondrial damage: a link between mitochondrial complex I activity and left ventricular dysfunction. *Free Radical Biology and Medicine* **46**, 462-470
150. Moe, G. W., Marin-Garcia, J., Konig, A., Goldenthal, M., Lu, X., and Feng, Q. (2004) In vivo TNF-α inhibition ameliorates cardiac mitochondrial dysfunction, oxidative stress, and apoptosis in experimental heart failure. *American Journal of Physiology-Heart and Circulatory Physiology* **287**, 1813-1820
151. Doll, D. N., Rellick, S. L., Barr, T. L., Ren, X., and Simpkins, J. W. (2015) Rapid mitochondrial dysfunction mediates TNF-alpha-induced neurotoxicity. *Journal of Neurochemistry* **132**, 443-451
152. Kida, Y., Tchao, B. N., and Yamaguchi, I. (2014) Peritubular capillary rarefaction: a new therapeutic target in chronic kidney disease. *Pediatric Nephrology* **29**, 333-342
153. Lacerda, L., McCarthy, J., Mungly, S. F. K., Lynn, E. G., Sack, M. N., Opie, L. H., and Lecour, S. (2010) TNFα protects cardiac mitochondria independently of its cell surface receptors. *Basic Research in Cardiology* **105**, 751-762
154. Shan, Y.-S., Hsu, H.-P., Lai, M.-D., Yen, M.-C., Chen, W.-C., Fang, J.-H., Weng, T.-Y., and Chen, Y.-L. (2015) Argininosuccinate synthetase 1 suppression and arginine restriction inhibit cell migration in gastric cancer cell lines. *Scientific Reports* **5**, 9783
155. Huang, Z., Wang, T.-S., Zhao, Y.-C., Zuo, R.-J., Deng, W.-B., Chi, Y.-J., and Yang, Z.-M. (2014) Cyclic adenosine monophosphate-induced argininosuccinate synthase 1 expression is essential during mouse decidualization. *Molecular and Cellular Endocrinology* **388**, 20-31
156. Herrera Sanchez, M. B., Previdi, S., Bruno, S., Fonsato, V., Deregibus, M. C., Kholia, S., Petrillo, S., Tolosano, E., Critelli, R., Spada, M., Romagnoli, R., Salizzoni, M., Tetta, C., and Camussi, G. (2017) Extracellular vesicles from human liver stem cells restore argininosuccinate synthase deficiency. *Stem Cell Research & Therapy* **8**, 176
157. Wieser, M., Stadler, G., Jennings, P., Streubel, B., Pfaller, W., Ambros, P., Riedl, C., Katinger, H., Grillari, J., and Grillari-Voglauer, R. (2008) hTERT alone immortalizes epithelial cells of renal proximal tubules without changing their functional characteristics. *American Journal of Physiology-Renal Physiology* **295**, 1365-1375

158. Slusser, A., Bathula, C. S., Sens, D. A., Somji, S., Sens, M. A., Zhou, X. D., and Garrett, S. H. (2015) Cadherin Expression, Vectorial Active Transport, and Metallothionein Isoform 3 Mediated EMT/MET Responses in Cultured Primary and Immortalized Human Proximal Tubule Cells. *PLoS ONE* **10**, e0120132
159. Czajka, A., and Malik, A. N. (2016) Hyperglycemia induced damage to mitochondrial respiration in renal mesangial and tubular cells: Implications for diabetic nephropathy. *Redox biology* **10**, 100-107
160. Gewin, L. S. (2018) Renal fibrosis: Primacy of the proximal tubule. *Matrix Biology* **68-69**, 248-262
161. Secker, P. F., Beneke, S., Schlichenmaier, N., Delp, J., Gutbier, S., Leist, M., and Dietrich, D. R. (2018) Canagliflozin mediated dual inhibition of mitochondrial glutamate dehydrogenase and complex I: an off-target adverse effect. *Cell Death & Disease* **9**, 226-226
162. Cohen, N. S., and Kuda, A. (1996) Argininosuccinate synthetase and argininosuccinate lyase are localized around mitochondria: an immunocytochemical study. *Journal of Cellular Biochemistry* **60**, 334-340
163. Loeffler, I., and Wolf, G. (2013) Transforming growth factor-β and the progression of renal disease. *Nephrology Dialysis Transplantation* **29**, 37-45
164. Casalena, G., Daehn, I., and Bottinger, E. (2012) Transforming growth factor-β, bioenergetics, and mitochondria in renal disease. *Seminars in Nephrology* **32**, 295-303
165. Pfleger, J., He, M., and Abdellatif, M. (2015) Mitochondrial complex II is a source of the reserve respiratory capacity that is regulated by metabolic sensors and promotes cell survival. *Cellular Death and Disease* **6**, e1835
166. Kobayashi, H., Gilbert, V., Liu, Q., Kapitsinou, P. P., Unger, T. L., Rha, J., Rivella, S., Schlondorff, D., and Haase, V. H. (2012) Myeloid cell-derived hypoxia-inducible factor attenuates inflammation in unilateral ureteral obstruction-induced kidney injury. *Journal of Immunology* **188**, 5106-5115
167. Malek, M., and Nematbakhsh, M. (2015) Renal ischemia/reperfusion injury; from pathophysiology to treatment. *Journal of Renal Injury Prevention* **4**, 20-27
168. Amdur, R. L., Feldman, H. I., Gupta, J., Yang, W., Kanetsky, P., Shlipak, M., Rahman, M., Lash, J. P., Townsend, R. R., Ojo, A., Roy-Chaudhury, A., Go, A. S., Joffe, M., He, J., Balakrishnan, V. S., Kimmel, P. L., Kusek, J. W., and Raj, D. S. (2016) Inflammation and Progression of CKD: The CRIC Study. *Clinical Journal of the American Society of Nephrology* **11**, 1546-1556
169. Hayden, M. S., and Ghosh, S. (2014) Regulation of NF-κB by TNF family cytokines. *Seminars in Immunology* **26**, 253-266
170. Szlosarek, P. W., Grimshaw, M. J., Wilbanks, G. D., Hagemann, T., Wilson, J. L., Burke, F., Stamp, G., and Balkwill, F. R. (2007) Aberrant regulation of argininosuccinate synthetase by TNF-alpha in human epithelial ovarian cancer. *International Journal of Cancer* **121**, 6-11
171. Ishikura, H., Takahashi, C., Kanagawa, K., Hirata, H., Imai, K., and Yoshiki, T. (1991) Cytokine regulation of ICAM-1 expression on human renal tubular epithelial cells in vitro. *Transplantation* **51**, 1272-1275
172. Datta De, D., Datta, A., Bhattacharjya, S., and Roychoudhury, S. (2013) NF-kappaB mediated transcriptional repression of acid modifying hormone gastrin. *PLoS One* **8**, e73409

173. Campbell, K. J., Rocha, S., and Perkins, N. D. (2004) Active Repression of Antiapoptotic Gene Expression by RelA(p65) NF-κB. *Molecular Cell* **13**, 853-865
174. Aggarwal, B. B. (2003) Signalling pathways of the TNF superfamily: a double-edged sword. *Nature Reviews Immunology* **3**, 745-756
175. Lkhagva, B., Kao, Y.-H., Lee, T.-I., Lee, T.-W., Cheng, W.-L., and Chen, Y.-J. (2018) Activation of Class I histone deacetylases contributes to mitochondrial dysfunction in cardiomyocytes with altered complex activities. *Epigenetics* **13**, 376-385
176. Tran, M., Tam, D., Bardia, A., Bhasin, M., Rowe, G. C., Kher, A., Zsengeller, Z. K., Akhavan-Sharif, M. R., Khankin, E. V., Saintgeniez, M., David, S., Burstein, D., Karumanchi, S. A., Stillman, I. E., Arany, Z., and Parikh, S. M. (2011) PGC-1alpha promotes recovery after acute kidney injury during systemic inflammation in mice. *Journal of Clinical Investigation* **121**, 4003-4014
177. Li, Z. L., and Liu, B. C. (2019) Hypoxia and Renal Tubulointerstitial Fibrosis. *Advances in Experimental Medicine and Biology* **1165**, 467-485
178. Tsai, W.-B., Aiba, I., Lee, S.-y., Feun, L., Savaraj, N., and Kuo, M. T. (2009) Resistance to arginine deiminase treatment in melanoma cells is associated with induced argininosuccinate synthetase expression involving c-Myc/HIF-1α/Sp4. *Molecular Cancer Therapeutics* **8**, 3223-3233
179. Long, Y., Tsai, W. B., Chang, J. T., Estecio, M., Wangpaichitr, M., Savaraj, N., Feun, L. G., Chen, H. H., and Kuo, M. T. (2016) Cisplatin-induced synthetic lethality to arginine-starvation therapy by transcriptional suppression of ASS1 is regulated by DEC1, HIF-1alpha, and c-Myc transcription network and is independent of ASS1 promoter DNA methylation. *Oncotarget* **7**, 82658-82670
180. Song, J., Yu, J., Prayogo, G. W., Cao, W., Wu, Y., Jia, Z., and Zhang, A. (2019) Understanding kidney injury molecule 1: a novel immune factor in kidney pathophysiology. *American Journal of Translational Research* **11**, 1219-1229
181. Knoppert, S. N., Valentijn, F. A., Nguyen, T. Q., Goldschmeding, R., and Falke, L. L. (2019) Cellular Senescence and the Kidney: Potential Therapeutic Targets and Tools. *Frontiers in Pharmacology* **10,** 770
182. Gewin, L., Zent, R., and Pozzi, A. (2017) Progression of chronic kidney disease: too much cellular talk causes damage. *Kidney International* **91**, 552-560
183. Tang, S. C. W., Leung, J. C. K., Chan, L. Y. Y., Tsang, A. W. L., and Lai, K. N. (2006) Activation of Tubular Epithelial Cells in Diabetic Nephropathy and the Role of the Peroxisome Proliferator–Activated Receptor-γ Agonist. *Journal of the American Society of Nephrology* **17**, 1633-1643
184. Sato, Y., and Yanagita, M. (2018) Immune cells and inflammation in AKI to CKD progression. *American Journal of Physiology-Renal Physiology* **315**, 1501-1512
185. Rabb, H., Daniels, F., O'Donnell, M., Haq, M., Saba, S. R., Keane, W., and Tang, W. W. (2000) Pathophysiological role of T lymphocytes in renal ischemia-reperfusion injury in mice. *American Journal of Physiology-Renal Physiology* **279**, 525-531
186. Erez, A., Nagamani, S. C., Shchelochkov, O. A., Premkumar, M. H., Campeau, P. M., Chen, Y., Garg, H. K., Li, L., Mian, A., Bertin, T. K., Black, J. O., Zeng, H., Tang, Y., Reddy, A. K., Summar, M., O'Brien, W. E., Harrison, D. G., Mitch, W. E., Marini, J. C., Aschner, J. L., Bryan, N.

S., and Lee, B. (2011) Requirement of argininosuccinate lyase for systemic nitric oxide production. *Nature Medicine* **17**, 1619-1626
187. Bateman, L. A., Ku, W. M., Heslin, M. J., Contreras, C. M., Skibola, C. F., and Nomura, D. K. (2017) Argininosuccinate Synthase 1 is a Metabolic Regulator of Colorectal Cancer Pathogenicity. *ACS Chemical Biology* **12**, 905-911
188. Yarmolinsky, M., and Hoess, R. (2015) The Legacy of Nat Sternberg: The Genesis of Cre-lox Technology. *Annual review of virology* **2**, 25-40
189. Feil, S., Valtcheva, N., and Feil, R. (2009) Inducible Cre mice. *Methods in Molecular Biology* **530**, 343-363
190. Muzumdar, M. D., Tasic, B., Miyamichi, K., Li, L., and Luo, L. (2007) A global double-fluorescent Cre reporter mouse. *Genesis* **45**, 593-605
191. Capecchi, M. R. (1989) The new mouse genetics: altering the genome by gene targeting. *Trends in Genetics* **5**, 70-76
192. Song, A. J., and Palmiter, R. D. (2018) Detecting and Avoiding Problems When Using the Cre-lox System. *Trends in Genetics* **34**, 333-340
193. Moeller, M. J., Sanden, S. K., Soofi, A., Wiggins, R. C., and Holzman, L. B. (2003) Podocyte-specific expression of cre recombinase in transgenic mice. *Genesis* **35**, 39-42
194. Nelson, R. D., Stricklett, P., Gustafson, C., Stevens, A., Ausiello, D., Brown, D., and Kohan, D. E. (1998) Expression of an AQP2 Cre recombinase transgene in kidney and male reproductive system of transgenic mice. *American Journal of Physiology-Cell Physiology* **275**, 216-226
195. Espana-Agusti, J., Zou, X., Wong, K., Fu, B., Yang, F., Tuveson, D. A., Adams, D. J., and Matakidou, A. (2016) Generation and Characterisation of a Pax8-CreER(T2) Transgenic Line and a Slc22a6-CreER(T2) Knock-In Line for Inducible and Specific Genetic Manipulation of Renal Tubular Epithelial Cells. *PLoS ONE* **11**, e0148055
196. Patejunas, G., Bradley, A., Beaudet, A. L., and O'Brien, W. E. (1994) Generation of a mouse model for citrullinemia by targeted disruption of the argininosuccinate synthetase gene. *Somatic Cell and Molecular Genetics* **20**, 55-60
197. Perez, C. J., Jaubert, J., Guénet, J.-L., Barnhart, K. F., Ross-Inta, C. M., Quintanilla, V. C., Aubin, I., Brandon, J. L., Otto, N. W., DiGiovanni, J., Gimenez-Conti, I., Giulivi, C., Kusewitt, D. F., Conti, C. J., and Benavides, F. (2010) Two Hypomorphic Alleles of Mouse Ass1 as a New Animal Model of Citrullinemia Type I and Other Hyperammonemic Syndromes. *The American Journal of Pathology* **177**, 1958-1968
198. Marion, V., Sankaranarayanan, S., de Theije, C., van Dijk, P., Hakvoort, T. B., Lamers, W. H., and Kohler, E. S. (2013) Hepatic adaptation compensates inactivation of intestinal arginine biosynthesis in suckling mice. *PLoS One* **8**, e67021
199. Kauffman, K., Oberli, M., Dorkin, R., Hurtado, J., Kaczmarek, J., Bhadini, S., Wyckoff, J., Langer, R., Jaklenec, A., and Anderson, D. (2017) Rapid, Single-Cell Analysis and Discovery of Vectored mRNA Transfection In Vivo with a loxP-Flanked tdTomato Reporter Mouse. *Molecular Therapy - Nucleic Acids* **10** 55–63
200. Drosos, G., Ampatzidou, F., Sarafidis, P., Karaiskos, T., Madesis, A., and Boutou, A. K. (2018) Serum Creatinine and Chronic Kidney Disease-Epidemiology Estimated Glomerular Filtration Rate: Independent Predictors of Renal Replacement Therapy following Cardiac Surgery. *American Journal of Nephrology* **48**, 108-117

201. DOSSETOR, J. B. (1966) Creatininemia Versus Uremia: The Relative Significance of Blood Urea Nitrogen and Serum Creatinine Concentrations in Azotemia. *Annals of Internal Medicine* **65**, 1287-1299
202. Tveitaras, M. K., Skogstrand, T., Leh, S., Helle, F., Iversen, B. M., Chatziantoniou, C., Reed, R. K., and Hultstrom, M. (2015) Matrix Metalloproteinase-2 Knockout and Heterozygote Mice Are Protected from Hydronephrosis and Kidney Fibrosis after Unilateral Ureteral Obstruction. *PLoS One* **10**, e0143390
203. Kraut, J. A., and Madias, N. E. (2016) Metabolic Acidosis of CKD: An Update. *American Journal of Kidney Diseases* **67**, 307-317
204. Batlle, D., Ba Aqeel, S. H., and Marquez, A. (2018) The Urine Anion Gap in Context. *Clinical Journal of the American Society of Nephrology* **13**, 195-197
205. Li, Y., Caballero, D., Ponsetto, J., Chen, A., Zhu, C., Guo, J., Demay, M., Juppner, H., and Bergwitz, C. (2017) Response of Npt2a knockout mice to dietary calcium and phosphorus. *PLoS One* **12**, e0176232
206. Wysowski, D. K., Kornegay, C., Nourjah, P., and Trontell, A. (2003) Sex and Age Differences in Serum Potassium in the United States. *Clinical Chemistry* **49**, 190-192
207. Baylis, C. (2008) Nitric oxide deficiency in chronic kidney disease. *American Journal of Physiology-Renal Physiology* **294**, 1-9
208. Sinha, A. D., and Agarwal, R. (2014) Hypertension Treatment for Patients with Advanced Chronic Kidney Disease. *Current Cardiovascular Risk Reports* **8**, 400
209. Babu, M., and Drawz, P. (2019) Masked Hypertension in CKD: Increased Prevalence and Risk for Cardiovascular and Renal Events. *Current Cardiology Reports* **21**, 58
210. Berkels, R., Purol-Schnabel, S., and Roesen, R. (2004) Measurement of nitric oxide by reconversion of nitrate/nitrite to NO. *Methods in Molecular Biology* **279**, 1-8
211. Wilde, E., Aubdool, A. A., Thakore, P., Baldissera, L., Jr., Alawi, K. M., Keeble, J., Nandi, M., and Brain, S. D. (2017) Tail-Cuff Technique and Its Influence on Central Blood Pressure in the Mouse. *Journal of the American Heart Association* **6**
212. Kruger, C., Nguyen, T.-T., Breaux, C., Guillory, A., Mangelli, M., Fridianto, K. T., Kovalik, J.-P., Burk, D. H., Noland, R. C., Mynatt, R., and Stadler, K. (2019) Proximal Tubular Cell-Specific Ablation of Carnitine Acetyl-Transferase Causes Tubular Disease and Secondary Glomerulosclerosis. *Diabetes*, db180090
213. Miao, J., Lesher, A. M., Miwa, T., Sato, S., Gullipalli, D., and Song, W.-C. (2014) Tissue-specific deletion of Crry from mouse proximal tubular epithelial cells increases susceptibility to renal ischemia–reperfusion injury. *Kidney International* **86**, 726-737
214. Breyer, M. D., and Susztak, K. (2016) Developing Treatments for Chronic Kidney Disease in the 21st Century. *Seminars in Nephrology* **36**, 436-447
215. Fioretto, P., Barzon, I., and Mauer, M. (2014) Is diabetic nephropathy reversible? *Diabetes Research and Clinical Practice* **104**, 323-328
216. Fiorentino, M., Grandaliano, G., Gesualdo, L., and Castellano, G. (2018) Acute Kidney Injury to Chronic Kidney Disease Transition. *Contributions to Nephrology* **193**, 45-54
217. Connaughton, D. M., and Hildebrandt, F. (2020) Personalized medicine in chronic kidney disease by detection of monogenic mutations. *Nephrology, Dialysis, Transplantation* **35**, 390-397

218. Moonen, L., D'Haese, P. C., and Vervaet, B. A. (2018) Epithelial Cell Cycle Behaviour in the Injured Kidney. *Internationa Journal of Molecular Science* **19**, 2038
219. Skrypnyk, N. I., Sanker, S., Skvarca, L. B., Novitskaya, T., Woods, C., Chiba, T., Patel, K., Goldberg, N. D., McDermott, L., Vinson, P. N., Calcutt, M. W., Huryn, D. M., Vernetti, L. A., Vogt, A., Hukriede, N. A., and Caestecker, M. P. d. (2016) Delayed treatment with PTBA analogs reduces postinjury renal fibrosis after kidney injury. *American Journal of Physiology-Renal Physiology* **310**, 705-716
220. Brilli Skvarca, L., Han, H. I., Espiritu, E. B., Missinato, M. A., Rochon, E. R., McDaniels, M. D., Bais, A. S., Roman, B. L., Waxman, J. S., Watkins, S. C., Davidson, A. J., Tsang, M., and Hukriede, N. A. (2019) Enhancing regeneration after acute kidney injury by promoting cellular dedifferentiation in zebrafish. *Disease Models & Mechanisms* **12**, dmm037390
221. Goldberg, I., Krause, I. (2016) The Role of Gender in Chronic Kidney Disease. *European Medical Journal* **1**, 58-64
222. Iseki, K. (2008) Gender differences in chronic kidney disease. *Kidney International* **74**, 415-417
223. Fanelli, C., Dell, #xea, , H., Cavaglieri, R. C., Dominguez, W. V., and Noronha, I. L. (2017) Gender Differences in the Progression of Experimental Chronic Kidney Disease Induced by Chronic Nitric Oxide Inhibition. *BioMed Research International* **2017**, 12
224. Menegatti, S., Bianchi, E., and Rogge, L. (2019) Anti-TNF Therapy in Spondyloarthritis and Related Diseases, Impact on the Immune System and Prediction of Treatment Responses. *Frontiers in Immunology* **10**
225. The National Institute for Health and Care Excellence. (2010) Etanercept, infliximab and adalimumab for the treatment of psoriatic arthritis. in *NICE Guideline TA199*
226. Nair, K., Ghushchyan, V., and Naim, A. (2013) Effectiveness and Costs of TNF-Alpha Blocker Use for Patients with Rheumatoid Arthritis. *American Health and Drug Benefits* **6**, 126-136
227. Murdaca, G., Spanò, F., Contatore, M., Guastalla, A., Penza, E., Magnani, O., and Puppo, F. (2015) Infection risk associated with anti-TNF-α agents: a review. *Expert Opinion on Drug Safety* **14**, 571-582